ALLOSTERIC CONTROL

OF TYPE III SECRETION SYSTEMS

BY THE SECOND MESSENGER

CYCLIC-DI-GMP

Eleftheria Trampari

September 2016

A thesis submitted for the degree of Doctor of Philosophy

Department of Molecular Microbiology, John Innes Centre

University of East Anglia

Abstract

Eleftheria Trampari, September 2016, John Innes Centre, University of East Anglia, PhD., UK

Allosteric control of Type III secretion systems by the second messenger Cyclic-di-GMP.

Cyclic di-GMP (cdG) is a ubiquitous second messenger in bacteria, regulating transcriptional and post-transcriptional processes and allosterically controlling protein function. While the mechanisms of cdG metabolism are well understood, the downstream targets of this molecule are poorly characterised.

To understand the role of cdG signalling in plant-associated species, cdG-capture compound pull-down experiments were performed to identify potential binding proteins in *Pseudomonas fluorescens*. One of the top targets identified was the flagella export AAA+ ATPase FliI, which was shown to bind specifically and tightly to cdG. FliI-cdG interaction was demonstrated for diverse bacterial FliI homologs. Excitingly, high-affinity binding was observed for the type-III secretion system (T3SS) homolog, HrcN and the type-VI ATPase, ClpB2. A combination of techniques was used to predict the FliI cdG binding site at the interface between two FliI subunits.

Although the addition of cdG inhibits the ATPase activity of both FliI and HrcN *in vitro*, this occurs at a non-physiological cdG concentration suggesting that this does not represent the *in vivo* role of binding. However, when cdG concentrations are artificially increased, the export of flagellin subunits is significantly reduced, suggesting a link between cdG binding and protein export. Changes in the *in vitro* multimerization state of the protein were also observed upon the addition of cdG.

As part of this study, novel and highly specific tools for nucleotide-protein interactions were developed and existing biochemistry techniques were optimised. These assays were

employed to characterise cdG binding to four more proteins, which were identified as cdG binders.

The results generated in this study broaden the existing knowledge about cdG binding protein diversity. The identification of FliI as a cdG binder suggests a novel cdG-dependent control mechanism for the function of bacterial export pathways including the flagellum and the T3SS, through allosteric interaction with export ATPase proteins.

Acknowledgements

I would like to express my deepest thanks to my supervisor, Dr Jacob Malone, for being the best supervisor I could ever have. His vision, support, and input were way beyond the expectations, and I am grateful for that. Many thanks go to my supervisory team members, Dr Gary Rowley and Professor Mark Banfield, for their advice and guidance.

I owe special thanks to Dr Richard Little, who has not only been a mentor to me, being always supportive and ready to help, but a great friend as well. I also owe my deepest gratitude to the other members of my group, who were willing to offer their assistance and advice in any chance given and made it so much more enjoyable to work on this project. Thanks, Sebastian Pfeilmeier, Lucia Grenga, Rosaria Campilongo, and Stuart Woodcock.

I consider myself extremely fortunate that I had the chance to work in the Molecular Microbiology department at the John Innes Centre, which I consider to be the ideal place to undertake research. Many thanks are due to all the members of the Molecular Microbiology department, who made it such a fantastic environment to work at. Special thanks to the Head of the Department, Professor Mark Buttner, for being so supportive in the course of this project. Many thanks to Dr David Lawson and Dr Clare Stevenson for their help with all the X-ray crystallography work and modelling. I would also like to thank Dr Thomas Wilhelm for the peptide shift analysis, Dr Patrick Gunning for his contribution to the AFM experiments and Dr. Gerhard Saalbach for the MS analysis.

I owe many thanks to Professor Miguel Camara and Professor Rafael Rivilla for allowing me to include the unpublished work I produced in this thesis.

Last but not least, my deepest heartfelt thanks go to my parents and sister for their daily support and for always being there for me. I also owe my deepest gratitude to my partner, Dimitris, for his warm encouragement and constructive comments on this project. Without their support and encouragement, this thesis wouldn’t have been possible.

Table of Contents

Table of Figures

Table of Abbreviations

Abbreviations	Definition
AAA+ ATPases	ATPases Associated with diverse cellular Activities
ADP	Adenosine diphosphate
AFM	Atomic Force Microscopy
APS	Ammonium Persulfate
ATP	Adenosine triphosphate
BSA	Bovine serum albumin
cAMP	Cyclic adenosine monophosphate
CC-CdG	Capture compound cdG
cdA	Cyclic-di-adenosine monophosphate
cdG	Bis-(3'-5')-cyclic dimeric guanosine monophosphate
cGMP	Cyclic Guanosine Monophosphate
DGC	Diguanylate cyclase
DNA	Deoxyribonucleic acid
DNase	Deoxyribonuclease
DRaCALA	Differential radial capillary of ligand assay
DSF	Differential Scanning Fluorimetry
FPLC	Fast Protein Liquid Chromatography
GSA	Gel shift assay
GTP	Guanosine-5'-triphosphate
IPTG	Isopropyl β-D-1-thiogalactopyranoside
ITC	Isothermal Titration Calorimetry
IVET	In Vivo Expression Technology
KB medium	King’s B medium
LB medium	Luria-Bertani Broth medium
LPS	Lipopolysaccharide
MS	Mass spectrometry
NADH	Nicotinamide adenine dinucleotide
Ni-NTA agarose	Nickel-Nitrilotriacetic acid agarose
PCR	Polymerase Chain Reaction
PDE	Phosphodiesterase
PEG	Polyethylene glycol
pGpG	2'-deoxy [5'-phosphate-guanylyl-(3'-5')-guanosine]
PGPR	Plant growth promoting rhizobacteria

PK/ LDH	Pyruvate Kinase/ Lactic Dehydrogenase
PMF	Proton Motive Force
PSA	Peptide Shift Analysis
PVDF	Polyvinylidene difluoride
Q-RT PCR	Quantitative reverse transcription PCR
RNA	Ribonucleic acid
SDS- PAGE	Sodium dodecyl sulfate- Polyacrylamide gel electrophoresis
SPR	Surface Plasmon Resonance
SUPr	Streptavidin UV Precipitation assay
T3SS	Type III secretion systems
T6SS	Type VI secretion systems
TB medium	Terrific Broth medium
TBS	Tris-buffered saline
TEM	Transmission Electron Microscopy
TEMED	Tetramethylethylenediamine
Tris-HCl buffer	Tris base-hydrochloride buffer
UV	UltraViolet

Chapter 1:

Introduction

Chapter 1: Introduction

Bacteria sense their environment using complex signalling networks, which allow them to receive environmental signals and translate them into cellular responses. These responses help the bacteria to "make different decisions", to either avoid or take advantage of their surroundings. Bacterial responses are orchestrated by complex intracellular signalling networks, an important part of which is the cyclic di-GMP (cdG) signalling system.

This study examines cdG networks in plant-associated bacteria, which can either have beneficial or harmful effects on plants. *Pseudomonas fluorescens* was selected as a model organism for studying the beneficial interactions between bacteria and plants, and *Pseudomonas syringae* for studying the bacterial plant infections. This work focuses on the identification of novel cdG targets in these *Pseudomonas sp.* and the characterisation of two particularly important cdG-binders, the ATPase complexes of the flagellum and the type III secretion system. Gaining more insights into the increasing importance of cdG networks in bacteria could have profound implications for the control of disease as well as the exploitation of these networks in beneficial microbes, for example, to promote more environmentally sustainable agricultural practices.

1.1 *Pseudomonas fluorescens*

Pseudomonas fluorescens is a Gram-negative, rod-shaped bacterium that lives saprophytically in the soil, for most of the time in close association with plants. *P. fluorescens* is characterised by its ability to produce fluorescent siderophores (e.g. pyoverdin), which are used by these microbes to extract the available iron from their environment (1).

P. fluorescens is an agronomically important bacterium due to its ability to act as a plant growth promoter (PGP) and a biocontrol agent. It effectively colonises roots and shoots, living of plant root exudates. In return *P. fluorescens* promotes plant growth and induces systemic resistence to pathogen attack in its host (2). *Pseudomonas* species also directly

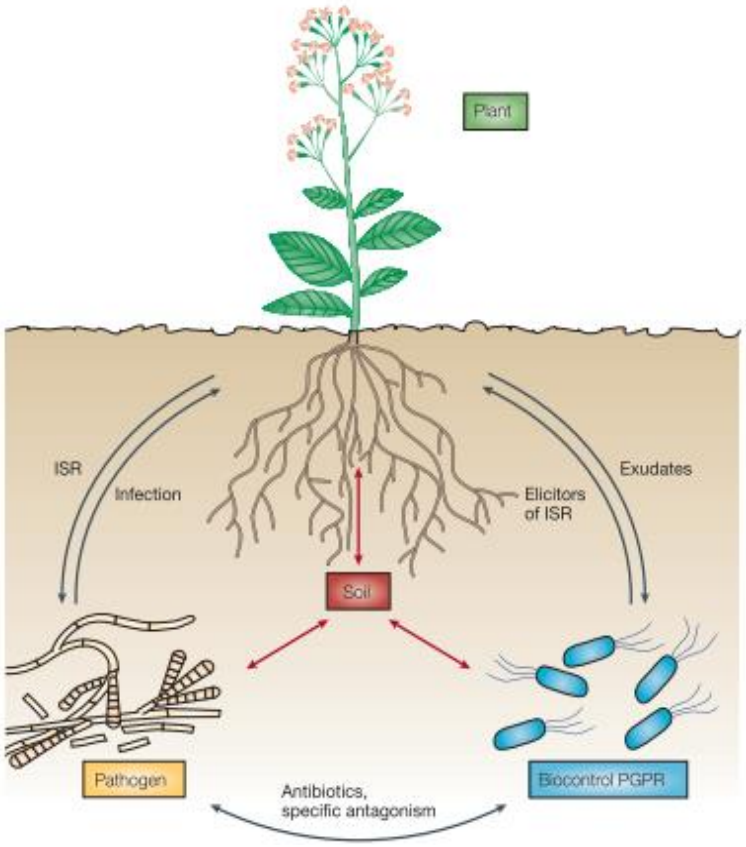

Figure 1.1: Representation of biological control in soil. The possible interaction between the biocontrol factors is described. Reprinted by permission from Macmillan Publishers Ltd: [Nature publishing group] (2), copyright (2005)

antagonise pathogens by secreting antibiotics and engaging in specific antimicrobial activity (Figure 1.1).

1.2 Biocontrol and plant growth promotion

Bacteria such as *P. fluorescens* that have the ability to promote plant growth are commonly known as plant growth-promoting rhizobacteria (PGPR). These microbes are able to colonise plant roots, leading to beneficial associations between the two species. PGPR can promote plant growth either directly, by altering plant hormone levels and/ or by making nutrients accessible to the plant roots, or indirectly, by fighting against pathogenic organisms that affect plant growth and development (3,4).

Biocontrol is a complicated process that is based on the specific properties of beneficial microorganisms to control plant diseases (5). Antagonism is the most well-known mechanism for controlling pathogenicity. In antagonistic relationships, certain microbial species have the ability to produce antibiotics and other secondary metabolites that are toxic to their competitors and as a result, they predominate in the rhizosphere (6), the soil area surrounding the roots.

In order for the biological control to be effective, two main conditions should be met. Firstly, bacteria need to produce a specific antibiotic, bacteriocin or other secondary metabolic products that will allow them to compete against other organisms in the soil environment successfully, and secondly, they must have the ability to colonise the plant root environment effectively. These two bacterial characteristics help them to efficiently protect plants (7).

1.3 Plant colonisation

The reason why microbes colonise plant roots is to exploit the secreted organic compounds the plant rhizosphere provides. By growing on plant root exudates, microbes

not only survive in a hostile environment but also develop into active microbial populations, which can then colonise plant surfaces (8). In addition to the nutrients that plants secrete, plant surfaces provide protection to the attached microbes, which have the opportunity to form a safe homeostatic environment (e.g. biofilm). It is also known that adherent populations develop stronger resistance against environmental factors and as a consequence prevails against free-living soil populations (9).

The colonising microbes benefit in multiple ways from their association with plants. However, plants also gain significant advantages, as bacteria both enhance plant growth and reduce the danger of plant disease. In addition to biocontrol activity against pathogenic microorganisms, PGPRs undertake several beneficial biological services for their plant hosts, such as phosphate solubilisation, nitrogen fixation, and the production of phytohormones (e.g. cytokinin and auxin) and growth stimulants such as ethylene. Beneficial microbes may also contribute towards natural environmental remediation, with some species having the ability to degrade dangerous chemical compounds in the soil (10).

In order for bacteria to achieve a successful association with plants they first need to attach to plant surfaces and then colonise plant tissues. There are two major ways under which bacteria can be deposited onto plant surfaces, the passive and active deposition. Passive mechanisms are usually environmental factors such as wind or rainwater that deposit bacteria onto the plant surfaces (11). Active deposition mechanisms involve motility and chemotaxis, which play a fundamental role in the successful plant root colonisation (12–14).

P. fluorescens colonises plant roots in a non-species specific manner and exploits root exudates as a carbon source. The colonisation process is highly regulated in all stages, from migration towards plant roots through to biofilm formation (7). To enable the initial stages of plant colonisation, these bacteria orchestrate a highly complex arsenal of

motility systems, which include the flagellum and the type IV pili as well as biosurfactants to enhance swarming motility (15,16).

1.4 Motility

One of the most important determinants for effective plant root colonisation is bacterial motility. Bacterial mutants that have lost their ability to swim are incapable of colonising plant roots efficiently, and as a result, they lose their biocontrol ability. The central organelle responsible for bacterial movement is the bacterial flagellum.

There are four distinct forms of motility (17): Twitching, requiring type IV pili (18); sliding motility, which is a form of passive translocation (19,20); and finally swimming and swarming motility, which are the most active forms of bacterial movement both depending on the presence of functional flagella (21,22).

Flagella-driven motility helps bacteria to move towards more advantageous environments and also to avoid dangerous environmental conditions, allowing them to compete against other organisms in the phyllosphere successfully.

1.5 Bacterial flagellum

The bacterial flagellum is the main organelle responsible for bacterial movement in Gram-negative species. It is the flagellated version of T3SS, as they both share the type III export machinery, a highly-conserved transmembrane export system, which initiates the formation of the flagellum filament and the injectisome needle in each system accordingly (23).

Formation of the flagellum has been linked to effective bacterial adherence and host colonisation, as well as multiplication inside host tissues. The main flagella filament subunit, flagellin, has been reported to employ adhesin-like properties, helping the bacteria to attach better to surfaces (24). Furthermore, the importance of flagella in the

invasion in mammalian cells has been demonstrated several times (25,26). As a result, the flagellum plays a crucial role not only in beneficial microbe-host interactions but also in bacterial virulence. Interestingly, the flagellum has also been implicated in the secretion of virulence factors (27).

The synthesis of this complex machinery requires more than 50 gene products. Regulation of flagellar synthesis occurs at every stage of its biogenesis, such as co-transcriptionally, post-transcriptionally, co-translationally and post-translationally (28–30). It is known that the transcription of flagellar genes is temporally-controlled and also depends on the environmental conditions. In certain bacteria flagella, gene expression is coordinated with the cell cycle (31).

1.5.1 Flagellum structure

The flagellum comprises of the basal body, the hook and the helical filament (32). The basal body includes protein rings attached to the bacterial membranes (L, P and the cytoplasmic C ring) and the central rod. The cytoplasmic C-ring acts as the rotor of the motor, and also as the input point for signals controlling flagellar rotation (33). Each component of the bacterial flagellum is synthesised at the correct time for its incorporation into the assembling machinery (34). The assembly starts by the build-up of the flagellum basal body, starting with FliF protein translocation at the inner membrane. The stator, formed by the motor proteins MotA and MotB, surrounds an ion-conducting channel complex which forms the basal body (35). The stator directly interacts with the rotor, which comprises of FliG, FliM and FliN (see Figure 1.2). Once the basal body has been built, the external components of the flagellum, the filament and the linker components are exported through the narrow central channel formed by this point.

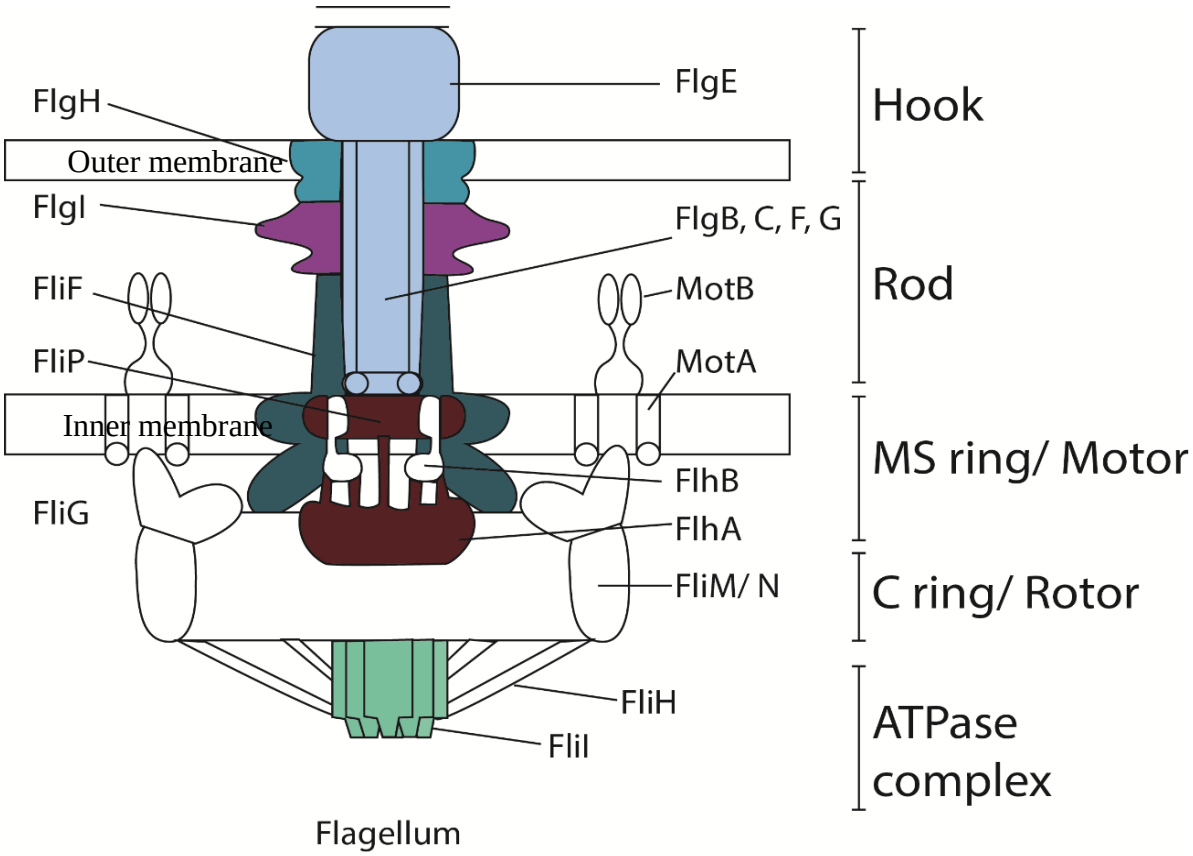

Figure 1.2: Structural representation of the bacterial flagellum. Figure based on (23)

1.5.1.1 The basal body

The basal body construction starts with the formation of the MS ring, a membrane ring structure attached to the rotor. The MS ring consists of 26 copies of FliF. The C ring formation follows, which is a second ring structure located in the cytoplasm (36). The next part assembled is the T3SS, which is thought to be built in the centre of the MS ring, a process followed by the rod assembly in the periplasmic space (37).

1.5.1.2 The rod

The rod consists of the proximal and the distal rod. The proximal rod is composed of 6 subunits of FlgB, FlgC and FlgF and the distal rod from around 26 subunits of FlgG (38,39). The secretion of the rod subunits occurs through the Sec secretion pathway instead of via flagellar type III secretion. FlhE is also a protein associated with the rod

and is required for efficient subunit secretion (40,41). Strains missing this protein are defective in swarming motility (42). FlgL is located at the proximal-distal rod junction, and deletion of the *flgL* gene affects its integrity, making the flagellum susceptible to breaking (43).

1.5.1.3 The motor-force generators

For the flagellum to rotate, both rotor and stator protein complexes are required. MotA and MotB, which are integral membrane proteins, form ion-conducting stator complexes (44,45), promoting the motor rotation. The rotor is built of FliG, FliN and FliM and it interacts with CheY, a component of the chemosensory system, directing the motor to a clockwise or a counter-clockwise direction (46,47). FliG is known to interact with MotA as well as the MS-ring protein FliF (48–50). FliM is the protein responsible for the interaction with phosphorylated CheY protein (51,52). FliN is involved in the rotation of the flagellum and directional switching, as well as contributing to protein export by direct interaction with FliH, the ATPase-complex protein (53–55). It is also known that FliN assembles onto the FliF ring prior to the localisation of the internal membrane components (FliF, FlhA, FlhB, FliP, FliQ and FliR). This indicates that FliN, being a cytoplasmic-directed component, may be essential for the correct localisation of the internal membrane proteins (54).

1.5.1.4 The hook

The hook is composed of about 120 copies of FlgE and resembles the structure of the filament (56,57). The main characteristic of the hook is its flexibility, which is essential for effective flagella function (58).

1.5.1.5 Capping proteins

FliD plays the role of the filament cap and is critical to its polymerization, enabling the filament proteins to polymerise by selectively allowing proteins to pass through the channel (59,60). The filament cap is made by five FliD molecules, forming a pentameric structure characterised by a flexible domain and a flat-top domain (61). FlgD is also a protein involved in the formation of the tip on the growing hook at an earlier stage of the assembly (48).

1.5.1.6 The flagellar propeller and filament

The rotation of the flagellar propeller is responsible for bacterial motility. The propeller is 20 nm thick and up to 15 μm long. The filament consists of up to 20,000 flagellin subunits (FliC). The rotation of this helical propeller is driven by the flagella motor. The direction in which bacteria move depends on the direction of the rotation, to change direction of movement they switch between clockwise and anti-clockwise motor rotation (62) (as a consequence of CheY-P interaction).

1.5.1.7 Junction proteins

Junction proteins are the proteins linking the flexible hook with the filament. For instance, when the hook is completely built, FlgD, the hook cap is discarded and three junction proteins take its place; FlgK and FlgL, both linking the hook with the filament and FliD, which links the filament with the cap. FlgK and FlgL stay in place during the assembly of the flagellum whereas FliD moves outwards as FliC polymerises (63–66).

1.5.1.8 Soluble cytosolic proteins; the ATPase complex

An important part of the flagellum export apparatus are three soluble proteins that form the ATPase complex. These are FliI; the main ATPase, FliH; a protein shown to negatively regulate ATPase activity and FliJ; a general chaperone (34,67). These three

proteins interact with each other forming the FliHIJ ATPase complex. It was initially believed that this complex was responsible for carrying substrates to the export gate of the flagellum, where it associated with the MS ring to secrete the proteins using the energy released by ATP hydrolysis. However, recent studies have shown that ATP hydrolysis is not essential for export, in comparison to the Proton Motive Force (PMF), but does help to effectively translocate the exported substrates (68,69). Recently, another potential role of the FliHIJ complex has been unravelled. FliI ATP hydrolysis is apparently required in the T3SS in pathogens for the unfolding of secretion substrates (70). These studies indicate that a more realistic role of the complex may lie in the correct localisation of substrates to be exported onto the export gate, and then unfolding them to enable their translocation via PMF-dependent secretion (71,72). FliJ has been demonstrated to directly interact with FliM on the C ring as well as FlhA of the T3SS, whereas FliH was shown to interact with FliN of the C ring (53–55,73). From their part, the secretion proteins cannot interact directly with the FliHI complex without the presence of their chaperones (74). FliJ on the other hand can only interact with unbound chaperones but is incapable of interacting with substrates only or substrates bound to their chaperones (72). Finally, the FliH and FliJ proteins potentially interact independently with FliI to either inhibit or enhance its activity (68).

1.5.2 Flagellum function

Both the flagellum and the T3SS are responsible for the export of substrates. This process is remarkably fast. For instance, for the filament growth, flagellin is transported at a rate of 10,000 amino acids per second (75). Similarly, the non-flagellated T3SS from *S. typhimurium* transfers several thousand copies of the effector protein SipA in a matter of a minutes after contacting the host tissue (76).

The quick rate of secretion of these components cannot only be due to the ATPase activity of the soluble T3SS components, which leads to the conclusion that it most probably

depends on the PMF, which is responsible for the system's protein translocation and function. The ATPase complex (FliH, FliI, FliJ) however is assumed to be responsible for the efficient localisation of the proteins for secretion (68,69).

1.5.3 Transcriptional regulation of flagellar genes biosynthesis

The transcriptional regulation of the flagellum has mostly been studied in *S. typhimurium*. The master flagellar operon, *flhDC* controls flagellum assembly and is regulated by various input signals, which lead to the inhibition or expression of the flagellar genes. The *flhDC* genes are expressed by a class I promoter (34). FlhD and FlhC proteins interact with each other forming a heteromultimeric complex (four molecules of FlhD and two molecules of FlhC), which acts as a transcriptional activator, triggering σ^{70}-dependent transcription of the class II promoters (77). In turn, class II promoters are responsible for the transcription of the structural genes, which are needed for the hook-basal body assembly. When the hook and basal body are completed, σ^{28}-dependent class III promoter transcription occurs (78,79). This transcriptional level of regulation is inhibited from the anti-σ^{28} factor protein FlgM. When the hook-basal body assembly is completed, FlgM is secreted from the cell, potentially through the unfinished machinery, and σ^{28}-dependent transcription of the class III promoters starts. In that way there is a temporal control of the flagellar gene transcription, ensuring that each protein will be transcribed at the right point of assembly.

1.5.4 Flagellum regulation by cdG

In recent years it has become clear that regulation of flagella function is even more complex than initially thought. Various studies have shown that motility inhibition is directly associated with increased levels of the ubiquitous bacterial second messenger cyclic di-GMP (cdG) in the cell. Generally, high levels of cdG have been associated with inhibition of flagella and pilus-mediated motility. On the other hand, low levels of cdG

in the cell have been linked to the promotion of motility (80–83). In *Pseudomonas aeruginosa* PAO1, cdG controls the transcription of the flagellum by interacting with the master transcriptional regulator, FleQ (84). FleQ is an enhancer binding protein, which contains a AAA σ^{54} interaction domain and a helix-turn-helix DNA binding domain. It acts as an activator of the regulatory genes *fleSR*, as well as the genes that are responsible for flagellar assembly (85). The regulation of the flagella is also under the control of FleN, the expression of which is under FleQ control. FleN is an ATPase protein containing a Walker A motif (86) which interacts with FleQ in the presence of cdG and inhibits FleQ activity leading to the activation of flagella gene expression (87).

1.5.5 Flagellum and virulence

Although the flagellum was initially regarded as an organelle responsible solely for bacterial movement, recent studies have shown that it has a number of other biological functions as well. For instance, in many bacterial species, the flagellum is a well-studied virulence factor, making the non-flagellated strains less virulent. Indeed, the flagellum is known to affect virulence several different ways (24).

Of course, the main mechanism in which flagellum affects virulence is through the facilitation of motility. Among other examples, in *Vibrio cholerae*, lack of a flagellum leads to less virulent strains with reduced absorption in mice intestines (88).

Another mechanism is through the facilitation of adhesion. The flagellum has been shown to mediate direct bacterial adhesion in enteropathogenic *E. coli*. This function is structural, and is not linked to the flagellar rotation - *E. coli* strains with inactivated FliC demonstrate significantly decreased adhesion, whereas strains having a non-functional flagellum nonetheless adhere to surfaces as efficiently as the wild type (89).

For effective plant colonisation and persistence, it is critical that bacteria adhere efficiently to the plant surfaces. To do so, they employ various surface structures such as

the fimbriae or pili, several surface proteins (90) as well as the bacterial flagellum. The expression of the genes encoding for these structures is closely integrated with the expression of the flagellum genes. Thus, bacteria can easily switch between a motile and a sessile lifestyle based on the different environmental stimuli (e.g. temperature, osmolarity, pH, etc.), which in turn alter the expression of the *flhDC* flagellar operon (91). This regulation of the flagellum genes occurs at the transcriptional level as well as the assembly level (34,91). The adherent properties of the flagellum also play a crucial role in biofilm formation. Non-flagellated mutants showed reduced adhesion compared to the wild type strain and as a result, reduced biofilm formation (89,92).

1.6 *Pseudomonas syringae*

P. syringae is closely related to *P. fluorescens*, but in contrast to the latter, is an aggressive plant pathogen with over 50 known pathovars infecting a broad range of different plant species. *P. syringae* pathovars cause plant diseases including bleeding canker, halo blight and tomato speck. *P. syringae* pv. *tomato* DC3000 (*Pto*), for instance, infects tomato plants and the model organism *Arabidopsis thaliana* (93). *P. syringae* is able to manipulate host plant cells by producing and secreting diverse phytotoxins and effector proteins. These induce a range of pathogenic phenotypes, including stomatal opening to enable bacteria access to the apoplast, chlorosis and tissue necrosis (94,95). *P. syringae* secretes and injects many of these phytotoxins and virulence factors by deploying a specialised organelle called the T3SS (96). Consequently, the T3SS plays a crucial role in *P. syringae* virulence (97).

1.7 Plant infection

Many plant pathogenic bacteria follow a traditional infectious cycle which is well-conserved among different bacterial species. This includes some well-determined stages such as the entry of the pathogen (usually through wounds on the plant tissue), establishment and multiplication in the apoplast, avoidance of the host defence mechanisms and finally the exit from the organism. Although the virulence factors differ from one organism to the other, many of the systems used during infection are remarkably conserved among different species (95).

Once a bacterium has encountered its host, the first step for a successful infection is the adhesion of the bacteria to the plant surface using specific surface proteins called adhesins. Adhesins are bacterial cell surface components, which enable bacteria to resist physical forces and enable them to attach to host cells effectively. Adhesins exhibit an increased selectivity for specific target molecules and recognise specific motifs on the

host surfaces (98). These molecules are usually located at the tip of distinct bacterial structures such as the pili or fimbriae; alternatively, they are anchored to the bacterial membrane. Following adhesion to the plant surface, bacteria migrate into the apoplast. This step is followed by the coordinated deployment of the bacterial secretion systems, which are employed to fight and avoid the host's defence mechanisms.

1.8 Secretion systems

Gram negative bacteria, including *P. fluorescens* and *P. syringae*, employ complex nano-machines for the export of virulence factors directly into host cells. These virulence factors are usually either toxins, which are critical to pathogenesis, or effector proteins. Two of the most important secretion systems, responsible for the establishment and maintenance of bacterial infections and cytotoxicity against different cell types are the Type III and Type VI secretion systems.

1.8.1 Type III secretion system (T3SS)

The T3SS is a needle-like structure that delivers bacterial effector proteins and toxins directly into the host cell in a highly regulated manner. It is well conserved both structurally and functionally among both symbiotic and Gram-negative pathogenic bacteria (99). It consists of multiple protein layers organised in the inner cytoplasmic membrane, the peptidoglycan layer and the bacterial outer membrane, as well as in the periplasmic and extracellular spaces (100,101). The T3SS is activated upon recognition of host cells, and effector proteins secreted by this system can inhibit or modify host metabolic pathways in a manner beneficial to the invading microbe (102). The gene cluster of the T3SS and the proteins it encodes resemble those involved in the assembly of the bacterial flagellum, suggesting some conserved similarities between the two systems.

The T3SS is one of the main organelles responsible for bacterial pathogenicity. Indeed, most pathogenic Gram-negative bacteria are equipped with an active T3SS, which they use for infecting plants and to facilitate multiplication in plant tissues (103). The T3SS is responsible for the translocation of effector proteins into the host cells resulting in the manipulation of the plant cellular mechanisms to the benefit of the pathogen (104–106).

T3SS are complex nanomachines anchored to bacterial membranes. They contain a pilus-like structure, which is used as a transport channel for secreting proteins and toxins (107–109). For the translocation of secreted proteins, a pore-like structure is formed on the plant cell membrane, which is called the translocon (110,111). Although the T3SS components are secreted from the cell into the space between the bacteria and the plant cell for the formation of the T3SS pilus, effector proteins are directly translocated into the host cell. This last function depends on a signal usually incorporated in the N-terminal end of the protein to be secreted. These signals usually follow a specific amino acid pattern, which is recognised by the bacterium and places them at the right location (112,113). Except for this pattern, the accurate localisation of effector proteins in the bacterial cytosol and the T3SS export gate is crucial and is catalysed by cytosolic chaperone proteins, which bind and potentially stabilise T3SS substrates, and as a result, promote the recognition of the secreted substrates by the secretion system (114–116).

1.8.1.1 T3SS Structure

The Type III secretion system is structurally characterised by the base, the needle, the inner rod, the export apparatus and the soluble cytosolic components.

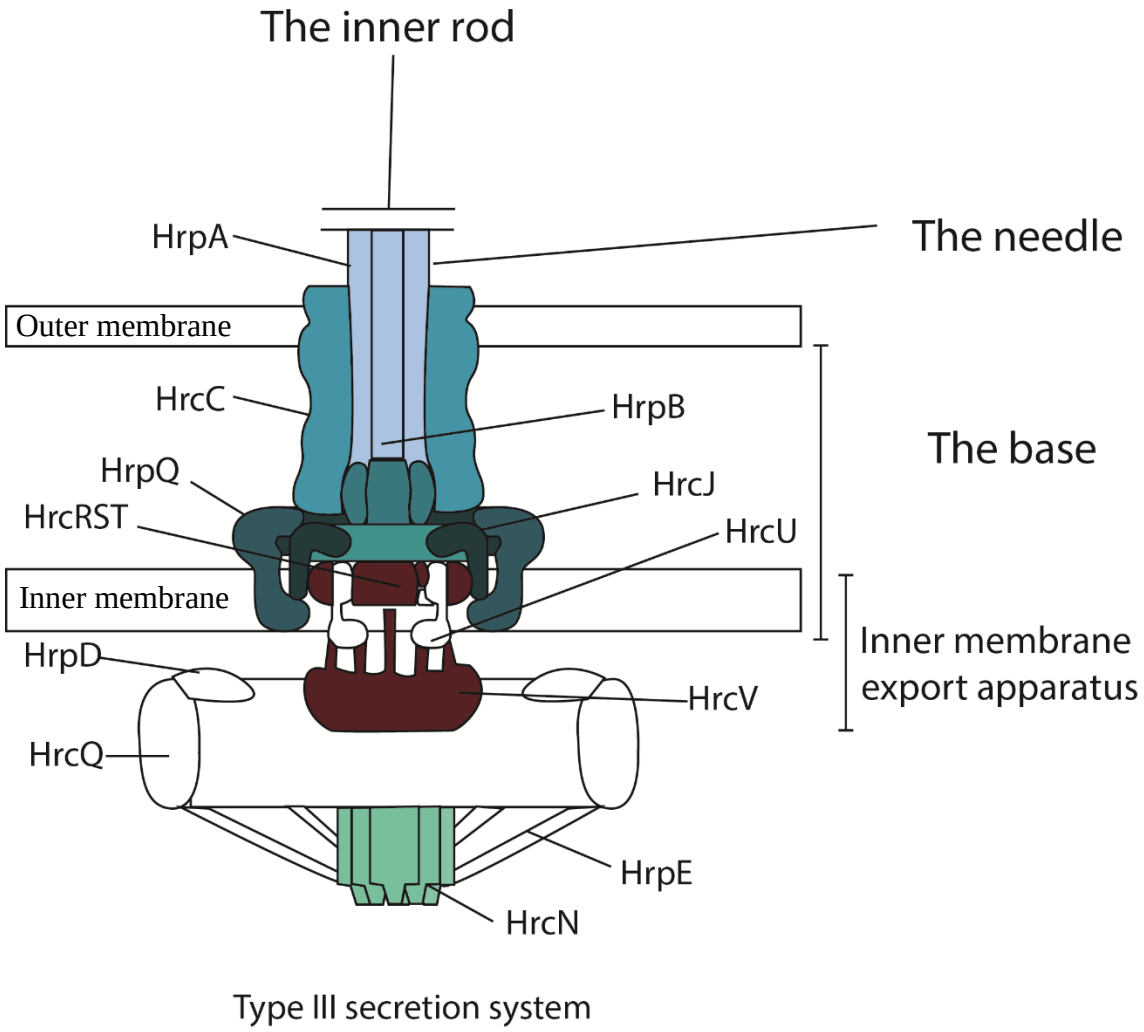

Figure 1.3: Structural representation of the type III secretion system. Figure based on (23)

1.8.1.1.1 The base

The part of the T3SS anchored to the inner membrane is called the base. It is also the first structure built in a new T3SS complex. The base consists of two inner rings and two outer rings connected by the neck (117). The inner rings are assembled from subunits of HrpQ and HrcJ, which form two concentric rings with diameters of 27 and 18 nm, respectively (118,119). The outer rings and neck are composed of the same protein; HrcC, a secretin

family protein. The neck links the inner rings with the outer rings. Once the base is completed, it acts as an export machine for the extracellular components of the T3SS (e.g. the needle).

1.8.1.1.2 The needle

The extracellular part of the T3SS is the needle. The needle is built from multiple subunits of HrpA, which are arranged in a helical fashion (120–123). It is 30 to 70 nm long in its native state with a width ranging from 10 to 13 nm. Solid-state NMR structure analysis has shown that the N-terminal domain of HrpA is orientated to the exterior of the needle in contrast to the C-terminus, which faces the lumen. The residues facing the lumen of the filament are highly conserved and polar, being positively or negatively charged, indicating that this charge distribution may be necessary for substrate transfer through the channel (124).

After the needle is built, it is either capped by a single protein, PcrV in *Pseudomonas* (125,126) or is extended to a longer structure by EspA, a trait observed in *E. coli* (127). The extension is structurally similar to the flagellum filament made by FliC and forms a helical structure more flexible than the T3SS needle filament (128).

1.8.1.1.3 The inner rod

The inner rod is the part of the T3SS that connects the needle to the base. It is built of a single protein, HrpB (129). HrpB is predicted to share similarities in structure with HrpA, with the two proteins having a similar α-helical hairpin shape surrounded by flexible regions (130).

1.8.1.1.4 Inner membrane export apparatus

The export apparatus consists of five well-conserved inner membrane proteins, which are essential for the T3SS function; HrcV, HrcR, HrcS, HrcT and HrcU (131–136). Recent

cryo-EM studies have shown that a number of these proteins are potentially located within the T3SS, facilitating the export of substrates through the inner membrane (137). It is still uncertain however if these proteins always function as a group or if they can operate individually (138).

1.8.1.1.5 Cytosolic components

There are a number of cytosolic proteins associated with the T3SS; HrpE, HrcQA, HrcQB, HrpO, HrcV and HrcN. These proteins are essential for substrate secretion and are highly conserved across all T3SSs (132,139–143). It is well reported that these proteins interact with each other, but their organisation is still poorly characterised (144–146). However, orthologs of some of these proteins exist in the better-characterised flagellum and are components of the well-defined C-ring structure, which is known to be required for altering the direction of flagellar rotation (147,148). A C-ring structure is absent in the T3SS, but there is some preliminary evidence that these proteins may cluster to form a complex, which associates with the main export apparatus (144).

HrcN one of the cytosolic proteins related to the T3SS base, and is a highly conserved ATPase with profound structural similarities to both FliI and the F_0F_1 ATPases (139,141). It forms a hexameric ring at the base of the export apparatus located at the bacterial inner membrane and provides the initial energy required for the secretion process (149–151) . In the human pathogen *Salmonella enterica*, it has been shown that ATP hydrolysis by HrcN is essential for the disassociation of effector proteins from their chaperones, with the chaperone-effector complexes shown to interact with the HrcN complex (70,74,152,153). It has also been suggested that HrcN may have an active role in the unfolding of effectors before they are loaded into the injectisome (70,154,155). In contrast to this, it has also been reported that HrcN is not required for the translocation of T3SS-associated proteins, as animal pathogenic bacteria are still virulent in the absence of a

functional ATPase (68,69). In conclusion, based on the latest studies on HrcN, the ATPase is responsible for the effective docking of effector proteins to the T3SS export gate, whereas the export of these proteins is potentially dependent on PMF (68–70,153),(156).

1.8.1.2 T3SS function

For the effective function of the T3SS, an activating signal is essential. Some studies have provided evidence that this signal may come from direct contact of the bacterial cell with the host cell (117), (157,158). It is possible that this mechanism exists to ensure that the secreted proteins will be delivered directly to the host cells and not the extracellular space. The way the bacterial cell senses the interaction is still poorly understood, but some initial evidence suggests that the tip complex proteins may be involved in the recognition process (109). Experiments with potential tip interacting compounds (e.g. Congo red, bile salts) have shown that the T3SS secretion can be activated even without a host cell present. The reason for this may be potential conformational changes on the tip of the needle, which mimic the contact with the host cell (159–163).

The signal that is presumably sensed by the tip of the needle is then transduced to the remaining components of the secretion machine. This process is potentially mediated by conformation changes in the protein components of the needle and the inner rod (109). In support of this, previous studies have identified mutations in the needle and inner rod protein domains that result in altered secretion patterns (164–167). Following the activation of the system, the next step is the deployment of translocase proteins, which will open the passage for effector protein translocation (168). As a result, the translocases are thought to interact with the T3SS prior to the effectors. Indeed, even prior to activation, the only proteins found to interact with the cytosolic components of the system are the translocases, and only in their absence can effector proteins be detected (144).

1.8.1.3 Effector proteins

Bacterial pathogenicity depends on the ability of bacteria to infect plants and to be able to survive inside the plant tissue. To achieve this, they secrete toxins and toxic protein factors (e.g. degradative enzymes), as well as effector proteins that manipulate cell behaviour, directly into the host cells (169). Effectors are proteins secreted by bacteria using the T3SS in a highly controlled manner, enabling them to effectively manipulate host components either structurally or functionally. Plant pathogenic bacteria are known to possess a large number of diverse effector proteins. For instance, the *P. syringae* genome sequence revealed that strains in this species are each equipped with up to 39 effectors (170,171). Deletion of individual effector genes usually produces little or no effect on bacterial virulence, indicating that pathogenicity is a bacterial behaviour orchestrated by complex and redundant mechanisms. In *P. syringae pv. tomato*, the deletion of 18 different effector genes, which are part of six genomic clusters, are required to produce an effect on bacterial growth *in planta* (172), whereas a minimum of 8 effectors is needed for the effective suppression of plant resistance mechanisms and to promote bacterial virulence (173,174). Recent studies have shown that effector proteins in animal pathogens are potentially secreted at different time points to achieve the maximum output (76,175–177). For many years, studies have focused on the characterisation of effector proteins and their targets in the plant cells, revealing roles of effector proteins in the manipulation of signal transduction, protein degradation, phytohormone signalling, pathogen-associated molecular pattern (PAMP)-triggered immunity and plant gene expression among others (169).

1.8.1.4 T3SS regulation

The expression of the T3SS in *P. syringae* is induced when the bacterium enters the apoplastic plant space. This induction is triggered by HrpR and HrpS, two NtrC-family

transcriptional regulators, which interact with each other (178). These two regulators induce the expression of HrpL, an alternative sigma factor binding to the conserved elements of the T3SS promoter regions (179). This positive regulation is inhibited by HrpV, a negative regulator, which potentially acts upstream of HrpL and interacts with HrpS (180,181). HrpV activity is suppressed by HrpG, a potential T3SS chaperone. The activation of the T3SS potentially triggers the release of HrpG from its interaction substrate, leading to the interaction with HrpV, and thus inhibiting the negative regulation promoted by the latest protein (181). Another player in the control of T3SS expression is the Lon protein, an ATP- dependent serine protease, the role of which is to degrade misfolded or unstable protein substrates. In this way, Lon contributes to the correct function of the T3SS (182,183). Lon also acts as a negative regulator of T3SS function by degrading HrpR (178,184–186). Although the Lon protease is able to degrade effectors, these are protected by its proteolytic activity when they are bound to their chaperones (187), (108).

1.8.2 Type VI secretion systems (T6SS)

The Type VI secretion system (T6SS) is one of the main export systems in bacteria, and more specifically is characteristic of Gram-negative proteobacteria, both pathogenic and commensal (188). Although the T6SS is more common in pathogens, there are also several nitrogen-fixing bacteria and rhizobia that have a functional T6SS (189). Pathogenic bacteria employing a T6SS usually pose a high threat to human health, having representatives in highly pathogenic categories (e.g. *Salmonella typhi*, the enteropathogenic *E. coli*, *Yersinia pestis,* etc.) (189).

Genetically, the T6SS regulon comprises of 15-25 genes, which were originally identified by their importance in the secretion of virulence factors (190–193). Some of these gene products are secreted as virulence factors, and others are thought to be either structural

components of the machinery or chaperones assisting with the translocation of the system components (194,195). One of these components, which is present in most T6SS clusters is the hexameric AAA+ ATPase, which is known to hydrolyse ATP to assist with the transportation of the proteins through the export system (196). For instance, in *P. aeruginosa* ClpV1 has been shown to act as an energy source for the secretory apparatus (192).

1.9 Cyclic-di-GMP

Bis- (3'-5') cyclic guanosine monophosphate or cyclic-di-GMP (cdG) is a ubiquitous second messenger, which is very widespread among different bacterial species. It was initially discovered from studies in *Gluconacetobacter xylinus* that identified its role in the regulation of cellulose biosynthesis (197). Today, we know that cdG is a soluble molecule associated with signal transduction networks in most bacterial species, where it functions as a second messenger. Second messengers transfer an environmental signal from the cell surface to the interior of the cell, after amplifying and converting it into a

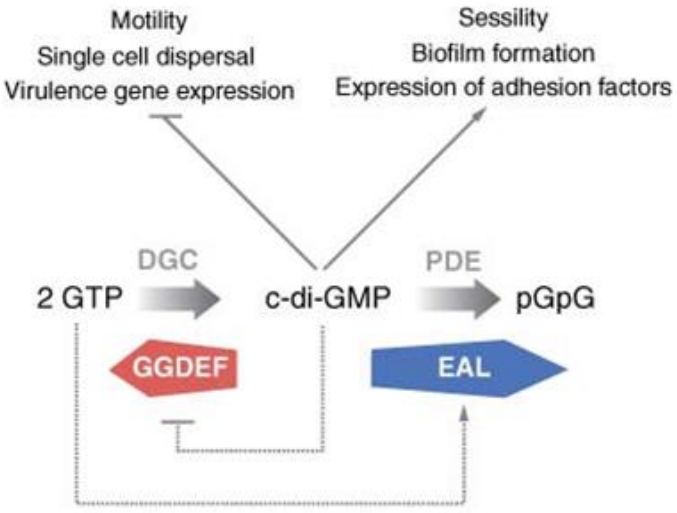

Figure 1.4: c-di-GMP metabolism in the bacterial cell, GGDEF domains synthesise c-di-GMP and EAL domains degrade it. Figure originally published by Urs Jenal and Jacob Malone in Annual Reviews (203).

biochemical response, and can have an enormous impact on the biological processes of the cell (198).

1.9.1 Metabolism

CdG is synthesised by two guanosine-5'-triphosphate (GTP) molecules in a reaction catalysed by diguanylate cyclases (DGCs) and is catabolised into 5’-phosphoguanylyl-

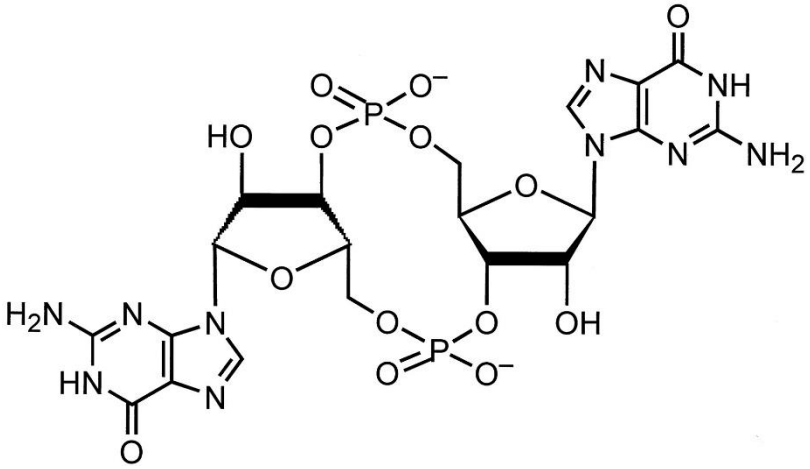

Figure 1.5: Structural representation of cyclic di-GMP.

(3’-5’)-guanosine (pGpG) by specific phosphodiesterases (PDEs) (199). The huge importance of this molecule became apparent after the advent of widespread whole genome sequencing when it was found that over 80% of bacterial genomes encode multiple cdG metabolic enzymes (200). These enzymes have conserved GGDEF and EAL domains, which were linked to cdG metabolism in a final contribution by the pioneering Benziman lab (201). In *P. fluorescens* Pf-01, 43 proteins containing GGDEF and EAL domains have been found (202), and other *P. fluorescens* genomes encode similar numbers of these enzymes. It was found that overexpression of genes containing the above domains modulates the intracellular levels of cdG, leading to the expression of different phenotypes. These include biofilm formation and cessation of motility when the GGDEF domain is overexpressed and a switch to a motile phenotype when an EAL domain is overexpressed (203). A minimal functional model which best describes cdG regulation comprises a DGC and a PDE, which synthesise and degrade cdG respectively,

an effector component which interacts with the cdG molecule, and its downstream phenotypic target. This whole system is controlled by alterations in the cellular cdG concentration (199). It regulates transcription and post-transcriptional procedures as well as allosterically controlling protein function. On the level of the microbial population, cdG action has been shown to lead to biofilm formation, secondary metabolite production and the switch between a planktonic state to a sessile state of living. Finally, cdG can also regulate the production of bacterial virulence factors (204). EAL and GGDEF domains are commonly located in multi-domain proteins and co-exist with other signalling domains commonly found in bacteria, suggesting a complex system of environmental regulation of PDE and DGC activity (205)(206,207). Common cdG-associated sensory domains include but are not limited to the following: REC, PAS, HAMP, BLUF and GAF, etc., and are responsible for sensing environmental stimuli such as light, oxygen availability, redox potential, nutrients, osmolarity, population density and other stimuli (208). The high number of different proteins, each with its own characteristic domains, reveals the complexity of the cdG regulatory network (209).

1.9.2 Importance to Pseudomonas plant associations

CdG plays a crucial role in many aspects of the bacterial lifestyle. For instance, it has been associated with the switch between a motile and a sessile way of living, i.e. biofilm formation. Biofilm formation has been shown to be essential for efficient plant root colonisation and as a consequence plays a major role in the successful establishment of a beneficial relationship between plants and bacteria (210). In *P. aeruginosa,* cdG has been shown to regulate biofilm formation via FleQ, a transcriptional regulator, which upon binding to cdG, activates the expression of biofilm-related genes such as the Pel and Psl exopolysaccharides operons. What is more, FleQ is known to repress the flagellar gene expression upon the interaction with cdG. As described previously, the flagellum is also

known to facilitate adhesion to surfaces and as a result to enhance biofilm formation (84,211).

Additionally, cdG has been linked to surface attachment in *Pseudomonas fluorescens* SBW25. More specifically cdG has been associated with the Wsp pathway, which is responsible for the aggregative, hyper-adherent wrinkly spreader phenotype (212). This phenotype is a result of the overproduction of a cellulosic polymer, a product of the *wss* operon, which is in turn regulated by the Wsp chemosensory pathway and WspR, a CheY-GGDEF like protein involved in cdG metabolism. CdG regulation of the system leads to cellulose expression and attachment enabling more efficient surface colonisation (213), (214).

To investigate further the role of cdG networks and rhizosphere colonisation Silby et al. have identified seven cdG-related genes, by In Vivo Expression Technology (IVET) analysis, which are upregulated in the sugar beet rhizosphere environment (215).

Further studies were carried out to identify genes and pathways related to swimming motility repression in *Pseudomonas fluorescens* F113. As part of the work of different labs, SadB was originally identified as a protein related to surface adhesion, which acts at the beginning of biofilm formation and represses swarming motility by rhamnolipid sensing (216,217). The linkage between SadB and cdG is yet unknown and remains to be identified. The Gac system is another system implicated in the repression of swimming motility in *P. fluorescens* F113. GacA/GacS is a two-component system which regulates the production of secondary metabolites and secreted proteins, like exoprotease and cyanide, through repression of the post-translational regulator RsmA (218,219). Recent studies have shown that the Gac system is also related to repression of motility and biofilm formation (217), and controls/is controlled by cdG signalling proteins (220–222).

1.9.3 Binding

The molecules that recognise and bind c-di-GMP, and trigger a downstream cellular response are called effectors and include both proteins and RNA molecules. Effectors differ widely from one another in both structure and function and are characterised by the different affinities with which they bind cdG. Previous studies have revealed various cdG targets. Currently, known cdG effectors and binding targets include PilZ domain proteins, diverse transcription factors, HD-GYP domain proteins, RNA riboswitches and even inactive GGDEF and EAL domain proteins (223–225). Through these effectors, cdG exerts its role and regulates processes at the transcriptional, post-transcriptional and post-translational levels (200).

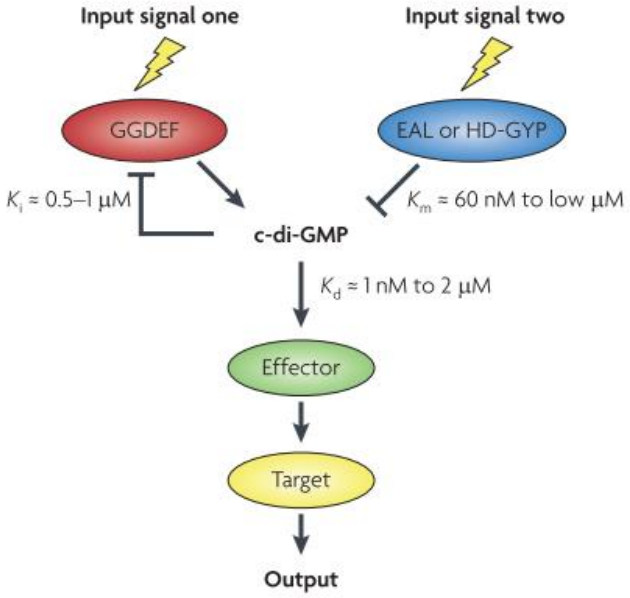

Figure 1.6: Representation of the characteristic c-di-GMP signalling model(3). Reprinted by permission from Macmillan Publishers Ltd: [Nature publishing group] (199), copyright (2009).

In the first cdG regulatory circuit identified, cellulose biosynthesis in the alpha-proteobacterium *Acetobacter xylinum* (197), cdG was shown to bind to BcsA, a 90-kDa PilZ-domain protein, involved in cellulose synthesis complex (226,227). Although it was initially thought that BcsA was the sole cdG target, subsequent studies showed that this

was not the case. This realisation, together with advances in genome sequencing technologies, revealed complex cdG signalling networks of GGDEF and EAL/ HD-GYP domain proteins in many different organisms, including several not known for cellulose synthesis (205,228). This indicated that cdG was likely to regulate other biological processes, and implying the existence of additional receptor proteins.

The perception for a number of years was that cdG should have a single characteristic binding protein or domain, resembling the well-understood cAMP binding protein CAP or CRP (200,229), which at the time was the only known cAMP binder. However, subsequent biochemical analyses have shown that nothing could be further from the case.

1.9.3.1 PilZ domain proteins

Further studies led to the identification of PilZ (230) a one-hundred amino acid protein domain first confirmed to bind cdG in *Pseudomonas aeruginosa* (230). To date, various examples of cdG based regulation via proteins containing PilZ domains have been identified. For instance, in *E. coli*, cdG interacts allosterically with the PilZ domain protein YcgR, resulting in a conformational change of the protein, enabling it to bind to and inhibit the rotation of the bacterium flagellum (231). In *P. aeruginosa*, cdG binding to the PilZ-domain protein Alg44 is suggested to regulate alginate production (232), while *P. fluorescens* contains five known proteins containing PilZ domains. PilZ domain proteins are well-characterised cdG effectors, and are widespread in bacterial species (233). However, although PilZ domain proteins as a family are known to bind cdG, they display significant diversity in cdG binding modes, quaternary structures and stoichiometries. In addition, some PilZ domain proteins do not bind to cdG, further complicating the picture.

1.9.3.2 Degenerate GGDEF/ EAL domain proteins

Another well-known category of cdG effectors are proteins containing either degenerate GGDEF or EAL domains. Whereas early studies on these domains focussed on their role in the synthesis and degradation of cdG, nowadays it is known that these domains not only metabolise cdG but that they also recognise it as a messenger, triggering in this way complex cellular and biochemical processes. In addition to the catalytic active site (A-site), GGDEF domains also have an allosteric inhibitory site (I site) which can bind c-di-GMP (234). LapD from *Pseudomonas fluorescens* is a well-studied example of the alternative role of these domains. LapD, despite containing both GGDEF and EAL domains, does not show any *in vitro* enzymatic activity but instead it acts as a receptor of cdG. CdG recognition by LapD leads to the maintenance of the outer membrane adhesin LapA on the surface of the cell (208,235). Other degenerate GGDEF/EAL domain proteins that bind cdG include PopA in *Caulobacter crescentus* (236), PelD in Pseudomonas, that controls exopolysaccharide production and Fim, which is involved in the regulation of pili function (237).

1.9.3.3 Binding diversity

Although the protein categories described above represent well-known cdG targets, in recent years more and more unconventional cdG binding proteins have been identified, some of them containing completely novel binding clusters. For instance, cdG has been recently strongly associated with transcriptional regulation by the identification of DNA-binding proteins as cdG targets. Some of these include VpsT, BldD, FleQ/ FlrA, VpsR, EpsI, LtmA, Bcam1349, MrkH (87,238–246). Several of these proteins employ novel ways of interacting with cdG. For example, in the case of MrkH, DNA binding combines a previously unknown type of DNA-binding domain with a cdG-binding PilZ domain (241). In the case of BldD, binding occurs at the interface between two subunits of the

protein, which are linked to a tetrameric cdG cluster in a novel binding site that contains no subunit-subunit interactions at all (238). Except for the transcriptional regulators, other proteins, in diverse categories, have recently been identified as cdG binding proteins. For instance, PgaC/D (247), a membrane-spanning poly-glcNAc synthase was shown to bind cdG, as well as the kinase/phosphatase CckA (248).

The discovery of these novel cdG binding mechanisms indicates the possibility that more cdG receptors exist and remain to be identified. In most cases, their prediction through bioinformatics approaches is not possible, as cdG binding requires a little more than three strategically placed glutamate/arginine residues (229). Identifying binding proteins generally requires more sophisticated lab techniques such as pull-down experiments and extensive binding tests (249).

In conclusion, our understanding of the cellular targets of cdG binding is far from complete. The discovery of novel, exciting targets is needed in order to understand further the mechanisms underpinning cdG metabolism and the processes controlled by this molecule in the cell.

Chapter 2:

Materials and methods

Chapter 2: Materials and methods

2.1 Materials

2.1.1 Antibiotics, enzymes and reagents

Antibiotics (Sigma) were used at the following concentrations: ampicillin and carbenicillin at 100 μg ml^{-1}, kanamycin at 50 μg ml^{-1}, and tetracycline at 12.5 μg ml^{-1} (in 80% ethanol). For inducible plasmids, isopropyl β-d-thiogalactopyranoside (IPTG) was added to a final concentration 0.5 mM-1 mM as appropriate. Digestions were performed with restriction enzymes (New England BioLabs), at 37°C for 2 hours unless otherwise stated. Ligations were performed O/N at 16ºC with T4 ligase (New England Biolabs) according to the manufacturer's instructions. Polymerase chain reactions (PCR) were carried out with Taq (New England BioLabs) and Phusion (New England BioLabs) enzymes according to the manufacturer instructions.

2.1.2 Media and Growth Conditions

Bacteria were cultured in Luria-Bertani (LB) medium (10 g NaCl, 10 g tryptone, 5 g yeast extract), King's B (KB) medium (10 g glycerol, 20 g Protease Peptone No.3, from BD, 1.5 g $K_2HPO_4.3H_2O$, 1.5 g $Mg_2SO_4.7H_2O$ L-1) and M9 minimal medium supplemented with 0.4% pyruvate as a carbon source [10 ml M9 salts (10x), 200 μl $MgSO_4$ (1M), 200 μl $CaCl_2$ (50mM), 2 ml pyruvate (20%) in 100 ml final volume]. Where appropriate, agar was added to a final concentration 1.5%. Bacteria were grown O/N in the appropriate medium at 37ºC for *E. coli* and 28ºC for *P. fluorescens* under shaking conditions. For protein overexpression, Terrific broth (Deionized H2O to 900 mL, 12 g tryptone, 24 g yeast extract, 4 ml glycerol, 100 mL of a sterile solution of 0.17 M KH_2PO_4, 0.72 M

K_2HPO_4) was used. The overexpressions were carried out at 18^oC O/N, under shaking conditions.

2.1.3 Strains and Plasmids

All the strains and plasmids used in this study are listed in Table 2.1. Primers are listed in Table 2.2.

Table 2.1: Strains and plasmids

Strains	Description	Reference
E. coli BL21-(DE3)	*SmR, K12 recF143 lacIq lacZΔ.M15, xylA*	Novagen
E. coli DH5α	*endA1, hsdR17(rK-mK+), supE44, recA1, gyrA (NalR), relA1, Δ(lacIZYA-argF) U169, deoR, Φ80dlacΔ(lacZ)M15*	(250)
SBW25	Environmental *P. fluorescens* isolate	(251)
Pto DC3000	Rif^R derivative of *P. syringae* pv. *tomato* NCPPB 1106	(252)
Salmonella enterica pv. *typhimurium*	Strain LT2	(253)
Sinorhizobium meliloti	Strain 1020	(254)
Plasmids		
pETNdeM-11	*Km^R, purification vector, N-terminal His6-tag*	(255)
pQLinkG2	*Amp^R purification vector, N-terminal GST tag*	(256)
pTYB12	*Amp^R purification vector, Intein tag*	(257,258)
pET42b	*Km^R, purification vector, C-terminal His6-tag*	Novagen
pME6032/ *wspR19*	*Tet^R, overexpression vector*	Malone lab unpublished
pET42b/ *PFLU4401*	*For the overexpression of PFLU_4401*	This study
pET42b/ *PFLU6126*	*For the overexpression of PFLU _6126*	This study
pET42b/ *PFLU0463*	*For the overexpression of PFLU_0463*	This study
pET42b/ *PFLU4320*	*For the overexpression of PFLU 4320*	This study
pET42b/ *PFLU4414*	*For the overexpression of PFLU 4414*	This study
pET42b/ *PFLU4531*	*For the overexpression of PFLU_4531*	This study
pTYB12/ *PFLU1582*	*For the overexpression of PFLU_1582*	This study
pTYB12/ *PFLU4531*	*For the overexpression of PFLU_4531*	This study
pTYB12/ *PFLU4622*	*For the overexpression of PFLU_4622*	This study

pETNdeM-11/ *PFLU*0001	*For the overexpression of PFLU_0001 (DnaA)*	This study
pETNdeM-11/ *PFLU3809*	*For the overexpression of PFLU_3809*	This study
pETNdeM-11/ *PFLU4732*	*For the overexpression of PFLU_4732*	This study
pETNdeM-11/ *PFLU4436*	*For the overexpression of PFLU_4436 (FliI)*	This study
pETNdeM-11/ *PFLU4436*/ Δ1-18	*For the overexpression of PFLU_4436 (FliI) truncated version Δ1-18,*	This study
pETNdeM-11/ *PFLU4436*/ G176A	*For the overexpression of PFLU_4436 (FliI) with a point mutation at G176A*	This study
pETNdeM-11/ *PFLU4436*/ K181A	*For the overexpression of PFLU_4436 (FliI) with a point mutation at K181A*	This study
pETNdeM-11/ *PFLU4436*/ S182A	*For the overexpression of PFLU_4436 (FliI) with a point mutation at S182A*	This study
pETNdeM-11/ *PFLU4436*/ D265A	*For the overexpression of PFLU_4436 (FliI) with a point mutation at D265A*	This study
pETNdeM-11/ *PFLU4436*/ R170H	*For the overexpression of PFLU_4436 (FliI) with a point mutation at R170H*	This study
pETNdeM-11/ *PFLU4436*/ E208Q	*For the overexpression of PFLU_4436 (FliI) with a point mutation at E208Q*	This study
pETNdeM-11/ *PFLU4436*/ R337H	*For the overexpression of PFLU_4436 (FliI) with a point mutation at R337H*	This study
pETNdeM-11/ *PFLU4895*	*For the overexpression of PFLU_4895*	This study
pETNdeM-11/ *PFLU4437*	*For the overexpression of PFLU_4437(FliH),*	This study
pETNdeM-11/ *PFLU0343*	*For the overexpression of PFLU_0343 (NtrC),*	This study
pETNdeM-11/ *PSPTO1400*	*For the overexpression of PSPTO_1400 (HrcN),*	This study
pETNdeM-11/ *PSPTO1400*/ K181A	*For the overexpression of PSPTO_1400 (HrcN)*	This study
pETNdeM-11/ *PSPTO1400*/ S182A	*For the overexpression of PSPTO_1400 (HrcN) with a point mutation at S182A*	This study
pETNdeM-11/ *PSPTO1400*/ D265A	*For the overexpression of PSPTO_1400 (HrcN) with a point mutation at D265A*	This study
pETNdeM-11/ *PSPTO1961*	*For the overexpression of PSPTO_1961 (FliI from P. syringae)*	This study
pETNdeM-11/ *STY2180*	*For the overexpression of STY_2180 (FliI from S. typhimurium)*	This study
pETNdeM-11/ *SMC03025*	*For the overexpression of SMC_03025 (FliI from S. meliloti)*	This study
pETNdeM-11/ *PFLU6025*	*For the overexpression of PFLU_6025 (ClpB2),*	This study
pETNdeM-11/ *PSPTO1960*	*For the overexpression of PSPTO_1960 (FliH from P. syringae)*	This study

pQlinkG2/ *PSPTO1960*	*For the overexpression of PSPTO_1960 (FliH from P. syringae)*	This study
pQlinkG2/ *PSPTO1961*	*For the overexpression of PSPTO_1961 (FliI from P. syringae)*	This study

2.1.4 Oligonucleotides

Oligonucleotides were ordered and synthesised by Sigma. They were stored at -20 °C in deionised water at a final concentration 100 μM. They were diluted at 10 μM to be used at a final concentration of 0.2 μM in PCR reactions. The primers used in this study are enlisted in the following table:

Table 2.2: Primers and expression vectors

Gene target	Description	Sequence
PFLU0001	DnaA Forward	CATTAATCATATGTCAGTGGAACTTTGGC
PFLU0001	DnaA Reverse	CTATCTCGAGCGTTGTCAGTGTACGC
PFLU4401	PFLU4401 Forward	CTTAATTCATATGGCCGGCATTCTCGACAC
PFLU4401	PFLU4401 Reverse	TAAGCTCGAGGGCGGGCACTTCGTC
PFLU4401	PFLU4401 XhoI site-directed mutagenesis Forward	GCGTGAAAAACTAGAGGACCCGGTCC
PFLU4401	PFLU4401 XhoI site-directed mutagenesis Reverse	GGACCGGGTCCTCTAGTTTTTCACGC
PFLU6126	PFLU6126 Forward	CATTAATCATATGGCCGTCAAGAAACGAG
PFLU6126	PFLU6126 Reverse	CTATCTCGAGGCGGATGTGAGCAAG
PFLU6126	PFLU6126 XhoI Site-directed mutagenesis Forward	ATCGCACGTCTAGAGCAGCGCCTG
PFLU6126	PFLU6126 XhoI Site-directed mutagenesis Reverse	CAGGCGCTGCTCTAGACGTGCGAT
PFLU0463	PFLU0463 Forward	CATTAATCATATGCGCGTACTGGTAATC
PFLU0463	PFLU0463 Reverse	CTATCTCGAGGTGCAGCTCCTCAGC
PFLU4320	PFLU4320 Forward	CATTAATCATATGTGCGGATTAGCTGGAG
PFLU4320	PFLU4320 Reverse	CTATCTCGAGGATTCCTTGTTCGCTG
PFLU4531	PFLU4531 Forward	GTTTAACTTTAAGAAGGAGATATACATATGAAAGCGCCCCGCGTTACCCT
PFLU4531	PFLU4531 Reverse	GTGGTGGTGGTGGTGGTGGTGCTCGAGGGCCTGCCGGGGCGCGGCGA
PFLU1582	PFLU1582 Forward	TTACATCATATGAGCGAACACGAGCGCG

PFLU1582	PFLU1582 Reverse	AGATTGAATTCTCAGCGCATTTTCAAG
PFLU4531	PFLU4531 Site directed mutagenesis, NdeI site Forward	TCGCCCACCACATGGAGCAGGGC
PFLU4531	PFLU4531 Site-directed mutagenesis, NdeI site, Reverse	GCCCTGCTCCATGTGGTGGGCGA
PFLU4531	PFLU4531 Forward	TTACATCATATGAAAGCGCCCCGCGTTAC
PFLU4531	PFLU4531 Reverse	AGATTGAATTCTCAGGCCTGCCGGGGC
PFLU4622	PFLU4622 Forward	TTACATCATATGGCTGTCAAAACAAATA
PFLU4622	PFLU4622 Reverse	AGATTGAATTCTTACAGGTGGAAGCG
PFLU3809	PFLU3809 Forward	TTACTTCATATGCCCACCCGCTCGAAGATC
PFLU3809	PFLU3809 Reverse	AGATTGAATTCTTACTTCAACTTGGCAATCGCCG
PFLU4732	PFLU4732 Forward	TTACTTCATATGTCTACGGGTAATTTGGA
PFLU4732	PFLU4732 Reverse	AGATTGAATTCTTACTTGGCCTGGTAAATG
PFLU4436	PFLU4436 Forward	TTACTTCATATGCGCCTTGATCGCACCAG
PFLU4436	PFLU4436 Reverse	ATATTCAATTGTTAGCCGCCCGGCGCG
PFLU4436	PFLU4436 G176A Forward	CCTGTTCGCCGCTACCGGCGTGG
PFLU4436	PFLU4436 G176A Reverse	CCACGCCGGTAGCGGCGAACAGG
PFLU4436	PFLU4436 K181A Forward	CGGCGTGGGTGCGTCGGTGTTGC
PFLU4436	PFLU4436 K181A Reverse	GCAACACCGACGCACCCACGCCG
PFLU4436	PFLU4436 S182A Forward	CGTGGGTAAGGCGGTGTTGCT
PFLU4436	PFLU4436 S182A Reverse	AGCAACACCGCCTTACCCACG
PFLU4436	PFLU4436 D265A Forward	GTTGCTGATGGCCTCGCTCACGC
PFLU4436	PFLU4436 D265A Reverse	GCGTGAGCGAGGCCATCAGCAAC
PFLU4436	PFLU4436 R170H Forward	CGCGGCCAGCATCTGGGCCTG
PFLU4436	PFLU4436 R170H Reverse	CAGGCCCAGATGCTGGCCGCG
PFLU4436	PFLU4436 E208Q Forward	CGGGGCCGTCAGGTGAAGGAA

PFLU4436	PFLU4436 E208Q Reverse	TTCCTTCACCTGACGGCCCCG
PFLU4436	PFLU4436 R337H Forward	GACTCGGCGCATGGCGTGCTC
PFLU4436	PFLU4436 R337H Reverse	GAGCACGCCATGCGCCGAGTC
PFLU4895	PFLU4895 Forward	TTACTTCATATGCGTATCCACGTCAGT
PFLU4895	PFLU4895 Reverse	AGATTGAATTCTCAGGGCTTGTTGGAG
PFLU4437	PFLU4437 (FliH) Forward	TTACTTCATATGTCGAACAAAGATGAG
PFLU4437	PFLU4437 (FliH) Reverse	AATCTGAATTCTCAAGGCGCATCGGG
PFLU4436	FliI Δ1-18 Forward	TTACTTCATATGACATCGTTGCCCGGCCAG
PFLU0343	NtrC Forward	TTACTTCATATGAGCCGTAGTGAAACCG
PFLU0343	NtrC Reverse	AATATCAATTGTCAGCCTTCATCGC
PSPTO1400	HrcN Forward	TTACTTCATATGAACGCCGCACTGAACCAG
PSPTO1400	HrcN Reverse	AATATGAATTCTTACTCCGGCAGTTGCGAG
PSPTO1961	Pto DC3000 *fliI* Forward	TTACTTCATATGCGCCTTGATCGCGTGAG
PSPTO1961	Pto DC3000 *fliI* Rev	AATATCAATTGTCAGCCGCCAGGGG
STY2180	S. typhimurium *fliI* Forward	TTACTTCATATGACCACGCGCCTGACC
STY2180	S. typhimurium *fliI* Rev	AATTGAGAATTCTCACACCGTCGGGAAAAT
SMc03025	S. meliloti *fliI* Forward	TTACTTCATATGGCACGCGAAGCCGCTG
SMc03026	S. meliloti *fliI* Rev	AATATCAATTGTCATCCCCTTCCGCGCA
PFLU6025	SBW25 *clpB2* Forward	TTACTTCATATGGGTGAAATCAGTCGC
PFLU6025	SBW25 *clpB2* Rev	AATATCAATTGTCAATCTGCGTCGC
PSPTO1400	HrcN K181A Forward	CGGTTGCGGCGCGACCACGCTGA
PSPTO1400	HrcN K181A Reverse	TCAGCGTGGTCGCGCCGCAACCG
PSPTO1400	HrcN S182A Forward	GCGGCAAGGCCACGCTGATG
PSPTO1400	HrcN S182A Reverse	CATCAGCGTGGCCTTGCCGC
PSPTO1400	HrcN D265A Forward	GCTGCTGCTCGCCTCCCTGACCC
PSPTO1400	HrcN D265A Reverse	GGGTCAGGGAGGCGAGCAGCAGC
PSPTO1960	FliH Pto His Forward	TTACTTCATATGTCCAGTTCCAATAAAG
PSPTO1960	FliH Pto His Reverse	AATATCAATTGTCAAGGCGCATCGAGAG
PSPTO1960	FliH Pto GST Forward	AATCGAGGATCCATGTCCAGTTCCAAT

PSPTO1960	FliH Pto GST Reverse	TCGATTGCGGCCGCTCAAGGCGCATCGAG
PSPTO1961	FliI Pto GST Forward	AATCGAGGATCCATGCGCCTTGATCGCGTGAG
PSPTO1961	FliI Pto GST Reverse	TCGATTGCGGCCGCTCAGCCGCCAGGGGCCGG

2.2 Methods

2.2.1 Molecular Biology Procedures

Cloning was performed according to standard molecular biology techniques. Purification/ overexpression vectors based on pET42b were produced by ligating PCR fragments between the NdeI and XhoI sites as appropriate. pETNdeM-11 backbone were generated by ligating PCR fragments between the NdeI and EcoRI sites of plasmid pETNdeM-11 (255) as necessary. pQLinkG2-based (Addgene plasmid #13671) overexpression and purification vectors were produced by ligating PCR fragments between the *BamH* I and *Not* I restriction sites (256). pTYB12 was used for the Intein Mediated Purification using an Affinity Chitin-binding Tag (New England Biolabs, IMPACT^{TM} kit, N6902S) based on the manufacturer's instructions (257,258). Overexpression vectors based on pTYB12 were produced by ligating PCR fragments between NdeI and EcoRI sites as appropriate. Site-directed mutagenesis by overlap extension (259) was used to generate the ATPase active site (Walker A and B motifs) and the binding site mutations in both FliI and HrcN using the appropriate primers (Table 2.2). The constructs were then cloned into the appropriate overexpression vectors (Table 2.1).

2.2.1.1 PCR

Polymerase chain reaction was carried out in an ARKTIK thermal cycler (Thermo Fisher Scientific). A standard 50 µl reaction contained: 10 µl dNTPs (2 mM), 5 µl polymerase buffer (10x), 0.5 µl Taq polymerase or 0.5 µl Phusion polymerase, 2.5 µl of each primer (10 µM), 1 µl DNA template, made up to 50 µl with deionised water. The standard protocol followed was based on the polymerase manufacturer's instructions. Based on that, the initial denaturation of the DNA template was carried out in a single step for 3 min at 95°C. For the amplification of the product of interest, 25 cycles of denaturation for

30 sec at 95°C were performed, followed by annealing for 30 sec at the appropriate temperature (56°C – 62°C depending on the primer melting temperature, Tm) and strand extension for 1-2 minutes at 72°C for 30 sec. A 5-minute extension step at 72°C was included before the sample was kept at 4°C.

2.2.1.2 q-RT PCR

For the RNA extractions, 100ml of LB were inoculated with the strains of interest and were grown O/N at 37ºC. For the overproduction of cdG in some of the strains, WspR, a cyclase was overexpressed in pME6032 vector by adding 0.5mM IPTG to the cultures when they reached an OD of 0.5-0.8 and growing them O/N at 37ºC. The cells were harvested by centrifugation and the RNA isolations were carried out using the RNeasy Mini kit by Qiagen according to the manufacturer's instructions. For the cDNA generation, the QuantiTect Reverse Transcription Kit was used, following a two-step approach. The first step towards the cDNA synthesis was the elimination of the genomic DNA from the RNA samples. For that, 500 ng of RNA were used and incubated for 2 minutes at 42ºC with the gDNA Wipeout buffer included in the kit. For the second step of the reaction, the reverse transcription mix (Quantiscript Reverse Transcriptase, RNase inhibitors, RT buffer, RT primer mix) was added to each reaction, and it was followed by 15 minutes' incubation at 42ºC and then at 95ºC for 3 minutes for the inactivation of the reverse transcriptase. The cDNA concentrations were quantified by Nanodrop, and they were normalised accordingly. For the qPCR step, the Bioline SensiFAST SYBR No-ROX Kit (#98005) was used. 50 μl final volume reactions were used with 100 ng cDNA, 250nM of the forward and reverse primer and 1x SensiMix™ SYBR® No-ROX respectively in each reaction.

For the analysis, the BioRad CFX96 Touch real-time PCR detection system was used. White plates were used (Bio-Rad hard-shell white PCR plates #HSP9601). The thermal

cycling conditions followed were 10 minutes at 95°C for the polymerase activation, and 40 cycles of 95°C for 15 seconds, 55°C for 15 seconds and 72°C for 15 seconds. The results obtained were normalised against the expression of the housekeeping gene RpoD, encoding for the σ^{70} factor.

2.2.1.3 Agarose gels

Agarose electrophoresis gels were prepared at a final agarose concentration of 0.8, 1 and 1.2% depending on the size of the DNA fragments for analysis. The gels were prepared in 1x TBE buffer (90 mM Tris-HCl pH 8.0, 0.55% boric acid, 2 mM EDTA) and 10 μg ml^{-1} ethidium bromide were added for the visualisation of DNA under ultraviolet (UV). The DNA samples were mixed with sample loading buffer (0.25% bromophenol blue, 0.25% xylene cyanol, 30% glycerol, Sambrook et al. 1989) before loaded onto the gel. Gel electrophoresis was carried out in TBE buffer using a PowerPac™ Universal Power Supply (BioRad) between 80 and 130 V until the DNA and dye bars were sufficiently separated. As a standard, 1 kb DNA ladder (NEB) was run in parallel with the DNA fragments for analysis. The gels were visualised using a UV Transilluminator and Gel Documentation System (UVP).

2.2.1.4 Digestion, purification and ligation

Cloning was performed by standard molecular biology techniques (260). Plasmid DNA extractions from liquid cultures were performed using the NucleoSpin® Plasmid extraction kits (Macherey-Nagel). DNA fragments generated by PCR were cleaned up by the NucleoSpin® Gel and PCR Clean-up (Macherey-Nagel). Ligations were carried out either O/N at 16°C or for 10 minutes at room temperature with 0.5 U T4 DNA ligase (New England Biolabs) in a final volume of 10 μl, containing ligase buffer and a 3:1 molar ratio of vector to insert.

2.2.1.5 Transformation of chemically competent Escherichia coli cells

Competent cells were prepared by growing *E. coli* cultures to mid-log phase in LB medium. The cells were harvested by centrifugation at 4,000g for 15 minutes and were washed with ice-cold 50 mM $CaCl_2$ buffer. 30 min incubation intervals on ice were carried out between the washing steps. Finally, the cells were pelleted and re-suspended in 100 µl ice-cold 50 mM $CaCl_2$ for storage at -80^{o}C until transformation. For the transformation, either plasmid DNA or the ligation reaction mix were mixed with 50 µl of competent cells and incubated on ice for 30 min. The transformations were performed by heat-shock at 42°C for 2 min, incubated on ice for a further 2 min. The cells were left to recover in 1 ml of LB medium at 37^{o}C for 2 hours before plating onto selective media.

2.2.2 Protein biochemistry techniques

2.2.2.1 Protein overexpression and purification

For the overexpression of proteins, the *E. coli* BL21-(DE3) pLysS strains were used. The strain was transformed with the overexpression vectors, as appropriate for its protein. For the overexpression, 5 ml cultures were grown O/N and were used in a 1:100 ratio to inoculate the overexpression cultures. The overexpression cultures were then grown at 37°C to an OD_{600} of 0.4 before protein expression was induced overnight with 0.5-1 mM IPTG at 18°C. Cells were then lysed by sonication on ice, and the soluble protein fraction was recovered by centrifugation at 10,000g for 30 minutes. His_6-tagged proteins were purified by NTA-Ni chromatography, in 1 ml HiTrap chelating HP columns (GE Healthcare). GST-tagged proteins were purified using glutathione pre-packed columns (GSTrap^{TM} HP, 1 ml, GE Healthcare). For the purifications, an AKTA Fast Protein Liquid Chromatography (FPLC) system was used (AKTA pure chromatography system, GE Healthcare, Life Sciences). For the His-tag protein purifications, the columns were equilibrated with 10 volumes of washing buffer (20 mM HEPES, 250 mM NaCl, 2 mM

$MgCl_2$, 2.5% glycerol pH 7.5). Cell lysates were loaded to the equilibrated columns, which were then washed with 10 volumes of washing buffer containing 50 mM imidazole. The proteins were eluted using washing buffer containing 500 mM imidazole, in a single step elution. For the GST-tagged proteins, the columns were equilibrated with 10 volumes of washing buffer (20 mM HEPES, 250 mM NaCl, 2 mM $MgCl_2$, 2.5% glycerol pH 7.5) and loaded with cell lysate. Following protein immobilisation, the proteins were eluted with a gradient of washing buffer containing 10 mM reduced glutathione. For the intein system purifications, chitin resin was used, and the purification was performed following the manufacturer's instructions (New England Biolabs, IMPACT™ kit, N6902S).

2.2.2.2 SDS-PAGE gels

Sodium dodecyl sulphate polyacrylamide gel electrophoresis (SDS-PAGE) was carried out in 4% stacking (0.83ml acrylamide (30%), 0.63ml Tris-HCl pH 6.8, 25µl SDS (20%), 50µl APS (10%), 8µl TEMED and 2.8ml deionised H2O) and 12 % resolving gels (4 ml acrylamide (30%), 3.75ml Tris-HCl pH 6.8, 50µl SDS (20%), 100µl APS (10%), 8µl TEMED and 2.1ml deionised H_2O). The gels were prepared in Mini-PROTEAN® Tetra Handcast Systems (BioRad) according to the manufacturer's instructions. Protein samples were mixed in 1:1 ratio with 2 x SDS loading buffer (0.005% bromophenol blue, 10% glycerol, 2% SDS, 10 mM Tris-HCl pH 6.8) and were incubated for 4 min at 95°C to denature proteins before loading. Broad Range Protein Markers or ColorPlus™ Prestained Protein Ladder, Broad Range (New England Biolabs) were used as a standard. The gel electrophoresis was performed in SDS running buffer (25 mM Tris, 192 mM glycine, 1% SDS) at 120-180 V until the dye front reached the bottom of the gel. Gels were stained in InstantBlue (Expedeon) for 1 hour with shaking and were destained with water for 1 hour.

2.2.2.3 Western blotting

For the preparation of the protein samples to be analysed by Western, 100ml of LB were inoculated with the FleQ-bypass mutants and were grown O/N. On the next day, the cells were harvested and the growing media was collected for the identification of exported flagellin subunits. The proteins in the media were mixed with an equal volume of ice-cold acetone and were left to precipitate at -20^{o}C O/N. They were then resuspended in 100μl of protein buffer. The protein concentration is each sample was normalised accordingly before the analysis. SDS-PAGE gels were loaded with the proteins of interest and ran as described in the previous section. For the Western blotting, no staining is required. Proteins were blotted onto an Immobilon-P PVDF membrane (Millipore) using a Western blot module (ThermoFisher Scientific) according to the manufacturer's instructions. The membrane was blocked by TBS-Tween20 solution containing 5% milk powder O/N at 8^{o}C. It was then rinsed with TBS-Tween20 and incubated with primary (1/10,000 dilution in TBS buffer) and secondary peroxidase antibodies (1/3,000 dilution in TBS buffer) (1-2 hours each), with washing steps with TBS-Tween20 in between the incubations. The rinsed membrane was developed by incubation of 2.5 ml Amersham ECL Western Blotting Detection Reagent (GE Healthcare Life Sciences) for 5 minutes. The western blots were visualised by using a CCD camera (ImageQuant LAS 500).

2.2.2.4 Capture compound screen for cyclic di-GMP binding proteins

The protocol was performed based on the Nesper *et al.* publication in 2012 (249). For the identification of novel cdG targets in *P. fluorescens* SBW25, bacteria were grown in M9-pyruvate and M9-pyruvate complemented with CAS aminoacids, KB and LB, to stationary phase and mid-logarithmic phase in 250ml cultures. The cells were isolated by centrifugation for 30 minutes at 5,000g. 0.5 g-1 g of the pellet was weighed and resuspended in 1- 1.5ml protein buffer (20 mM HEPES, 250 mM NaCl, 2 mM $MgCl_2$,

2.5% glycerol pH 7.5) complemented with pellets of protease inhibitor and DNaseI (Roche) according to the manufacturers' instructions. Cells were lysed by sonication on ice, and the soluble fraction of the proteins was isolated by centrifugation at 100,000 g for 1 hour. The analysis was performed on the soluble fraction of the cell lysates. 600 µg of the soluble protein fraction were mixed with the capture compound cdG (CC-cdG) at a final concentration of 10 µM. To produce the method's control samples, cdG, at a final concentration of 1mM, was pre-incubated with the soluble lysate fraction to be used as a reference. The final volume of the reaction was adjusted to 100 µL with protein buffer, and the reactions were incubated for 2 hours at 4°C on a rotary wheel. The reactions were UV irradiated for 4 minutes using the caproBox (Caprotec Bioanalytics GmbH, Berlin). 50 µl streptavidin magnetic beads (Dynabeads, ThermoFisher Scientific) were added together with 25 µL of 5x wash buffer (250 mM Tris pH7.5, 5M NaCl, 0.1% n-octyl-β-glucopyranoside). The samples were further incubated for 30-60 minutes at 4°C on a rotary wheel. The target proteins, bound to the magnetic beads, were isolated using the provided magnet (caproMag) and the samples were washed five- ten times with 200 µL of 1x wash buffer. The beads were resuspended in 20 µL SDS loading buffer (0.005% bromophenol blue, 10% glycerol, 2% SDS, 10 mM Tris-HCl pH 6.8) and were incubated at 95°C for ten minutes. The samples were loaded on a 12% SDS-PAGE acrylamide gel and were ran at 100 Volts for ten minutes. The protein bands were cut and analysed by Mass Spectrometry.

2.2.2.5 Gel filtration chromatography

Soluble protein extracts were prepared in protein buffer (20 mM HEPES, 100 mM NaCl pH 7.5). Gel filtration chromatography was performed on a Superdex 200 10/300 GL column by FPLC (AKTA pure, GE Healthcare). The column was equilibrated with 3 volumes of protein buffer. 100 µL injections of 60 µM of FliI and $FliI_{\Delta 1\text{-}18}$ were performed

at a flow rate of 0.5 ml/min. ATP and cyclic di-GMP were added to the protein mix at a concentration of 500 μM accordingly and were pre-incubated O/N at 4^{o}C on a rotary wheel. The results were plotted in Excel, the baseline for the different samples was normalised, and the curves were smoothed using GraphPad.

2.2.3 Binding tests

2.2.3.1 Differential Radial Capillary of Ligand Assay (DRaCALA)

The method was performed as previously described by Roelofs *et al.* (63). The assays were conducted by mixing 4 nM radiolabelled cdG with variable concentrations of the proteins of interest. For the synthesis of radiolabelled cdG from [γ^{32}-P]- GTP, the well-characterized DGC protein, PleD* was used. 10 μM of PleD* was mixed with 1 μl of [γ^{32}-P]- GTP and was incubated at 37^{o}C for 1 hour. The reaction was inactivated by 10 minutes' incubation at 95^{o}C, and the radiolabelled cdG was isolated by centrifuging the reaction for 5 minutes at 13,000g. For the analysis, each protein was incubated for 2-5 minutes with 4nM radiolabelled cdG in protein buffer (20 mM HEPES, 250 mM NaCl, 2 mM $MgCl_2$, 2.5% glycerol pH 7.5). 5 μL of the sample was spotted on nitrocellulose, and a phosphorimager was used for the visualisation of the results. As an alternative to [γ-^{32}P] cdG, 2′-Fluo-AHC-c-diGMP was used (BioLog 009) at a final concentration of 0.6 μM in some of the experiments. For the DRaCALA nucleotide competition experiments of $FliI_{\Delta 1\text{-}18}$, 1 mM of each nucleotide was mixed with 10 μM of the protein and incubated for 30 min. 0.6 μM of the fluorescent cdG analogue were then added to the reaction and were incubated for 2 minutes before spotting 5 μL on a nitrocellulose membrane for the analysis. The results were visualised using a charge-coupled device camera.

2.2.3.2 Isothermal Titration Calorimetry (ITC)

ITC experiments were conducted using an ITC200 Calorimeter instrument (MicroCal Inc.). The experiments were performed at 25ºC in 20 mM HEPES, 150 mM NaCl, pH 8 buffer. For the FliI experiment, the calorimetric cell was filled with protein at a final concentration of 54 μM, which was titrated with 1 mM cdG. For the PFLU_1582 experiment, the cell was filled with protein at a final concentration of 100 μM, which was titrated with 1mM cdG. A total number of 18 injections were carried out of a volume of 1 μL for the first, followed by 2 μL injections for the rest. The ITC data was analysed, plotted and fitted to a one-site binding model using the MicroCal Origin software. Injections were made at 150 seconds intervals with a stirring speed of 1000 rpm.

2.2.3.3 Surface plasmon resonance (SPR)

For the cdG binding experiments, the SPR experiments were conducted using a Biacore T200 system. 100 nM biotinylated cdG (Biolog B098) were immobilised on a streptavidin chip (GE Healthcare) at a final immobilisation level of 50 RU, with a flow rate of 5 μL/ min. An empty cell was used as a reference for subtraction of non-specific interactions subtraction. After the immobilisation, the chip was washed with 1 M NaCl, 50 mM NaOH for the removal of any unconjugated streptavidin. The protein samples were prepared at the required concentrations in SPR buffer (10 mM HEPES, 150 mM NaCl, 0.1% Tween 20, 2 mM $MgCl_2$) and were injected with a flow rate of 5 μl/min over the chip for 60 sec, 90 sec or 120 sec until they reached their saturation level. The buffer was then injected onto the chip for 60 or 90 seconds for the calculation of the disassociation time of the protein from the chip. 1 M NaCl was used after each injection for the chip regeneration. For each protein concentration, three replicates were included as appropriate.

For the FliH/ FliI interaction experiments, N-terminal His-tagged FliH from *Pseudomonas syringae* DC3000 was immobilised on an NTA sensor chip (GE

Healthcare, BR100407) at a final 50 RU immobilisation level. N-terminal GST-tagged FliI full length at a final concentration of 10 μM, from *P. syringae* DC3000, was injected at a flow rate of 5 μl/ min over the reference and the FliH cell for 60 seconds, followed by the buffer for 60 seconds. To test the effects of cdG on the interaction, a range of cdG concentrations (0, 1, 10, 100, 1000 μM) were pre-incubated with FliI O/N at 4^{o}C.

2.2.3.4 Differential Scanning Fluorimetry (DSF)

Shifts in the protein melting temperature were measured by DSF. Reactions of a final volume of 20 μl were set up. The final protein concentration used was 10 μM; SYPRO Orange was used as the detection dye at a final concentration of 5x, and the reactions were prepared in 20 mM HEPES, 100 mM NaCl, 2 mM $MgCl_2$ pH 8 buffer. For the identification of potential shifts in the melting temperature of the proteins in association with cdG, a titration of cdG was carried out (0, 10, 30, 100, 300, 1000 μM cdG). The reactions were set up in a clear bottom 96-well plate, and the experiment was conducted using a Biorad CFX96 instrument. The protocol followed was: 10 minutes at 10^{o}C followed by 0.5^{o}C increment up to 90^{o}C and the reactions were kept at 4^{o}C. The results were analysed using the Biorad CFX Manager 2.1.

2.2.3.5 Streptavidin UV Precipitation assay (SUPr)

The method was carried out as described in (261). 5 ml cultures of *E. coli* strains carrying overexpression vectors for EpsI/ Nla24 and SadB were induced with 0.5 mM IPTG for 5 hours at 28°C. Empty-vector and non-induced strains were used as controls. The cells were collected by centrifugation were resuspended in 400 μl protein wash buffer before they were lysed by sonication. The soluble fraction was collected after centrifugation at 13000g at 4°C for 1 hour and 45μl of it were mixed with biotinylated cdG (BioLog B098) at a final concentration of 30 μM. The mix was then incubated O/N on a rotary wheel at 8°C and was UV cross-linked for the complexes stabilisation, on the next day. The UV

cross-linking was performed on ice for 4 minutes in a UV Stratalinker (Stratagene). For the isolation of the biotinylated-cdG bound proteins, 25 µl of Streptavidin magnetic beads (Invitrogen) were added and incubated for 1 hour on a rotary wheel at 8°C. A magnet was used for the isolation of the Streptavidin magnetic beads. To remove any un bound proteins, five-ten washing steps were carried out with 200 µl of protein wash buffer (20 mM HEPES, 250 mM NaCl, 2 mM $MgCl_2$, and 2.5% (v/v) glycerol pH 6.8). The washed Streptavidin beads were resuspended in 15 µl wash buffer with 4x SDS loading buffer added. The samples were incubated at 95°C for 10 min and were loaded on a 12% SDS-PAGE protein gel. The gel was then developed using InstantBlue (Expedeon).

2.2.3.6 Native acrylamide gel shift assays

10 µM of protein were incubated with 120 µM of cdG for 15minutes on ice. The mix was UV cross-linked for 1 minute in round-bottom 96-well plates, in a UV Stratalinker on ice. A protein-only sample was used as a reference to the method. The samples were mixed with 2x sample buffer (62.5 mM Tris-HCl, pH 6.8, 25% glycerol, 1% Bromophenol Blue) and loaded onto a native acrylamide gel. For the native gel preparation, 10 ml of 12% native PAGE separating gel were prepared by mixing 4 ml of Acrylamide/Bis-acrylamide (30%/0.8% w/v), 5.89 ml of 0.375 M Tris-HCl (pH 8.8), 100 µL of 10% (w/v) ammonium persulfate and 10 µL TEMED. The electrophoresis was performed in 25 mM Tris and 192 mM glycine running buffer, at 180 V for 1 hour. The gel was stained using InstantBlue (Expedeon).

2.2.3.7 Native Agarose gel shift assays

The assay was carried out as described in (262). For the identification of protein shifts in agarose gels upon the addition of cdG, 5 µM final protein concentration was used and was incubated with 100 µM of cdG for 15 minutes on ice. The protein mix was UV cross-linked using a Stratalinker for 1 minute on ice. As a reference, a protein-only sample was

included. The samples were loaded on a horizontal 0.8% native agarose gel, which was prepared in 25 mM Tris-HCl, pH 8.5, 19.2 mM glycine, with the comb placed in the middle. The samples were mixed 1:1 with sample buffer (20% glycerol, 0.2% Bromophenol blue, 0.12 M Tris base) and were loaded on the gel. The electrophoresis was performed at 50 V constant voltage, for 1 hour, at room temperature. The gels were stained with 0.12% Coomassie brilliant blue, 45% methanol, 10% acetic acid for 20 minutes and were then destained with 45% methanol and 10% acetic acid.

2.2.3.8 Capture compound competition assay

For the competition assay, 10 μM of $FliI_{\Delta 1\text{-}18}$ were mixed with 1 mM of cdG, ATP, ADP, NADH, cAMP, cGMP, cdA in separate reactions and were incubated for 30 minutes at 4ºC on a rotary wheel. 10 μM of the capture compound (chemically modified, biotinylated cdG from Caprotec) was then added to the reaction mixes, which were then incubated O/N at 4ºC on a rotary wheel. On the next day, the reactions were UV-cross-linked for 4 minutes using the UV Stratalinker (Stratagene) on ice for the stabilisation of the interactions. For the isolation of the cdG-protein complexes, streptavidin magnetic beads (Invitrogen) were used in a 1:5 ratio with the protein mixture. The samples were then washed 5x with protein washing buffer (20 mM HEPES, 250 mM NaCl, 2 mM $MgCl_2$, and 2.5% (v/v) glycerol pH 6.8), they were mixed with SDS-protein loading dye, were incubated at 95ºC for 10minutes and they were analysed on an SDS-PAGE gel.

2.2.4 Activity analysis

2.2.4.1 Linked Pyruvate Kinase / Lactate Dehydrogenase (PK/LDH) ATPase activity assay

The ATPase activity of the proteins of interest was measured indirectly by monitoring NADH oxidation. For the analysis, each protein was prepared in ATPase activity buffer (50 mM Tris-Cl, 2 mM $MgCl_2$, 1 mM DTT and 10 mM KCl, pH 8.0). For each reaction, 1μM final protein concentration was mixed with 5 mM NADH in 10 mM NaOH, 80 mM phosphoenolpyruvic acid, 1.5 μl PK/LDH (Sigma) and the appropriate concentrations of cdG. The reactions were initiated by the addition of suitable ATP concentrations. Experiments were carried out in clear bottom 96-well plates (Elkay laboratory products (UK) Limited) in a plate reader (BioTek Instruments inc.) and the enzymatic activity of each protein was determined by monitoring the absorbance at A_{340} with 1-minute intervals. The results were analysed by plotting the specific activity of the enzyme (nmol ATP hydrolysed/ min/ mg of protein) versus ATP concentration, and the kinetic

parameters were calculated by non-linear enzyme kinetics modelling (Hill equation) in GraphPad Prism.

2.2.5 Microscopy techniques

2.2.5.1 Transmission electron microscopy (TEM)

For the visualisation of FliI full-length complex formation in TEM, 1-3 μg/ml of FliI full length from *Pseudomonas fluorescens* SBW25 were used. CdG was added to the protein mix accordingly, at a final concentration of 1 mM and incubated with the protein O/N at 4^{o}C. For the visualisation of the samples, the protein sample was negatively stained as described by Harris and Horne (1991) (263) in 2% aqueous uranyl acetate, pH 4.5, on a 400 mesh copper grid with a carbon-coated pyroxylin support film. The grids were viewed in a Tecnai 20 transmission electron microscope (FEI, Eindhoven, Netherlands) at 200kV and digital TIFF images were taken using an AMT XR60B digital camera (Deben, Bury St Edmunds, UK).

2.2.5.2 Atomic force microscopy (AFM)

For the visualisation of FliI and FliI alleles complexes using AFM, 1-3 μg/ ml of protein in 10 mM HEPES, 3 mM $MgCl_2$ buffer, were used. CdG and ATP were added, where needed at 100μM final concentration. The protein samples were immobilised on mica slides. The samples were analysed in MFP-3D-BIO (Asylum Research, Santa Barbara, CA, USA) AFM instrument. Imaging was performed in tapping mode in air in the repulsive regime using Olympus AC160TS cantilevers (Olympus, Japan). The cantilevers were driven into oscillation at 10% below their fundamental resonant frequency (typically around 320 kHz) and the feedback loop operated using amplitude control. The set-point was kept at the minimal value (~ 90% of the free amplitude) that enabled stable tracking of the sample surface to eliminate any sample damage. The scan rate was 1 Hz.

2.2.6 Mass spectroscopy analysis

2.2.6.*1 Mass spectrometry of cross-linked FliI for the peptide shift analysis*

All the MS analysis was carried out by Dr. Gerhard Saalbach. FliI full length was mixed with cdG capture compound (Caprotec) in a 1:1 ratio (10 μM final concentration) and cross-linked by UV irradiation for 4 minutes on ice, in a Stratalinker. The cross-linked protein molecules were washed with protein wash buffer and were isolated using streptavidin magnetic beads and a magnet. The procedure is described in detail in the capture compound method above. A non-cross-linked control was included as a reference. The two samples were isolated on an SDS-PAGE gel; the protein bands were cut out, and the samples were given for MS-analysis. The analysis was carried out using a nanoLC-MSMS on an Orbitrap Fusion™ Tribrid™ Mass Spectrometer coupled to an UltiMate® 3000 RSLCnano LC system (Thermo Scientific, Hemel Hempstead, UK). A PepMap™ 100 C18 LC Column (C18, 2 μm, 500x0.75 mm, Thermo) was used to separate the peptides, with a gradient of 0.75% min^{-1} acetonitrile from 6% to 40% in water/0.1% formic acid at a flow rate of 0.3 μl min^{-1} and infused directly into the mass spectrometer. The precursor scans were performed in positive ion mode, at 120 K resolution over the mass range 350-1800 (m/z) with no quad isolation (Orbitrap). One microscan of 50 ms with an AGC target of $2e^5$ was used. The threshold for MS^2 was set to $1.5e^4$, and both CID and HCD were utilised for the fragmentation of the precursor ions, with CE=30 and an isolation window of 1.6 Da (quadrupole) using the automatic maximum speed option with ion injection for all available parallelizable time. Dynamic exclusion was set to 1 count and 30 s. MaxQuant 1.5.2.8 (www.MaxQuant.org) was used to generate recalibrated peak lists. Mascot 2.4 (Matrixscience, London, UK) was used to compare the merged HCD and CID peak lists against a partial E. coli database, including the expected FliI protein sequence. The precursor and the fragment error tolerances were

set to 6 ppm and 0.6 Da, respectively. The enzyme was set to trypsin/P, and a maximum of two missed cleavages were allowed. Carbamidomethyl (C) was set as fixed modification, and oxidation (M) and acetylation (Protein N-term) were used as variable modifications. The Mascot search results were imported into Scaffold 4.4.1.1 (www.proteomsoftware.com) using identification probabilities of 99% and 95% for proteins and peptides.

2.2.6.2 Mass Spectrometry-Peptide Shift Analysis (MS-PSA)

MS-PSA analysis was performed as described previously in (264). For the analysis two different samples were included, the treated (UV-cross-linked with the cdG CC) and the untreated (reference sample). Accordingly, many peptides in the treated samples were found to have shifts in their size compared to the untreated sample. The most heavily modified peptide after the treatment with cdG CC was identified to be the NVLLLMDSLTR peptide. More specifically, the following MS-PSA parameters were used for both analyses: num = 8 pmr = 0.001 t1 = 5 t2 = 100 fmr = 0.5 mnds = 2 clusterq = True signif = 1 tol = 1 outl = 0.1 nmfp = 20 mofp = 9 mnspg = 2 csf = 2 peakfreq = 2 nummods = 1 pwss = 4 cp = 3 qual1 = 0.2 qual2 = 0.2 qual1pl2 = 0.5 mrms = 150 maxdev = 1.

2.2.7 Structural analysis

2.2.7.1 Crystallisation trials

For the crystallisation experiments, N-terminally His-tagged $FliI_{\Delta 1\text{-}18}$ at a concentration 6 mg/mL was used. The protein was crystallised by sitting-drop vapour diffusion in 96-well crystallisation plates (Swissci) by mixing 0.3 µl well solution with 0.3 µl protein solution. The plates were set up by using either an OryxNano or an Oryx8 crystallisation robot (Douglas Instruments). The crystal optimisation experiments were performed manually

in 24-well plates (Hampton Research) by the hanging-drop vapour diffusion technique by varying the composition of the precipitant solution to improve crystal quality. The best $FliI_{\Delta 1\text{-}18}$ crystals were obtained from 20% (w/v) PEG 4000, 40% (v/v) Glycerol, 0.1 M Bicine/ Tris pH 8.5, 0.3 M magnesium chloride and 0.3 M calcium chloride in the presence of 1 mM cdG and 1 mM ADP. The crystals were harvested and flash-cooled in liquid nitrogen using LithoLoops (Molecular Dimensions). Additional cryoprotection was not required due to the presence of glycerol in the crystallisation solution. They were then transported to the Diamond Light Source (Oxfordshire, UK), in Unipuck cassettes (MiTeGen), where they were maintained at -173°C with a Cryojet cryocooler (Oxford Instruments) during data collection. A Pilatus 6M hybrid photon counting detector (Dectris) was used for the recording of the X-ray diffraction data on either beamline I02 or I03, which were then integrated using XDS (265), and scaled and merged using AIMLESS (266) via the XIA2 expert system (267). The structure was solved by molecular replacement with PHASER (268) starting from the known FliI structure (PDB accession code 2DPY) using a dataset collected to 2.4 Å resolution for $FliI_{\Delta 1\text{-}18}$, in the presence of cdG and ADP.

The protein model and the electron density maps were generated by COOT (269). The model was built manually by altering it to fit in the electron density until the observed and calculated data were assessed to have the closest possible match with the data set by monitoring the Rfactor and Rfree values. For the refinement of the protein, structure REFMAC was used (270). The water molecules were fitted and refined by ARP/wARP (271).

2.2.7.2 Homology Model Production

The homology model of the hexameric FliI from *P. fluorescens* SBW25 was based on the published crystal structure of FliI from *S. enterica* (Protein Databank accession code:

2DPY) (272). The two proteins share 63% sequence similarities, and the model was created by the Phyre2 server (273). The model prediction was based on the broad structural similarities between FliI and the a and β subunits of the F_0F_1 ATP synthase. The hexameric model was generated by superposing six copies of the monomeric structure onto each of the a and β subunits of the bovine F_0F_1 ATP synthase complex (Protein Data Bank accession code: 2JIZ) (274), using the secondary structure matching algorithm (275), in the COOT software (269). The structural figures were all generated using CCP4 mg (276).

Chapter 3:

Identification of novel cdG binding proteins

Chapter 3: Identification of novel cdG binding proteins

3.1 Introduction

CdG is a widespread bacterial second messenger, which regulates growth and behaviour in both Gram-positive and negative bacteria. CdG is well known to trigger the switch between a motile lifestyle and a sessile one. It has also been associated with biofilm formation, one of the leading causes of chronic infections caused by pathogenic bacterial strains (e.g. *Pseudomonas aeruginosa*) (277). An increasing number of cellular processes controlled by cdG are emerging, such as the synthesis and export of exopolysaccharide (EPS), synthesis of secondary metabolites, different ways of regulating bacterial motility, cell cycle control, etc. (224,277,278). As described in the introduction, cdG has various binding targets in the bacterial cell. To be able to predict and analyse the pathways and processes that are triggered and regulated by cdG, it is imperative to identify these targets. Although we have a good understanding of cdG metabolism, surprisingly little is currently known about the downstream targets of this molecule.

In recent years more and more cdG binding proteins have been discovered. While many of the established cdG targets have been identified following bioinformatics approaches, it is becoming increasingly clear that cdG networks contain many more target proteins whose nature cannot be determined bioinformatically. To further understand the mechanisms underpinning cdG metabolism and the processes controlled by this molecule in the cell, it is essential to identify these missing cdG targets. Although there have been some previous attempts that aimed to determine cdG targets from whole cell lysates using cdG immobilised to sepharose and affinity chromatography (279,280), there were major problems with the physical stability of the sepharose beads, and limited availability rendering it difficult to carry out large-scale experiments.

For the identification of cdG targets in complex bacterial cell lysates, Urs Jenal's group developed a global approach in 2012 (249). His group introduced a novel tri-functional capture compound screen (cdG-CC) as a tool for the effective identification of cdG targets from a complex mixture of cell lysates. CdG-CC is a chemically modified cdG molecule (Figure 3.1), which has a biotin group attached to it for sorting purposes, and a UV reactivity group for the stabilisation of the complexes formed.

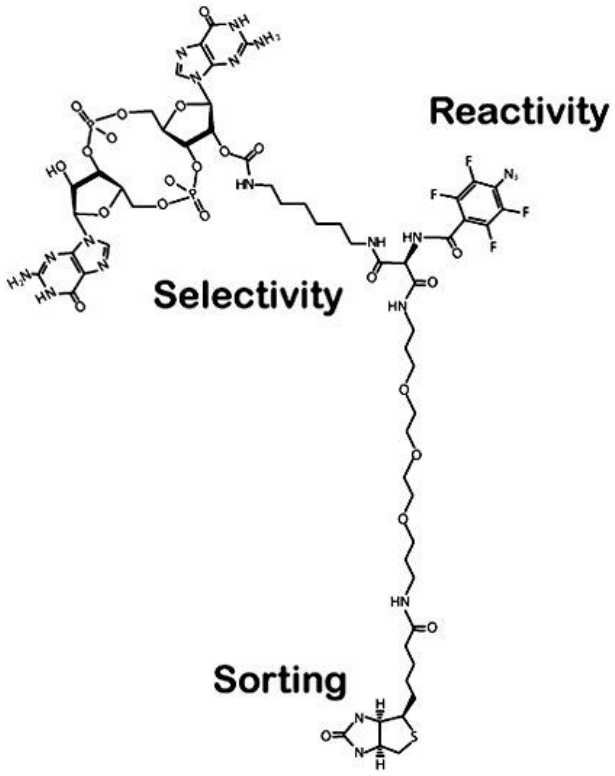

Figure 3.1: CdG capture compound as described in (249). Reprinted by permission from Elsevier.

The capture compound is incubated with a crude extract of bacterial cells, and protein-cdG complexes are stabilised by UV cross-linking. Finally, for the isolation of the complexes, streptavidin magnetic beads are employed. The analysis of the bound proteins is achieved by Mass Spectrometry (MS) analysis. To reduce the number of false positive binders, various nucleotides are incubated with the cdG-CC and whole cell lysates and are used as controls for the method. For the evaluation of the method, it is important that some known cdG binding proteins can be detected following MS/MS. In both of the

publications describing the method, as well as in the experiments carried out here, several known cdG binding proteins were identified.

3.2 Aims

1. To identify novel cdG binding targets by performing pull-down screens.

2. To select the most interesting targets, and confirm binding using a selection of biochemical tools.

3.3 Results

3.3.1 Identification of novel cdG targets

To identify novel cdG binding proteins in *Pseudomonas fluorescens* SBW25, a cdG capture compound screen was performed in multiple media conditions. The bacteria were grown in the following media; M9-pyruvate, M9-pyruvate complemented with CAS amino acids, KB and LB to logarithmic and stationary growth phases. The experiment was repeated twice per condition and samples pre-incubated with an excess of cdG were included as controls. A merged list of potential binding targets, which resulted from the different experimental conditions, are presented in the following table 3.1.

Interestingly, three of the 17 identified potential targets are already known to interact with cdG (*i.e.* PFLU_4738, 1582, 1571). All three are known PilZ domain proteins. The other PilZ domain proteins encoded in the *P. fluorescens* genome are membrane proteins and could not be identified in this experiment, as only water soluble fractions were studied. Among the identified PilZ proteins, PFLU_4738 is a homolog of *E. coli* YcgR, the flagella brake protein, and a well-established cdG target in *E. coli* (281). A YcgR homolog in *P. putida* (FlgZ) has also been characterised (282).

Table 3.1: Merged list of potential cdG binding targets as emerged by the different screen conditions.

Protein name	Predicted function
PFLU_0001	**Chromosomal replication initiation protein DnaA**
PFLU_0017	Methionyl-tRNA formyltransferase
PFLU_0022	Quinone oxidoreductase
PFLU_0142	Uncharacterised- putative membrane protein
PFLU_0251	Predicted oxidoreductases
PFLU_0290	glucose-1-phosphate thymidylyltransferase
PFLU_0355	Fructose bisphosphatase
PFLU_0463	**Lipopolysaccharide heptosyltransferase-1**
PFLU_0667	Adenosine deaminase
PFLU_0760	Sulphate adenylyltransferase subunit 2
PFLU_0771	4-Hydroxy-3-methylbut-2-enyl diphosphate reductase IspH
PFLU_0840	30s ribosomal protein S9
PFLU_0879	Hypothetical protein
PFLU_0998	ATP-dependent RNA helicase RhlB
PFLU_1164	DNA mismatch repair protein MutS
PFLU_1327	Hypothetical protein- outer membrane
PFLU_1454	Uncharacterised protein
PFLU_1571	PilZ domain protein- cdG binding
PFLU_1582	**PilZ domain protein- cdG binding**
PFLU_1597	Hypothetical protein- ppGpp synthetase- RelA/SpoT family
PFLU_1667	Putative aminotransferase- cell wall biogenesis
PFLU_2160	Putative dehydrogenase
PFLU_3017	Two-component system protein
PFLU_3199	3-oxoacyl-ACP synthase II
PFLU_3406	Cysteine synthase(only in one)
PFLU_3481	Hypothetical- AAA
PFLU_3796	Siroheme synthase
PFLU_3809	**Isocitrate dehydrogenase**
PFLU_4144	Phenylalanyl-tRNA synthetase subunit alpha
PFLU_4320	**Putative asparagine synthetase**
PFLU_4401	**Putative Chemotaxis protein**
PFLU_4436	**Putative flagellum ATPase**
PFLU_4531	**LysR family transcriptional regulator**
PFLU_4578	DNA polymerase III subunits gamma and tau
PFLU_4589	Cell division protein ZipA
PFLU_4622	**Transcriptional regulator**
PFLU_4738	PilZ domain protein- c di-GMP binding
PFLU_4874	16S rRNA uridine-516 pseudouridylate synthase
PFLU_4895	**Putative regulatory protein**
PFLU_4900	Cold shock
PFLU_4908	Translocation protein
PFLU_4974	Uncharacterised
PFLU_5043	GMP synthase
PFLU_5427	Gamma-glutamyl phosphate reductase
PFLU_5543	Biotin protein ligase
PFLU_5615	Biotin synthase
PFLU_5772	tRNA (guanine-N(7)-)-methyltransferase
PFLU_5828	GlycolatePutative oxidase
PFLU_5932	Putative uroporphyrin-III C-methyltransferase
PFLU_6001	Putative exported
PFLU_6122	Proton-transporting ATP synthase activity, rotational mechanism
PFLU_6126	**Putative chromosome partitioning protein ParB**

3.3.2 Target selection and analysis

Following the identification of potential cdG targets (table 3.1), it was necessary to confirm that the proteins identified in our screens were indeed specific cdG binding proteins. To do this, key targets from the screen were selected (highlighted in bold, table 3.1), cloned into overexpression vectors, and purified. These were: the chromosomal replication initiation protein DnaA (PFLU_0001), the lipopolysaccharide heptosyltransferase protein PFLU_0463, the previously unidentified PilZ domain protein PFLU_1582, the isocitrate dehydrogenase PFLU_3809, the putative asparagine synthetase PFLU_4320, the putative chemotaxis protein PFLU_4401, the flagellum ATP synthase PFLU_4436, the LysR transcriptional regulator PFLU_4531, a second transcriptional regulator (PFLU_4622), the putative regulatory protein PFLU_4895, and the chromosome partitioning protein, PFLU_6126.

The target genes were cloned into either pET42b, pETM-NdeI-11 or pTYB12 vectors, resulting in the attachment of an C-terminal His tag in each case. They were purified using an AKTA FPLC system with anti-His Nickel columns. The purifications were optimised for each protein, to achieve high purity products that remain soluble and active in solution.

3.3.3 Binding testing

In order to test the purified proteins, it was essential to develop and optimise simple and rapid assays that would allow the simultaneous examination of a large number of proteins for cdG binding.

The first assay used was the Differential Radial Capillary Action of Ligand Assay (DRaCALA). In DRaCALA, radiolabelled cdG is mixed with the protein, or the lysate overexpressing the protein of interest, and binding is indicated by the formation of an inner ring in the middle of the spot on a nitrocellulose membrane (283).

Initially, *E. coli* whole cell lysates overexpressing PFLU_0001, PFLU_4401, PFLU_6126, PFLU_0463 and PFLU_4320 were tested. PleD* was used as a positive control. This protein is a phosphorylation-independent, constitutively active form of the PleD diguanylate cyclase (284). Strong, unambiguous binding could not be detected for any of the selected proteins (Figure 3.2). However, in some cases, there was a hint of an inner ring, which encouraged us to investigate further by testing the purified proteins instead of the lysates. The most promising targets were examined with a series of additional assays to confirm that the results were reproducible.

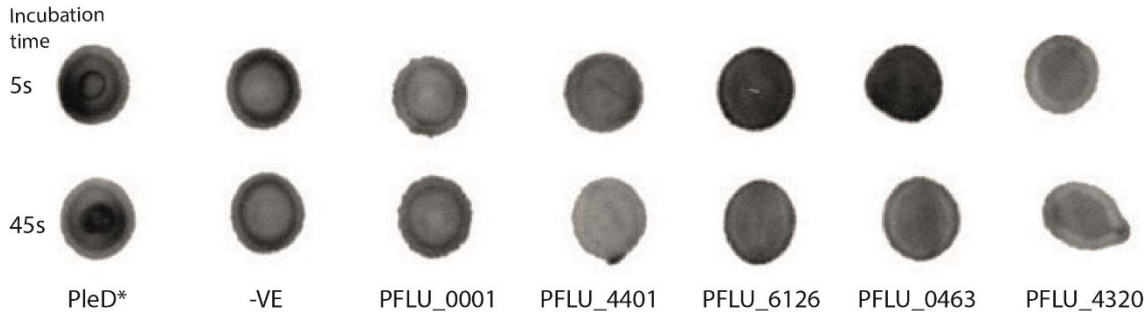

Figure 3.2: DRaCALA on whole cell lysates overexpressing a selection of potential cdG targets identified in the capture compound screen. PleD was used as a positive control for binding. Non-induced whole cell lysates were used as a negative control. The lysates were incubated with the radiolabelled cdG either for 5 or 45 seconds.*

*3.3.4 Method evaluation using the cdG-binding protein, PleD**

The first protein tested for evaluating the methods was PleD*, a known cdG binding protein. Firstly, the overexpression and purification of the protein were optimised to achieve a high protein yield (Figure 3.3- A). The purified protein was then tested for binding by DRaCALA, where a clear inner, binding ring was formed, strongly indicating binding (Figure 3.3- B-II). Once PleD* binding had been confirmed by DRaCALA, the next assay carried out was Differential Scanning Fluorimetry (DSF) (285), a method measuring changes in the melting temperature of the protein upon addition of a ligand. An increase in the melting temperature of PleD* was demonstrated upon the addition of increasing concentrations of cdG (Figure 3.3- C). This directly indicates the effect cdG has on the conformation of PleD*, which leads to changes in the stability of the complex and as a result on the T_m of the protein.

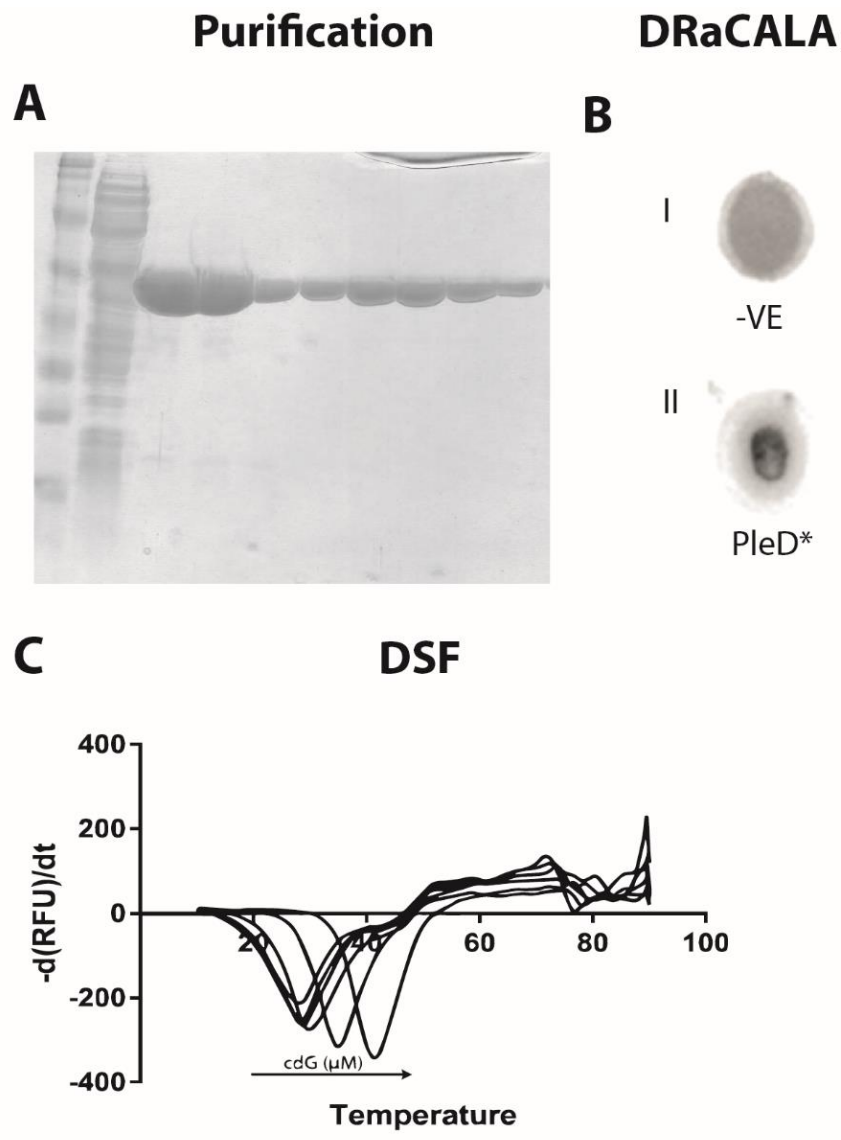

Figure 3.3: Purification and analysis of PleD as a positive control for cdG binding. A. Protein purification fractions. The protein was purified using an FPLC-AKTA system to high quantities and extra purity. B. DRaCALA assay. Negative, non-binding control. PleD* (3 μM) binding spot C. Differential Scanning Fluorimetry (DSF). The melting temperature of the protein increases as the cdG concentration raises (0 μM, 1 μM, 3 μM, 10 μM, 30 μM, 100 μM), indicating a role of cdG in the conformation of the protein.*

3.3.5 Testing putative binding targets

3.3.5.1 Lipopolysaccharide heptosyltransferase (PFLU_0463)

PFLU_0463 is a lipopolysaccharide heptosyltransferase-1, an enzyme known to transfer heptoses in lipopolysaccharides. *PFLU_0463* is homologous to *E. coli* and *Salmonella rfaC*, mutations in which were shown to produce an LPS core free of oligosaccharides, This, in turn, resulted in reduced motility and the absence of functional flagellum filaments, suggesting that oligosaccharides attached to the LPS core are essential for both the assembly of the flagellum and for protein secretion (286).

The protein was purified in high amounts and purity (Figure 3.4- A) and tested for binding using DRaCALA. As indicated in Figure 3.4- C, an inner ring was observed for the protein sample, indicating binding to cdG. To test if the cdG binding was condition-dependent, *P. fluorescens* whole cell lysates were added to the mix, although this did not trigger any profound change in binding. Different reagents were also added such as ATP and chromosomal DNA, but no changes in binding intensity were observed. In DSF (Figure 3.4- B), a mild shift of the melting temperature was observed upon the addition of increasing concentrations of cdG. The final binding test carried out was a gel shift assay (GSA), an assay monitoring potential size shifts on the protein upon the addition of cdG, when analysed on an agarose gel. This assay is differentiated from the native gel shift assay, as the proteins are analysed both based on their size and their isoelectric point (see Materials and Methods for the description of the assay). In the case of PFLU_0463, a clear shift of the protein size was observed upon the addition of raising cdG concentrations, strongly indicating binding.

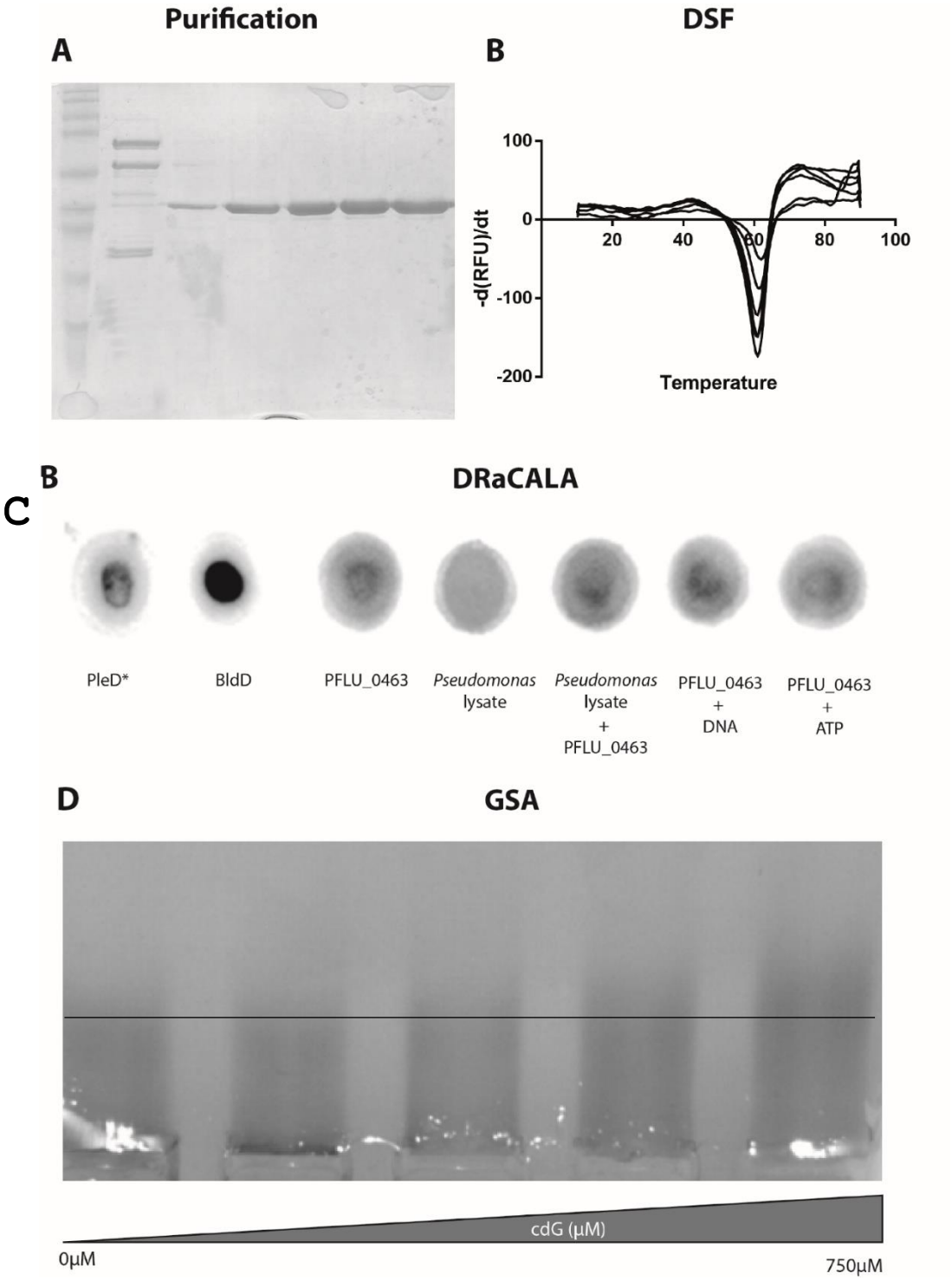

*Figure 3.4: Purification and analysis of PFLU_0463 for cdG binding. A. Protein purification fractions. The protein was purified using an FPLC-AKTA system to high quantities and extra purity. B. Differential Scanning Fluorimetry (DSF). A mild change in the melting temperature of the protein was observed upon the addition of increasing concentrations of cdG. C. DRaCALA assay - PleD*and BldD (238) were used as positive controls (3 µM of each), PFLU_0463 (3 µM) gave a positive binding spot, additions of Pseudomonas whole cell lysates (0.5 mg/ml) didn't produce a binding ring, addition of the lysate to the protein didn't change the binding profile, addition of ATP (10 µM) didn't change the binding profile. D. Gel shift assay (GSA), upon the addition of increasing concentrations of cdG (0µM, 100 µM, 200 µM, 400 µM, and 750 µM), shift in the size of the protein is observed.*

3.3.5.2 PilZ domain hypothetical protein (PFLU_1582)

The next protein tested was the PilZ domain protein PFLU_1582. PilZ domain proteins are known cdG binders. However, not every protein containing a PilZ domain binds to cdG. PFLU_1582 is a previously unidentified PilZ domain protein with no previous association with cdG binding, so it was necessary to biochemically test binding for this protein.

Once again, the overexpression and purification parameters of the protein were optimised (Figure 3.5- A) and the protein was tested in DRaCALA. As presented in Figure 3.5, the formation of an inner ring is evident in the DRaCALA assay (Figure 3.5- B- III). To further confirm binding, a DSF experiment was carried out, in which it is evident that upon the addition of increasing concentrations of cdG the melting temperature of the protein increases (Figure 3.5- C). Finally, the GSA assay was used to confirm cdG binding. In this assay the addition of cdG led to a shift in the size of PFLU_1582, indicating cdG binding to the protein leading to its conformational change. Lastly, the protein was incubated with 120 μM of cdG and was analysed on a native gel, under non-denaturing conditions. However, there was no effect on the size of the protein after the addition of cdG.

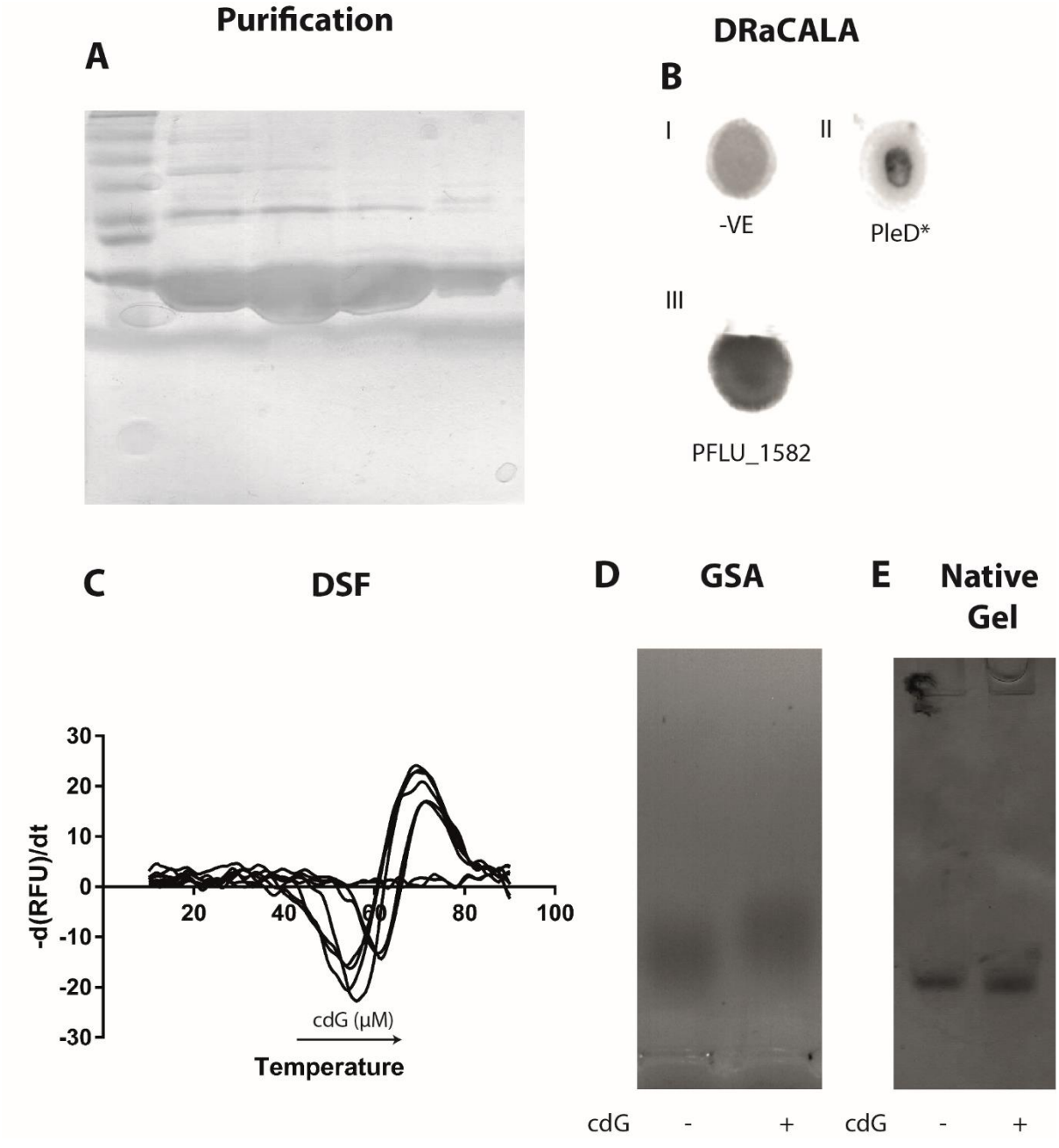

Figure 3.5: Purification and analysis of PFLU_1582 for cdG binding. A. Protein purification fractions. The protein was purified using an FPLC-AKTA system to high quantities and extra purity. B. DRaCALA assay, I. Negative, non-binding control, II. PleD binding spot (3 μM), III. PFLU_1582 binding spot (3 μM) C. Differential Scanning Fluorimetry (DSF). The melting temperature of the protein increases as the cdG concentration raises (0 μM, 10 μM, 30 μM, 100 μM, 400 μM, 500 μM), indicating a role of cdG in the conformation of the protein. D. Gel shift assay (GSA) on PFLU_1582 (5 μM), upon the addition of 100 μM of cdG, a shift in the size of the protein is observed. E. Native gel of PFLU_1582 (6 μM) without cdG and upon the incubation with 100 μM cdG. No shift in the size of the protein was observed.*

At this stage, we decided to use an analytical binding assay to PFLU_1582, to acquire more information about the nature of the interaction (e.g. the stoichiometry). Isothermal Titration Calorimetry (ITC) was employed to probe the cdG-protein interaction (Figure

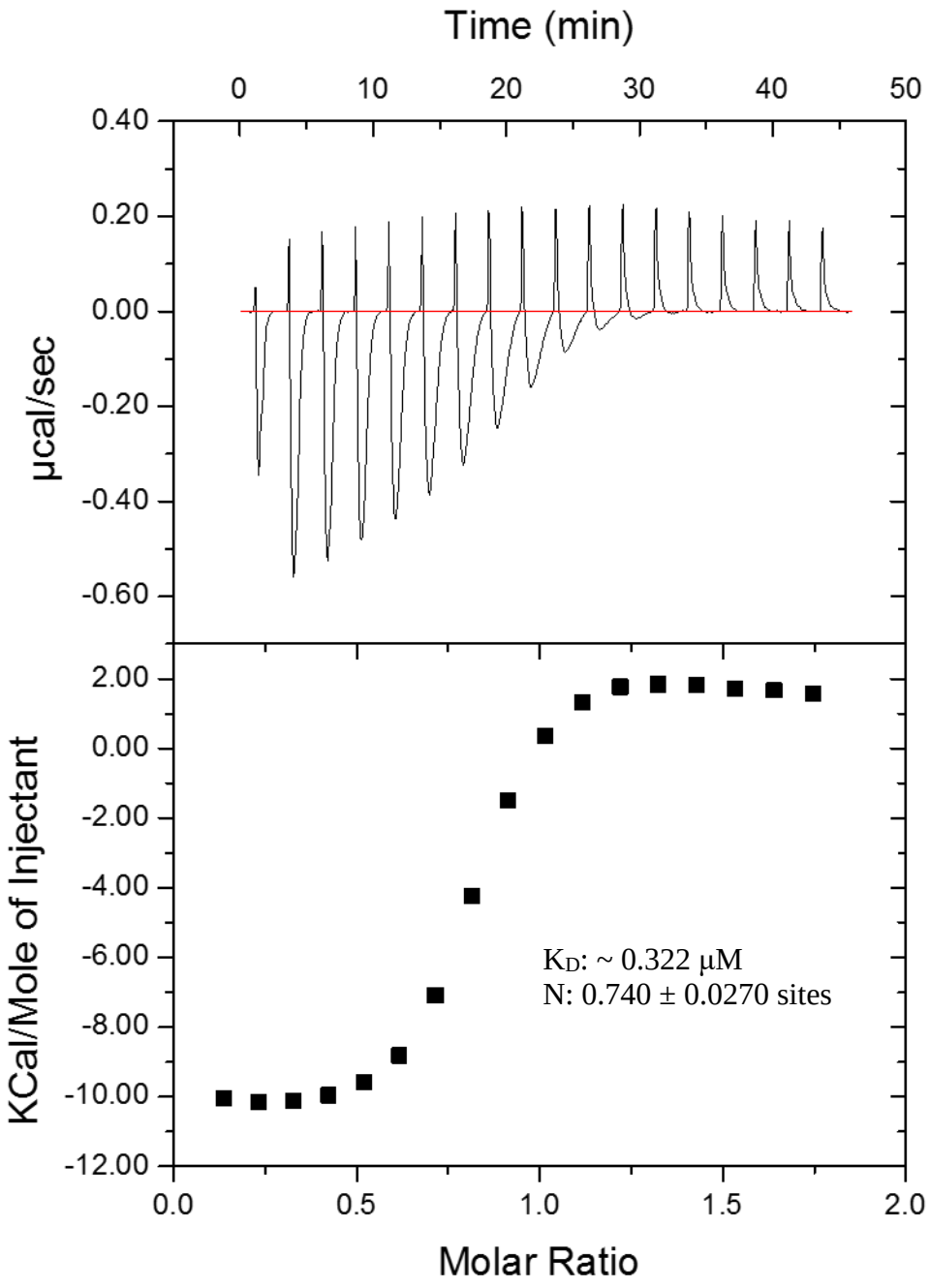

Figure 3.6: Isothermal titration calorimetry result showing the interaction between PFLU_1582 and cdG. Data collected is shown on the top and the affinity fit on the bottom. The K_D was calculated to be ~322nM and the stoichiometry of the interaction was calculated to be 1:1. MicroCal Origin software was used to fit a single-site fit model.

3.6). Through these experiments, the K_D of the PFLU_1582 interaction with cdG was determined to be ~322 nM. One molecule of protein was shown to interact with one molecule of cdG.

3. 3.5.3 Flagellum-specific ATP synthase FliI (PFLU_4436)

The next protein tested was the flagellar ATPase PFLU_4436. PFLU_4436, or FliI, is a well-conserved protein among flagellated microorganisms, which forms hexamers at the base of the bacterial flagellum and hydrolyses ATP to provide the system with the initial energy required for the export of proteins through the flagellum export gate.

PFLU_4436 was purified in high amounts and purity (Figure 3.7- A). It was first tested with DRaCALA, where an inner binding ring was formed, indicating cdG binding (Figure 3.7- B- III). However, no shift in the melting temperature of the protein was observed in DSF (Figure 3.7- C) and also no change in the size of the protein was seen in GSA (Figure 3.7- D).

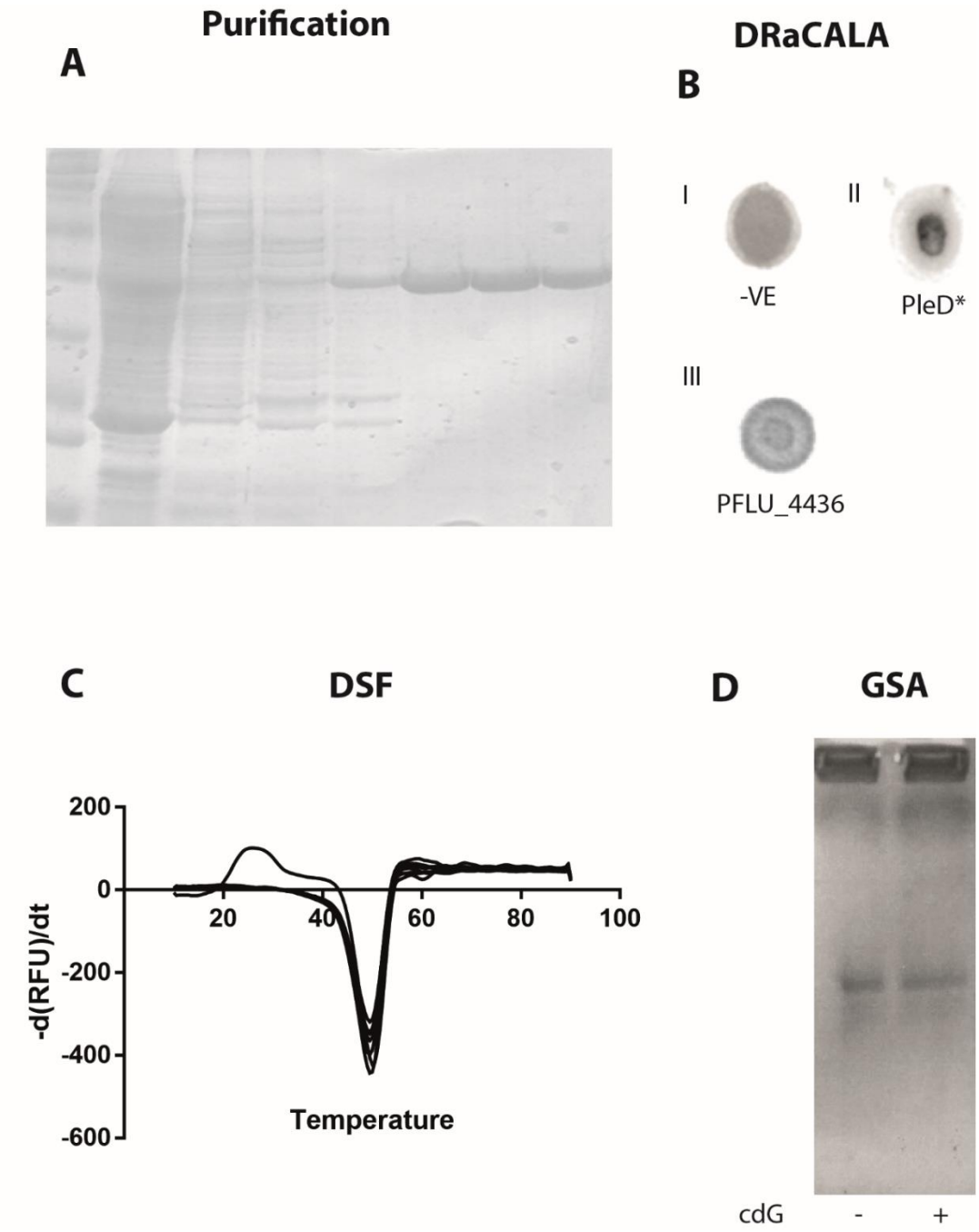

Figure 3.7: Purification and analysis of PFLU_4436 for cdG binding. A. Protein purification fractions. The protein was purified using an FPLC-AKTA system to high quantities and extra purity. B. DRaCALA assay, I. Negative, non-binding control, II. PleD binding spot (3 μM), III. PFLU_4436 binding spot (2.5 μM) C. Differential Scanning Fluorimetry (DSF). No change in the melting temperature of the protein was observed upon the addition of increasing concentrations of cdG (0 μM, 1 μM, 3 μM, 10 μM, 30 μM, 100 μM, 300 μM and 1 mM). D. Gel shift assay (GSA), upon the addition of 100 μM of cdG, no shift in the size of the protein was observed.*

Similarly to PFLU_1582, and based on the positive DRaCALA result, the PFLU_4436 protein was examined further by ITC to confirm binding and find out more about the nature of the dinucleotide interaction (Figure 3.8).

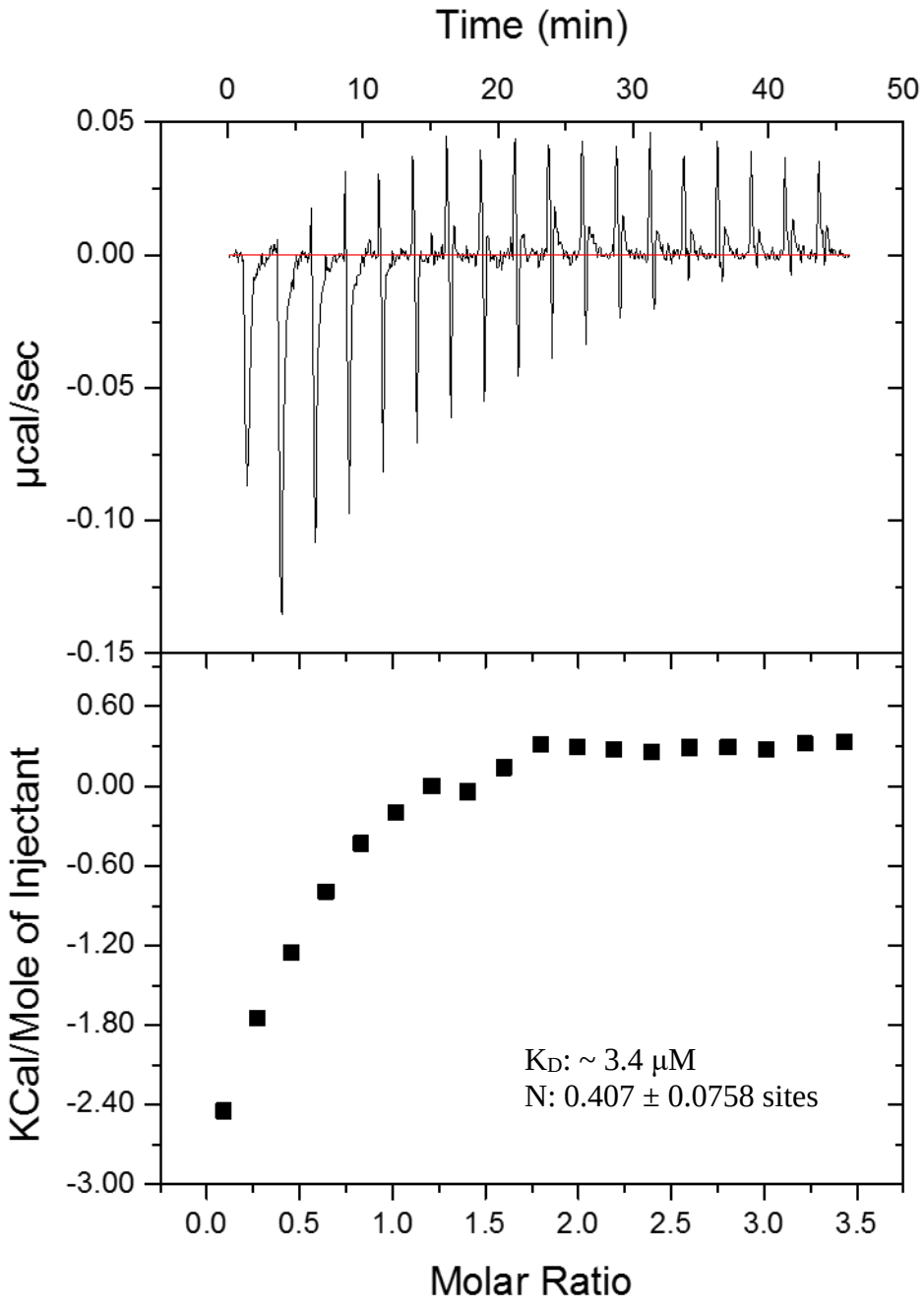

Figure 3.8: Isothermal titration calorimetry result showing the interaction between PFLU_4436 and cdG. Data collected is shown on the top and the affinity fit on the bottom. The K_D was calculated to be ~3.4 µM and the stoichiometry of the interaction was calculated to be 2:1. MicroCal Origin software was used to fit a single-site fit model.

The K_D of PFLU_4436 (FliI) interaction with cdG was determined to be ~3.4 μM. The stoichiometry of the reaction was calculated to be N~ 0.4. This stoichiometry either implies that two molecules of the protein are needed for binding of 1 molecule of cdG (assuming that N is closer to 0.5), or that the binding happens in a 3:1 protein: cdG ratio (assuming that N is closer to 0.3). A possible interprantation is discussed at the end of this chapter.

3. 3.5.4 False positive targets- Isocitrate dehydrogenase (PFLU_3809)

Although the proteins described above were proven to be positive binding targets, this was not the case for all of the initially selected proteins. PFLU_0001, PFLU_4401, PFLU_4531, PFLU_4895, PFLU_6126 as well as PFLU_3809, were shown to be false positives (more examples in Appendix 1). For instance, although PFLU_3809 (isocitrate dehydrogenase), came up in the capture compound screen as a strong positive target, when tested with DRaCALA, DSF and GSA, we saw no indication of cdG binding (Figure 3.9).

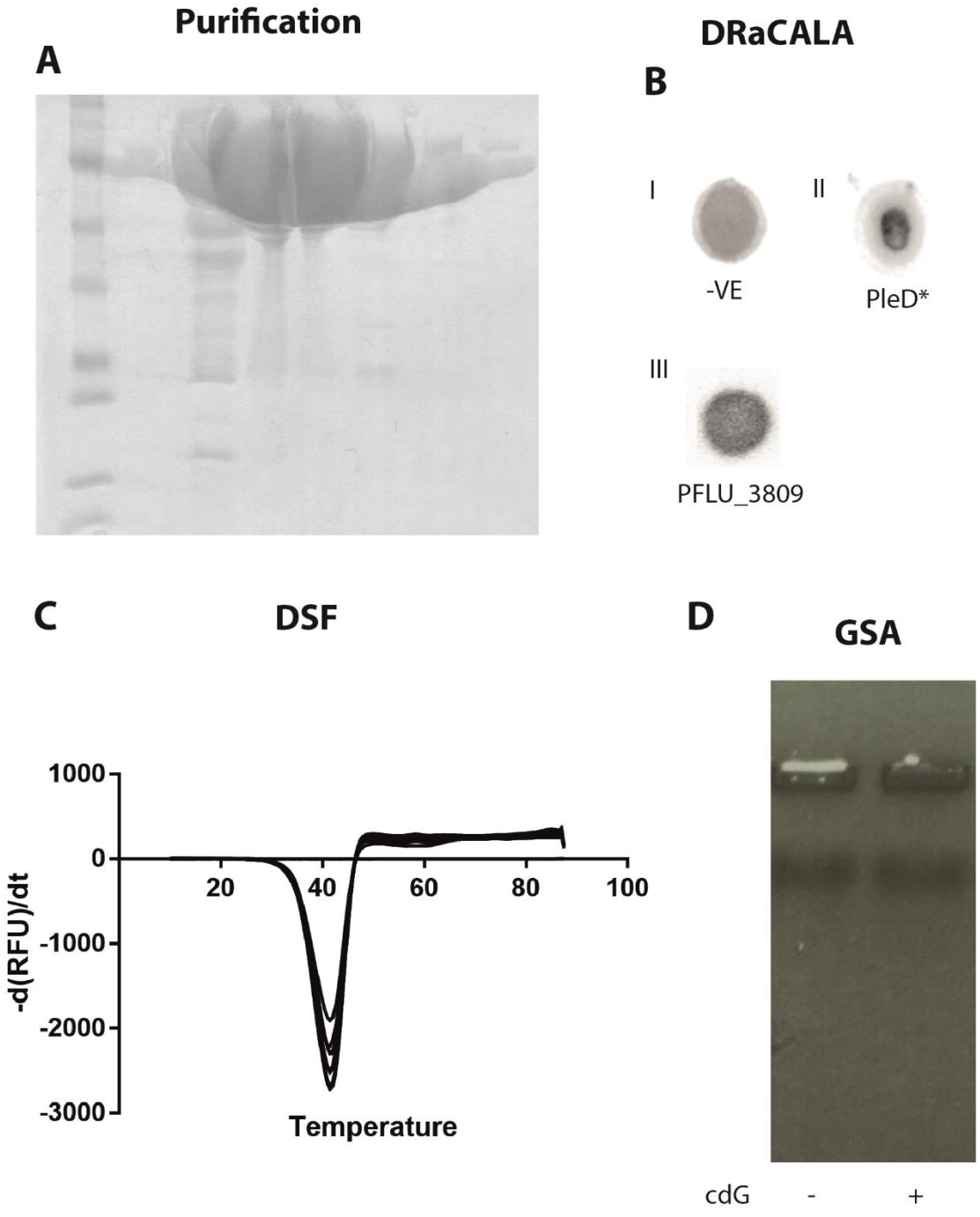

Figure 3.9: Purification and analysis of PFLU_3809 for cdG binding. A. Protein purification fractions. The protein was purified using an FPLC-AKTA system to high quantities and extra purity. B. DRaCALA assay, I. Negative, non-binding control, II. PleD binding spot (3 μM), III. PFLU_3809 spot (25 μM), not binding was observed. C. Differential Scanning Fluorimetry (DSF). No change in the melting temperature of the protein was observed upon the addition of increasing concentrations of cdG. D. Gel shift assay (GSA), upon the addition of 100 μM of cdG, no shift in the size of the protein was observed.*

3.4 Discussion

CdG has been known to function as a second messenger for many years. However, it has recently become apparent that its importance to bacterial behaviour is broader than initially thought. This small molecule has been associated with changes in bacterial lifestyle, lipo/exopolysaccharide production and virulence but recently it has also been linked to unexpected functions such as the control of *Streptomyces* development (238). To further unravel its importance in bacteria, it is essential to identify novel cdG binding targets in the cell. To do so, *Pseudomonas fluorescens* SBW25 was selected as a model organism for the identification of novel cdG targets. *P. fluorescens* is a biocontrol agent, which promotes plant growth by fighting pathogenic microorganisms in the soil, and by secreting growth hormones and other beneficial molecules.

To identify novel cdG binding proteins in *P. fluorescens*, a series of pull-down experiments were carried out based on the cdG capture compound screen, initially developed by the Jenal group (249). By carrying out the capture compound screen in multiple conditions, many potential cdG targets were identified. However, it was essential for these proteins to be tested further by biochemical tools to confirm binding to cdG. To do so, the potential targets were cloned, overexpressed and purified in *E. coli* and tested using various biochemical assays. The first assay used was the capillary-action radiolabelled assay, DRaCALA. The reason for selecting this assay first was because of its simplicity and its speed. DRaCALA simply involves the incubation of radiolabeled cdG with the protein of interest, or even with whole cell lysates overexpressing the protein of interest before spotting onto a nitrocellulose membrane. Being a quick and easy method for the identification of cdG binding proteins, this assay was the ideal initial screening tool to test multiple potential binding candidates. Unfortunately, after testing multiple proteins of interest, it became evident that results obtained with the DRaCALA assay

were inconsistent and prone to false negative results. For these reasons, it was necessary to test the potential targets using alternative biochemical assays, in order to give more reproducible and consistent results and to support the initial DRaCALA data. One of the assays selected was DSF, a straightforward and precise assay producing consistent and reproducible results. DSF gives information about potential alterations in the conformation of the protein, and as a result its melting temperature (T_m), upon the addition of increasing concentrations of cdG. Although DSF is a valuable tool for the indirect identification of protein-ligand interactions, getting positive results from this assay requires the addition of the ligand, in this case, cdG, to have a direct effect on the conformation of the protein and as a result to cause a change in melting temperature. Unsurprisingly, not every protein-ligand interaction leads to an alteration in the protein folding and as a result, getting a negative result in DSF doesn't mean that the protein does not interact with the ligand of interest.

Both DRaCALA and DSF are simple, rapid assays that act as a first indication to confirm cdG binding. However, these methods are both highly dependent on the nature of the interaction of the protein with cdG. Based on the idea that an interaction between cdG and the potential binding proteins will lead to a multimerization effect of the protein or a change in folding that would cause it to behave differently in a native gel environment, native gel shift assays were proposed as an alternative binding test. However, no changes in the multimerization state of the protein were observed for any of the proteins tested, so this method was not pursued further. An easier and simpler assay, which was optimised for the proteins of interest was the Gel Shift Assay (GSA), an assay conducted in agarose gels. The aim of this assay is similar to the Native gel assay. However, it produces more consistent and reproducible results, in a shorter time than native gels.

PleD* was used as a positive control in all these experiments. This protein is a response regulator, which is required for the pole development of *Caulobacter crescentus* during its cell cycle (82). During the *Caulobacter* cell cycle, PleD is specifically localised to one pole of the cell, a procedure which is coupled by the activation of the C-terminal GGDEF domain of the protein via the phosphorylation of its N-terminal domain (284). As a cyclase, PleD* binds cdG with a high affinity and it is well reported that the condensation of GTP to cdG requires the dimerization of the protein (287), making this a highly suitable positive control.

All the assays described above worked nicely for the initial stages of testing as they are quick and easy and give multiple options for testing a number of proteins simultaneously in various different conditions. However, they do not provide any information about the nature of the interaction between the protein and cdG, or the affinity of binding. To further characterise proteins of interest, several other tools were employed to more closely probe the nature of the cdG-interaction. The first of these was Isothermal Titration calorimetry (ITC), which allowed the determination of a cdG binding affinity for PFLU_1582 in the low μM range (~0.322 μM). ITC was also used to confirm further and characterise cdG binding to PFLU_4436. In this case, the K_D of the reaction was a little higher than for PFLU_1582, but was again in the low μM range (~3.4 μM), well within the range of physiologically relevant binding affinities (288). The stoichiometry of the reaction was calculated to be ~0.4. This value can either represent a stoichiometry of 3:1 protein: cdG, if closer to 0.3 or a stoichiometry of 2:1 protein: cdG if closer to 0.5. There are a variety of reasons why the exact value could not be calculated. For example, changes in the conformation and multimerisation state of the protein upon the addition of cdG may introduce a consistent inaccuracy in the data, making it impossible to calculate the physiological value. It seems more probable that binding happens in a 2:1 ratio, as FliI *in vivo* is frequently present as a dimer; the only possible ratios for binding to this form

being 1:1 or 2:1 (289). Although ITC provides lots of information about the nature of the interaction, it has high concentration requirements for both protein and ligand. For this reason, it is not an ideal method to examine unstable or low-abundance proteins. This was a factor for PFLU_4436, which easily precipitates in high concentrations, making it tough to test and produce consistent results for this protein with ITC.

After testing all the proteins described in this chapter, PFLU_4436 (FliI) was selected for more detailed analysis. FliI represents an exciting and highly important new cdG target, with implications for both the survival and the control of pathogenicity of pseudomonads. Although no effects were observed for FliI in the conformation change based assays (Figure 3.6- B, C, and D), the DRaCALA binding result was strong and consistent, and the initial positive ITC results were encouraging enough to warrant further analysis of this protein.

All the proteins tested are summarised in the following table (Table 3.2).

Table 3.2: List of proteins tested for cdG binding and outcome in different assays. (+) indicates a positive outcome, (-) indicates a negative outcome. Absence of a (+)/ (-) symbol indicates that the protein was not tested with the specific assay. Positive cdG binders are highlighted in bold.

Locus	Name	DraCALA	DSF	GSA	N-PAGE	ITC	Outcome
PFLU_0001	DnaA	-	-		-	-	Negative
PFLU_0463	**-**	+	+	+	-		**Positive**
PFLU_1582	**PilZ**	**+**	**+**	**+**	**-**	**+**	**Positive**
PFLU_3809	-	-	-	-	-	-	Negative
PFLU_4320	-	-	-	-	-		Negative
PFLU_4401	-	-	-	-	-		Negative
PFLU_4436	**FliI**	**+**	**-**	**-**		**+**	**Positive**
PFLU_4531	-	-	-		-		Negative
PFLU_4622	-	-	-		-		Negative
PFLU_4895	-	-	-	-			Negative
PFLU_6126	ParB	-	-	-	-		Negative

Chapter 4:

FliI binding, characterisation and universality

Chapter 4: FliI binding to cdG, characterisation and universality

4.1 Introduction

The bacterial flagellum is one of the most important organelles for efficient host colonization by both commensal and pathogenic species. *P. fluorescens* flagella-mediated motility is crucial during both the initial stages of plant root colonization as the flagellum helps the bacterium to move through the soil towards plant roots, and during later stages where the bacterium colonizes plant surfaces, and further migrates into the apoplastic space (15).

Assembly of the bacterial flagellum is a complex process starting from the export of extracellular subunits via the flagellum export gate (28,37,290). The AAA+ ATPase FliI interacts with FliH and FliJ and forms the soluble, cytosolic fraction of the flagellum machinery (67,291). FliI and FliH associate in a heterotrimer ($FliH_2$-FliI) in *vivo*, which acts as a chaperone for the transfer of substrates from the cytoplasm to the flagellum export gate. There, FliI forms a hexameric ring and hydrolyses ATP to provide the initial energy required for export via the flagellum gate (68). Although it is well reported that the majority of the energy needed for flagellum formation is provided by the proton motive force (PMF), FliI ATPase activity is essential for the initiation of the export process (292,293).

FliI is a very well-conserved protein among different bacterial species, characterised by homologs in every bacterium species equipped with a flagellum. FliI homologs are found in major plant pathogens such as *Pseudomonas syringae,* major human pathogens such as *Salmonella enterica pv typhimurium* and plant symbionts such as *Sinorhizobium meliloti*. In addition to FliI homologs in different species, FliI has well-conserved

orthologs in different export systems, such as the closely related Type III secretion system (T3SS) and even the more distantly related Type VI secretion system (T6SS). Although FliI orthologs among these systems do not share huge similarities, they all form hexamers or even dodecamers at the cytoplasmic basal body of the organelle, and have the same broad function; to catalyse the hydrolysis of ATP to provide energy for the initial export of substrates.

CdG has been linked several times with the regulation of the bacterial flagellum. For example, the expression of the flagellar gene cluster is controlled by the cdG-binding transcriptional regulator FleQ (84,87). The control of flagella function has also been associated with cdG, which binds to YcgR and FlgZ, basal body-associated proteins, leading to reduced flagellar rotation speed in both *Escherichia coli* and *Pseudomonas putida*, respectively (231,282).

The flagellar export ATPase FliI (PFLU4436), was among the proteins positively identified in the capture compound screening experiment and subsequently confirmed as a cdG binding protein with a K_D in the low micromolar range. Due to its widespread nature, and the importance of *Pseudomonas* colonisation and infection, FliI was selected from the binding targets identified in chapter 3, and subjected to in-depth biochemical analysis.

After having confirmed cdG binding by DRaCALA and ITC, Surface Plasmon Resonance (SPR) was used to further characterise the interaction. SPR is an assay using biotinylated cdG immobilised on a streptavidin chip to monitor changes in the resonance of the system upon the addition of the protein of interest. When the protein is a positive binder, the addition of increasing levels of the protein should result in higher responses until a saturating level is achieved. The responses are then plotted against the injected

concentrations of protein, and an affinity curve is formed, giving more information about the stoichiometry of the reaction.

4.2 Aims

1. To biochemically characterise the interaction between cdG and FliI.
2. To examine the extent to which cdG binding is conserved among FliI proteins from different bacterial species, and orthologs in different secretion systems.
3. To determine the effect of cdG binding on the ATPase activity of FliI.

4.3 Results

4.3.1 Biochemical characterisation of FliI-cdG binding

4.3.1.1 Confirmation of FliI binding by DRaCALA

To further characterise the interaction between FliI and cdG, a set of assays was used with the aim to produce more consistent and reproducible results. To complement the previously results, a DRaCALA assay was performed using a series of different concentrations of FliI assayed against a stable concentration of cdG. As shown in Figure 4.1, the higher the concentration of FliI, the more pronounced the binding results were seen for cdG. To confirm that the results obtained with DRaCALA are specific to cdG, the experiment was repeated with radiolabelled GTP and no binding was observed (Figure 4.1).

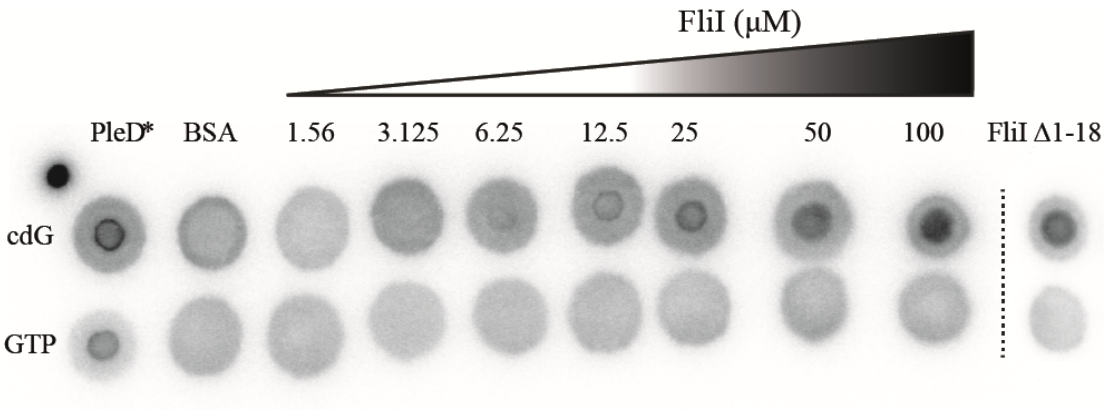

Figure 4.1: DRaCALA FliI titration experiment, FliI full length was added in raising increasing concentrations in the assay with a stable radiolabelled-cdG concentration at 4nm. Radiolabelled GTP was also included in the assayed but gave no positive binding for FliI. Positive (10 μM PleD) and negative (10 μM BSA) binding controls were included. FliI lacking the first 18 amino acids ($FliI_{\Delta 1-18}$) was also included in the assay (10μM) giving a positive binding spot for cdG but not for GTP. Figure adapted from (326).*

To overcome the problem of FliI protein aggregate formation, a truncated version of the protein lacking the first 18 amino acids was produced. This modification affects FliI multimerization, with the truncated allele unable to form hexamers *in vitro* (294).

4.3.1.2 FliI binding to cdG is specific

To further complement these results, a variety of nucleotides (cyclic di-GMP, ADP, ATP, NADH, cAMP, cGMP, and cyclic di-AMP), some of which closely resemble the cdG structure, were added to the DRaCALA assay to try and outcompete cdG binding. As shown in Figure 4.2, cdG was only out-competed when cold cdG was added. In any other case, no effect on the binding pattern was observed. To complement these results, a pull-down experiment, using the chemically modified cdG used in the capture compound screen, was carried out in parallel. This was incubated with the purified FliI protein, and various nucleotides were added to the mix (cyclic di-GMP, NADH, ADP, ATP, cAMP, cGMP, and cyclic di-AMP) to outcompete the capture compound. The same procedure used for the capture compound screen was followed, starting with normalised concentrations of the protein. After washing the unbound proteins off the capture compound, the samples were analysed on an acrylamide gel. The results were in agreement with the DRaCALA results, showing that competition is only present in the case of externally added cdG.

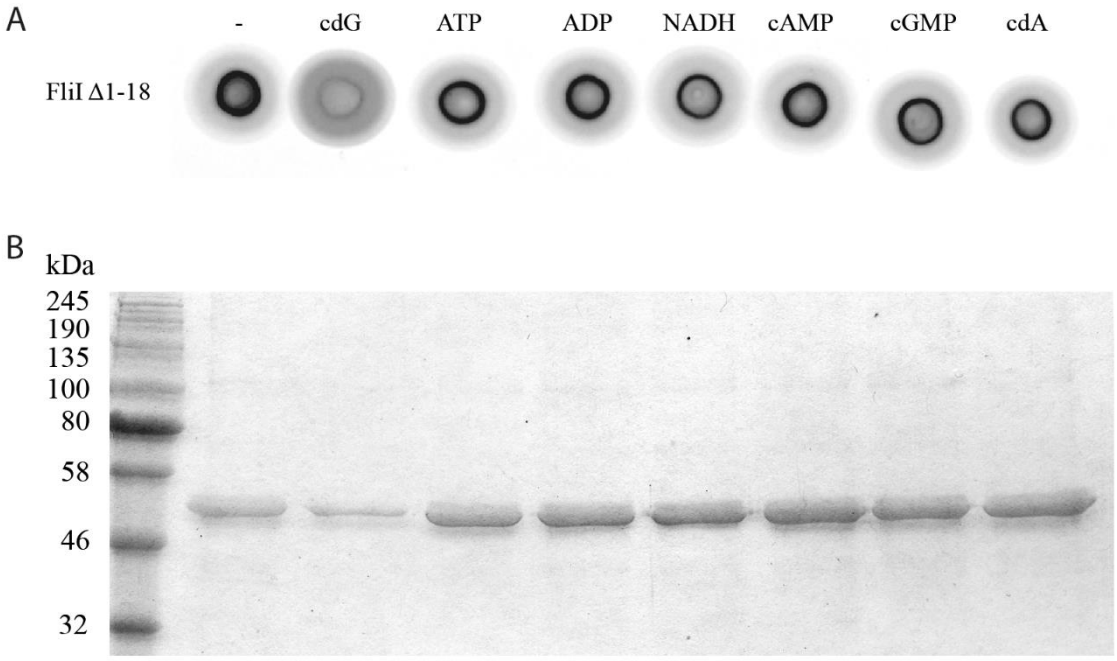

Figure 4.2: A. DRaCALA competition experiment performed on $FliI_{\Delta 1-18}$. A variety of nucleotides were included in the reaction to test the specificity of cdG binding. ***B.*** *SDS-PAGE gel showing protein bound to the capture compound after pre-incubation with different nucleotides. Figure adapted from (326).*

4.3.1.3 Testing the FliI-cdG interaction using Surface Plasmon Resonance (SPR)

As described in chapter 1, ITC was initially used to define the biochemical parameters of cdG binding to FliI. This technique showed tight cdG binding with a K_D of ~3.4 μM. However, it was not possible to refine the ITC protocol sufficiently to produce reproducible data. Consequently, surface plasmon resonance (SPR) was employed, producing positive, tight binding data with a K_D of 2.4 ± 0.2 μM (Figure 4.3).

Having confirmed that full-length FliI binds to cdG, the $FliI_{\Delta 1\text{-}18}$ allele was purified and tested for binding, resulting in a positive DRaCALA result (Figure 4.1) and an even tighter binding affinity (K_D: 0.8 ± 0.03 μM) when tested in SPR (Figure 4.4).

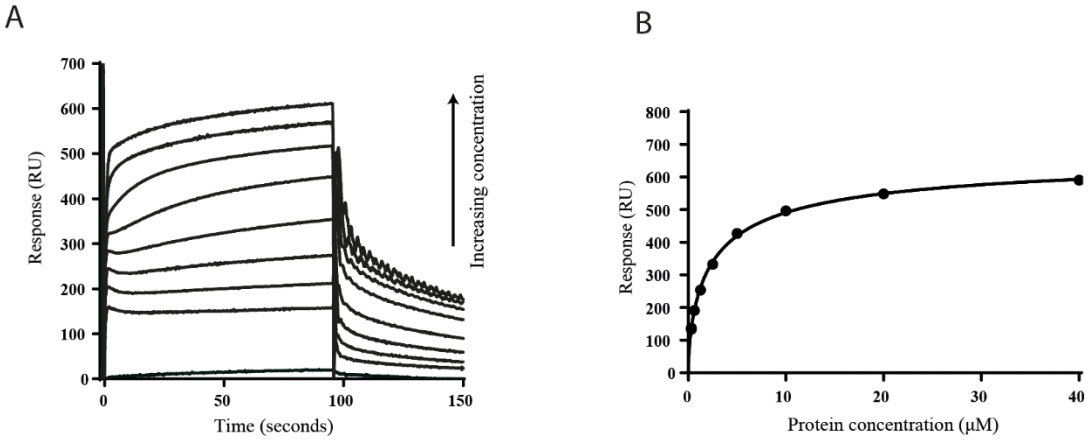

Figure 4.3: A. SPR sensorgrams showing affinity measurements for FliI full-length protein binding to biotinylated cdG. A range of FliI concentrations was used (0.312, 0.625, 1.25, 2.5, 5, 10, 20, and 40 μM), with three concentration replicates per concentration, included as appropriate. Buffer only and BSA were included as negative controls. B*. Affinity fit for FliI-cdG binding. The binding response for each concentration was recorded 4 s before the end of the injection. The* K_D *values for FliI binding to cdG (2.4 ± 0.2 μM) were calculated using by GraphPad Prism. Figure adapted from (326).*

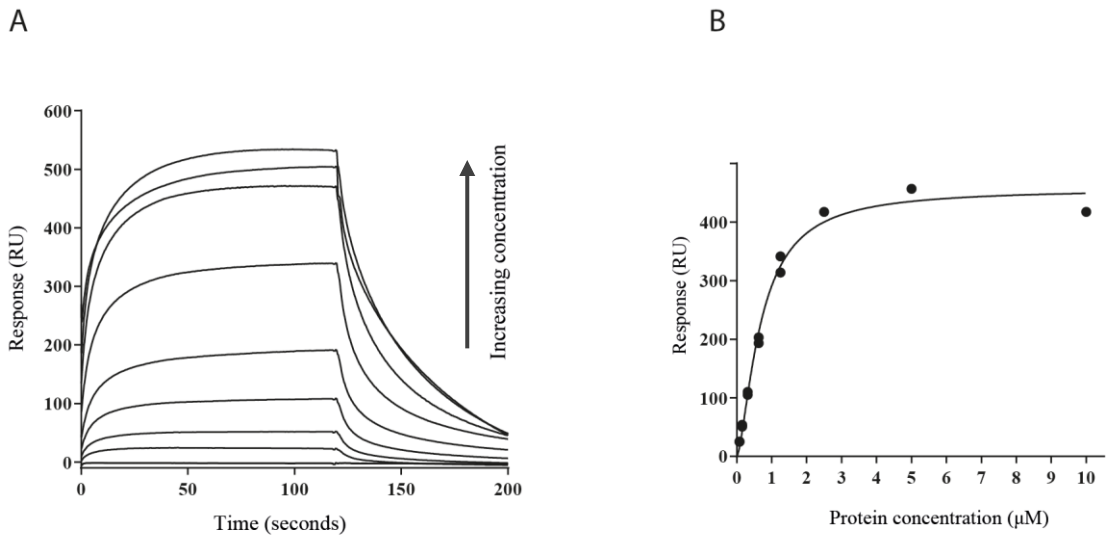

Figure 4.4: A. SPR sensorgrams showing affinity measurements for FliI$_{\Delta 1–18}$ binding to biotinylated cdG. A range of protein concentrations was used (0.078, 0.156, 0.3125, 0.625, 1.25, 2.5, 5, and 10 μM with three concentration replicates per concentration, included as appropriate. Buffer only and BSA were included as negative controls. ***B.*** *Affinity fit for FliI$_{\Delta 1–18}$-cdG binding. Binding responses were measured 4 s before the end of the injection, and the K_D values for FliI$_{\Delta 1–18}$ binding to cdG (0.8 ± 0.03 μM) were calculated by GraphPad Prism. Figure adapted from (326).*

4.3.2 FliI –cdG binding universality

4.3.2.1 FliI homologs from other species

To examine the degree of conservation among FliI proteins from different bacterial species, The FliI homologs from *Pseudomonas syringae*, *Salmonella enterica pv* typhimurium, and *Sinorhizobium meliloti* were selected for examination by SPR. If these diverse homologs bind to cdG, this will go a long way towards establishing this interaction as a universal trait among flagella. The *fliI* genes from the three species were

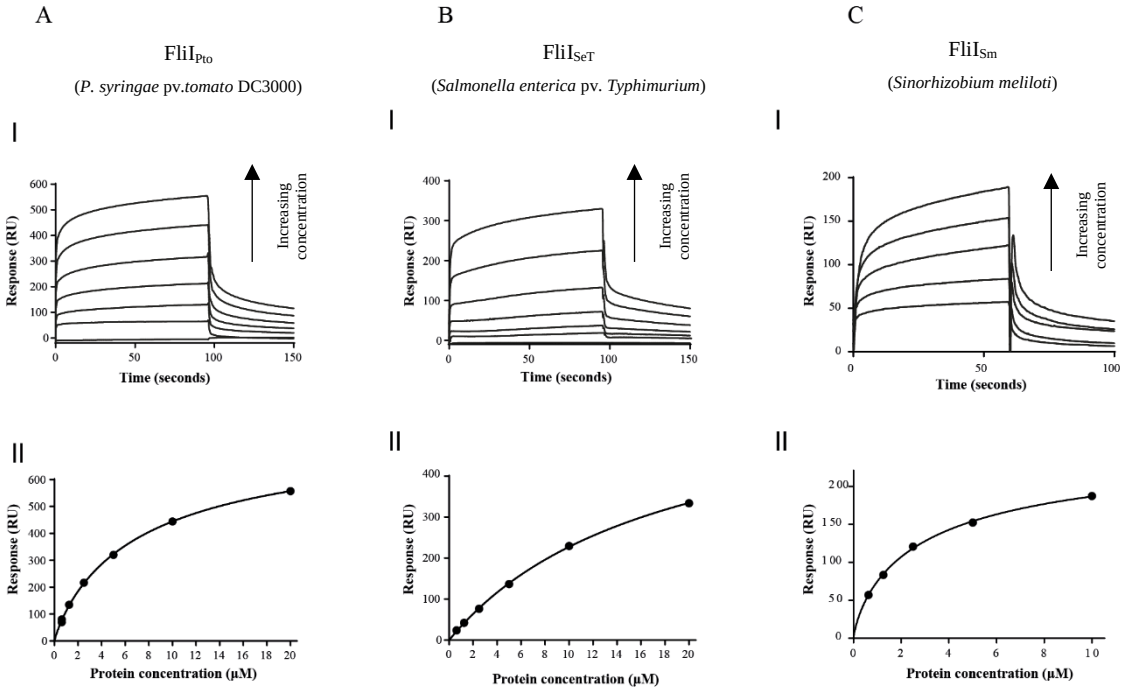

Figure 4.5: A- I, A-II, SPR sensorgrams and resulting affinity fit for FliIPto binding to biotinylated cdG. B-I and B-II, SPR sensorgrams and affinity fit for FliISeT binding to biotinylated cdG. C-I and C-II, SPR sensorgrams and affinity fit for FliISm binding to biotinylated cdG. In all three cases, a range of protein concentrations was used (0.625, 1.25, 2.5, 5, 10, and for FliIPto/FliISeT 20 μM) with three concentration replicates per concentration, included as appropriate. Buffer only and BSA were included as negative controls. The protein binding and dissociation phases for all sensorgrams are shown. For the affinity fits, binding responses were measured 4 s before the end of the injection, and K_D values for each protein were calculated by GraphPad Prism. Figure adapted from (326).

cloned into overexpression vectors, and the proteins were overexpressed, purified and analysed by SPR. In each case, this resulted in positive binding results (Figure 4.5).

4.3.2.2 FliI orthologs from the type III and type VI secretion systems

Next, FliI orthologs from the T3SS as well as the T6SS were selected and tested for binding. More specifically, the T3SS ortholog HrcN from *P. syringae* DC3000 and the T6SS ortholog ClpB2 from *P. fluorescens* SBW25 were chosen. Once again, the genes encoding the proteins of interest were cloned, purified and subjected to SPR analysis.

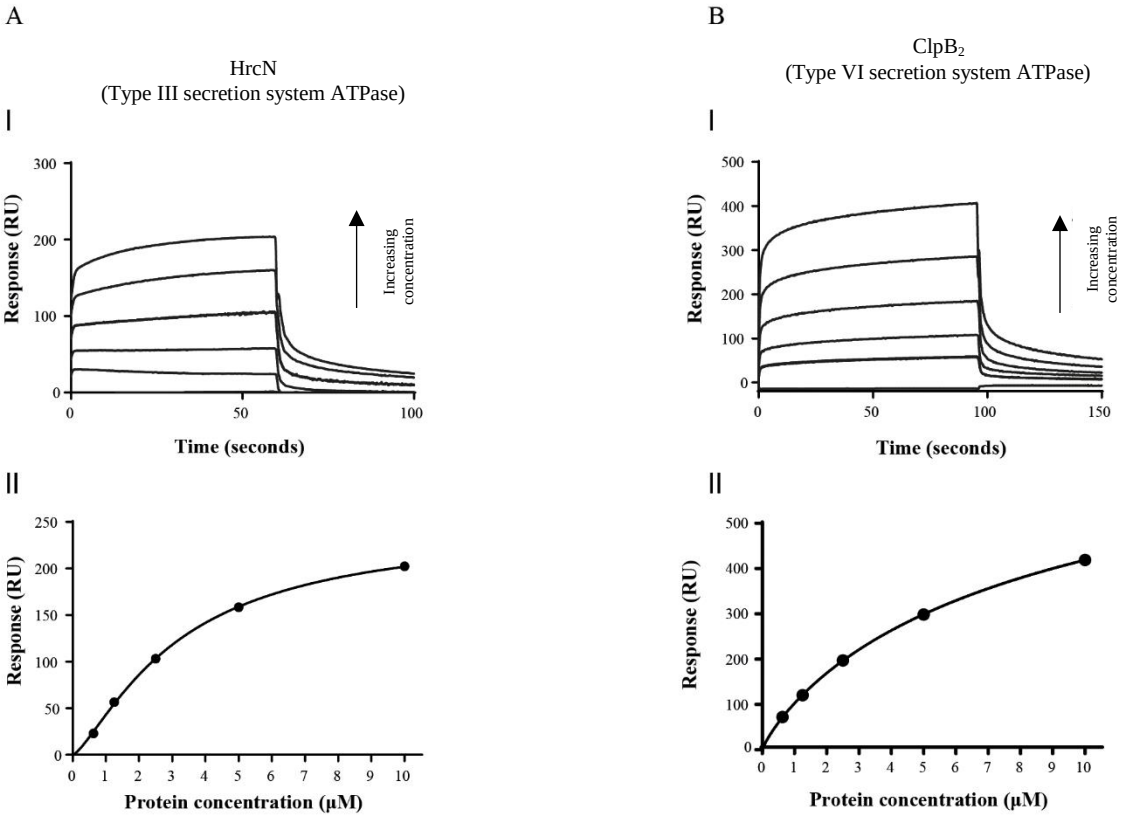

Figure 4.6: A-I and A-II, SPR sensorgram and resulting affinity fit for HrcN (type III export ATPase) binding to biotinylated cdG. B-I and B-II, SPR sensorgram and resulting affinity fit for ClpB2 (Type VI export ATPase) binding to biotinylated cdG. In both cases, a range of protein concentrations was used (0.625, 1.25, 2.5, 5, and 10 μM), with three concentration replicates per concentration, included as appropriate. Buffer only and BSA were included as negative controls. The protein binding and dissociation phases for all sensorgrams are shown. For the affinity fits, binding responses were measured 4 s before the end of the injection, and K_D values for each protein were calculated by GraphPad. Figure adapted from (326).

Tight, concentration-dependent binding to cdG was confirmed by SPR in each case (Figure 4.6).

4.3.3 FliI activity and the role of cdG

4.3.3.1 CdG binding inhibits ATPase activity

FliI and its orthologs are active ATPases in the cell, being responsible for the hydrolysis of ATP when associated with the export gate of the flagellum or the base of the T3SS / T6SS. To test the effect of cdG addition on the activity of these enzymes, the pyruvate kinase/ lactate dehydrogenase (PK/LDH) linked assay was used. It was observed that FliI is an active ATPase (with a V_{max} at 1262 ± 54.46 nmol ATP/min/mg), characterised by a sigmoidal ATPase activity curve, which could potentially indicate cooperative binding of ATP. Addition of 50 μM cdG resulted in a significant drop in FliI ATPase activity (V_{max} dropped noticeably at 867.2 ± 51.65 nmol ATP/min/mg) (Figure 4.7).

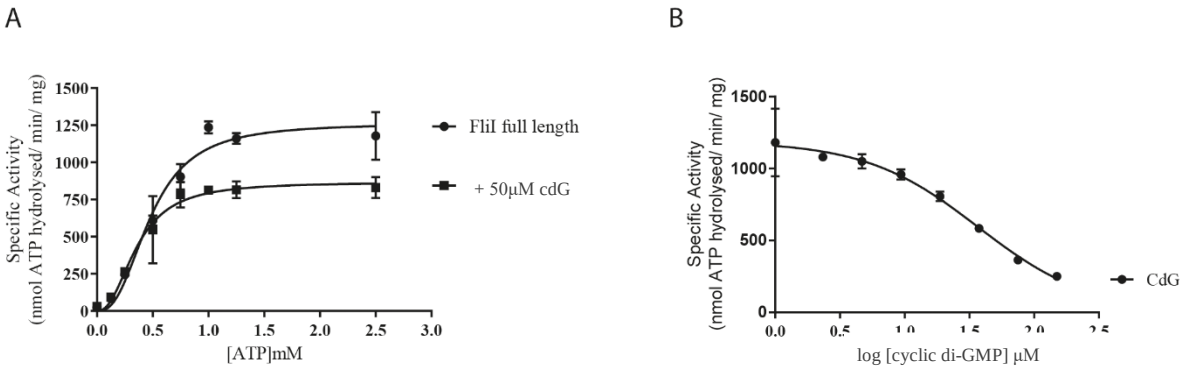

Figure 4.7: A, ATPase activity for FliIHis ± 50 μM cdG. FliIHis specific activity (nmol ATP hydrolysed/min/mg protein) is shown under increasing ATP concentrations. CdG addition causes a decrease of the Vmax of FliIHis ATPase activity. B, IC_{50} curve for FliIHis ATPase activity upon addition of increasing cdG concentrations. A constant concentration of ATP (1 mM) was included alongside 1 μg of FliIHis protein. Figure adapted from (326).

In order to evaluate the scale of the inhibition observed, a cdG titration was conducted for the ATPase assay and the IC_{50} value for the competition calculated (Figure 4.7). The

ATPase activity of FliI was progressively inhibited by rising concentrations of cdG, and the IC_{50} of the interaction was calculated to be 36.7 ± 1.13 μM (Figure 4.7).

Following the ATPase results for FliI, the T3SS protein HrcN was selected for further analysis. HrcN was active in solution giving a V_{max} of 1183 ± 68.2 nmol ATP/min/mg. Upon the addition of 50 μM of cdG a similar reduction in activity to FliI was observed (to 832.4 ± 119.7 nmol ATP/min/mg (Figure 4.8). A cdG titration experiment was then performed to characterise the interaction further and led to an IC_{50} calculation of 25.11 ± 1.14 μM.

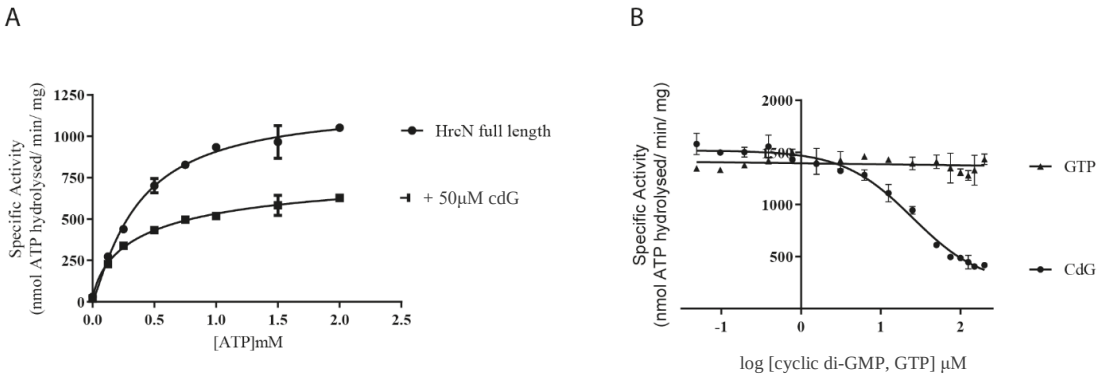

Figure 4.8: A. ATPase activity for HrcN ± 50 μM cdG. HrcN specific activity (nmol ATP hydrolyzed/min/mg protein) is shown under increasing ATP concentrations. CdG addition causes a decrease of the Vmax of HrcN ATPase activity. ***B.*** *IC_{50} curve for HrcN ATPase activity upon addition of increasing cdG concentrations. A constant concentration of ATP (1 mM) was included alongside 1 μg of HrcN protein. The IC_{50} curve also includes results for GTP titration showing no ATPase inhibition. Figure adapted from (326).*

4.3.3.2 ATPase activity and cdG-binding can be decoupled

Following the ATPase inhibition results, the question to be addressed was whether cdG binding occurs at the same site as ATP, and if so, does cdG-binding competitively inhibit ATPase activity? To test this, the residue positions essential for the ATPase activity (Walker A motif positions G176 and K181 and the Walker B motif position D265) were mutated by overlap extension mutagenesis. The mutated genes were cloned in pETNdeM-

11 expression vector and were overexpressed. The proteins were purified and tested for both ATPase activity and cdG binding. Their activity was tested using the PK/LDH linked assay, and cdG binding was tested by SPR (Figure 4.9).

The results obtained showed that whereas in the K181A and D265A mutants, the ATPase activity was completely abolished, the mutants still bound to cdG with affinities close to the WT. In the case of G176A (a mutant not essential for ATPase activity), a small drop in the ATPase activity was observed, whereas the affinity curve produced by SPR was indicative for non-specific binding (Figure 4.9).

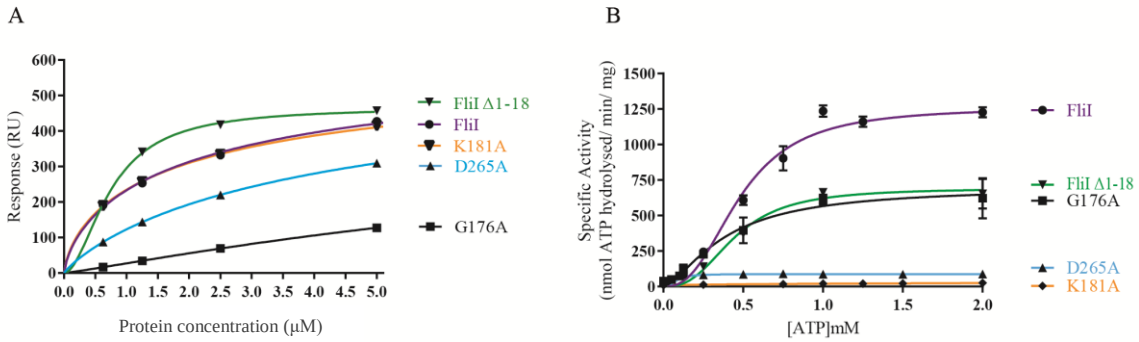

Figure 4.9: A, Affinity fit for cdG binding to different FliI alleles (FliI$_{His}$, Δ1–18, K181A, D265A, and G176A). Sensorgrams obtained using biotinylated cdG were used to calculate the K_D values for FliI binding to cdG. At each protein concentration, the responses were recorded 4s before the end of the injection. ***B,*** *ATPase activity for different FliI alleles. Protein specific activity in each case (nmol ATP hydrolyzed/min/mg protein) is shown for increasing ATP concentrations. Figure adapted from (326).*

4.4 Discussion

In this chapter, I provide further evidence that the second messenger cdG binds to the bacterial flagellum export ATPase FliI. Binding was confirmed by surface plasmon resonance and shown to occur in the same physiological range as other characterised cdG binding proteins. Binding specificity was confirmed by two independent competition assays, providing evidence that binding is not only tight but is also highly specific to cdG.

FliI is a protein that naturally forms dimers, hexamers or even higher order complexes in solution. This effect is even more pronounced at higher concentrations of the protein and leads to a non-uniform solution making it hard to use the full-length protein for analytical biochemistry. To overcome this problem, a truncated version of the protein lacking the first 18 amino acids was produced. It is well reported that the N-terminal end of the protein is responsible for the multimerization of the protein (294). As a result, the truncated version of FliI cannot form multimers and remains in a uniform, monomeric population in solution.

Having established SBW25 FliI binding to cdG, the next step was to test the universality of binding. FliI is a very well-conserved protein among different bacterial species, with homologs in every microorganism equipped with a flagellum. FliI homologs from multiple bacterial species were tested showing strong, concentration-dependent binding activity upon the addition of cdG in surface plasmon resonance. Excitingly, when the closely related type III secretion system ortholog HrcN from *P. syringae* DC3000 and the much more distantly related Type VI ATPase $ClpB_2$ from *P. fluorescens* SBW25 were tested, I was able to determine cdG binding at physiologically relevant (low micromolar) affinities in each case. These findings are a first indication that cdG may be involved in the direct regulation of export via the flagellar, the T3SS as well as the T6SS for a range of pathogenic and beneficial bacterial species.

To begin to unravel the role of the cdG interaction on protein function, the ATPase activity of both FliI and HrcN was measured to determine the effect of cdG on the enzymatic function of the protein. Interestingly in the case of FliI, the activity curve follows a sigmoid pattern, suggesting positive cooperative binding of ATP. This result implies that one molecule of ATP enhances the binding of the next molecule. It was also observed that the activity of both proteins is suppressed by the addition of cdG. In this respect, the relationship between cdG and the export ATPase proteins resembles binding to the transcriptional motility regulators FleQ and FlrA (87,245). These proteins are both active AAA+ ATPases and are known binders of cdG, which has been shown to bind close to the Walker A motif of the protein. However, this is apparently not the case for the export ATPases, as the ATPase activity could be effectively uncoupled from cdG binding. FliI/HrcN K181A (Walker A motif) mutants were shown to bind to cdG, in affinity levels close to the wild type but lost their ATPase activity, whereas the G176A mutant, although it showed severely compromised cdG binding, retained substantial ATPase activity.

Recent studies have shown that energy produced by the enzymatic activity of FliI is only required for the initial stages of export and the majority of the energy for protein export is provided by the proton motive force (293). My biochemical data shows that the ATPase activity of FliI and HrcN is suppressed in the presence of increased cdG levels. CdG may, therefore, exert a direct inhibitory effect on the export activity of these proteins. The allosteric suppression of AAA^+ ATPases by cdG would be consistent with the wider literature (87). The fact that the IC_{50} inhibition value is much higher than the expected cdG concentration in the cell (199), indicates that there may be a missing piece in this interaction. For instance, it is possible that the ATPase inhibition value may drop to a physiological range at the presence of one of FliI/ HrcN's protein partners in the cell. Another possibility is that maybe at a local level, cdG concentrations may reach a higher

level, that could be closer to the calculated IC_{50} value. To date, the highest reported concentrations of cdG levels in bacteria have been monitored to be in the low μM range (1-10μM) (199). However, at the moment it is impossible to monitor the local cdG concentrations in the cell to prove this point, due to the lack of a suitable method and the nature of the molecule itself (easily diffusible in the cytoplasm or bound to metabolising or receptor proteins).

The presence of FliI is essential for the efficient export of protein substrates through the flagellum and also plays a gatekeeper role, providing the basal body with the energy required to initiate protein export (292). At this stage, it is unclear what the biological role of cdG binding is in this system. Based on my results, which showed well-conserved FliI binding among diverse bacterial species with a relatively high affinity in each case (implying a regular interaction between cdG and the protein *in vivo*), I propose that cdG binding may play a very fundamental role in the control of flagellar function and assembly. For example, cdG binding may be required at a basal level for the initiation of protein export, perhaps via the promotion of multimerization or the imposition of rotational asymmetry to the FliI hexamer (295). It has been reported that basal levels of cdG are required for flagella synthesis in both *S. enterica* and *Caulobacter crescentus* (296,297). In both cases, deletion of all the cdG synthesis proteins resulted in a strain unable to produce cdG and led to the loss of flagella-driven motility. In the *Salmonella* cdG- strain, increased expression of flagellar basal body genes was observed, but the export of the flagellum filament subunit FliC was severely compromised (297). It is unclear at this point whether the mechanism of cdG control at the flagellum would be the same for the T3SS and the T6SS but considering that the two systems are reversely regulated (222) , it is unlikely for both to be controlled in the same way by cdG.

CdG has been associated with flagellar regulation at multiple levels of control. For instance, it is known that flagella gene expression in *Pseudomonas* sp. is controlled by FleQ, a known cdG binder, which binds to multiple flagellar loci. FleQ-cdG binding results in the abolition of flagella gene expression (84). Flagella rotation is also likely to be associated with cdG control in both *P. fluorescens* and *P. syringae*, which both contain close homologs to the *P. putida* flagellum brake protein, FlgZ (282). Swarming motility in *P. aeruginosa* is also a behaviour controlled by cdG interference with the two different stator complexes; MotAB and MotCD (298). Indirect effects on flagellar construction and motility are also caused by exopolysaccharide production and pili biosynthesis, which are both regulated by cdG (84,299–302).

CdG has also been associated with the control of the *P. aeruginosa* type III and type VI secretion systems. However the regulatory pathways, in this case, are less well understood. Studies have shown that cdG mediates the switch between the production of type III and the type VI secretion pathways by the sRNAs RsmY and RsmZ, via interactions with the small translational regulatory protein RsmA (222). RsmA controls the translation of both flagella and type III mRNAs in *P. aeruginosa* (220) and is part of a complex regulatory cdG signalling network (221,303).

Chapter 5:

Structural analysis of FliI and cdG binding site determination

Chapter 5: Structural analysis of FliI and cdG binding site determination

5.1 Introduction

In chapter 4, the relationship between the hexameric export ATPase, FliI and cdG was established. It was shown that cdG binds to FliI and its homologs, as well as FliI orthologs in the Type III and Type VI secretion systems both tightly and specifically. To fully understand the relationship between cdG binding and the FliI complex, it is essential to identify and characterise the cdG binding site.

Although certain cdG binding proteins have characteristic binding sites, which are conserved among many other cdG targets, recent studies have shown that cdG can bind to certain target proteins via novel binding motifs, which are not always possible to predict *in silico* (238). The structural diversity of cdG is one of the potential reasons that cdG binding motifs can be so different from one another. CdG is a flexible molecule that adopts a variety of conformations depending on the specific target. These conformations range from a fully stacked form to an extended monomer, through adjustments around the glycosidic bond. The guanine base of cdG, being hydrophobic can interact with an arginine or a phenylalanine/tyrosine residue, further increasing the range of its interaction partners. An interesting characteristic of cdG is also its capacity to oligomerise. CdG has been found in a monomeric, dimeric and even the recently-identified tetrameric form (238). CdG in the dimeric form is a very versatile molecule, which can adopt even more conformations; for instance, the guanine bases can be stacked together or stacked partially, and the remaining de-stacked guanine residues to be free to interact with available hydrophobic regions in target proteins (229).

Determination of the FliI cdG binding site is crucial for the identification of the role of this interaction. Although a FliI crystal structure has been resolved for *Salmonella enterica* pathovar *typhimurium* (272), the interaction of FliI to cdG was unknown when this structure was resolved. Nonetheless, this study was of crucial importance as it pointed out similarities between the F_0F_1 ATP synthetase and FliI, by modelling FliI as a hexamer. The model was based on the F_0F_1 structure composed of the $\alpha_3\beta_3\gamma$ subunits. The two proteins share similarities at the main chain structures in the interface between the two subunits, whereas they are very different when it comes to the outer surface of the hexameric ring. The results generated by this study imply a co-evolution of the two proteins as, although their function is different, they share similarities in their mechanism of action (272). Determination of the binding site not only will it give insights about the role of this interaction but also will potentially unravel a new mechanism of cdG binding, broadening our understanding of cdG signalling mechanisms.

5.2 Aims

1. To structurally characterise the FliI-cdG complex.
2. To identify and analyse the binding site of cdG to FliI.

5.3 Results

5.3.1 Crystallisation trials

The first step towards the determination of the binding site was the initiation of crystallisation trials in *P. fluorescens* SBW25.

The FliI full-length protein has been extensively studied, and it is well-reported for the formation of higher order complexes in solution, making it not suitable for crystallisation purposes. For that reason, the truncated version of FliI (Δ1-18) from *P. fluorescens* SBW25 was selected for crystallisation purposes as it is unable to form hexamers and remains soluble in high concentrations. However, although the protein is highly soluble and stays in a monomeric form, it could not be crystallised when it was added to a number of different commercial screens. In addition to commercial screening attempts, the published crystallisation conditions for the *Salmonella* protein were applied but again did not result in protein crystals.

Having confirmed cdG binding in a number of different species, my next crystallisation efforts focused on the FliI homolog from *Salmonella enterica* ($FliI_{SeT}$). Although this crystal structure is already published (272), the aim was to co-crystallise the protein with cdG to determine the binding site. For this reason, the $FliI_{\Delta 1\text{-}18}$ mutant was used and was applied to a number of different commercially available screens. The protein was finally crystallised in the Morpheus screen under 20 % w/v PEG 4000, 40% v/v Glycerol, 0.1 M Bicine/ Tris pH 8.5, 0.3 M magnesium chloride and 0.3 M calcium chloride, in the presence of 1 mM cdG and 1 mM ADP. The crystals had a needle-like structure and in order to be diffracted, they needed to grow further in size. To achieve this, a series of optimisation experiments were carried out, which gave crystals of a nice size and shape (see Figure 5.1).

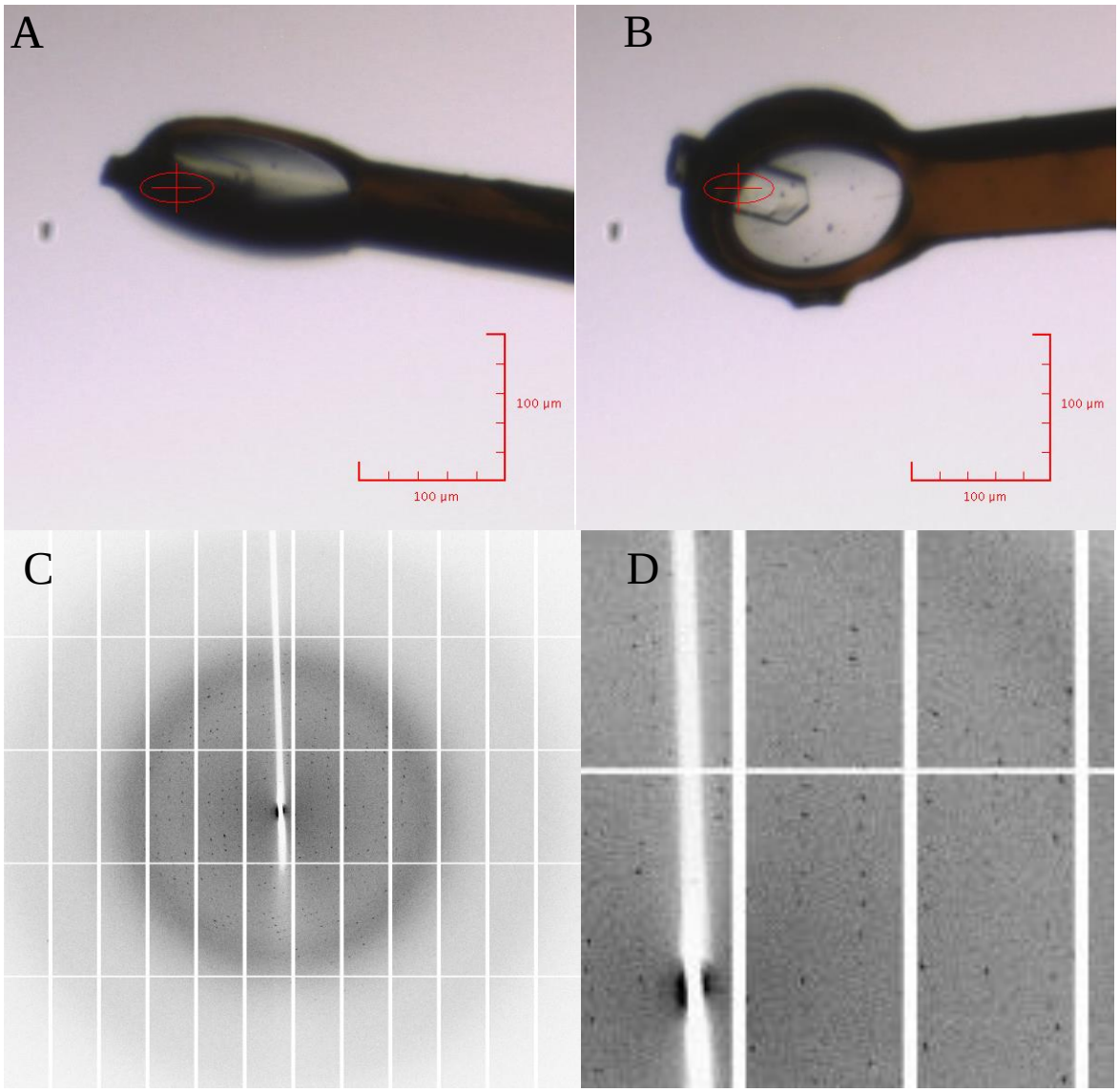

Figure 5.1: A-B. Orthogonal view of mounted crystal (top panels). C-D. Example of diffraction pattern for the best FliI$_{\Delta 1\text{-}18}$ crystal (bottom panels). Crystals were obtained from S. enterica in complex with ADP. Inset highlights the weak and diffuse diffraction spots.

A B

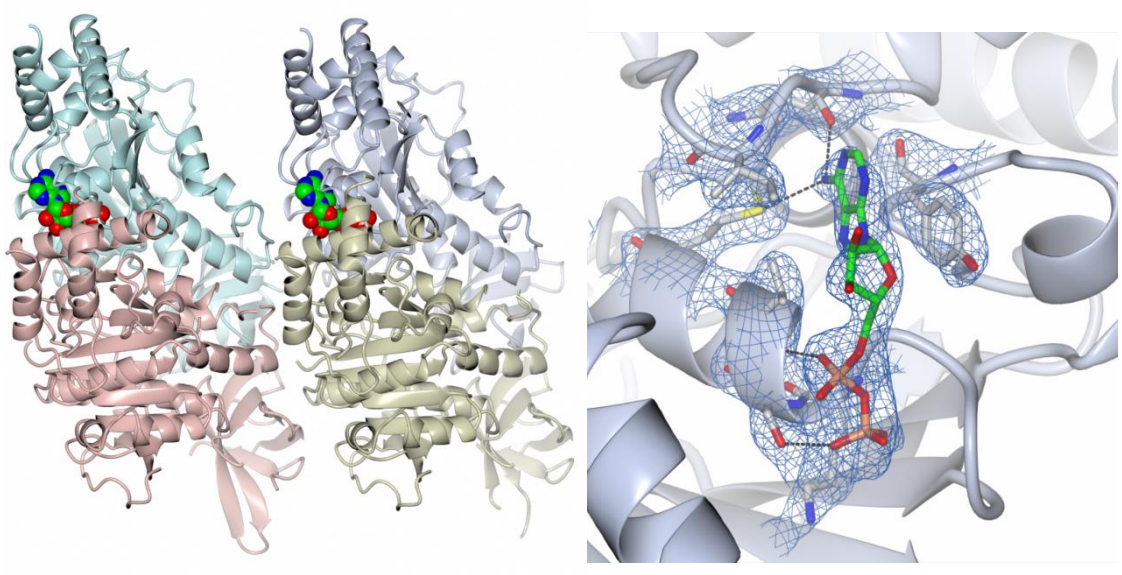

Figure 5.2: A. Overview of the asymmetric unit of FliI$_{\Delta 1\text{-}18}$ showing, as a cartoon representation, the four copies of the subunit in different colours and arranged as a pair of parallel dimers. Also shown as van der Waals spheres are the two bound ADP molecules (one per dimer). B. Close-up of the ADP binding site showing the residues involved in binding the nucleotide together with their associated electron density (calculated at 2.6 Å resolution and contoured at ~1.0 σ).

The FliI$_{\Delta 1\text{-}18}$ crystals were analysed on beamlines I02 and I03 at the Diamond Light Source. Generally, the X-ray diffraction was weak and gave diffuse spots indicative of poorly ordered crystals (Figure 5.1). Nevertheless, a number of datasets were collected to a maximum resolution of 2.4 Å from crystals of the protein alone, as well as crystals that had been soaked with ATP and cdG. All datasets were processed in space group $P2_1$ with approximate cell parameters of a = 95 Å, b = 73 Å, c = 126 Å, α = 90°, β = 94°, γ = 90°, these being very similar to those obtained for the deposited structure of FliI$_{\Delta 1\text{-}18}$ (PDB accession code 2DPY) in the same space group (a = 48 Å, b = 73 Å, c = 126 Å, α = 90°, β = 94°, γ = 90°). The doubling of the a-axis with respect to the deposited structure led to a doubling of the unit cell volume and an expected increase from two to four copies of the protein monomer in the asymmetric unit (ASU) while retaining the same solvent content of 47%. The structure was solved with PHASER using one subunit from 2DPY

as the search template. This was successful in placing four copies of the subunit in the ASU that were arranged as two dimers (Figure 5.2).

In the soaked crystal, only ADP was visible in the electron density plot, with a single ADP molecule bound equivalently to one subunit of each $FliI_{\Delta 1\text{-}18}$ dimer (Figure 5.2). Due to the poor data quality, refinement of the ligand-free and ADP-bound structures was less than satisfactory. As the resulting models did not provide any additional biological insights beyond those given by the published structure, this aspect of the project was suspended at this point.

Table 5.1: *X-Ray Data Collection and Refinement Statistics for* $FliI_{\Delta 1\text{-}18}$

Values in parentheses are for the outer resolution shell. [a] $R_{merge} = \sum_{hkl} \sum_i |I_i(hkl) - \langle I(hkl)\rangle| / \sum_{hkl} \sum_i I_i(hkl)$. [b] $R_{meas} = \sum_{hkl} [N/(N-1)]^{1/2} \times \sum_i |I_i(hkl) - \langle I(hkl)\rangle| / \sum_{hkl} \sum_i I_i(hkl)$, *where* $I_i(hkl)$ *is the ith observation of reflection hkl,* $\langle I(hkl)\rangle$ *is the weighted average intensity for all observations i of reflection hkl and N is the number of observations of reflection hkl.* [c] $CC_{½}$ *is the correlation coefficient between equivalent symmetry intensities from random halves of the dataset.* [d] *The data set was split into "working" and "free" sets consisting of 95 and 5% of the data respectively. The free set was not used for refinement.* [e] *The R-factors* R_{work} *and* R_{free} *are calculated as follows:* $R = \Sigma(|F_{obs} - F_{calc}|)/\Sigma|F_{obs}| \times 100$, *where* F_{obs} *and* F_{calc} *are the observed and calculated structure factor amplitudes, respectively.* [f] *Not fully refined.*

	Ligand-free	ADP-bound
Data collection		
Beamline	I02	I03
Wavelength (Å)	0.9795	0.9795
Detector	Pilatus 6M	Pilatus 6M
Resolution range (Å)	53.14 – 2.40 (2.46 – 2.40)	78.08 – 2.60 (2.67 – 2.60)
Space Group	$P2_1$	$P2_1$
Cell parameters (Å)	a = 94.6, b = 72.6, c = 125.6	a = 94.9, b = 72.7, c = 126.2
	α = 90.0, β = 94.0, γ = 90.0	α = 90.0, β = 93.6, γ = 90.0
Unique reflections	66398 (4871)	52797 (3846)
Multiplicity	5.7 (5.7)	4.2 (4.4)
Mean $I/\sigma(I)$	7.8 (1.2)	7.2 (1.0)
Completeness (%)	99.5 (99.1)	99.4 (98.9)
R_{merge}[a]	0.177 (1.555)	0.178 (1.537)
R_{meas}[b]	0.195 (1.714)	0.204 (1.746)
$CC_{½}$[c]	0.996 (0.509)	0.994 (0.465)
Refinement		
Reflections: working/free[d]	63093/3304	50138/2659
R_{work}/ R_{free}[e, f]	0.261/0.288	0.261/0.291
R.m.s. bond distance deviation (Å)	0.012	0.011
R.m.s. bond angle deviation (°)	1.61	1.51
Asymmetric unit contents	4 x $FliI_{\Delta 1\text{-}18}$	4 x $FliI_{\Delta 1\text{-}18}$ + 2 x ADP

5.3.2 Biochemical and in silico analysis of the cdG binding site

5.3.2.1 Peptide shift analysis

Since it was not possible to co-crystallise FliI with cdG, a combination of biochemical and *in silico* analysis experiments was carried out to determine the FliI cdG binding site.

The first experiment was a novel peptide-shift analysis (264), which was conducted in collaboration with Dr Thomas Wilhelm from the Institute of Food Research (IFR). For this assay, the chemically modified cdG used in the capture compound screen (cdG-CC) was incubated and cross-linked to purified $FliI_{\Delta 1\text{-}18}$. A sample of the cross-linked protein, alongside the unmodified protein as a reference, were digested with trypsin. The digested samples were analysed by Mass Spectrometry (MS) and differences between the profiles of identified peptides were analysed to provide clues as to the location of the cdG binding site. Comparison of the treated sample (cross-linked to cdG-CC) and the untreated $FliI_{His}$ as a reference resulted in the identification of many spectra relations corresponding to modified peptides (Figure 5.3).

One single peptide came back as the most densely modified after UV-cross-linking with the cdG-CC (residues 259–269, peptide sequence NVLLLMDSLTR). For this peptide, 52 spectra relations were identified where the heavier modification was >150 Da larger than the unmodified peptide. The identified peptide forms the central strand of a β-sheet in the centre of the SBW25 FliI homology model. Interestingly, the C-terminus of the same β-strand contains the conserved aspartate (Asp-265) of the Walker B motif. Importantly, the identified peptide is facing towards the interface between the two monomeric FliI subunits (Figure 5.5- A).

A

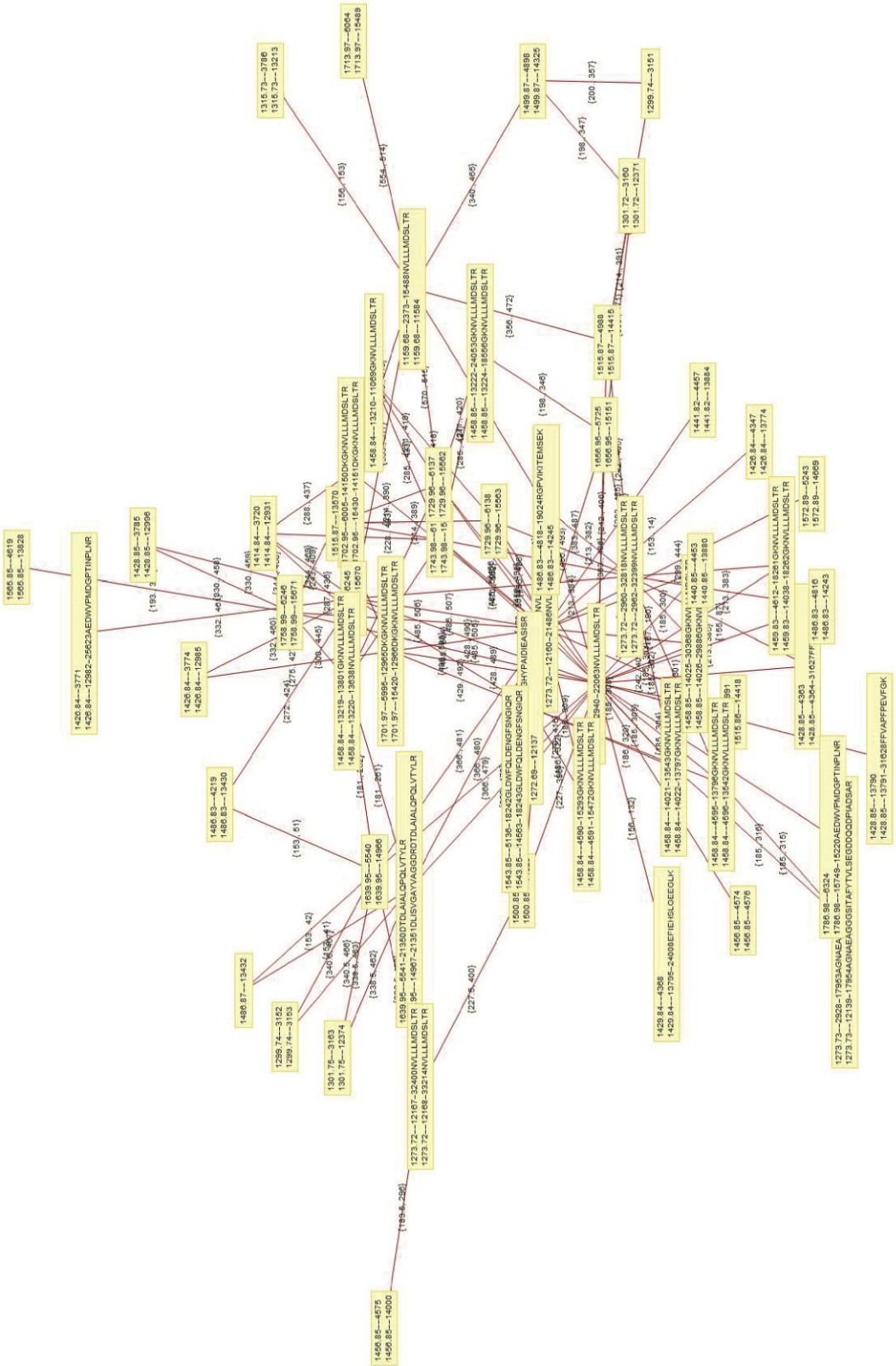

B

Figure 5.3: Mass Spectrometry Peak Shift Analyses for treated (i.e. cross-linked to cdG) vs untreated. A. The particularly dense clusters of related spectra in both analyses correspond to the most densely-modified peptides following cdG-capture compound crosslinking. B. The denser network corresponds to the most highly-modified peptide (NVLLLMDSLTR), which comprises residues 259-269 of FliI.

5.3.2. 2 Analysis of highly conserved residues

A second round of *in silico* analysis was performed to complement the previous results, in collaboration with Dr David Lawson. This analysis was based on the conserved amino acid residues found in every cdG binding ATPase protein (Figure 5.4), which were then mapped on a homology model of FliI from SBW25, constructed based on the published *Salmonella enterica* crystal structure (Figure 5.5).

The peptide identified from the previous *in silico* analysis as the most heavily modified upon the UV-cross-linking with the cdG-CC emerges close to the cluster of the identified highly conserved residues. Together, these two *in silico* analysis techniques present a plausible candidate for the cdG binding pocket, which is potentially formed by residues from two FliI subunits, as shown in the model illustrated in Figure 5.5.

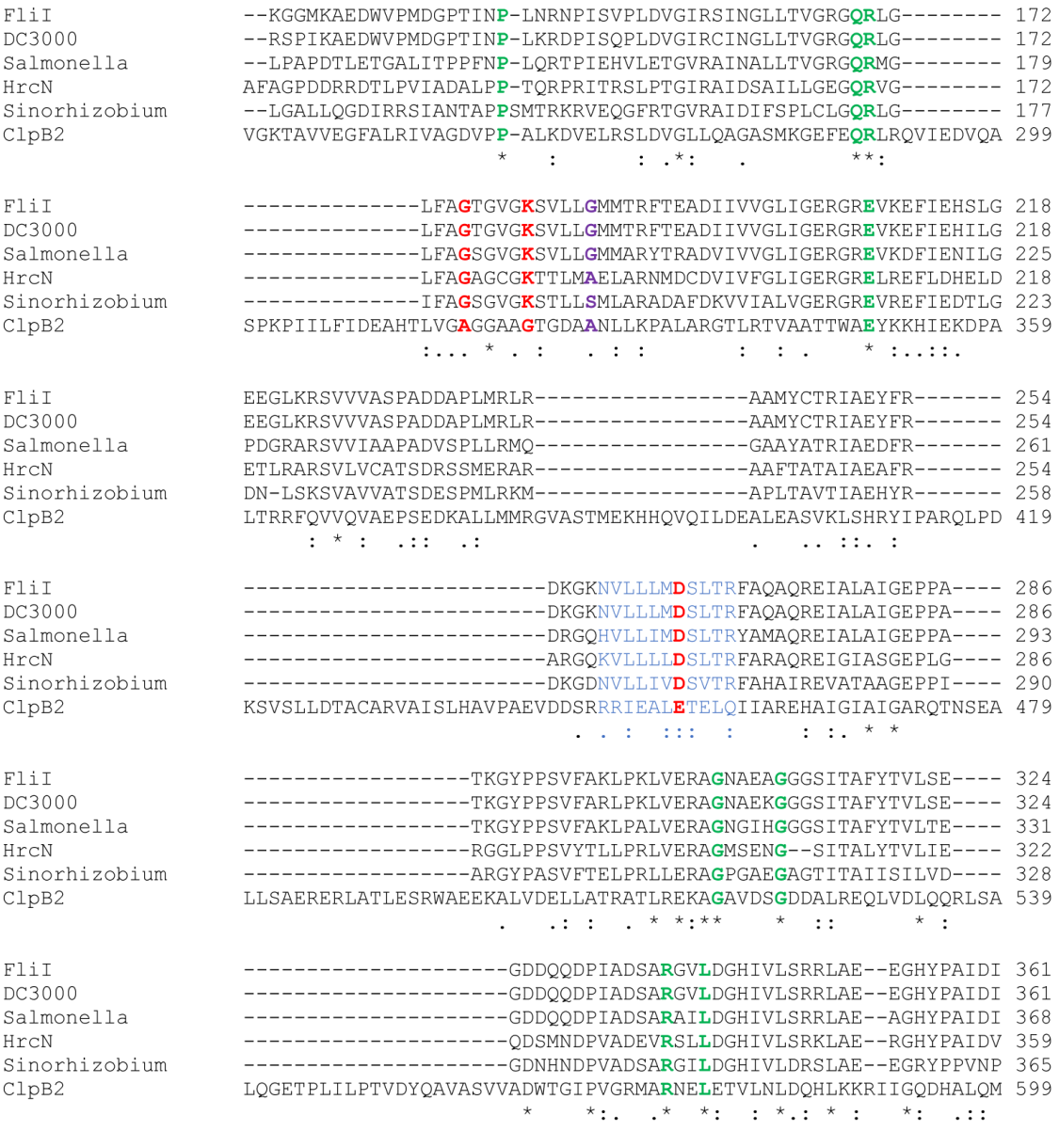

Figure 5.4: Clustal alignment of conserved residues between FliI homologs from other species and orthologs from other export systems (HrcN, and ClpB2). Residues similarities between all proteins are marked with asterisks (*), and similarities across all six with periods (.) or colons (:). The FliI Walker A/B residues are marked in red while in blue is highlighted the capture compound-binding NVLLLMDSLTR peptide, in purple is marked the position of the conserved cdG binding arginine in FlrA (Arg-176), and in green are the conserved residues of the proposed cdG binding. Figure adapted from (326).

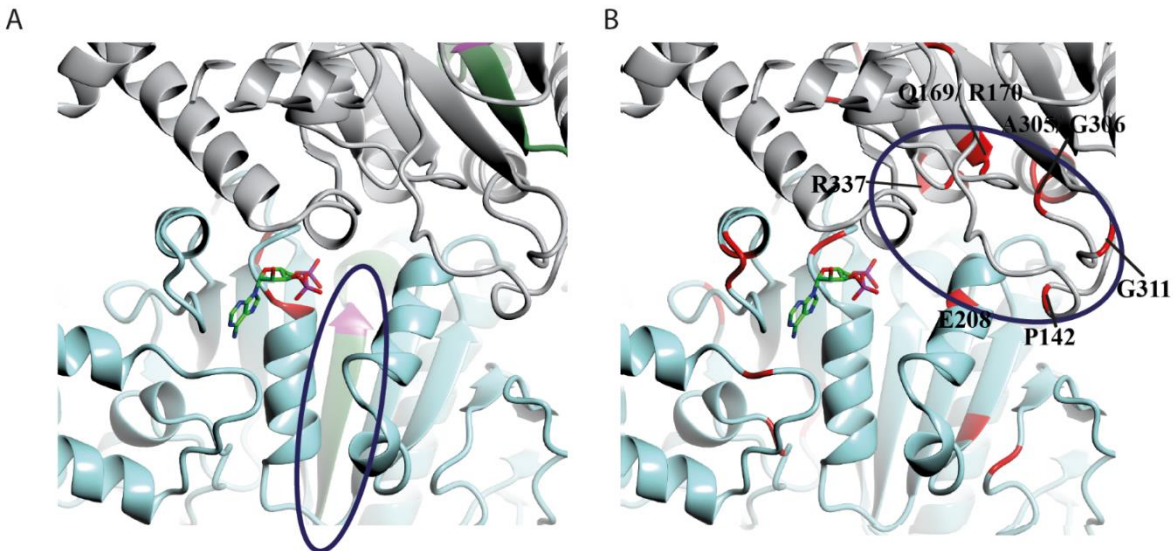

Figure 5.5: Homology model of the predicted hexameric SBW25 FliI, based on the published crystal structure of FliI from S. typhimurium *(Protein Data Bank code 2DPY).* ***A.*** *Interface between two FliI subunits, marked in green is the identified NVLLLMDSLTR peptide, implicated in cdG capture compound binding and marked in pink is the conserved Walker B aspartate (Asp-265)* ***B.*** *Marked in red are the conserved residues between the six cdG-binding proteins tested in this study (based on the conserved residues analysis), ADP is included in the structure, shown to bind at the interfaces between the individual FliI subunits. Figure adapted from (326).*

5.3.3 Mutagenesis of 'binding' residues (R, E, G) and subsequent cdG-binding and ATPase activity assays

Following the identification of the potential binding site from the *in silico* analysis described above, some of the key residues identified as part of the potential binding site were mutated and tested to confirm their importance in cdG binding. To do this, specific amino acid substitutions were introduced (R170H, E208Q, and R337H) in the $FliI_{\Delta 1-18}$ background; then the purified proteins were examined for cdG binding and ATPase activity (Figure 5.6).

The binding ability of the mutants to cdG was monitored by SPR, and it was observed that binding was heavily compromised in all three cases (R170H, E208Q, and R337H) as the K_D of the interaction was beyond the method's detection limit and could not be accurately determined (Figure 5.6- A). The mutants were also tested for their ATPase activity (Figure 5.6- B) and were found to be enzymatically inactive.

A

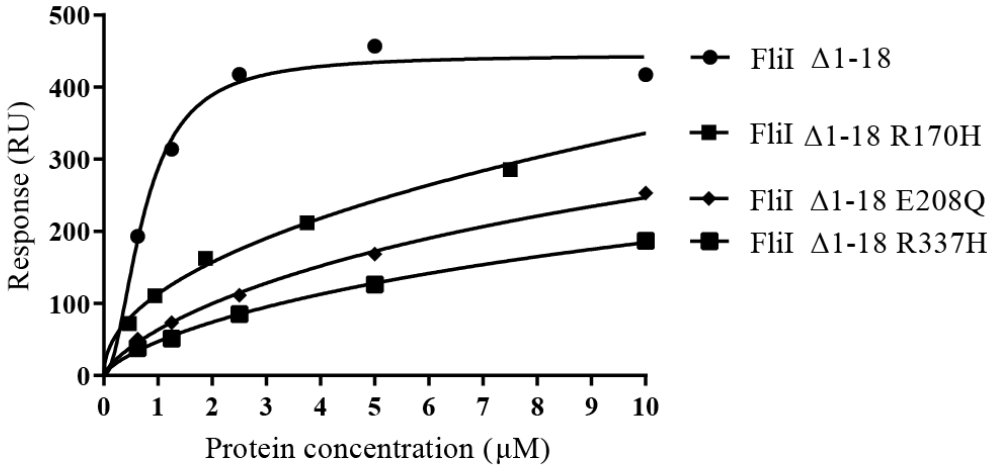

B

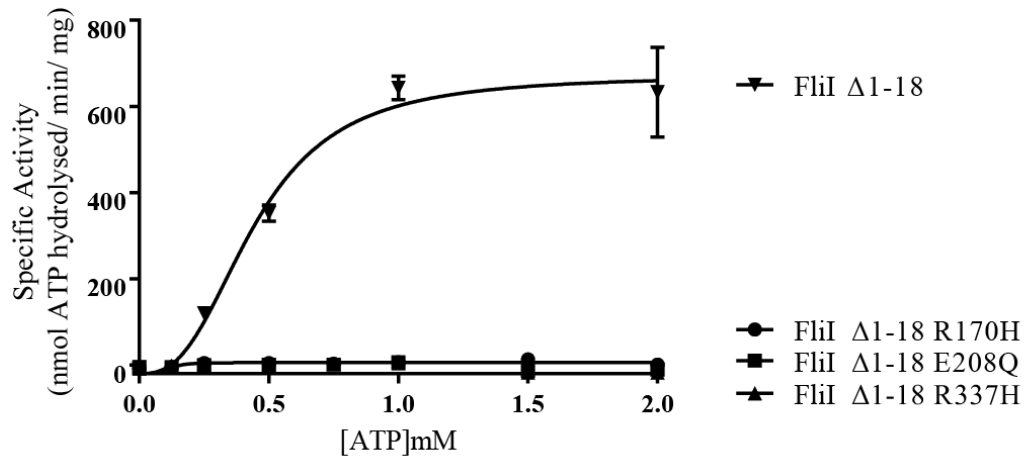

Figure 5.6: A. SPR affinity fit for cdG binding to FliI alleles with amino acid substitutions (FliIΔ1–18, FliIΔ1–18 R170H, FliIΔ1–18 E208Q, and FliIΔ1–18 R337H). B. ATPase activity for different FliI and the mutated alleles. Specific activity for each protein (nmol ATP hydrolysed/min/mg protein) was monitored under increasing ATP concentrations. Figure adapted from (326).

5.4 Discussion

To identify the cdG binding site of FliI, crystallisation trials were carried out firstly on FliI full length from *P. fluorescens* SBW25 and then on the truncated allele $FliI_{\Delta 1\text{-}18}$. After several failed attempts, the crystallisation efforts were refocused on the FliI homolog from *Salmonella enterica*, the crystal structure of which has already been published (272). Although the protein was crystallised in the presence of cdG, it was not possible to resolve the cdG molecule in the protein structure. However, our crystals could only be generated in the presence of cdG, strongly suggesting that cdG may be essential for crystallisation of the protein under the specific conditions tested. Although it was not possible to resolve cdG structure in the crystals obtained, this may indicate that cdG was indeed present as crystals couldn't be obtained without it but in not a high enough concentration to produce a dense enough electron density that would allow the structure to be resolved.

To identify the cdG binding site and get more information about the nature of binding, two independent *in silico* analyses were employed; the first was a recently developed method for the identification of unknown peptide modifications, the peptide shift analysis. This analysis resulted in one single peptide, which was identified as the most heavily modified upon the addition of cross-linked cdG. The peptide identified consisted of 11 amino acid residues (NVLLLMDSLTR) and is located in the core of the SBW25 FliI homology model. The end of the peptide emerges at the interface created by the two FliI subunits and in close proximity to a cluster of highly conserved residues, as identified by the seconds *in silico* analysis. To focus more on the cdG binding site, a predicted model was built based on the published FliI structure from *Salmonella enterica*, with the quaternary structure of the complex based on the hexameric F_1F_0 ATPase, which shares many structural similarities with FliI. FliI homologs and orthologs share a small number

of highly conserved residues including several glutamate and arginine residues, which are known to be required for cdG binding (234) (Figure 5.4).

As part of this second analysis, the conserved residues among the FliI homologs were identified and were mapped on the model. Interestingly the residues were all facing towards a pocket formed between the two FliI subunits. These results complemented the first *in silico* analysis, which showed that the end of the modified peptide is also directed to the same pocket. The conserved pocket identified contained two arginines (Arg-170 and Arg-337) from the first subunit and a glutamate (Glu-208) from the second. Both arginine and glutamate residues are known to be highly important for cdG binding in previously characterised cdG binding proteins (234,238). Residues R170, E208, and R337, were mutated and tested for both binding and activity. The residues substitutions led to a heavily compromised binding and a loss in ATPase activity.

The mutated proteins, except for the loss of cdG binding, they also lost their ATPase activity. However, this does not come as a surprise since the amino acid substitutions were located in the interface between the two FliI subunits. By mutating these residues, it is possible that the active site of the protein was altered because of multimerization changes. Another possibility is that these mutations may have direct effects on the folding of the protein causing it to lose its activity. The fact that the mutations did not cause the protein to precipitate, neither did they lead to a different behaviour when tested by AFM (see chapter 6), gives a strong indication that the proteins remained soluble and the loss of binding was specific to the residue change in each case.

The fact that the binding site was shown to be at the interface between the two FliI subunits could have great implications on the role of cdG binding in this class of ATPases. For instance, this strategic binding position may serve as a catalyst for cdG to control the function of the protein by altering its multimerization state.

Chapter 6:

Towards the in vivo characterisation of FliI-cdG binding

Chapter 6: Towards the *in vivo* characterisation of FliI-cdG binding

6.1 Introduction

FliI is an active ATPase, hydrolysing ATP to provide the initial energy required for the export of the flagellar subunits and as a result the construction of a functional flagellum. However, it is still unclear how the chemical energy acquired from ATP hydrolysis is converted to the mechanical energy required for protein export. Sharing broad structural similarities with the F_0F_1 ATP synthase (272), FliI forms a homo-hexameric complex that docks on the export gate of the flagellum, where it exerts its activity. Although the role of FliI in protein export is well-reported, recent studies have shown that FliI null mutants can still export their substrates via the flagellum export gate, using the proton motive force (PMF) alone (68).

In addition to its role as an ATPase during protein export, FliI also forms heterotrimers in the bacterial cytoplasm with another protein, FliH. Together they act as chaperones for flagellar subunits, which they then direct to the export gate. FliH also acts on anchoring the FliI hexamer to the export gate, where it exerts its full enzymatic activity (304).

The recent identification of FliI as a cdG binder creates numerous questions concerning the *in vivo* role of this binding. CdG signalling networks are highly complex and characterising the interaction of FliI to the cdG molecule *in vivo* could prove to be a hard task. CdG is known to be involved in flagella biosynthesis and function at various regulatory levels. To begin with, cdG controls the flagella gene expression by directly interacting with the master transcriptional regulator FleQ. The next level of regulation by cdG comes at the post-translational level, by the direct interaction of the molecule with the flagellar brake protein, YcgR. This leads to a conformational change in the protein,

enabling it to bind to, and inhibit the rotation of, the bacterial flagellum (231,281). Finally, a newly discovered mechanism of regulation is through cdG interaction with the flagella stator complexes (298). The MotCD stator is responsible for swarming motility in *Pseudomonas aeruginosa*, whereas the MotAB stator does not support swarming. When cdG levels are increased in the bacterial cell, swarming motility is repressed by the MotAB stator. It has been shown that introducing mutations in these stator proteins recovers cdG-mediated repression of swarming.

All these different levels of regulation by cdG, create lots of questions about the newly-identified role of cdG regulation via FliI. To approach this matter and investigate it further, I looked at some common roles of FliI (e.g. flagellar genes expression, export via the flagellum) and investigated how these may be affected by increased cdG levels.

Having proposed that cdG binding occurs at the interface between the two FliI subunits, and given that FliI is a protein known to exert its maximum activity and role via multimerising in higher order complexes, in this chapter, I focused on the characterisation of cdG effects on the multimerization state of the protein.

6.2 Aims

1. To investigate the effect of cdG on the flagellar gene expression and protein export.
2. To examine how cdG addition affects the multimeric state of FliI.

6.3 Results

6.3.1 Effect of cdG on the flagellum genes expression and export via the flagellum

The first step towards the biological characterisation of FliI binding to cdG was to test if this interaction has a direct effect on the export of the flagellum subunits via the export gate. The first step towards this goal was to investigate whether the expression levels of the flagellum genes are affected by increasing levels of cdG in the recently-published FleQ-bypass mutants (305). In the FleQ-bypass mutants, the flagellum genes transcription is no longer under the FleQ control but under the control of NtrC, a transcriptional regulator in the same family as FleQ. The reason for using these mutants was to overcome the well-known cdG-dependent transcriptional control of flagella expression exerted by FleQ.

Quantitative RT-PCR experiments were carried out to monitor the expression of FliC, FliI and NtrC in the presence of low and high levels of cdG in the cell accordingly (Figure 6.1- A). The results presented in Figure 6.1 were normalised against the expression of the σ^{70} factor, RpoD. Overproduction of cdG in the cells was mediated by overexpression of the WspR cyclase. As shown in Figure 6.1- A, *fliC* expression was abolished in the Δ*fleQ* mutant, as expected by the lack of the transcriptional regulator. The overproduction of cdG in the wild-type background also led to heavily compromised *fliC* expression, due to the FleQ-cdG interaction. However, in the FleQ-bypass mutants, no cdG-mediated effect was observed, proving that cdG has no longer an effect on the expression of the flagellum genes.

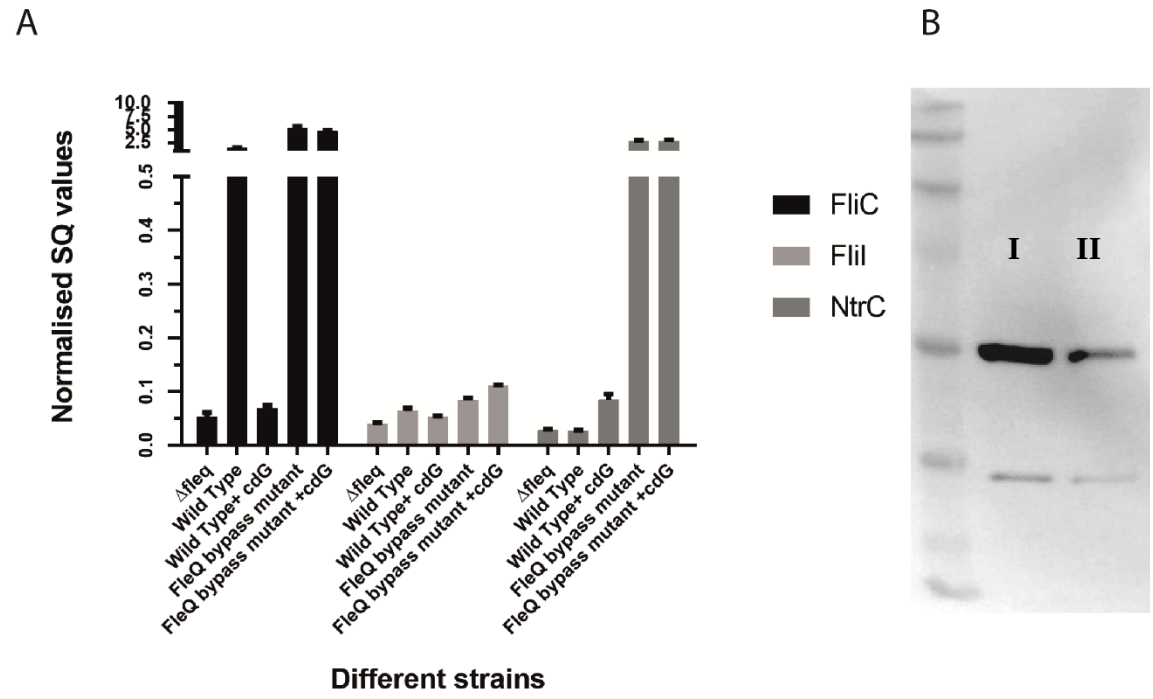

Figure 6.1: A. q-RT PCR data monitoring the expression levels of FliC, FliI and NtrC in the wild type background, ΔfleQ background, wild type strain overproducing cdG, FleQ bypass mutant and FleQ bypass mutant overproducing cdG. The data obtained was normalised against the expression of the housekeeping sigma factor gene, q-RT. B. Western blot monitoring the flagellin (FliC) export levels. The exported levels of flagellin were monitored in the media, where the bacteria were grown, as described in the Materials and Methods relevant section. I. FleQ bypass mutant, II. FleQ bypass mutant overproducing cdG by the overexpression of the WspR cyclase.

FliI expression occurs at much lower levels in the cell compared to FliC. Furthermore, FliI expression is not significantly affected by cdG overproduction in the cell. NtrC expression is much higher in the FleQ-bypass mutants with no effect from cdG overproduction. However, a significant increase in its expression was observed in the wild-type background when the levels of cdG were increased.

Having established that cdG has no other effect on the expression of the flagellum genes in the FleQ bypass mutant, the next step was to test whether increasing cdG levels have an effect on FliC export via the flagellum. To test this, a Western blot was performed monitoring the levels of the exported FliC in the FleQ-bypass strain overproducing cdG in comparison to a strain with basal cdG levels. To monitor the exported levels of

flagellin, the media where the bacteria were grown O/N was collected and the proteins present in it were concentrated by acetone precipitation before being analysed further. As presented in Figure 6.1- B, the export of FliC is heavily compromised in the presence of high cdG levels. This implies that cdG may play a direct role in controlling protein export via the flagellum machinery.

6.3.2 Effects of cdG on the multimerization state of FliI

6.3.2.1 Size exclusion chromatography

Having acquired some first indications about cdG involvement in protein export via the flagellum, the next step was to test if alterations at the export levels of the flagellum are due to changes in the multimerization state of FliI, and as a result a loss of activity.

To test this, and to monitor the effects that cdG has on the conformation of the protein, a series of gel filtration experiments were carried out. As presented in Figure 6.2- A, full-length FliI runs mostly in the void volume with only a small percentage of the protein population running as a dimer. The addition of ATP to the protein had no effect on the running size of the complexes. However, when cdG was added, a peak corresponding to a dodecameric state was formed (Figure 6.2- A). The truncated version of the protein was also used for the identification of potential conformational changes upon the addition of cdG and ATP. As expected, this allele is unable to form hexamers by itself and runs as a monomer in the size exclusion chromatography column. CdG addition had no effect on this allele of the protein in contrast to ATP, the addition of which leads to higher order complex formation (dimers and hexamers) (Figure 6.2- B).

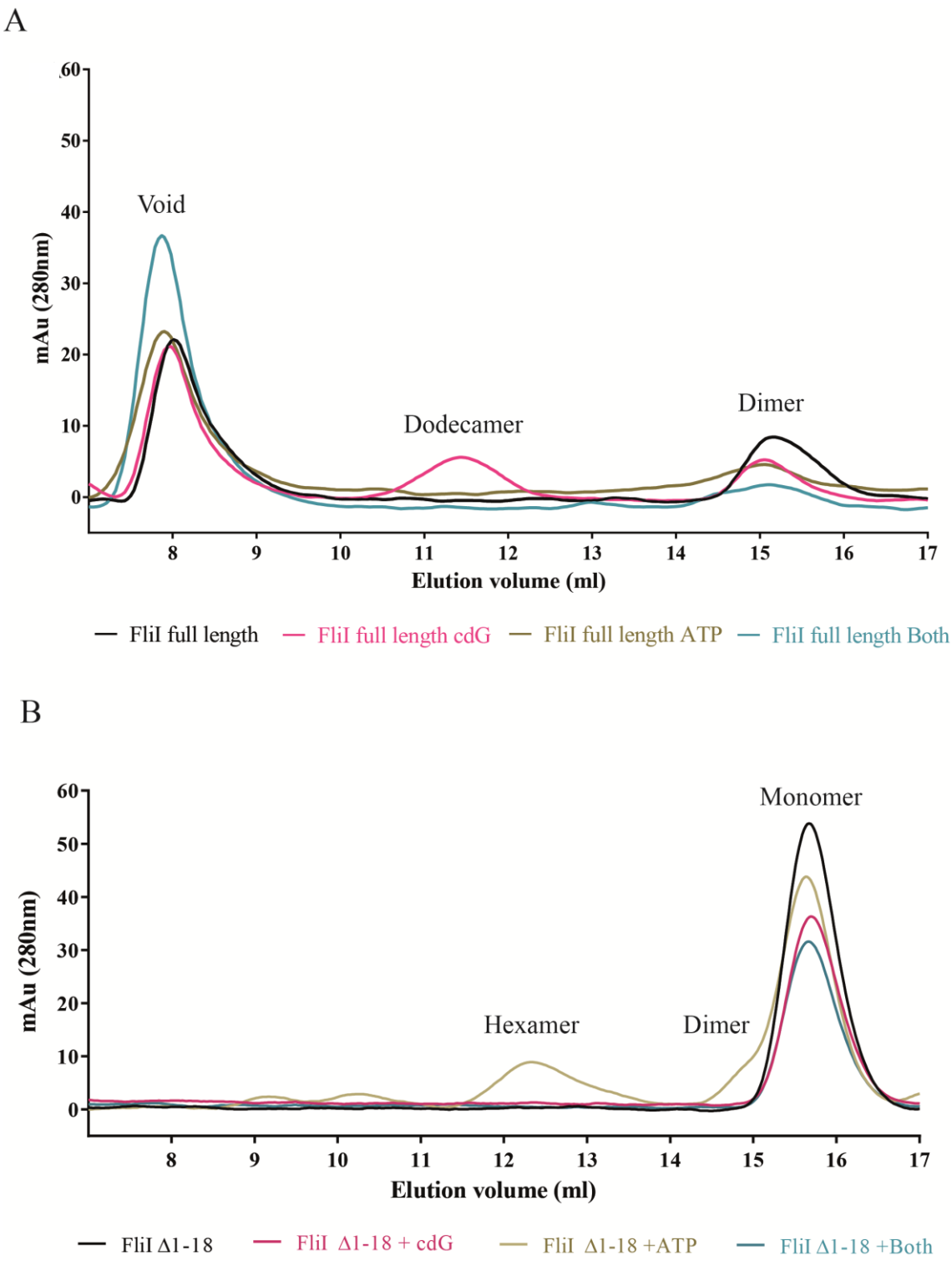

Figure 6.2: A. Size exclusion chromatography on FliI full length, cdG and ATP nucleotides were added at a concentration of 500 μM accordingly. B. Size exclusion chromatography on FliI Δ1-18, cdG and ATP nucleotides were added at a concentration of 500 μM accordingly.

6.3.2.3 Transmission electron microscopy

To expand on the gel filtration data, two complementary imaging approaches were conducted. First, Transmission Electron Microscopy (TEM) was carried out. The TEM experiments showed that the FliI full-length protein forms higher order complexes as expected. However, these corresponded to units of a larger size than would be expected from the hexameric complexes described in the literature (150). The protein complex population was uniformly distributed, and no precipitation was observed (Figure 6.3- A). Surprisingly, the addition of cdG caused the protein complexes to cluster together, forming distinct ring-like structures (Figure 6.3- B).

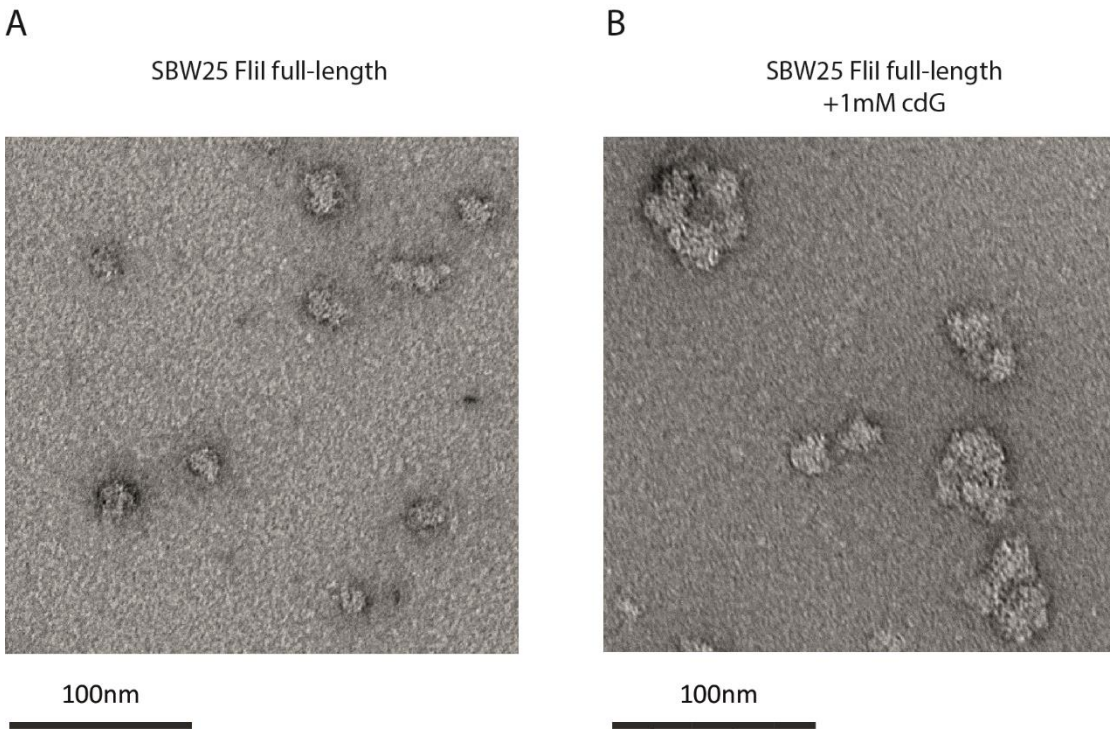

Figure 6.3: Transmission electron microscopy (TEM) experiments on FliI full length from P. fluorescens SBW25. A. Purified FliI full-length was analysed by TEM. Multimers of 20 nm-50 nm were observed corresponding to hexamers, dodecamers and higher order complexes. B. TEM analysis of full length FliI upon the addition of 1 mM cdG, ring like structures were observed upon the addition of cdG consisting of FliI higher-order multimers.

6.3.2.4 Atomic force microscopy (AFM)

The second approach followed for the visualisation of FliI complexes was AFM. Similarly to the TEM assays, the AFM experiments revealed the formation of higher order complexes of distinct shape and size for FliI full-length (Figure 6.4- A). It was observed that FliI full-length population was distributed among hexamers, dodecamers and higher order complexes. As expected, in the case of the truncated version of the protein, which is unable to form higher order complexes, no protein clusters were observed as the size of the protein in the monomeric and dimeric form is much smaller than the detection limit of AFM (Figure 6.4- B). The addition of 100 μM cdG led to clustering of the hexamers and the formation of circular structures (Figure 6.4- C), dependent on the addition of cdG specifically, as no clustering was observed when ATP was added to the protein solution (Figure 6.4- D). The FliI G176A mutant, which maintains its ATPase activity but is no longer sensitive to cdG, was then tested by AFM. This mutant was able to form higher order complexes, as observed in the wild-type background. However, an unexpected effect was also noted, the hexameric FliI hexamers accumulate around the bigger FliI complexes, creating a 'halo-like' effect (Figure 6.4- E). This effect was only observed for this specific mutant, whereas the other mutants, introduced in Chapter 5, behaved in a similar manner to the wild type (Figure 6.4- F).

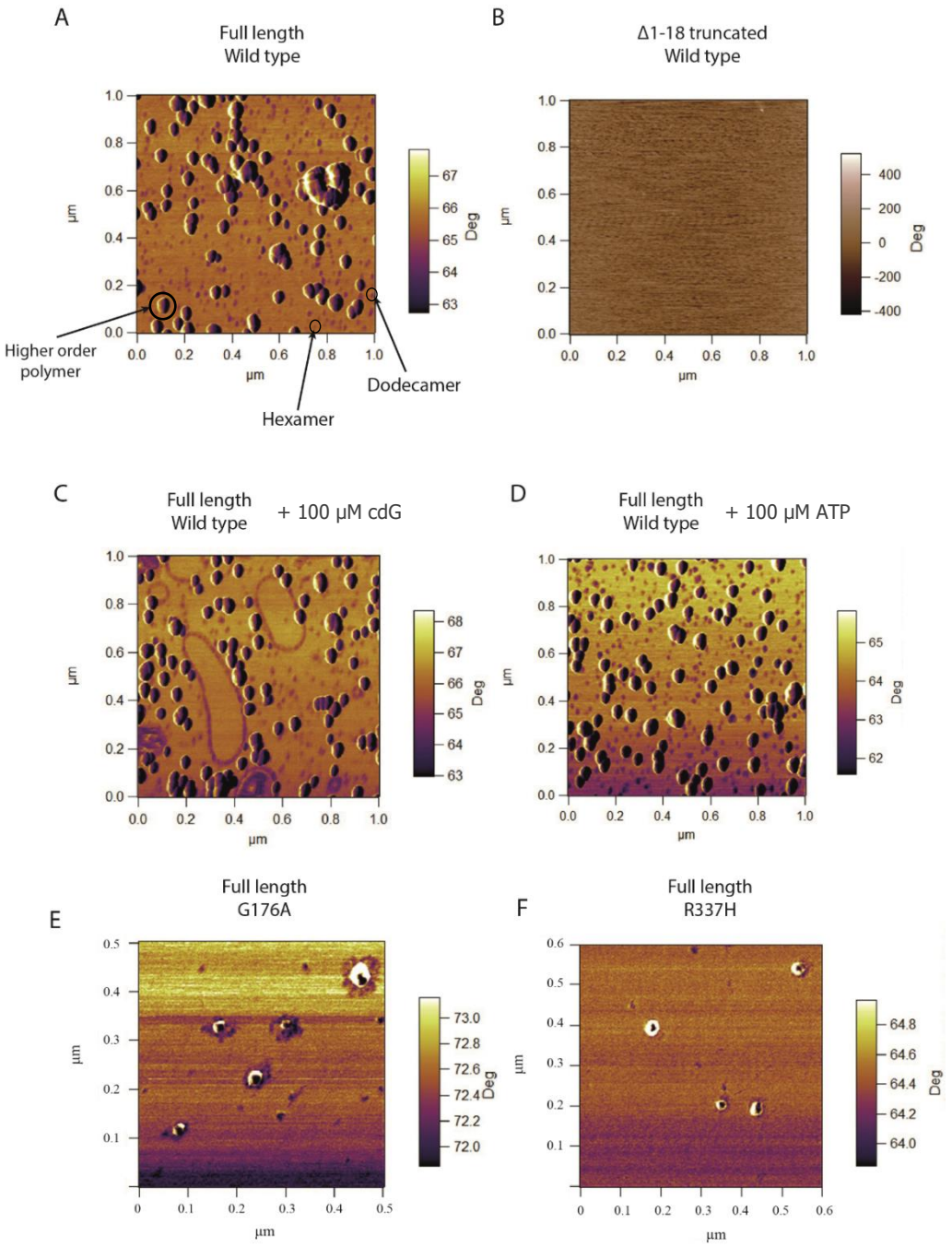

Figure 6.4: Atomic Force Microscopy (AFM) experiments for the determination of FliI multimerization state. A. FliI full length forms hexamers, dodecamers and higher order, regular-sized complexes. B. FliI Δ1-18, the truncated protein forms monomers and dimers, which are below the detection limit of the method. C. 100 µM cdG were added to the FliI full length mix, resulting in the formation of ring like structures, comprising of the hexameric/ dodecameric complexes of the protein. D. 100 µM ATP were added to the FliI full length mix with no obvious results on the multimerization state of the protein. E. FliI full length G176A mutant, accumulation of the hexameric and dodecameric complexes was observed around the higher order complexes. No cdG or ATP were added. F. FliI full length R337H mutant, forming higher order complexes in a similar to the WT way. No cdG or ATP were added.

6.3.3 FliI interaction with FliH

FliI is part of a complex system *in vivo*, being closely associated with its protein partners, FliH and FliJ. To test how FliI-FliH interaction is affected by cdG addition, a series of SPR experiments were carried out in which the proteins were introduced in turn to the assay. FliH with an N-terminal His tag was immobilised on a nickel SPR chip and the association with FliI was monitored by flowing purified GST-tagged FliI over the chip. CdG was also added in increasing concentrations to the FliI mixture and was pre-incubated with it before passing it through the FliH chip. It was observed that FliI interacts with FliH, filling almost 88% percent of the chip's capacity (Figure 6.5). The chip's capacity was calculated by subtracting FliI's binding response by the maximal number of binding sites (Rmax) on the SPR chip, which was calculated based on FliH molecules bound to the chip.

Upon the addition of cdG the responses obtained were greater than 100% and even reached 450% of the FliI-only response (Figure 6.5). These results strongly indicate that cdG causes FliI to multimerize, and for that reason, the response is much greater than the capacity of the SPR chip, even if a maximal 1:2 ratio of FliH-FliI is assumed.

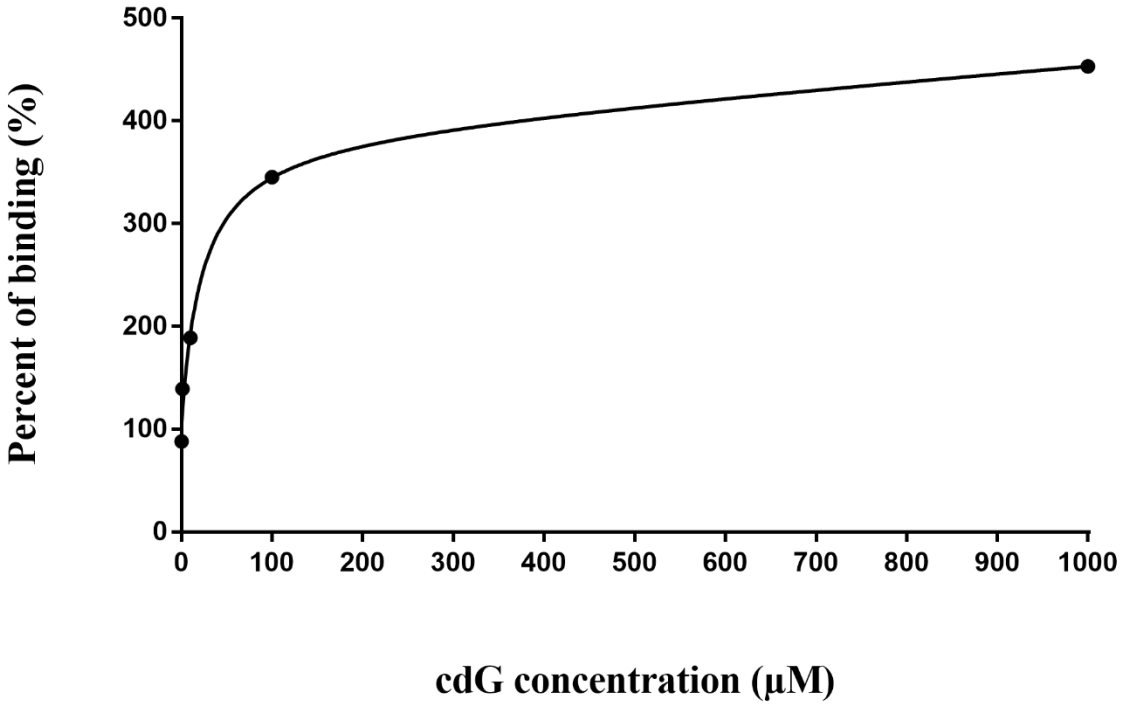

Figure 6.5: Surface plasmon resonance monitoring the interaction between FliI and FliH. The percent of FliI binding to the FliH chip was calculated in increasing cdG concentrations. CdG addition to the FliI solution led to multimerization of the protein resulting in higher percentages of binding on the FliH chip.

6.4 Discussion

CdG is a small signalling molecule that is involved at multiple levels of regulation of the bacterial flagellum. As part of this study, a previously unknown mechanism of regulation was identified; direct interaction of cdG with the main flagellum ATPase, FliI. After having established the nature of this binding, the next step was to determine the biological role of this interaction. As cdG control of flagellar expression and function is complex and pleiotropic, this presented some technical challenges. The most important one was the cdG-dependent FleQ-mediated transcription of the flagellum genes. To overcome that, we were kindly provided specific FleQ-bypass mutants (305). In these mutants, the regulation of the flagellum genes is no longer controlled by the master transcriptional regulator FleQ but are constitutively expressed under the control of another transcriptional regulator, NtrC.

The initial working hypothesis was that cdG may have a direct effect on the export of flagellin (FliC) subunits via the flagellum. To test this, the expression of flagellin (FliC) was monitored by q-RT-PCR in the FleQ-bypass mutants, and no change in the level of the protein was observed upon the overproduction of cdG in the cells. However, when the export of FliC was monitored by Western blotting, the FliC export was shown to be significantly reduced in the strain overproducing cdG. This result presents a first indication that cdG may have a role in the inhibition of the export via the flagellum export gate. FliI expression levels, on the other hand, were much lower and didn't change significantly upon the overexpression of cdG in the cells. This can easily be explained as fewer copies of the protein are required for the export, compared to FliC, which is the major subunit of the flagellum filament and is required in high abundance.

The next step was to investigate the reason that FliC export levels dropped by increasing levels of cdG. Having established that the binding happens at the interface between the

two subunits, we examined the possibility that the effects observed may be due to changes in the multimerization state of the protein. A size exclusion chromatography (gel filtration) experiment was performed to characterise the multimeric state of the protein as well as potential changes in its running pattern. FliI full length, as it is well reported in the literature, tends to form higher order complexes, and this was verified by gel filtration experiments. The largest part of FliI full length runs above the detection limit of the column (>600 KDa) with a minority of the protein running as a dimer. However, the addition of cdG led to the formation of complexes corresponding to a dodecameric complex. This result gives a first indication that cdG may indeed have a direct effect on the multimerization state of the protein. The truncated version of the protein, lacking the first 18 amino acids is unable to multimerize to a hexamer and runs in the monomeric form. However, the addition of ATP led the protein to multimerize and form dimers and hexamers, whereas the addition of cdG had no obvious results.

Although the full-length protein runs in the void volume, it was found to have fully active ATPase activity, and no obvious precipitation was observed in solution. What is more, it binds cdG tightly, in the low μM range. This suggests that the protein doesn't form inactive aggregates as originally thought, but higher order complexes, which are still active and functional. To test this, TEM and AFM experiments were carried out to visualise the conformation of the protein in solution. In TEM, it was observed that the protein indeed forms higher order complexes corresponding to sizes greater than the hexameric size. In AFM, formation of regular-shaped higher order complexes was also observed. Interestingly, no precipitation of the protein was observed in any of these techniques, confirming that FliI multimerizes in a controlled manner, in contradiction to what was originally believed. These complexes tend to cluster together, forming ring-like structures when cdG is added to the protein mixture. This observation was backed up by the results obtained by AFM, which showed that cdG addition leads to clustering of FliI

hexamers or dodecamers into ring-like structures. This effect was specific to cdG as no effects were observed when ATP was added to the mix. These results may have no physiological role, but they give the first indication that cdG does, in fact, have a role in the clustering of FliI complexes. An unexpected and exciting result came from the analysis in AFM of the G176A mutant. This mutant is active but insensitive to cdG. Although the regular-shaped and sized complexes were still formed, interestingly the structures corresponding to hexamers or dodecamers accumulated around the bigger complexes, creating a halo-like effect. This effect was unique to the specific mutant as it was not observed in any of the other mutants tested by this method, which behaved like the wild-type protein. Further tests need to be carried out to better characterise this unique conformation of the specific mutant.

Finally, the effect of cdG on the multimerization state of the protein was confirmed when FliI interaction to FliH was tested. The interaction of the two proteins was tested in the presence of increasing cdG concentrations, and it was observed that pre-incubation of cdG with FliI leads to higher binding responses when tested against FliH, indicating the formation of larger FliI complexes interacting with FliH.

Based on the results presented in this chapter, there are strong indications leading to the conclusion that cdG does indeed have an effect on the multimerization state of the protein, potentially leading to inhibition of FliC export via the flagellum export gate. However, further investigation is required to establish the biological role of cdG interaction with FliI.

Chapter 7:

Towards the determination of novel cdG targets

Chapter 7: Towards the determination of novel cdG targets

7.1 Introduction

As part of the work presented in this study, the importance of nucleotide-protein binding was emphasised and more specifically the importance of identifying novel targets of the small second messenger cdG. Although the metabolism of this molecule has been extensively studied, surprisingly little is known about its downstream targets. One of the reasons for that is that there is significant variation among cdG targets, which makes it impossible to predict them bioinformatically.

Following the Capture compound screen (described in Chapter 3), it was essential to test a large number of proteins to identify the true cdG targets and exclude false positives. The established cdG binding assays used by the field, although useful for certain proteins, did not give consistent results for all of them and are lacking in specificity and selectivity. To overcome this problem, an arsenal of biochemical tools was developed, which allowed the identification and characterisation of novel cdG targets. These tools not only helped with the identification of previously unknown cdG targets (e.g. the export ATPases) but also contributed to the characterisation of binding for a number of different proteins for international labs.

In this chapter, the testing and identification of four novel cdG binders are described:

7.1.1 EpsI/ Nla24

The first protein tested is EpsI/ Nla24, a transcriptional regulator protein, which is part of the NtrC-like transcriptional regulator family. EpsI/Nla24 controls the transcription of the EPS synthesis genes in *Myxococcus xanthus* and is essential for EPS production in this species. EpsI/Nla24 is associated with the regulation of *EPS* gene transcription both at

the developmental stage and also at the vegetative growth stage (306). It is structurally composed of three distinct domains; a receiver domain, part of a two component system, located at the N-terminal end of the protein, a AAA+ ATPase domain, and a helix-turn-helix (HTH) DNA-binding domain.

In many bacterial species, the regulation of EPS synthesis is directly associated with cdG levels in the cell (307). The regulation of EPS synthesis by cdG can either occur at the transcriptional or the post-translational level. Two of the most well-studied regulation mechanisms at the transcriptional level are the FleQ-mediated regulation of *EPS* gene expression in *Pseudomonas aeruginosa* and VpsR regulation in *Vibrio cholerae (84,246)*. Binding of cdG to FleQ releases its binding to the *pel* operon, responsible for the EPS production, and as a result, it activates EPS expression. On the other hand, VpsR is able to bind to its cognate promoters even at the absence of cdG, but it only exerts its activity when bound to cdG.

EpsI/ Nla24 has a similar function to FleQ in *M. xanthus*, and after having established the effects of cdG perturbation on *M. xanthus* cells (308), the protein was tested for cdG binding. EpsI/ Nla24 was first tested by DRaCALA but did not give a positive response. However, as this protein shares similarities in structure and function, as well as some of the key cdG binding residues of FleQ, it remained a likely cdG binding target. Consequently, I tested EpsI/ Nla24 cdG binding using both SPR and a novel, benchtop cdG binding assay, whose development is described in this thesis.

7.1.2 ToxR

ToxR/ RegA is a transcriptional regulator that has been associated with regulating the expression of an important virulence factor in *Pseudomonas aeruginosa*, exotoxin A (309,310). ToxR positively regulates exotoxin A production, as overproduction of the

ToxR protein *in trans* increases the production of the toxin. ToxR has also been associated with pyocin uptake and cell viability via positive regulation of the *tol-oprL* operon (311) as well as the regulation of a 42kDa iron protein (312).

Recent research conducted by Professor Miguel Camara's group at the University of Nottingham identified a new role of ToxR in the regulation of swarming, polysaccharide synthesis and biofilm formation in *P. aeruginosa* PAO1 (unpublished data). These phenotypes are well known to be very closely associated with cdG, so it was decided to further investigate ToxR's association with cdG. ToxR was shown to be a previously uncharacterised EAL domain protein (cdG diguanylate phosphodiesterase). Although it lacks the conserved catalytic residues responsible for the phosphodiesterase activity, it is possible that ToxR may be a cdG effector-like its closely related homologs LapD (235) and FimX (313). To confirm this, the first step was to test if *toxR* deletion has an effect on cdG levels in the cells. Indeed, when the levels of cdG were monitored in the cell, the *toxR* null mutant shows elevated dinucleotide concentrations compared to the wild type.

7.1.3 SadB

SadB has been associated with surface attachment and biofilm formation in *P. aeruginosa* PA14. This finding established the SadB protein as essential for surface monolayer formation (216). SadB was also found to be implicated in affecting swarming motility by exerting a direct effect on rhamnolipid sensing (314). The protein has also been linked to swarming motility in a FleQ-dependent manner (217). In *P. fluorescens*, SadB has been associated with the Gac system, which negatively regulates flagella-mediated motility (315). Finally, SadB is known to be involved in the Type IV pilus (T4P) biogenesis, as it acts upstream of the Pil-Chp chemotactic cluster (316,317). Structurally, SadB contains an HD(N)-GYP at the C-terminus, which does not exhibit any phosphodiesterase activity,

and a Ybak domain at the N-terminus. Both of these domains are required for function (216,315,316).

Although the exact function of SadB is not yet clear, it is well-established that the protein acts downstream of SadC in the cdG signalling cascade (221). However, there are a lot of hypotheses on how the protein may act. It was considered that SadB may assist SadC to its phosphodiesterase activity, acting upstream of cdG synthesis (221).

Another hypothesis is that SadB could act as a cdG effector, and form part of the signalling network responsible for transmitting the cdG signal to its downstream targets. Based on this hypothesis, SadB was tested as a potential cdG target in collaboration with Professor Rafael Rivilla's group (data not published).

7.1.4 RimK

RimK is an α-L-glutamate ligase enzyme, which catalyses the addition of glutamate residues to the C-terminal end of the ribosomal 30S subunit protein RpsF (318). Although the function of this protein has been well-documented, it has only recently been shown that the activity of this enzyme leads to alterations in ribosomal protein levels. It has also been demonstrated that deletion of the *rimK* gene has direct effects on bacterial behaviour in *Pseudomonas* species (319). RimK is part of an operon encoding for two more proteins; RimB and RimA, which tightly control its activity (319). RimA is an active phosphodiesterase involved in cdG metabolism, providing a potential link between RimK and cdG signalling.

7.2 Aims

1. To test previously uncharacterised proteins for cdG binding using the novel tools developed in this study.

7.3 Results

7.3.1 Identification of EpsI/ Nla24 transcriptional regulator as a cdG binder

To test EpsI/ Nla24 binding to cdG, the novel Streptavidin UV Precipitation (SUPr) assay was developed and employed. For this assay, whole cell lysates overexpressing the protein of interest were incubated with biotinylated cdG; then UV cross-linked before streptavidin magnetic beads were used to select and pull-down the proteins bound to the biotinylated-cdG. The bound proteins were then analysed on an SDS gel (Figure 7.1- A). Non-binding protein controls were included as appropriate (data not shown). As presented in Figure 7.1, EpsI/ Nla24 was selectively pulled down from the cell lysate.

Having established that cdG interacts with EpsI/ Nla24, the protein was then tested by SPR, to characterise the interaction better. In SPR, EpsI/ Nla24 gave a clear positive, concentration-dependent response confirming cdG binding (Figure 7.1- B). The SPR responses for different cdG concentrations were then plotted, producing an affinity curve (Figure 7.1- C) from which the binding affinity was calculated to be 0.53 ±0.06 μM, which is physiologically relevant for cdG binding proteins in *Myxococcus* (261).

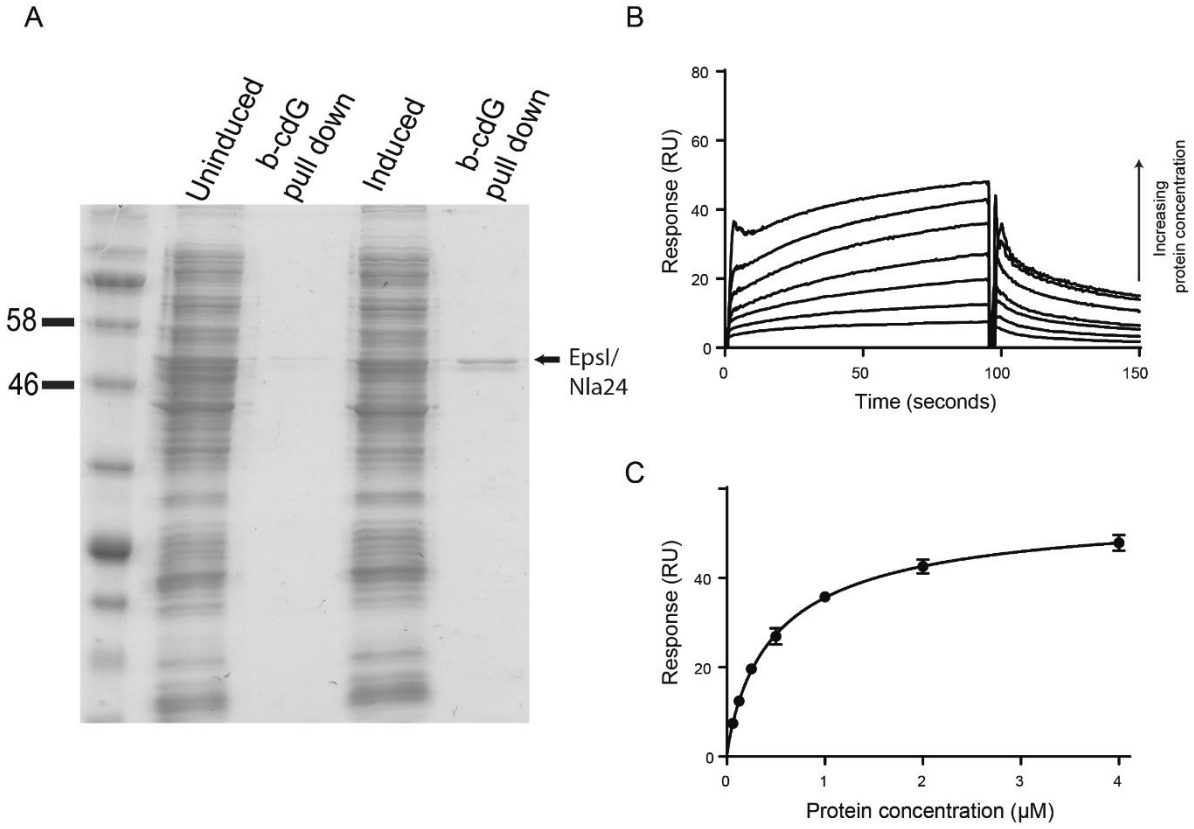

Figure 7.1: A. Streptavidin UV Precipitation (SUPr) assay on EpsI/ Nla24. Biotinylated cdG was used to pull down EpsI/ Nla24 from a complex protein mix. Non-induced lysate was used as a reference. B: SPR sensorgrams showing affinity measurements for EpsI/ Nla24 binding to biotinylated cdG. A range of EpsI/ Nla24 concentrations was used (ranging from 62.5 nM -lowest curve to 4 μM- highest curve), for each concentration 3 replicates were included. Buffer only and BSA controls were also included as negative controls. C. Affinity fit describing EpsI/ Nla24-cdG binding. Binding responses was recorded 4 s before the end of the injection for each concentration, the K_D value for EpsI/ Nla24 binding to cdG was calculated to be 0.53 ± 0.06 μM and the analysis was carried out on BiaEvaluation software and confirmed by GraphPad Prism. Figure adapted from (261).

7.3.2 Identification of the transcriptional regulator ToxR as a cdG binder

To test the possibility of ToxR being a cdG binder, the binding was tested using the well-established SPR method.

Although the ToxR was rather unstable in solution and exhibited a rapid degradation rate, it was possible to purify it and test it by SPR in the first few hours after purification. As presented in Figure 7.2, it was possible to detect concentration-dependent responses in a series of SPR experiments. The K_D of the interaction was calculated to be 2.36 ± 0.7 μM, which is biologically relevant for a cdG binding protein in *P. aeruginosa* (Figure 7.2- B).

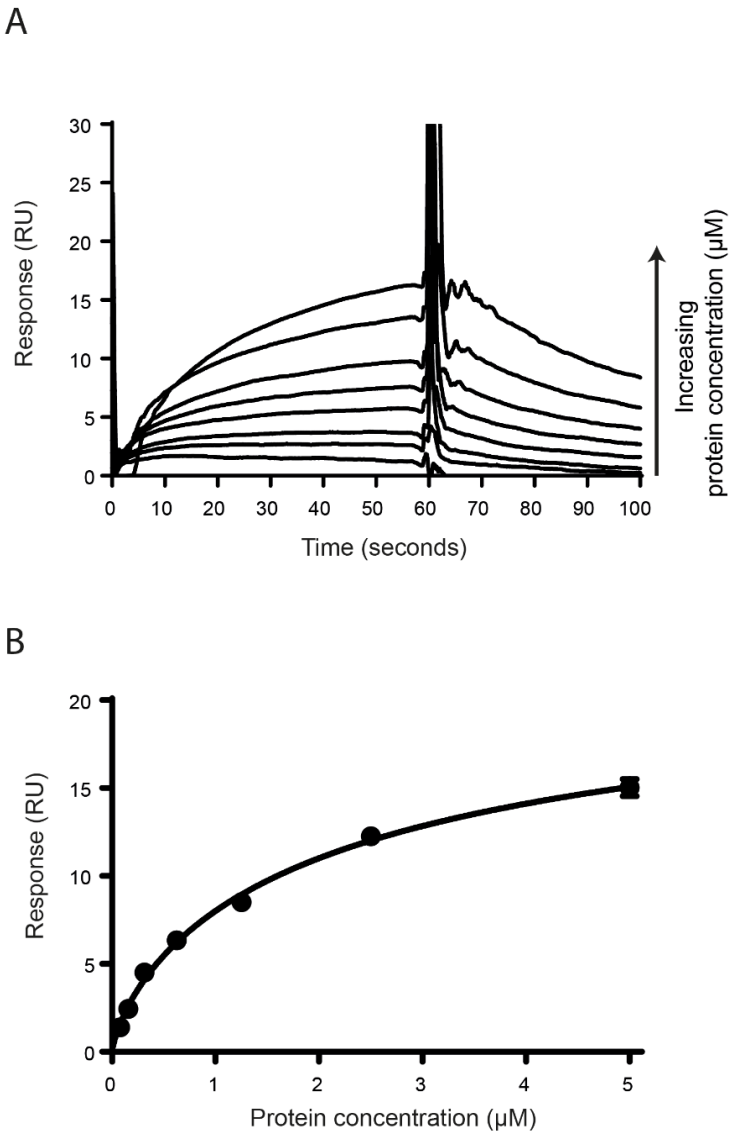

Figure 7.2: A. SPR sensorgrams showing affinity measurements for ToxR binding to biotinylated cdG. A range of ToxR concentrations was used (ranging from 78.125 nM -lowest curve to 5.0 µM - highest curve), for each concentration 3 replicates were included. Buffer only and BSA controls were also included as negative controls. B. Affinity fit describing ToxR -cdG binding. Binding responses were recorded 4 s before the end of the injection for each concentration, the K_D value for ToxR binding to cdG was calculated to be 2.36 ± 0.7 µM and the analysis was carried out on BiaEvaluation software and confirmed by GraphPad Prism.

7.3.3 Identification of the transcriptional regulator SadB as a cdG binder

To test SadB for cdG binding, the protein was first tested by the SUPr assay. Whole cell lysates overexpressing SadB were used. The lysates were incubated and cross-linked with biotinylated cdG for the stabilisation of the complex formation. The complexes were then isolated by streptavidin magnetic beads and the fractions were analysed on SDS-PAGE gels. As presented in Figure 7.3- A SadB was clearly isolated from the complex protein mixture. Non-induced cell lysates and non-binding protein controls were used as negative controls for the pull-down experiment.

To further characterise the cdG interaction with SadB, SPR was employed. The protein gave positive concentration-dependent responses, strongly indicating binding to cdG (Figure 7.3- B). To calculate the affinity of this interaction the responses for each concentration were plotted to produce an affinity curve (Figure 7.3- C). The K_D of the interaction was calculated to be 0.23± 0.034 μM, which again is biologically relevant in *Pseudomonas* cdG binders.

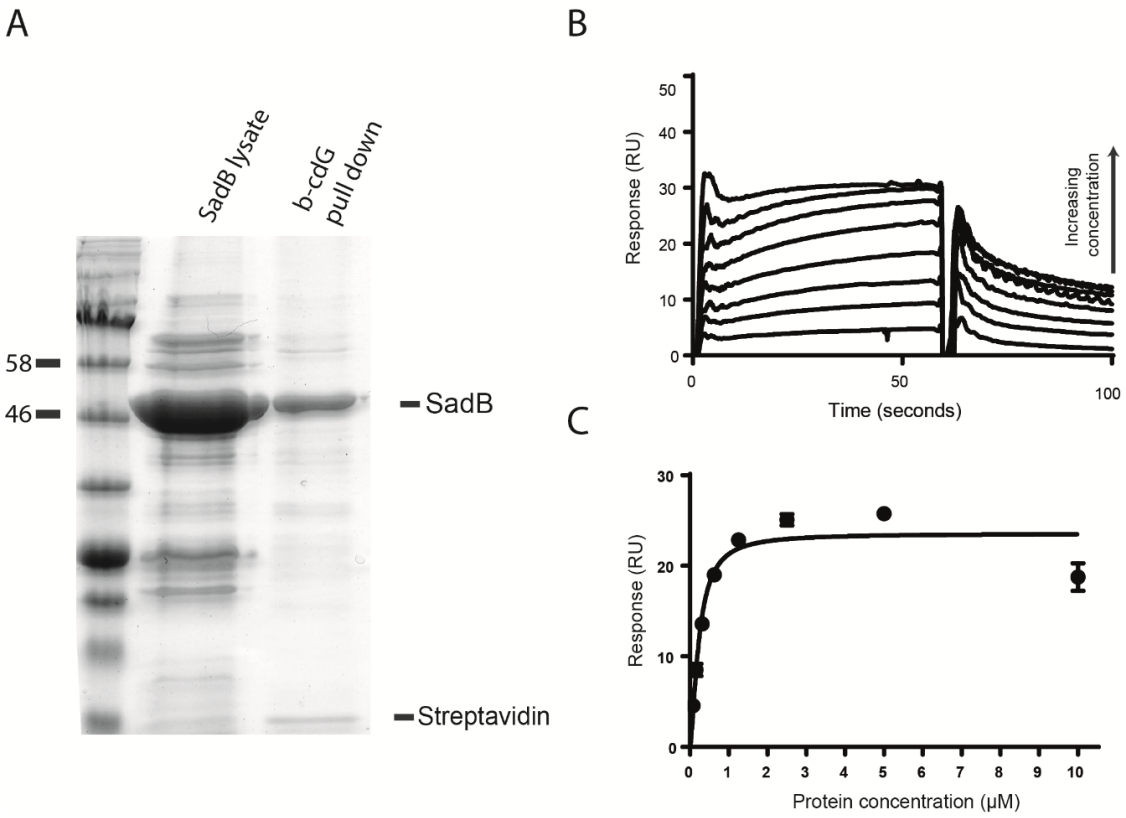

Figure 7.3: A. Streptavidin UV Precipitation (SUPr) assay on SadB. Biotinylated cdG was used for the isolation of SadB from a complex mix of proteins. Non-binding proteins as well as non-induced cell lysates were included as negative controls (data not shown) B: SPR sensorgrams showing affinity measurements for SadB binding to biotinylated cdG. A range of SadB concentrations was used (ranging from 78.125 nM -lowest curve to 10 μM - highest curve), for each concentration 3 replicates were included. Buffer only and BSA controls were also included as negative controls. C. Affinity fit describing SadB-cdG binding. Binding responses was recorded 4 s before the end of the injection for each concentration, the K_D value for SadB binding to cdG was calculated to be 0.23± 0.034 μM and the analysis was carried out on BiaEvaluation software and confirmed by GraphPad Prism.

7.3.4 Identification of the *L-glutamate ligase* RimK as a cdG binder

In this project, RimK proteins from *P. fluorescens* and *E. coli* were tested for binding. Each protein was first tested for cdG binding by the SUPr assay. Whole cell lysates overexpressing RimK were incubated with biotinylated cdG, cross-linked and isolated with streptavidin magnetic beads, before being analysed on an SDS-PAGE gel. As presented in Figure 7.4- A RimK could be isolated from the complex whole cell lysate mix. Cell lysates from non-induced cultures were used as a negative control.

SPR was the next assay employed to further characterise the interaction, resulting in positive concentration-dependent responses, which strongly indicate binding to cdG (Figure 7.4- B). The affinity of the interaction in each case was calculated by an affinity curve (Figure 7.4- C). The K_D of the interaction for RimK from *P. fluorescens* was calculated to be 1.0 μM and for *E. coli* the K_D was 3.8 μM.

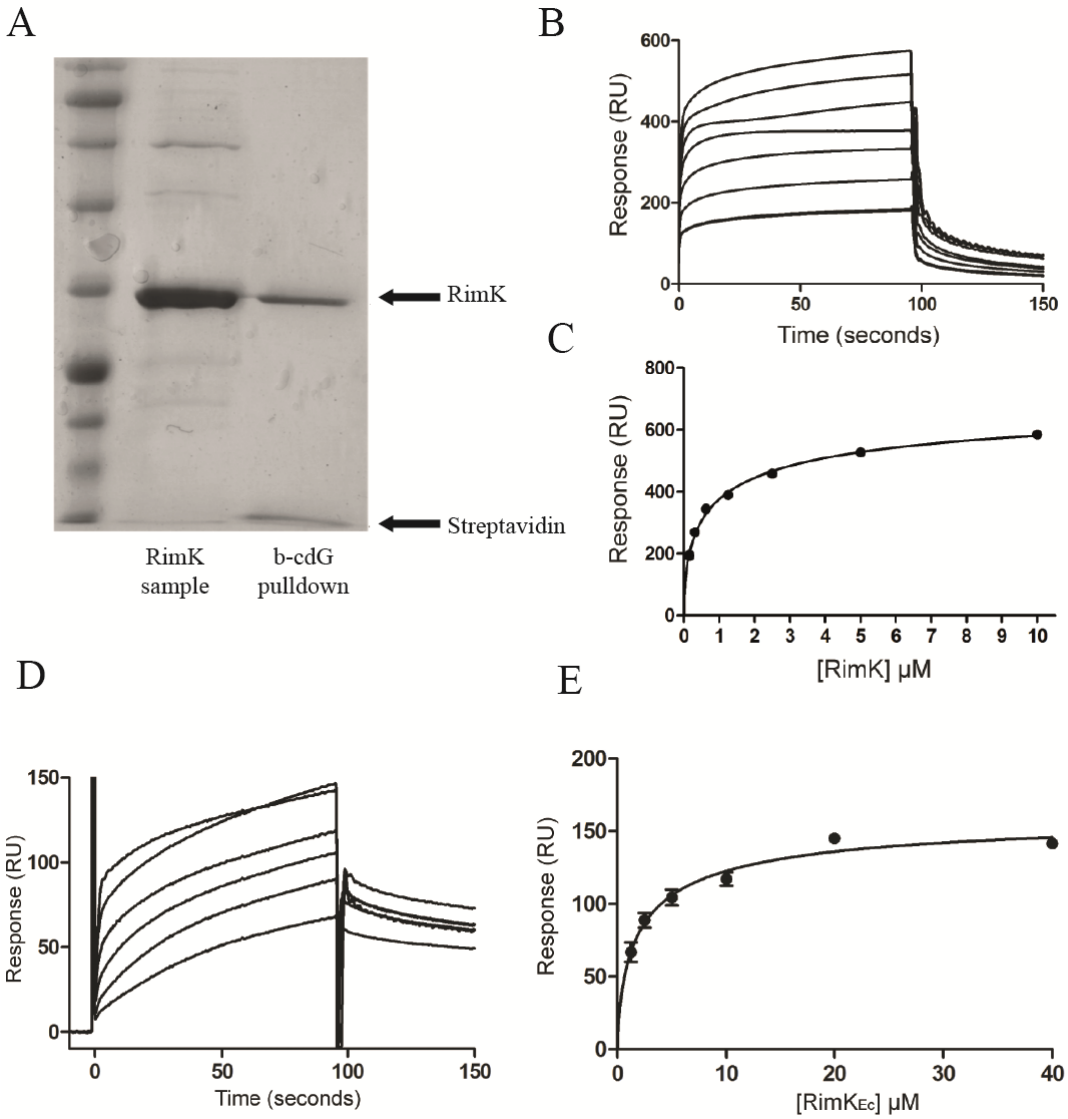

Figure 7.4: A. Streptavidin UV Precipitation (SUPr) assay on RimK. Biotinylated cdG was used for the isolation of RimK from E. coli overexpression cell lysate, the b-cdG pull down is loaded alongside B, D: SPR sensorgrams showing affinity measurements for RimK binding to biotinylated cdG (for RimK from P. fluorescens and E. coli respectively). A range of RimK concentrations was used (ranging from 156 nM -lowest curve to 10 µM - highest curve for P. fluorescens and 1.25 µM -lowest curve to 40 µM - highest curve for E. coli). For each concentration 3 replicates were included. Buffer only and BSA controls were also included as negative controls as appropriate. C, E. Affinity fit describing RimK -cdG binding (for RimK from P. fluorescens and E. coli respectively). Binding responses was recorded 4 s before the end of the injection for each concentration, the K_D value for RimK from P. fluorescens and from E. coli were 1 µM and 3.8 respectively. The analysis was carried out on BiaEvaluation software and confirmed by GraphPad Prism. Figure adapted from (319).

7.4 Discussion

In recent years, it has become clear that the mechanisms underpinning cdG regulation networks are much more complicated than originally thought. In response to this realisation, there has been a constant effort to identify novel cdG targets and characterise them to get a better understanding of how cdG-mediated signalling is regulated. The limiting factor, however, is the lack of highly efficient screens and biochemical tools to characterise the potential binders.

In this chapter, I describe two new cdG analytical tools, developed as part of this study and applied to different proteins to test them and characterise their cdG binding behaviour. The first protein tested was the transcriptional regulator EpsI/ Nla24, from Lotte Søgaard-Andersen's group, in Germany. Although these were strong experimental indications that the protein may act as a cdG binder, the lack of effective biochemical assays for nucleotide-protein interactions, prevented the characterisation of this protein's association with cdG. Here, a dual approach was followed that allowed the efficient characterisation of this interaction. The first method used to test binding was the novel Streptavidin UV Precipitation (SUPr) assay, which I developed as part of this study. This assay is highly specific, resulting in consistent and reproducible results. It is also ideal for screening of multiple targets simultaneously, which makes it an invaluable tool for the analysis of 'big-screening' targets. When the SUPr assay was applied to EpsI/ Nla24, it was possible to specifically isolate this protein from a complex cell lysate, strongly indicating binding to cdG. As a negative control for the method, non-induced lysates were used where no isolation of EpsI/ Nla24 was detected.

Although SUPr is a very efficient assay for rapid binding detection, it doesn't provide any information about the nature of the interaction or its affinity. To complement this method and further characterise the interaction between EpsI/ Nla24 and cdG, SPR was used,

following its effective application to FliI and HrcN. EpsI/ Nla24 binding to cdG has significant implications for our understanding of cdG signalling networks in *M. xanthus*. This result strongly indicates that EPS synthesis in this bacterium is controlled at the transcriptional level by EpsI/ Nla24, via direct regulation from cdG (261).

A second example of a previously unidentified cdG binding protein presented in this chapter is the transcriptional regulator ToxR. ToxR is a previously unidentified EAL domain protein, which lacks cdG phosphodiesterase activity. However, it is not uncommon for a degenerate EAL domain protein to be a cdG binder. Results from Professor Miguel Camara's group showed that the deletion of this protein leads to increased levels of cdG in the cell, indicating a role of ToxR in the cdG-controlled regulatory network. To test binding of cdG to the protein, the SPR approach was followed as the protein was rather unstable and exhibited a fast degradation rate, which made it unsuitable for the SUPr assay. However, in SPR the protein demonstrated positive concentration-dependent responses to increasing levels of cdG, indicating binding with a K_D in the low μM range. Since similar cdG regulatory pathways have previously been identified in *Xanthomonas campestris* (320) and *E. coli* (321), this result suggests that cdG regulation at the transcriptional level may be a common trait among different bacterial species.

The third protein tested was SadB, a protein that has been implicated many times in common bacterial behaviours associated with cdG but has not previously been linked to cdG binding. A similar approach was used for this protein; binding of the protein to cdG was firstly shown by SUPr, where the protein was very efficiently separated from the complex protein mixture. The interaction was then tested further by SPR resulting in a K_D for the interaction in the low μM range. Although the interaction of SadB to cdG has been previously hypothesised, it was first shown experimentally as part of this study.

Another previously unknown cdG binder, identified in this study is RimK. Binding was tested both in *E. coli* and *P. fluorescens* giving affinities in the low μM range, implying that the binding may be widespread among RimK homologs. CdG binding to RimK was shown to boost its glutamate ligase activity (319). RimA, which is part of the same operon as RimK, is an active phosphodiesterase, making it likely that it may hydrolyse cdG under certain conditions to alter RimK activity. This study unravelled a novel regulatory pathway linking cdG binding proteins to the ribosome function and proteome remodelling (319).

The identification of these novel cdG binding proteins gives a good indication of how complex cdG networks are, and how important is to be able to rely on efficient biochemical tools to characterise these targets. Here I present two valuable new analytical tools for the study of cdG binding proteins in bacteria and demonstrate their utility to the examination of different signalling systems in a variety of bacterial species.

Chapter 8:

General discussion

Chapter 8: General Discussion

8.1 Summary

The wider aim of this study was to identify and characterise novel cdG binding proteins in *P. fluorescens* SBW25. To this end, an array of pull-down screens were performed (249), which led to the identification of a number of potential cdG targets. Several of the most biologically interesting targets were then selected and biochemically tested for binding. Among these targets, the flagellum main ATPase FliI was identified as a novel cdG binder. Molecular biology and biochemistry techniques were employed to characterise the nature of cdG binding to FliI, to examine the degree of conservation of cdG binding among FliI homologs and to determine the effect of binding on the protein's activity. Determination of the binding site at the interface between the two FliI subunits opened the path to further investigate the physiological role of binding, and the effects that this has on the multimerization state of the protein. Finally, the important biochemical tools developed and optimised in this study were used to identify more protein targets for cdG binding, expanding our understanding on how cdG signalling networks operate.

8.2 Discussion

To identify novel cdG binding proteins, the capture compound pull-down screening experiment (249) was performed in various media and growth conditions. The reason for repeating the screen in these different experimental conditions (described in detail in Chapter 3) was to compensate for the well-reported characteristic of bacteria to express genes both conditionally and transiently, to meet the immediate needs of the organism in a specific growth condition (322). For instance, FliI was identified as a potential candidate only in the stationary phase in LB. The isolation of the protein at this stage could potentially be due to experimental variation or due to the absence of other cdG binders at

this growth phase, which made it possible for FliI to interact with cdG. The cells exhibited a motile phenotype at the stationary phase, when observed under the microscope, which indicates a strong presence of FliI, together with the rest of the flagellum components at this growth phase. Minimal media (M9-pyruvate) was used to induce the expression of genes that may be required to survive in poor growth conditions, and that would not be expressed in rich media.

Although the pull-down screens led to the identification of a number of potential cdG targets, many of these were shown to be false positives when tested using the biochemical assays available at the beginning of this study. However, I strongly believe that the lack of more sophisticated and precise tools at this early stage of the project may have led to the mis-characterisation of some of these targets. In my opinion it would be well worth testing some of these proteins again, using the novel tools developed in the course of this study (e.g. by SUPr or SPR).

Strikingly, FliI ATPase was identified as one of the stronger binding proteins in the capture compound screen, and when tested by DRaCALA gave strong concentration-dependent responses. To further characterise cdG binding to this protein, I performed several state-of-the-art biochemical techniques such as ITC and SPR. These techniques provided a deep insight into the nature of binding. For instance, ITC provided information about the stoichiometry of the interaction, which was found to be a ratio of 2:1 protein to cdG. This result was a first indication that two molecules of the protein are needed for binding to one molecule of cdG, and that cdG binding may therefore occur at the interface between two protein subunits. The binding affinity was calculated by SPR in the low μM range, a physiologically relevant affinity for cdG binders (229). Excitingly, binding was also confirmed for FliI homologs from other organisms. These homologs were strategically selected to cover a wide range of organisms from distinct categories (plant

pathogen, plant symbiotant and human pathogen). Confirming binding in all these three categories shows how widespread the binding is and implies that cdG binding to FliI is a universal trait.

The next step after confirming and characterising the nature of binding, was to identify the exact binding site. Knowing the location of the FliI-cdG binding site is a very important step towards the identification of the role of binding to the protein. Knowing the exact binding location allows not only to generate specific mutants and perturb protein function in *vivo* but also it enables the prediction of cdG binding proteins having the same sharing domains. To achieve this, several attempts to crystallise FliI from SBW25 were carried out. Unfortunately, however, these yielded no promising results. Finally, FliI from *S. enterica* was crystallised in the presence of cdG and ADP. Unfortunately, the location of cdG could not be resolved in the FliI structure. Since its presence in the trials was essential for crystals to be produced, it is possible that the molecule was present, but only in a percentage of the available binding sites of the protein, resulting in a too-low electron density to enable the resolution of its structure. Another possibility is that the binding pocket could not be formed properly because the truncated version of the *Salmonella* protein was used for crystallisation. This truncated allele is well-reported as being unable to form multimers higher in order than dimers (323). As a result, the binding site may not be available when the truncated protein is crystallised in the monomeric state as it may only occur in the hexameric state of the protein. Another possibility is that given that it was shown that the binding occurs at the interface between the two FliI subunits, with specific amino acid contributions from each subunit, it may be that $FliI_{\Delta 1\text{-}18}$ crystallises in a way, which doesn't allow for these residues to come together and form the binding pocket.

Despite the lack of a crystal structure of FliI bound to cdG, the importance of determining the binding site led me to look for other methods and tools to achieve it. Two complementary *in silico* analyses were performed (described in detail in chapter 5), both pointing to a conserved binding site at the interface between the two FliI subunits. This binding site was subsequently confirmed by producing the mutated protein analogues by site-directed mutagenesis, purifying them and testing them for binding by SPR. The determination of the binding site at the interface between the two subunits strongly indicates, given the way FliI functions, that cdG binding may affect the multimerization state of the protein and thus, its function in the wider flagellar context.

The specific *in vivo* role of the FliI-cdG interaction remains to be unravelled, and at this stage we can only speculate as to what it may be. The first hypothesis is that it may act as a fine control of the export via the flagellum by altering the multimerization state of the protein. Indeed, preliminary data, presented in chapter 6, shows that the flagellin export levels drop when cdG concentration in the cells increases. However, although I eliminated the FleQ cdG-dependent transcriptional control mechanism (see Chapter 6), we cannot rule out the possibility that another, as yet uncharacterised cdG-dependent flagellar control mechanism may exist. Another hypothesis, is that given that cdG binding occurs at the interface between the two FliI subunits, it may lead to an asymmetry in the hexameric complex, facilitating the association and dissociation of ATP at the enzyme active sites. Although our ATPase activity results suggest an inhibition of ATPase activity by cdG, the IC_{50} values are far from physiological, making it unlikely that this represents the actual role of cdG binding in vivo. A third theory is that cdG binding to FliI may influence the direction of rotation of the protein, affecting protein export as a consequence of this. Finally, it is also possible that cdG is required for the rapid disassembly of the filament of the flagellum in circumstances where the bacterium needs to detection by the

host, given that flagellin is well-reported to be triggering the innate immune response of host cells (324).

The role of cdG binding to the T3SS and T6SS export systems is very uncertain and needs further characterisation. However, it is well-known that these two systems are reciprocally regulated by cdG (222) during the switch between acute and chronic infection, and it is possible that cdG triggers the rapid switching between these two systems. In this model, HrcN and ClpB2 would facilitate the assembly and disassembly of the needle structures of the two organelles in response to cdG binding. Another hypothesis is that cdG interaction with FliI may be a control mechanism for the export of structural subunits the effector proteins exported by the secretory complexes. In this model, cdG binding to the T3/6SS would play a similar role to that observed for the flagellum (Chapter 6).

The initial aim of this study was to expand our understanding of cdG signalling mechanisms by the identification of novel targets of the molecule. The development of novel biochemical tools for the characterisation of binding targets, together with the optimisation of existing assays worked towards this direction. During the course of this study, I developed and pioneered the use of novel tools for the examination of protein-nucleotide interactions (e.g. the SUPr assay), which proved to be valuable assets for the investigation for novel cdG targets. In chapter 7, I describe how these tools were used for the characterisation of binding to four previously unknown cdG targets (EpsI/Nla24, ToxR, SadB and RimK).

8.3 Implications

CdG binding to FliI and its orthologs is a discovery with great implications. Although the export ATPases have been extensively studied, binding to a new ligand, which potentially

alters their function and multimerization state, make the existing models of hexameric export ATPases incomplete. Additionally, our perception of the flagellum organelle assembly and function change in light of this discovery as it was shown that are controlled by cdG, something previously unknown. Finally, modifications in the function of the ATPases as well as in the organelle assembly, lead to direct effects of cdG in motility and virulence, implying that existing models describing how these behaviours function are now incomplete and need to change in light of this discovery.

Furthermore, new tools developed in the course of this study will advance and speed up cdG research and can also expand into other nucleotide second messengers.

Finally, the identification of a new class of cdG receptors, the export ATPases, together with the characterisation of binding for a number of different transcriptional regulators as well as the ribosomal modification protein RimK, changes what we know so far for cdG binding. Through the course of this study, more diverse cdG binding proteins were discovered, broadening the existing knowledge about cdG binding protein diversity.

8.4 Future directions of research

By carrying out a number of screening experiments aimed at the identification of novel cdG binders, an exhaustive database of potential cdG targets was produced. In this study, only a small number of the proteins was tested for binding. Hence, an obvious starting point for future analysis would be to start testing some of the most exciting targets using the tools developed in the course of this study.

My attempts to co-crystallise cdG with the truncated version of FliI were unsuccessful. Nonetheless, it would be reasonable to return to this by attempting to crystallise the full-length protein and its orthologs, HrcN and $ClpB_2$. Using the full-length proteins will certainly be a harder task for the purposes of crystallisation because of the higher order

formation and aggregation of the proteins in higher concentrations. It is also possible that one of the orthologs from the T3SS or the T6SS may be more amenable to crystallisation.

To investigate the biological role of the FliI-cdG interaction further, the first obvious step would be to chromosomally introduce the mutations of the binding site into the *fliI* gene and test the resulting mutants for export, flagellum assembly, and rotation. We could also examine the impact of cdG perturbation on motility in the mutant background. In this case, the mutations would need to be introduced in the FleQ-bypass background to avoid the cdG-dependent regulation of flagellar transcription by FleQ.

To test protein export via the flagellum, a similar approach to the one described in Chapter 6 would be followed, in which the levels of exported flagellin subunits would be monitored by Western blotting. For the evaluation of flagella assembly, TEM could be employed to look for extracellular forming structures on the cells. Lastly, the flagellar rotation could be tested by artificially re-building the FliI-FliJ system in vitro, then monitoring rotation by the detection of the rotation speed of a fluorescently labelled actin filament, attached to FliJ. This method was previously carried out for the F_0F_1 ATPase (325). Rotary ATPase proteins are central players in control of bacterial virulence and motility. This work establishes a fundamental role for the second messenger cdG in the function of these proteins.

Bibliography

1. Kloepper JW, Leong J, Teintze M, Schroth MN. Enhanced plant growth by siderophores produced by plant growth-promoting rhizobacteria. Nature. 1980 Aug 28;286(5776):885–886.

2. Haas D, Défago G. Biological control of soil-borne pathogens by fluorescent pseudomonads. Nat Rev Microbiol. 2005 Apr;3(4):307–319.

3. Glick BR. Plant growth-promoting bacteria: mechanisms and applications. Scientifica (Cairo). 2012 Sep 19;2012:963401.

4. Glick BR. The enhancement of plant growth by free-living bacteria. Can J Microbiol. 1995 Feb;41(2):109–117.

5. Compant S, Duffy B, Nowak J, Clément C, Barka EA. Use of plant growth-promoting bacteria for biocontrol of plant diseases: principles, mechanisms of action, and future prospects. Appl Environ Microbiol. 2005 Sep;71(9):4951–4959.

6. Chin-A-Woeng TF, Bloemberg GV, Mulders IH, Dekkers LC, Lugtenberg BJ. Root colonization by phenazine-1-carboxamide-producing bacterium *Pseudomonas chlororaphis* PCL1391 is essential for biocontrol of tomato foot and root rot. Mol Plant Microbe Interact. 2000 Dec;13(12):1340–1345.

7. Chin-A-Woeng TFC, de Priester W, van der Bij AJ, Lugtenberg BJJ. Description of the Colonization of a Gnotobiotic Tomato Rhizosphere by *Pseudomonas fluorescens* Biocontrol Strain WCS365, Using Scanning Electron Microscopy. Mol Plant Microbe Interact. 1997 Jan;10(1):79–86.

8. Whipps JM. Microbial interactions and biocontrol in the rhizosphere. J Exp Bot. 2001 Mar;52(Spec Issue):487–511.

9. Stoodley P, Sauer K, Davies DG, Costerton JW. Biofilms as complex differentiated communities. Annu Rev Microbiol. 2002 Jan 30;56:187–209.

10. Lugtenberg BJ, Dekkers LC. What makes *Pseudomonas* bacteria rhizosphere competent? Environ Microbiol. 1999 Feb;1(1):9–13.

11. Pedgley DE. Aerobiology: The Atmosphere as a Source and Sink for Microbes. In: Andrews JH, Hirano SS, editors. Microbial Ecology of Leaves. New York, NY: Springer New York; 1991. p. 43–59.

12. Broek AV. The Role of Bacterial Motility, Chemotaxis, and Attachment in Bacteria-Plant Interactions. Mol Plant Microbe Interact. 1995;8(6):800.

13. Lugtenberg B, Kamilova F. Plant-growth-promoting rhizobacteria. Annu Rev Microbiol. 2009;63:541–556.

14. Ramey BE, Koutsoudis M, von Bodman SB, Fuqua C. Biofilm formation in plant-microbe associations. Curr Opin Microbiol. 2004 Dec;7(6):602–609.

15. Lugtenberg BJ, Dekkers L, Bloemberg GV. Molecular determinants of rhizosphere colonization by *Pseudomonas*. Annu Rev Phytopathol. 2001; 39:461–490.

16. Alsohim AS, Taylor TB, Barrett GA, Gallie J, Zhang X-X, Altamirano-Junqueira AE, et al. The biosurfactant viscosin produced by *Pseudomonas fluorescens* SBW25 aids spreading motility and plant growth promotion. Environ Microbiol. 2014 Jul;16(7):2267–2281.

17. Harshey RM. Bacterial motility on a surface: many ways to a common goal. Annu Rev Microbiol. 2003; 57:249–273.

18. Mattick JS. Type IV pili and twitching motility. Annu Rev Microbiol. 2002 Jan 30; 56: 289–314.

19. Matsuyama T, Bhasin A, Harshey RM. Mutational analysis of flagellum-independent surface spreading of *Serratia marcescens* 274 on a low-agar medium. J Bacteriol. 1995 Feb;177(4):987–991.

20. Martínez A, Torello S, Kolter R. Sliding motility in mycobacteria. J Bacteriol. 1999 Dec;181(23):7331–7338.

21. Harshey RM. Bees aren't the only ones: swarming in gram-negative bacteria. Mol Microbiol. 1994 Aug;13(3):389–394.

22. Macfarlane S, Hopkins MJ, Macfarlane GT. Toxin synthesis and mucin breakdown are related to swarming phenomenon in *Clostridium septicum*. Infect Immun. 2001 Feb;69(2):1120–1126.

23. Diepold A, Armitage JP. Type III secretion systems: the bacterial flagellum and the injectisome. Philos Trans R Soc Lond, B, Biol Sci. 2015 Oct 5;370(1679).

24. Haiko J, Westerlund-Wikström B. The role of the bacterial flagellum in adhesion and virulence. Biology. 2013 Oct 25;2(4):1242–1267.

25. Parthasarathy G, Yao Y, Kim KS. Flagella promote *Escherichia coli* K1 association with and invasion of human brain microvascular endothelial cells. Infect Immun. 2007 Jun;75(6):2937–2945.

26. Dons L, Eriksson E, Jin Y, Rottenberg ME, Kristensson K, Larsen CN, et al. Role of flagellin and the two-component CheA/CheY system of *Listeria monocytogenes* in host cell invasion and virulence. Infect Immun. 2004 Jun;72(6):3237–3244.

27. Young GM, Schmiel DH, Miller VL. A new pathway for the secretion of virulence factors by bacteria: the flagellar export apparatus functions as a protein-secretion system. Proc Natl Acad Sci U S A. 1999 May 25;96(11):6456–6461.

28. Macnab RM. Type III flagellar protein export and flagellar assembly. Biochim Biophys Acta. 2004 Nov 11;1694(1-3):207–217.

29. Aldridge P, Hughes KT. Regulation of flagellar assembly. Curr Opin Microbiol. 2002 Apr;5(2):160–165.

30. Chilcott GS, Hughes KT. Coupling of flagellar gene expression to flagellar assembly in *Salmonella enterica serovar typhimurium* and *Escherichia coli*. Microbiol Mol Biol Rev. 2000 Dec;64(4):694–708.

31. Aldridge P, Jenal U. Cell cycle-dependent degradation of a flagellar motor component requires a novel-type response regulator. Mol Microbiol. 1999 Apr;32(2):379–391.

32. Evans LDB, Hughes C, Fraser GM. Building a flagellum outside the bacterial cell. Trends Microbiol. 2014 Oct;22(10):566–572.

33. Roberts MAJ, Papachristodoulou A, Armitage JP. Adaptation and control circuits in bacterial chemotaxis. Biochem Soc Trans. 2010 Oct;38(5):1265–1269.

34. Chevance FFV, Hughes KT. Coordinating assembly of a bacterial macromolecular machine. Nat Rev Microbiol. 2008 Jun;6(6):455–465.

35. Leake MC, Chandler JH, Wadhams GH, Bai F, Berry RM, Armitage JP. Stoichiometry and turnover in single, functioning membrane protein complexes. Nature. 2006 Sep 21;443(7109):355–358.

36. Blair DF. Fine structure of a fine machine. J Bacteriol. 2006 Oct;188(20):7033–7035.

37. Macnab RM. How bacteria assemble flagella. Annu Rev Microbiol. 2003 May 1; 57: 77–100.

38. Homma M, Kutsukake K, Hasebe M, Iino T, Macnab RM. FlgB, FlgC, FlgF and FlgG. A family of structurally related proteins in the flagellar basal body of *Salmonella typhimurium*. J Mol Biol. 1990 Jan 20;211(2):465–477.

39. Jones CJ, Macnab RM. Flagellar assembly in *Salmonella typhimurium*: analysis with temperature-sensitive mutants. J Bacteriol. 1990 Mar;172(3):1327–1339.

40. Lee HJ, Hughes KT. Posttranscriptional control of the *Salmonella enterica* flagellar hook protein FlgE. J Bacteriol. 2006 May;188(9):3308–3316.

41. Hirano T, Minamino T, Macnab RM. The role in flagellar rod assembly of the N-terminal domain of *Salmonella* FlgJ, a flagellum-specific muramidase. J Mol Biol. 2001 Sep 14;312(2):359–369.

42. Stafford GP, Hughes C. *Salmonella typhimurium* flhE, a conserved flagellar regulon gene required for swarming. Microbiology (Reading, Engl). 2007 Feb;153(Pt 2):541–547.

43. Attmannspacher U, Scharf BE, Harshey RM. FliL is essential for swarming: motor rotation in absence of FliL fractures the flagellar rod in swarmer cells of *Salmonella enterica*. Mol Microbiol. 2008 Apr;68(2):328–341.

44. Blair DF, Berg HC. The MotA protein of E. coli is a proton-conducting component of the flagellar motor. Cell. 1990 Feb 9;60(3):439–449.

45. Berg HC. The rotary motor of bacterial flagella. Annu Rev Biochem. 2003;72:19–54.

46. Zhao R, Pathak N, Jaffe H, Reese TS, Khan S. FliN is a major structural protein of the C-ring in the *Salmonella typhimurium* flagellar basal body. J Mol Biol. 1996 Aug 16;261(2):195–208.

47. Zhao R, Amsler CD, Matsumura P, Khan S. FliG and FliM distribution in the *Salmonella typhimurium* cell and flagellar basal bodies. J Bacteriol. 1996 Jan;178(1):258–265.

48. Kubori T, Yamaguchi S, Aizawa S. Assembly of the switch complex onto the MS ring complex of *Salmonella typhimurium* does not require any other flagellar proteins. J Bacteriol. 1997 Feb;179(3):813–817.

49. Kihara M, Miller GU, Macnab RM. Deletion analysis of the flagellar switch protein FliG of *Salmonella*. J Bacteriol. 2000 Jun;182(11):3022–3028.

50. Grünenfelder B, Gehrig S, Jenal U. Role of the cytoplasmic C terminus of the FliF motor protein in flagellar assembly and rotation. J Bacteriol. 2003 Mar;185(5):1624–1633.

51. Bren A, Eisenbach M. The N terminus of the flagellar switch protein, FliM, is the binding domain for the chemotactic response regulator, CheY. J Mol Biol. 1998 May 8;278(3):507–514.

52. Toker AS, Macnab RM. Distinct regions of bacterial flagellar switch protein FliM interact with FliG, FliN and CheY. J Mol Biol. 1997 Oct 31;273(3):623–634.

53. González-Pedrajo B, Minamino T, Kihara M, Namba K. Interactions between C ring proteins and export apparatus components: a possible mechanism for facilitating type III protein export. Mol Microbiol. 2006 May;60(4):984–998.

54. Paul K, Harmon JG, Blair DF. Mutational analysis of the flagellar rotor protein FliN: identification of surfaces important for flagellar assembly and switching. J Bacteriol. 2006 Jul;188(14):5240–5248.

55. McMurry JL, Murphy JW, González-Pedrajo B. The FliN-FliH interaction mediates localization of flagellar export ATPase FliI to the C ring complex. Biochemistry. 2006 Oct 3;45(39):11790–11798.

56. Samatey FA, Matsunami H, Imada K, Nagashima S, Shaikh TR, Thomas DR, et al. Structure of the bacterial flagellar hook and implication for the molecular universal joint mechanism. Nature. 2004 Oct 28;431(7012):1062–1068.

57. Shaikh TR, Thomas DR, Chen JZ, Samatey FA, Matsunami H, Imada K, et al. A partial atomic structure for the flagellar hook of *Salmonella typhimurium*. Proc Natl Acad Sci U S A. 2005 Jan 25;102(4):1023–1028.

58. Hirano T, Yamaguchi S, Oosawa K, Aizawa S. Roles of FliK and FlhB in determination of flagellar hook length in *Salmonella typhimurium*. J Bacteriol. 1994 Sep;176(17):5439–5449.

59. Ikeda T, Asakura S, Kamiya R. Cap" on the tip of *Salmonella* flagella. J Mol Biol. 1985 Aug 20;184(4):735–737.

60. Homma M, Iino T. Locations of hook-associated proteins in flagellar structures of S*almonella typhimurium*. J Bacteriol. 1985 Apr;162(1):183–189.

61. Imada K, Vonderviszt F, Furukawa Y, Oosawa K, Namba K. Assembly characteristics of flagellar cap protein HAP2 of *Salmonella*: decamer and pentamer in the pH-sensitive equilibrium. J Mol Biol. 1998 Apr 10;277(4):883–891.

62. Larsen SH, Reader RW, Kort EN, Tso WW, Adler J. Change in direction of flagellar rotation is the basis of the chemotactic response in *Escherichia coli*. Nature. 1974 May 3;249(452):74–77.

63. Homma M, DeRosier DJ, Macnab RM. Flagellar hook and hook-associated proteins of *Salmonella typhimurium* and their relationship to other axial components of the flagellum. J Mol Biol. 1990 Jun 20;213(4):819–832.

64. Homma M, Kutsukake K, Iino T, Yamaguchi S. Hook-associated proteins essential for flagellar filament formation in *Salmonella typhimurium*. J Bacteriol. 1984 Jan;157(1):100–108.

65. Ikeda T, Asakura S, Kamiya R. Total reconstitution of *Salmonella* flagellar filaments from hook and purified flagellin and hook-associated proteins in vitro. J Mol Biol. 1989 Sep 5;209(1):109–114.

66. Homma M, Kutsukake K, Iino T. Structural genes for flagellar hook-associated proteins in *Salmonella typhimurium*. J Bacteriol. 1985 Aug;163(2):464–471.

67. Minamino T, Macnab RM. Components of the *Salmonella* flagellar export apparatus and classification of export substrates. J Bacteriol. 1999 Mar;181(5):1388–1394.

68. Minamino T, Namba K. Distinct roles of the FliI ATPase and proton motive force in bacterial flagellar protein export. Nature. 2008 Jan 24;451(7177):485–488.

69. Paul K, Erhardt M, Hirano T, Blair DF, Hughes KT. Energy source of flagellar type III secretion. Nature. 2008 Jan 24;451(7177):489–492.

70. Akeda Y, Galán JE. Chaperone release and unfolding of substrates in type III secretion. Nature. 2005 Oct 6;437(7060):911–915.

71. Stafford GP, Evans LDB, Krumscheid R, Dhillon P, Fraser GM, Hughes C. Sorting of early and late flagellar subunits after docking at the membrane ATPase of the type III export pathway. J Mol Biol. 2007 Dec 7;374(4):877–882.

72. Evans LDB, Stafford GP, Ahmed S, Fraser GM, Hughes C. An escort mechanism for cycling of export chaperones during flagellum assembly. Proc Natl Acad Sci U S A. 2006 Nov 14;103(46):17474–17479.

73. Fraser GM, González-Pedrajo B, Tame JRH, Macnab RM. Interactions of FliJ with the *Salmonella* type III flagellar export apparatus. J Bacteriol. 2003 Sep;185(18):5546–5554.

74. Thomas J, Stafford GP, Hughes C. Docking of cytosolic chaperone-substrate complexes at the membrane ATPase during flagellar type III protein export. Proc Natl Acad Sci U S A. 2004 Mar 16;101(11):3945–3950.

75. Iino T. Polarity of flagellar growth in *Salmonella*. J Gen Microbiol. 1969 May;56(2):227–239.

76. Schlumberger MC, Müller AJ, Ehrbar K, Winnen B, Duss I, Stecher B, et al. Real-time imaging of type III secretion: *Salmonella* SipA injection into host cells. Proc Natl Acad Sci U S A. 2005 Aug 30;102(35):12548–12553.

77. Wang S, Fleming RT, Westbrook EM, Matsumura P, McKay DB. Structure of the *Escherichia coli* FlhDC complex, a prokaryotic heteromeric regulator of transcription. J Mol Biol. 2006 Jan 27;355(4):798–808.

78. Ohnishi K, Kutsukake K, Suzuki H, Iino T. Gene fliA encodes an alternative sigma factor specific for flagellar operons in *Salmonella typhimurium*. Mol Gen Genet. 1990 Apr;221(2):139–147.

79. Karlinsey JE, Tanaka S, Bettenworth V, Yamaguchi S, Boos W, Aizawa SI, et al. Completion of the hook-basal body complex of the *Salmonella typhimurium* flagellum is coupled to FlgM secretion and fliC transcription. Mol Microbiol. 2000 Sep;37(5):1220–1231.

80. Tischler AD, Camilli A. Cyclic diguanylate (c-di-GMP) regulates *Vibrio cholerae* biofilm formation. Mol Microbiol. 2004 Aug;53(3):857–869.

81. Simm R, Morr M, Kader A, Nimtz M, Römling U. GGDEF and EAL domains inversely regulate cyclic di-GMP levels and transition from sessility to motility. Mol Microbiol. 2004 Aug;53(4):1123–1134.

82. Aldridge P, Paul R, Goymer P, Rainey P, Jenal U. Role of the GGDEF regulator PleD in polar development of *Caulobacter crescentus*. Mol Microbiol. 2003 Mar;47(6):1695–1708.

83. Boles BR, McCarter LL. *Vibrio* parahaemolyticus scrABC, a novel operon affecting swarming and capsular polysaccharide regulation. J Bacteriol. 2002 Nov;184(21):5946–5954.

84. Hickman JW, Harwood CS. Identification of FleQ from *Pseudomonas aeruginosa* as a c-di-GMP-responsive transcription factor. Mol Microbiol. 2008 Jul;69(2):376–389.

85. Jyot J, Dasgupta N, Ramphal R. FleQ, the major flagellar gene regulator in *Pseudomonas aeruginosa*, binds to enhancer sites located either upstream or atypically downstream of the RpoN binding site. J Bacteriol. 2002 Oct;184(19):5251–5260.

86. Koonin EV. A superfamily of ATPases with diverse functions containing either classical or deviant ATP-binding motif. J Mol Biol. 1993 Feb 20;229(4):1165–1174.

87. Baraquet C, Harwood CS. Cyclic diguanosine monophosphate represses bacterial flagella synthesis by interacting with the Walker A motif of the enhancer-binding protein FleQ. Proc Natl Acad Sci U S A. 2013 Nov 12;110(46):18478–18483.

88. Guentzel MN, Berry LJ. Motility as a virulence factor for *Vibrio cholerae*. Infect Immun. 1975 May;11(5):890–897.

89. Girón JA, Torres AG, Freer E, Kaper JB. The flagella of enteropathogenic *Escherichia coli* mediate adherence to epithelial cells. Mol Microbiol. 2002 Apr;44(2):361–379.

90. Klemm P, Vejborg RM, Hancock V. Prevention of bacterial adhesion. Appl Microbiol Biotechnol. 2010 Sep;88(2):451–459.

91. Prüss BM, Besemann C, Denton A, Wolfe AJ. A complex transcription network controls the early stages of biofilm development by *Escherichia coli*. J Bacteriol. 2006 Jun;188(11):3731–3739.

92. Mahajan A, Currie CG, Mackie S, Tree J, McAteer S, McKendrick I, et al. An investigation of the expression and adhesin function of H7 flagella in the interaction of *Escherichia coli* O157: H7 with bovine intestinal epithelium. Cell Microbiol. 2009 Jan;11(1):121–137.

93. Whalen MC, Innes RW, Bent AF, Staskawicz BJ. Identification of *Pseudomonas syringae* pathogens of Arabidopsis and a bacterial locus determining avirulence on both *Arabidopsis* and soybean. Plant Cell. 1991 Jan;3(1):49–59.

94. Kunkel BN, Chen Z. Virulence Strategies of Plant Pathogenic Bacteria. In: Dworkin M, Falkow S, Rosenberg E, Schleifer K-H, Stackebrandt E, editors. The Prokaryotes. New York, NY: Springer New York; 2006. p. 421–440.

95. Pfeilmeier S, Saur IM-L, Rathjen JP, Zipfel C, Malone JG. High levels of cyclic-di-GMP in plant-associated *Pseudomonas* correlate with evasion of plant immunity. Mol Plant Pathol. 2016 May;17(4):521–531.

96. Göhre V, Robatzek S. Breaking the barriers: microbial effector molecules subvert plant immunity. Annu Rev Phytopathol. 2008; 46:189–215.

97. Xin X-F, He SY. *Pseudomonas syringae* pv. *tomato* DC3000: a model pathogen for probing disease susceptibility and hormone signaling in plants. Annu Rev Phytopathol. 2013 May 31;51:473–498.

98. Klemm P, Schembri MA. Bacterial adhesins: function and structure. Int J Med Microbiol. 2000 Mar;290(1):27–35.

99. McCann HC, Guttman DS. Evolution of the type III secretion system and its effectors in plant-microbe interactions. New Phytol. 2008;177(1):33–47.

100. Moraes TF, Spreter T, Strynadka NC. Piecing together the type III injectisome of bacterial pathogens. Curr Opin Struct Biol. 2008 Apr;18(2):258–266.

101. Erhardt M, Namba K, Hughes KT. Bacterial nanomachines: the flagellum and type III injectisome. Cold Spring Harb Perspect Biol. 2010 Nov;2(11): a000299.

102. Boller T, Felix G. A renaissance of elicitors: perception of microbe-associated molecular patterns and danger signals by pattern-recognition receptors. Annu Rev Plant Biol. 2009; 60: 379–406.

103. Chang JH, Desveaux D, Creason AL. The ABCs and 123s of bacterial secretion systems in plant pathogenesis. Annu Rev Phytopathol. 2014 Jun 2;52:317–345.

104. Lee AH-Y, Middleton MA, Guttman DS, Desveaux D. Phytopathogen type III effectors as probes of biological systems. Microb Biotechnol. 2013 May;6(3):230–240.

105. Dean P. Functional domains and motifs of bacterial type III effector proteins and their roles in infection. FEMS Microbiol Rev. 2011 Nov;35(6):1100–1125.

106. He SY, Nomura K, Whittam TS. Type III protein secretion mechanism in mammalian and plant pathogens. Biochim Biophys Acta. 2004 Nov 11;1694(1-3):181–206.

107. Li C-M, Brown I, Mansfield J, Stevens C, Boureau T, Romantschuk M, et al. The Hrp pilus of *Pseudomonas syringae* elongates from its tip and acts as a conduit for translocation of the effector protein HrpZ. EMBO J. 2002 Apr 15;21(8):1909–1915.

108. Büttner D. Protein export according to schedule: architecture, assembly, and regulation of type III secretion systems from plant- and animal-pathogenic bacteria. Microbiol Mol Biol Rev. 2012 Jun;76(2):262–310.

109. Blocker AJ, Deane JE, Veenendaal AKJ, Roversi P, Hodgkinson JL, Johnson S, et al. What's the point of the type III secretion system needle? Proc Natl Acad Sci U S A. 2008 May 6;105(18):6507–6513.

110. Guignot J, Tran Van Nhieu G. Bacterial Control of Pores Induced by the Type III Secretion System: Mind the Gap. Front Immunol. 2016 Mar 9; 7: 84.

111. Matteï P-J, Faudry E, Job V, Izoré T, Attree I, Dessen A. Membrane targeting and pore formation by the type III secretion system translocon. FEBS J. 2011 Feb;278(3):414–426.

112. Arnold R, Brandmaier S, Kleine F, Tischler P, Heinz E, Behrens S, et al. Sequence-based prediction of type III secreted proteins. PLoS Pathog. 2009 Apr 24;5(4): e1000376.

113. Samudrala R, Heffron F, McDermott JE. Accurate prediction of secreted substrates and identification of a conserved putative secretion signal for type III secretion systems. PLoS Pathog. 2009 Apr 24;5(4): e1000375.

114. Feldman MF, Cornelis GR. The multitalented type III chaperones: all you can do with 15 kDa. FEMS Microbiol Lett. 2003 Feb 28;219(2):151–158.

115. Ménard R, Sansonetti P, Parsot C, Vasselon T. Extracellular association and cytoplasmic partitioning of the IpaB and IpaC invasins of S. flexneri. Cell. 1994 Nov 4;79(3):515–525.

116. Tucker SC, Galán JE. Complex function for SicA, a *Salmonella enterica* serovar *typhimurium* type III secretion-associated chaperone. J Bacteriol. 2000 Apr;182(8):2262–2268.

117. Galán JE, Lara-Tejero M, Marlovits TC, Wagner S. Bacterial type III secretion systems: specialized nanomachines for protein delivery into target cells. Annu Rev Microbiol. 2014 Jun 18; 68:415–438.

118. Schraidt O, Lefebre MD, Brunner MJ, Schmied WH, Schmidt A, Radics J, et al. Topology and organization of the *Salmonella typhimurium* type III secretion needle complex components. PLoS Pathog. 2010 Apr 1;6(4):e1000824.

119. Spreter T, Yip CK, Sanowar S, André I, Kimbrough TG, Vuckovic M, et al. A conserved structural motif mediates formation of the periplasmic rings in the type III secretion system. Nat Struct Mol Biol. 2009 May;16(5):468–476.

120. Galkin VE, Schmied WH, Schraidt O, Marlovits TC, Egelman EH. The structure of the *Salmonella typhimurium* type III secretion system needle shows divergence from the flagellar system. J Mol Biol. 2010 Mar 12;396(5):1392–1397.

121. Cordes FS, Komoriya K, Larquet E, Yang S, Egelman EH, Blocker A, et al. Helical structure of the needle of the type III secretion system of *Shigella flexneri*. J Biol Chem. 2003 May 9;278(19):17103–17107.

122. Kubori T, Sukhan A, Aizawa SI, Galán JE. Molecular characterization and assembly of the needle complex of the *Salmonella typhimurium* type III protein secretion system. Proc Natl Acad Sci U S A. 2000 Aug 29;97(18):10225–10230.

123. Loquet A, Sgourakis NG, Gupta R, Giller K, Riedel D, Goosmann C, et al. Atomic model of the type III secretion system needle. Nature. 2012 Jun 14;486(7402):276–279.

124. Demers J-P, Sgourakis NG, Gupta R, Loquet A, Giller K, Riedel D, et al. The common structural architecture of *Shigella flexneri* and *Salmonella typhimurium* type three secretion needles. PLoS Pathog. 2013 Mar 21;9(3): e1003245.

125. Mueller CA, Broz P, Müller SA, Ringler P, Erne-Brand F, Sorg I, et al. The V-antigen of *Yersinia* forms a distinct structure at the tip of injectisome needles. Science. 2005 Oct 28;310(5748):674–676.

126. Epler CR, Dickenson NE, Bullitt E, Picking WL. Ultrastructural analysis of IpaD at the tip of the nascent MxiH type III secretion apparatus of *Shigella flexneri*. J Mol Biol. 2012 Jun 29;420(1-2):29–39.

127. Knutton S, Rosenshine I, Pallen MJ, Nisan I, Neves BC, Bain C, et al. A novel EspA-associated surface organelle of enteropathogenic *Escherichia coli* involved in protein translocation into epithelial cells. EMBO J. 1998 Apr 15;17(8):2166–2176.

128. Yip CK, Finlay BB, Strynadka NCJ. Structural characterization of a type III secretion system filament protein in complex with its chaperone. Nat Struct Mol Biol. 2005 Jan;12(1):75–81.

129. Marlovits TC, Kubori T, Lara-Tejero M, Thomas D, Unger VM, Galán JE. Assembly of the inner rod determines needle length in the type III secretion injectisome. Nature. 2006 Jun 1;441(7093):637–640.

130. Lefebre MD, Galán JE. The inner rod protein controls substrate switching and needle length in a *Salmonella* type III secretion system. Proc Natl Acad Sci U S A. 2014 Jan 14;111(2):817–822.

131. Galán JE, Ginocchio C, Costeas P. Molecular and functional characterization of the *Salmonella* invasion gene invA: homology of InvA to members of a new protein family. J Bacteriol. 1992 Jul;174(13):4338–4349.

132. Fields KA, Plano GV, Straley SC. A low-Ca2+ response (LCR) secretion (ysc) locus lies within the lcrB region of the LCR plasmid in *Yersinia pestis*. J Bacteriol. 1994 Feb;176(3):569–579.

133. Allaoui A, Woestyn S, Sluiters C, Cornelis GR. YscU, a *Yersinia enterocolitica* inner membrane protein involved in Yop secretion. J Bacteriol. 1994 Aug;176(15):4534–4542.

134. Plano GV, Barve SS, Straley SC. LcrD, a membrane-bound regulator of the *Yersinia pestis* low-calcium response. J Bacteriol. 1991 Nov;173(22):7293–7303.

135. Groisman EA, Ochman H. Cognate gene clusters govern invasion of host epithelial cells by *Salmonella typhimurium* and *Shigella flexneri*. EMBO J. 1993 Oct;12(10):3779–3787.

136. Ginocchio CC, Galán JE. Functional conservation among members of the *Salmonella typhimurium* InvA family of proteins. Infect Immun. 1995 Feb;63(2):729–732.

137. Wagner S, Königsmaier L, Lara-Tejero M, Lefebre M, Marlovits TC, Galán JE. Organization and coordinated assembly of the type III secretion export apparatus. Proc Natl Acad Sci U S A. 2010 Oct 12;107(41):17745–17750.

138. Abrusci P, Vergara-Irigaray M, Johnson S, Beeby MD, Hendrixson DR, Roversi P, et al. Architecture of the major component of the type III secretion system export apparatus. Nat Struct Mol Biol. 2013 Jan;20(1):99–104.

139. Woestyn S, Allaoui A, Wattiau P, Cornelis GR. YscN, the putative energizer of the *Yersinia* Yop secretion machinery. J Bacteriol. 1994 Mar;176(6):1561–1569.

140. Morita-Ishihara T, Ogawa M, Sagara H, Yoshida M, Katayama E, Sasakawa C. *Shigella* Spa33 is an essential C-ring component of type III secretion machinery. J Biol Chem. 2006 Jan 6;281(1):599–607.

141. Eichelberg K, Ginocchio CC, Galán JE. Molecular and functional characterization of the *Salmonella typhimurium* invasion genes invB and invC: homology of InvC to the F0F1 ATPase family of proteins. J Bacteriol. 1994 Aug;176(15):4501–4510.

142. Collazo CM, Galán JE. Requirement for exported proteins in secretion through the invasion-associated type III system of *Salmonella typhimurium*. Infect Immun. 1996 Sep;64(9):3524–3531.

143. Collazo CM, Zierler MK, Galán JE. Functional analysis of the *Salmonella typhimurium* invasion genes invl and invJ and identification of a target of the protein secretion apparatus encoded in the inv locus. Mol Microbiol. 1995 Jan;15(1):25–38.

144. Lara-Tejero M, Kato J, Wagner S, Liu X, Galán JE. A sorting platform determines the order of protein secretion in bacterial type III systems. Science. 2011 Mar 4;331(6021):1188–1191.

145. Jackson MW, Plano GV. Interactions between type III secretion apparatus components from *Yersinia pestis* detected using the yeast two-hybrid system. FEMS Microbiol Lett. 2000 May 1;186(1):85–90.

146. Spaeth KE, Chen Y-S, Valdivia RH. The *Chlamydia* type III secretion system C-ring engages a chaperone-effector protein complex. PLoS Pathog. 2009 Sep 11;5(9): e1000579.

147. Driks A, DeRosier DJ. Additional structures associated with bacterial flagellar basal body. J Mol Biol. 1990 Feb 20;211(4):669–672.

148. Khan IH, Reese TS, Khan S. The cytoplasmic component of the bacterial flagellar motor. Proc Natl Acad Sci U S A. 1992 Jul 1;89(13):5956–5960.

149. Zarivach R, Vuckovic M, Deng W, Finlay BB, Strynadka NCJ. Structural analysis of a prototypical ATPase from the type III secretion system. Nat Struct Mol Biol. 2007 Feb;14(2):131–137.

150. Müller SA, Pozidis C, Stone R, Meesters C, Chami M, Engel A, et al. Double hexameric ring assembly of the type III protein translocase ATPase HrcN. Mol Microbiol. 2006 Jul;61(1):119–125.

151. Yip CK, Strynadka NCJ. New structural insights into the bacterial type III secretion system. Trends Biochem Sci. 2006 Apr;31(4):223–230.

152. Gauthier A, Finlay BB. Translocated intimin receptor and its chaperone interact with ATPase of the type III secretion apparatus of enteropathogenic *Escherichia coli*. J Bacteriol. 2003 Dec;185(23):6747–6755.

153. Wilharm G, Dittmann S, Schmid A, Heesemann J. On the role of specific chaperones, the specific ATPase, and the proton motive force in type III secretion. Int J Med Microbiol. 2007 Feb;297(1):27–36.

154. Marlovits TC, Kubori T, Sukhan A, Thomas DR, Galán JE, Unger VM. Structural insights into the assembly of the type III secretion needle complex. Science. 2004 Nov 5;306(5698):1040–1042.

155. Blocker A, Jouihri N, Larquet E, Gounon P, Ebel F, Parsot C, et al. Structure and composition of the *Shigella flexneri* "needle complex", a part of its type III secreton. Mol Microbiol. 2001 Feb;39(3):652–663.

156. Lorenz C, Büttner D. Functional characterization of the type III secretion ATPase HrcN from the plant pathogen *Xanthomonas campestris* pv. *vesicatoria*. J Bacteriol. 2009 Mar;191(5):1414–1428.

157. Zierler MK, Galán JE. Contact with cultured epithelial cells stimulates secretion of *Salmonella typhimurium* invasion protein InvJ. Infect Immun. 1995 Oct;63(10):4024–4028.

158. Ménard R, Sansonetti P, Parsot C. The secretion of the *Shigella flexneri* Ipa invasins is activated by epithelial cells and controlled by IpaB and IpaD. EMBO J. 1994 Nov 15;13(22):5293–5302.

159. Bahrani FK, Sansonetti PJ, Parsot C. Secretion of Ipa proteins by *Shigella flexneri*: inducer molecules and kinetics of activation. Infect Immun. 1997 Oct;65(10):4005–4010.

160. Olive AJ, Kenjale R, Espina M, Moore DS, Picking WL, Picking WD. Bile salts stimulate recruitment of IpaB to the *Shigella flexneri* surface, where it colocalizes with IpaD at the tip of the type III secretion needle. Infect Immun. 2007 May;75(5):2626–2629.

161. Wang Y, Nordhues BA, Zhong D, De Guzman RN. NMR characterization of the interaction of the *Salmonella* type III secretion system protein SipD and bile salts. Biochemistry. 2010 May 18;49(19):4220–4226.

162. Chatterjee S, Zhong D, Nordhues BA, Battaile KP, Lovell S, De Guzman RN. The crystal structures of the *Salmonella* type III secretion system tip protein SipD in complex with deoxycholate and chenodeoxycholate. Protein Sci. 2011 Jan;20(1):75–86.

163. Dickenson NE, Zhang L, Epler CR, Adam PR, Picking WL, Picking WD. Conformational changes in IpaD from *Shigella flexneri* upon binding bile salts provide insight into the second step of type III secretion. Biochemistry. 2011 Jan 18;50(2):172–180.

164. Cherradi Y, Schiavolin L, Moussa S, Meghraoui A, Meksem A, Biskri L, et al. Interplay between predicted inner-rod and gatekeeper in controlling substrate specificity of the type III secretion system. Mol Microbiol. 2013 Mar;87(6):1183–1199.

165. Kenjale R, Wilson J, Zenk SF, Saurya S, Picking WL, Picking WD, et al. The needle component of the type III secreton of *Shigella* regulates the activity of the secretion apparatus. J Biol Chem. 2005 Dec 30;280(52):42929–42937.

166. Veenendaal AKJ, Hodgkinson JL, Schwarzer L, Stabat D, Zenk SF, Blocker AJ. The type III secretion system needle tip complex mediates host cell sensing and translocon insertion. Mol Microbiol. 2007 Mar;63(6):1719–1730.

167. Davis AJ, Mecsas J. Mutations in the *Yersinia pseudotuberculosis* type III secretion system needle protein, YscF, that specifically abrogate effector translocation into host cells. J Bacteriol. 2007 Jan;189(1):83–97.

168. Lara-Tejero M, Galán JE. *Salmonella enterica* serovar *typhimurium* pathogenicity island 1-encoded type III secretion system translocases mediate intimate attachment to nonphagocytic cells. Infect Immun. 2009 Jul;77(7):2635–2642.

169. Büttner D. Behind the lines-actions of bacterial type III effector proteins in plant cells. FEMS Microbiol Rev. 2016 Aug 14;

170. Baltrus DA, Nishimura MT, Romanchuk A, Chang JH, Mukhtar MS, Cherkis K, et al. Dynamic evolution of pathogenicity revealed by sequencing and comparative genomics of 19 *Pseudomonas syringae* isolates. PLoS Pathog. 2011 Jul 14;7(7): e1002132.

171. Lindeberg M, Cunnac S, Collmer A. *Pseudomonas syringae* type III effector repertoires: last words in endless arguments. Trends Microbiol. 2012 Apr;20(4):199–208.

172. Kvitko BH, Park DH, Velásquez AC, Wei C-F, Russell AB, Martin GB, et al. Deletions in the repertoire of *Pseudomonas syringae* pv. *tomato* DC3000 type III secretion effector genes reveal functional overlap among effectors. PLoS Pathog. 2009 Apr 17;5(4): e1000388.

173. Cunnac S, Chakravarthy S, Kvitko BH, Russell AB, Martin GB, Collmer A. Genetic disassembly and combinatorial reassembly identify a minimal functional repertoire of type III effectors in *Pseudomonas syringae*. Proc Natl Acad Sci U S A. 2011 Feb 15;108(7):2975–2980.

174. Wei H-L, Chakravarthy S, Mathieu J, Helmann TC, Stodghill P, Swingle B, et al. *Pseudomonas syringae* pv. *tomato* DC3000 Type III Secretion Effector Polymutants Reveal an Interplay between HopAD1 and AvrPtoB. Cell Host Microbe. 2015 Jun 10;17(6):752–762.

175. Van Engelenburg SB, Palmer AE. Quantification of real-time *Salmonella* effector type III secretion kinetics reveals differential secretion rates for SopE2 and SptP. Chem Biol. 2008 Jun;15(6):619–628.

176. Enninga J, Mounier J, Sansonetti P, Tran Van Nhieu G. Secretion of type III effectors into host cells in real time. Nat Methods. 2005 Dec;2(12):959–965.

177. Mills E, Baruch K, Charpentier X, Kobi S, Rosenshine I. Real-time analysis of effector translocation by the type III secretion system of enteropathogenic *Escherichia coli*. Cell Host Microbe. 2008 Feb 14;3(2):104–113.

178. Bretz J, Losada L, Lisboa K, Hutcheson SW. Lon protease functions as a negative regulator of type III protein secretion in *Pseudomonas syringae*. Mol Microbiol. 2002 Jul;45(2):397–409.

179. Tang X, Xiao Y, Zhou J-M. Regulation of the type III secretion system in phytopathogenic bacteria. Mol Plant Microbe Interact. 2006 Nov;19(11):1159–1166.

180. Preston G, Deng WL, Huang HC, Collmer A. Negative regulation of *hrp* genes in *Pseudomonas syringae* by HrpV. J Bacteriol. 1998 Sep;180(17):4532–4537.

181. Wei C-F, Deng W-L, Huang H-C. A chaperone-like HrpG protein acts as a suppressor of HrpV in regulation of the *Pseudomonas syringae* pv. *syringae* type III secretion system. Mol Microbiol. 2005 Jul;57(2):520–536.

182. Tomoyasu T, Mogk A, Langen H, Goloubinoff P, Bukau B. Genetic dissection of the roles of chaperones and proteases in protein folding and degradation in the *Escherichia coli* cytosol. Mol Microbiol. 2001 Apr;40(2):397–413.

183. Rosen R, Biran D, Gur E, Becher D, Hecker M, Ron EZ. Protein aggregation in *Escherichia coli*: role of proteases. FEMS Microbiol Lett. 2002 Jan 22;207(1):9–12.

184. Ortiz-Martín I, Thwaites R, Mansfield JW, Beuzón CR. Negative regulation of the Hrp type III secretion system in *Pseudomonas syringae* pv. *phaseolicola*. Mol Plant Microbe Interact. 2010 May;23(5):682–701.

185. Yang HJ, Lee JS, Cha JY, Baik HS. Negative regulation of pathogenesis in *Pseudomonas syringae* pv. *tabaci* 11528 by ATP-dependent Lon protease. Mol Cells. 2011 Oct;32(4):317–323.

186. Lan L, Deng X, Xiao Y, Zhou J-M, Tang X. Mutation of Lon protease differentially affects the expression of *Pseudomonas syringae* type III secretion system genes in rich and minimal media and reduces pathogenicity. Mol Plant Microbe Interact. 2007 Jun;20(6):682–696.

187. Losada LC, Hutcheson SW. Type III secretion chaperones of *Pseudomonas syringae* protect effectors from Lon-associated degradation. Mol Microbiol. 2005 Feb;55(3):941–953.

188. Das S, Chaudhuri K. Identification of a unique IAHP (IcmF associated homologous proteins) cluster in *Vibrio cholerae* and other proteobacteria through in silico analysis. In Silico Biol (Gedrukt). 2003;3(3):287–300.

189. Pukatzki S, McAuley SB, Miyata ST. The type VI secretion system: translocation of effectors and effector-domains. Curr Opin Microbiol. 2009 Feb;12(1):11–17.

190. Pukatzki S, Ma AT, Sturtevant D, Krastins B, Sarracino D, Nelson WC, et al. Identification of a conserved bacterial protein secretion system in *Vibrio cholerae* using the *Dictyostelium* host model system. Proc Natl Acad Sci U S A. 2006 Jan 31;103(5):1528–1533.

191. Aubert DF, Flannagan RS, Valvano MA. A novel sensor kinase-response regulator hybrid controls biofilm formation and type VI secretion system activity in *Burkholderia cenocepacia*. Infect Immun. 2008 May;76(5):1979–1991.

192. Mougous JD, Cuff ME, Raunser S, Shen A, Zhou M, Gifford CA, et al. A virulence locus of *Pseudomonas aeruginosa* encodes a protein secretion apparatus. Science. 2006 Jun 9;312(5779):1526–1530.

193. Schell MA, Ulrich RL, Ribot WJ, Brueggemann EE, Hines HB, Chen D, et al. Type VI secretion is a major virulence determinant in *Burkholderia mallei*. Mol Microbiol. 2007 Jun;64(6):1466–1485.

194. Zheng J, Leung KY. Dissection of a type VI secretion system in *Edwardsiella tarda*. Mol Microbiol. 2007 Dec;66(5):1192–1206.

195. De Bruin OM, Ludu JS, Nano FE. The *Francisella* pathogenicity island protein IglA localizes to the bacterial cytoplasm and is needed for intracellular growth. BMC Microbiol. 2007 Jan 17; 7:1.

196. Lee S, Sowa ME, Watanabe Y, Sigler PB, Chiu W, Yoshida M, et al. The structure of ClpB: a molecular chaperone that rescues proteins from an aggregated state. Cell. 2003 Oct 17;115(2):229–240.

197. Ross P, Weinhouse H, Aloni Y, Michaeli D, Weinberger-Ohana P, Mayer R, et al. Regulation of cellulose synthesis in *Acetobacter xylinum* by cyclic diguanylic acid. Nature. 1987 Jan 21;325(6101):279–281.

198. Pesavento C, Hengge R. Bacterial nucleotide-based second messengers. Curr Opin Microbiol. 2009 Apr;12(2):170–176.

199. Hengge R. Principles of c-di-GMP signalling in bacteria. Nat Rev Microbiol. 2009 Apr;7(4):263–273.

200. Römling U, Gomelsky M, Galperin MY. C-di-GMP: the dawning of a novel bacterial signalling system. Mol Microbiol. 2005 Aug;57(3):629–639.

201. Tal R, Wong HC, Calhoon R, Gelfand D, Fear AL, Volman G, et al. Three cdg operons control cellular turnover of cyclic di-GMP in *Acetobacter xylinum*: genetic organization and occurrence of conserved domains in isoenzymes. J Bacteriol. 1998 Sep;180(17):4416–4425.

202. Newell PD, Yoshioka S, Hvorecny KL, Monds RD, O'Toole GA. Systematic analysis of diguanylate cyclases that promote biofilm formation by *Pseudomonas fluorescens* Pf0-1. J Bacteriol. 2011 Sep;193(18):4685–4698.

203. Jenal U, Malone J. Mechanisms of cyclic-di-GMP signaling in bacteria. Annu Rev Genet. 2006; 40: 385–407.

204. Povolotsky TL, Hengge R. Life- style' control networks in *Escherichia coli*: signaling by the second messenger c-di-GMP. J Biotechnol. 2012 Jul 31;160(1-2):10–16.

205. Galperin MY, Nikolskaya AN, Koonin EV. Novel domains of the prokaryotic two-component signal transduction systems. FEMS Microbiol Lett. 2001 Sep 11;203(1):11–21.

206. Jenal U. Cyclic di-guanosine-monophosphate comes of age: a novel secondary messenger involved in modulating cell surface structures in bacteria? Curr Opin Microbiol. 2004 Apr;7(2):185–191.

207. Tamayo R, Pratt JT, Camilli A. Roles of cyclic diguanylate in the regulation of bacterial pathogenesis. Annu Rev Microbiol. 2007; 61:131–148.

208. Mills E, Pultz IS, Kulasekara HD, Miller SI. The bacterial second messenger c-di-GMP: mechanisms of signalling. Cell Microbiol. 2011 Aug;13(8):1122–1129.

209. Boyd CD, O'Toole GA. Second Messenger Regulation of Biofilm Formation: Breakthroughs in Understanding c-di-GMP Effector Systems. Annu Rev Cell Dev Biol. 2012 Nov 10;28(1):439–462.

210. Espinosa-Urgel M, Kolter R, Ramos J-L. Root colonization by *Pseudomonas putida*: love at first sight. Microbiology (Reading, Engl). 2002 Feb;148(Pt 2):341–343.

211. Baraquet C, Murakami K, Parsek MR, Harwood CS. The FleQ protein from *Pseudomonas aeruginosa* functions as both a repressor and an activator to control gene expression from the pel operon promoter in response to c-di-GMP. Nucleic Acids Res. 2012 Aug;40(15):7207–7218.

212. Goymer P, Kahn SG, Malone JG, Gehrig SM, Spiers AJ, Rainey PB. Adaptive divergence in experimental populations of *Pseudomonas fluorescens*. II. Role of the GGDEF regulator WspR in evolution and development of the wrinkly spreader phenotype. Genetics. 2006 Jun;173(2):515–526.

213. Spiers AJ, Kahn SG, Bohannon J, Travisano M, Rainey PB. Adaptive divergence in experimental populations of *Pseudomonas fluorescens*. I. Genetic and phenotypic bases of wrinkly spreader fitness. Genetics. 2002 May;161(1):33–46.

214. Spiers AJ, Bohannon J, Gehrig SM, Rainey PB. Biofilm formation at the air-liquid interface by the *Pseudomonas fluorescens* SBW25 wrinkly spreader requires an acetylated form of cellulose. Mol Microbiol. 2003 Oct;50(1):15–27.

215. Silby MW, Cerdeño-Tárraga AM, Vernikos GS, Giddens SR, Jackson RW, Preston GM, et al. Genomic and genetic analyses of diversity and plant interactions of *Pseudomonas fluorescens*. Genome Biol. 2009 May 11;10(5): R51.

216. Caiazza NC, O'Toole GA. SadB is required for the transition from reversible to irreversible attachment during biofilm formation by *Pseudomonas aeruginosa* PA14. J Bacteriol. 2004 Jul;186(14):4476–4485.

217. Navazo A, Barahona E, Redondo-Nieto M, Martínez-Granero F, Rivilla R, Martín M. Three independent signalling pathways repress motility in *Pseudomonas fluorescens* F113. Microb Biotechnol. 2009 Jul;2(4):489–498.

218. Blumer C, Heeb S, Pessi G, Haas D. Global GacA-steered control of cyanide and exoprotease production in *Pseudomonas fluorescens* involves specific ribosome binding sites. Proc Natl Acad Sci U S A. 1999 Nov 23;96(24):14073–14078.

219. Martínez-Granero F, Capdevila S, Sánchez-Contreras M, Martín M, Rivilla R. Two site-specific recombinases are implicated in phenotypic variation and competitive rhizosphere colonization in *Pseudomonas fluorescens*. Microbiology (Reading, Engl). 2005 Mar;151(Pt 3):975–983.

220. Brencic A, Lory S. Determination of the regulon and identification of novel mRNA targets of *Pseudomonas aeruginosa* RsmA. Mol Microbiol. 2009 May;72(3):612–632.

221. Moscoso JA, Jaeger T, Valentini M, Hui K, Jenal U, Filloux A. The diguanylate cyclase SadC is a central player in Gac/Rsm-mediated biofilm formation in *Pseudomonas aeruginosa*. J Bacteriol. 2014 Dec;196(23):4081–4088.

222. Moscoso JA, Mikkelsen H, Heeb S, Williams P, Filloux A. The *Pseudomonas aeruginosa* sensor RetS switches type III and type VI secretion via c-di-GMP signalling. Environ Microbiol. 2011 Dec;13(12):3128–3138.

223. Breaker RR. Prospects for riboswitch discovery and analysis. Mol Cell. 2011 Sep 16;43(6):867–879.

224. Hengge R. Cyclic-di-GMP reaches out into the bacterial RNA world. Sci Signal. 2010 Nov 23;3(149):pe44.

225. Ryan RP, Fouhy Y, Lucey JF, Crossman LC, Spiro S, He Y-W, et al. Cell-cell signaling in *Xanthomonas campestris* involves an HD-GYP domain protein that functions in cyclic di-GMP turnover. Proc Natl Acad Sci U S A. 2006 Apr 25;103(17):6712–6717.

226. Weinhouse H, Sapir S, Amikam D, Shilo Y, Volman G, Ohana P, et al. c-di-GMP-binding protein, a new factor regulating cellulose synthesis in *Acetobacter xylinum*. FEBS Lett. 1997 Oct 20;416(2):207–211.

227. Ross P, Mayer R, Benziman M. Cellulose biosynthesis and function in bacteria. Microbiol Rev. 1991 Mar;55(1):35–58.

228. Galperin MY, Natale DA, Aravind L, Koonin EV. A specialized version of the HD hydrolase domain implicated in signal transduction. J Mol Microbiol Biotechnol. 1999 Nov;1(2):303–305.

229. Chou S-H, Galperin MY. Diversity of Cyclic Di-GMP-Binding Proteins and Mechanisms. J Bacteriol. 2016 Jan;198(1):32–46.

230. Amikam D, Galperin MY. PilZ domain is part of the bacterial c-di-GMP binding protein. Bioinformatics. 2006 Jan 1;22(1):3–6.

231. Boehm A, Kaiser M, Li H, Spangler C, Kasper CA, Ackermann M, et al. Second messenger-mediated adjustment of bacterial swimming velocity. Cell. 2010 Apr 2;141(1):107–116.

232. Merighi M, Lee VT, Hyodo M, Hayakawa Y, Lory S. The second messenger bis-(3’-5')-cyclic-GMP and its PilZ domain-containing receptor Alg44 are required for alginate biosynthesis in *Pseudomonas aeruginosa*. Mol Microbiol. 2007 Aug;65(4):876–895.

233. Ko J, Ryu K-S, Kim H, Shin J-S, Lee J-O, Cheong C, et al. Structure of PP4397 reveals the molecular basis for different c-di-GMP binding modes by Pilz domain proteins. J Mol Biol. 2010 Apr 23;398(1):97–110.

234. Ryan RP, Tolker-Nielsen T, Dow JM. When the PilZ don’t work: effectors for cyclic di-GMP action in bacteria. Trends Microbiol. 2012 May;20(5):235–242.

235. Newell PD, Monds RD, O’Toole GA. LapD is a bis-(3’,5')-cyclic dimeric GMP-binding protein that regulates surface attachment by *Pseudomonas fluorescens* Pf0-1. Proc Natl Acad Sci U S A. 2009 Mar 3;106(9):3461–3466.

236. Duerig A, Abel S, Folcher M, Nicollier M, Schwede T, Amiot N, et al. Second messenger-mediated spatiotemporal control of protein degradation regulates bacterial cell cycle progression. Genes Dev. 2009 Jan 1;23(1):93–104.

237. Kazmierczak BI, Lebron MB, Murray TS. Analysis of FimX, a phosphodiesterase that governs twitching motility in *Pseudomonas aeruginosa*. Mol Microbiol. 2006 May;60(4):1026–1043.

238. Tschowri N, Schumacher MA, Schlimpert S, Chinnam NB, Findlay KC, Brennan RG, et al. Tetrameric c-di-GMP mediates effective transcription factor dimerization to control *Streptomyces* development. Cell. 2014 Aug 28;158(5):1136–1147.

239. Krasteva PV, Fong JCN, Shikuma NJ, Beyhan S, Navarro MVAS, Yildiz FH, et al. *Vibrio cholerae* VpsT regulates matrix production and motility by directly sensing cyclic di-GMP. Science. 2010 Feb 12;327(5967):866–868.

240. Chin K-H, Lee Y-C, Tu Z-L, Chen C-H, Tseng Y-H, Yang J-M, et al. The cAMP receptor-like protein CLP is a novel c-di-GMP receptor linking cell-cell signaling to virulence gene expression in *Xanthomonas campestris*. J Mol Biol. 2010 Feb 26;396(3):646–662.

241. Wilksch JJ, Yang J, Clements A, Gabbe JL, Short KR, Cao H, et al. MrkH, a novel c-di-GMP-dependent transcriptional activator, controls Klebsiella pneumoniae biofilm formation by regulating type 3 fimbriae expression. PLoS Pathog. 2011 Aug 25;7(8): e1002204.

242. Fazli M, O'Connell A, Nilsson M, Niehaus K, Dow JM, Givskov M, et al. The CRP/FNR family protein Bcam1349 is a c-di-GMP effector that regulates biofilm formation in the respiratory pathogen *Burkholderia cenocepacia*. Mol Microbiol. 2011 Oct;82(2):327–341.

243. Chambers JR, Liao J, Schurr MJ, Sauer K. BrlR from *Pseudomonas aeruginosa* is a c-di-GMP-responsive transcription factor. Mol Microbiol. 2014 May;92(3):471–487.

244. Li W, He Z-G. LtmA, a novel cyclic di-GMP-responsive activator, broadly regulates the expression of lipid transport and metabolism genes in Mycobacterium smegmatis. Nucleic Acids Res. 2012 Dec;40(22):11292–11307.

245. Srivastava D, Hsieh M-L, Khataokar A, Neiditch MB, Waters CM. Cyclic di-GMP inhibits Vibrio cholerae motility by repressing induction of transcription and inducing extracellular polysaccharide production. Mol Microbiol. 2013 Dec;90(6):1262–1276.

246. Srivastava D, Harris RC, Waters CM. Integration of cyclic di-GMP and quorum sensing in the control of vpsT and aphA in Vibrio cholerae. J Bacteriol. 2011 Nov;193(22):6331–6341.

247. Steiner S, Lori C, Boehm A, Jenal U. Allosteric activation of exopolysaccharide synthesis through cyclic di-GMP-stimulated protein-protein interaction. EMBO J. 2013 Feb 6;32(3):354–368.

248. Dubey BN, Lori C, Ozaki S, Fucile G, Plaza-Menacho I, Jenal U, et al. Cyclic di-GMP mediates a histidine kinase/phosphatase switch by noncovalent domain cross-linking. Science advances. 2016 Sep 16;2(9):e1600823.

249. Nesper J, Reinders A, Glatter T, Schmidt A, Jenal U. A novel capture compound for the identification and analysis of cyclic di-GMP binding proteins. J Proteomics. 2012 Aug 3;75(15):4874–4878.

250. Woodcock DM, Crowther PJ, Doherty J, Jefferson S, DeCruz E, Noyer-Weidner M, et al. Quantitative evaluation of *Escherichia coli* host strains for tolerance to cytosine methylation in plasmid and phage recombinants. Nucleic Acids Res. 1989 May 11;17(9):3469–3478.

251. Rainey PB, Bailey MJ. Physical and genetic map of the *Pseudomonas fluorescens* SBW25 chromosome. Mol Microbiol. 1996 Feb;19(3):521–533.

252. Cuppels DA. Generation and Characterization of Tn5 Insertion Mutations in *Pseudomonas syringae* pv. *tomato*. Appl Environ Microbiol. 1986 Feb;51(2):323–327.

253. Lucchini S, Rowley G, Goldberg MD, Hurd D, Harrison M, Hinton JCD. H-NS mediates the silencing of laterally acquired genes in bacteria. PLoS Pathog. 2006 Aug;2(8): e81.

254. Galibert F, Finan TM, Long SR, Puhler A, Abola P, Ampe F, et al. The composite genome of the legume symbiont *Sinorhizobium meliloti*. Science. 2001 Jul 27;293(5530):668–672.

255. Little R, Salinas P, Slavny P, Clarke TA, Dixon R. Substitutions in the redox-sensing PAS domain of the NifL regulatory protein define an inter-subunit pathway for redox signal transmission. Mol Microbiol. 2011 Oct 1;82(1):222–235.

256. Scheich C, Kümmel D, Soumailakakis D, Heinemann U, Büssow K. Vectors for co-expression of an unrestricted number of proteins. Nucleic Acids Res. 2007 Feb 20;35(6): e43.

257. Chong S, Mersha FB, Comb DG, Scott ME, Landry D, Vence LM, et al. Single-column purification of free recombinant proteins using a self-cleavable affinity tag derived from a protein splicing element. Gene. 1997 Jun;192(2):271–281.

258. Chong S, Montello GE, Zhang A, Cantor EJ, Liao W, Xu MQ, et al. Utilizing the C-terminal cleavage activity of a protein splicing element to purify recombinant proteins in a single chromatographic step. Nucleic Acids Res. 1998 Nov 15;26(22):5109–5115.

259. Ho SN, Hunt HD, Horton RM, Pullen JK, Pease LR. Site-directed mutagenesis by overlap extension using the polymerase chain reaction. Gene. 1989 Apr 15;77(1):51–59.

260. Molecular cloning: a laboratory manual / J. Sambrook, E.F. Fritsch, T. Maniatis - Details - Trove [Internet]. [cited 2016 Aug 8]. Available from: http://trove.nla.gov.au/work/13615226

261. Skotnicka D, Smaldone GT, Petters T, Trampari E, Liang J, Kaever V, et al. A Minimal Threshold of c-di-GMP Is Essential for Fruiting Body Formation and Sporulation in *Myxococcus xanthus*. PLoS Genet. 2016 May 23;12(5):e1006080.

262. Kim R, Yokota H, Kim SH. Electrophoresis of proteins and protein-protein complexes in a native agarose gel. Anal Biochem. 2000 Jun 15;282(1):147–149.

263. Electron Microscopy in Biology: A Practical Approach by Harris, J.R.: Oxford University Press 9780199632190 - Anybook Ltd. [Internet]. [cited 2016 Aug 2]. Available from: http://www.abebooks.co.uk/Electron-Microscopy-Biology-Practical-Approach-Harris/9104614611/bd

264. Wilhelm T, Jones AME. Identification of related peptides through the analysis of fragment ion mass shifts. J Proteome Res. 2014 Sep 5;13(9):4002–4011.

265. Kabsch W. Integration, scaling, space-group assignment and post-refinement. Acta Crystallogr D Biol Crystallogr. 2010 Feb;66(Pt 2):133–144.

266. Evans PR, Murshudov GN. How good are my data and what is the resolution? Acta Crystallogr D Biol Crystallogr. 2013 Jul;69(Pt 7):1204–1214.

267. Winter G. xia2: an expert system for macromolecular crystallography data reduction. J Appl Crystallogr. 2010 Feb 1;43(1):186–190.

268. McCoy AJ, Grosse-Kunstleve RW, Adams PD, Winn MD, Storoni LC, Read RJ. Phaser crystallographic software. J Appl Crystallogr. 2007 Aug 1;40(Pt 4):658–674.

269. Emsley P, Cowtan K. Coot: model-building tools for molecular graphics. Acta Crystallogr D Biol Crystallogr. 2004 Dec;60(Pt 12 Pt 1):2126–2132.

270. Murshudov GN, Skubák P, Lebedev AA, Pannu NS, Steiner RA, Nicholls RA, et al. REFMAC5 for the refinement of macromolecular crystal structures. Acta Crystallogr D Biol Crystallogr. 2011 Apr;67(Pt 4):355–367.

271. Perrakis A, Harkiolaki M, Wilson KS, Lamzin VS. ARP /wARP and molecular replacement. Acta Crystallogr D Biol Crystallogr. 2001 Oct 1;57(10):1445–1450.

272. Imada K, Minamino T, Tahara A, Namba K. Structural similarity between the flagellar type III ATPase FliI and F1-ATPase subunits. Proc Natl Acad Sci U S A. 2007 Jan 9;104(2):485–490.

273. Kelley LA, Sternberg MJE. Protein structure prediction on the Web: a case study using the Phyre server. Nat Protoc. 2009;4(3):363–371.

274. Gledhill JR, Montgomery MG, Leslie AGW, Walker JE. Mechanism of inhibition of bovine F1-ATPase by resveratrol and related polyphenols. Proc Natl Acad Sci U S A. 2007 Aug 21;104(34):13632–13637.

275. Krissinel E, Henrick K. Secondary-structure matching (SSM), a new tool for fast protein structure alignment in three dimensions. Acta Crystallogr D Biol Crystallogr. 2004 Dec;60(Pt 12 Pt 1):2256–2268.

276. McNicholas S, Potterton E, Wilson KS, Noble MEM. Presenting your structures: the CCP4mg molecular-graphics software. Acta Crystallogr D Biol Crystallogr. 2011 Apr;67(Pt 4):386–394.

277. Furukawa S, Kuchma SL, O'Toole GA. Keeping their options open: acute versus persistent infections. J Bacteriol. 2006 Feb;188(4):1211–1217.

278. Sondermann H, Shikuma NJ, Yildiz FH. You've come a long way: c-di-GMP signaling. Curr Opin Microbiol. 2012 Apr 1;15(2):140–146.

279. Christen M, Christen B, Allan MG, Folcher M, Jenö P, Grzesiek S, et al. DgrA is a member of a new family of cyclic diguanosine monophosphate receptors and controls flagellar motor function in *Caulobacter crescentus*. Proc Natl Acad Sci U S A. 2007 Mar 6;104(10):4112–4117.

280. Düvel J, Bertinetti D, Möller S, Schwede F, Morr M, Wissing J, et al. A chemical proteomics approach to identify c-di-GMP binding proteins in *Pseudomonas aeruginosa*. J Microbiol Methods. 2012 Feb;88(2):229–236.

281. Paul K, Nieto V, Carlquist WC, Blair DF, Harshey RM. The c-di-GMP binding protein YcgR controls flagellar motor direction and speed to affect chemotaxis by a "backstop brake" mechanism. Mol Cell. 2010 Apr 9;38(1):128–139.

282. Martínez-Granero F, Navazo A, Barahona E, Redondo-Nieto M, González de Heredia E, Baena I, et al. Identification of flgZ as a flagellar gene encoding a PilZ domain protein that regulates swimming motility and biofilm formation in *Pseudomonas*. PLoS ONE. 2014 Feb 4;9(2): e87608.

283. Roelofs KG, Wang J, Sintim HO, Lee VT. Differential radial capillary action of ligand assay for high-throughput detection of protein-metabolite interactions. Proc Natl Acad Sci U S A. 2011 Sep 13;108(37):15528–15533.

284. Paul R, Weiser S, Amiot NC, Chan C, Schirmer T, Giese B, et al. Cell cycle-dependent dynamic localization of a bacterial response regulator with a novel di-guanylate cyclase output domain. Genes Dev. 2004 Mar 15;18(6):715–727.

285. Niesen FH, Berglund H, Vedadi M. The use of differential scanning fluorimetry to detect ligand interactions that promote protein stability. Nat Protoc. 2007;2(9):2212–2221.

286. Crhanova M, Malcova M, Mazgajova M, Karasova D, Sebkova A, Fucikova A, et al. LPS structure influences protein secretion in *Salmonella enterica*. Vet Microbiol. 2011 Aug 26;152(1-2):131–137.

287. Chan C, Paul R, Samoray D, Amiot NC, Giese B, Jenal U, et al. Structural basis of activity and allosteric control of diguanylate cyclase. Proc Natl Acad Sci U S A. 2004 Dec 7;101(49):17084–17089.

288. Pultz IS, Christen M, Kulasekara HD, Kennard A, Kulasekara B, Miller SI. The response threshold of *Salmonella* PilZ domain proteins is determined by their binding affinities for c-di-GMP. Mol Microbiol. 2012 Dec;86(6):1424–1440.

289. Kazetani K-I, Minamino T, Miyata T, Kato T, Namba K. ATP-induced FliI hexamerization facilitates bacterial flagellar protein export. Biochem Biophys Res Commun. 2009 Oct 16;388(2):323–327.

290. Minamino T, Imada K, Namba K. Mechanisms of type III protein export for bacterial flagellar assembly. Mol Biosyst. 2008 Nov;4(11):1105–1115.

291. Minamino T, MacNab RM. Interactions among components of the *Salmonella* flagellar export apparatus and its substrates. Mol Microbiol. 2000 Mar;35(5):1052–1064.

292. Minamino T. Protein export through the bacterial flagellar type III export pathway. Biochim Biophys Acta. 2014 Aug;1843(8):1642–1648.

293. Minamino T, Morimoto YV, Kinoshita M, Aldridge PD, Namba K. The bacterial flagellar protein export apparatus processively transports flagellar proteins even with extremely infrequent ATP hydrolysis. Sci Rep. 2014 Dec 22; 4:7579.

294. Minamino T, Kazetani K, Tahara A, Suzuki H, Furukawa Y, Kihara M, et al. Oligomerization of the bacterial flagellar ATPase FliI is controlled by its extreme N-terminal region. J Mol Biol. 2006 Jul 7;360(2):510–519.

295. Iino R, Noji H. Intersubunit coordination and cooperativity in ring-shaped NTPases. Curr Opin Struct Biol. 2013 Apr;23(2):229–234.

296. Abel S, Bucher T, Nicollier M, Hug I, Kaever V, Abel Zur Wiesch P, et al. Bi-modal distribution of the second messenger c-di-GMP controls cell fate and asymmetry during the caulobacter cell cycle. PLoS Genet. 2013 Sep 5;9(9):e1003744.

297. Solano C, García B, Latasa C, Toledo-Arana A, Zorraquino V, Valle J, et al. Genetic reductionist approach for dissecting individual roles of GGDEF proteins within the c-di-GMP signaling network in *Salmonella*. Proc Natl Acad Sci U S A. 2009 May 12;106(19):7997–8002.

298. Kuchma SL, Delalez NJ, Filkins LM, Snavely EA, Armitage JP, O'Toole GA. Cyclic di-GMP-mediated repression of swarming motility by *Pseudomonas aeruginosa* PA14 requires the MotAB stator. J Bacteriol. 2015 Feb;197(3):420–430.

299. Qi Y, Chuah MLC, Dong X, Xie K, Luo Z, Tang K, et al. Binding of cyclic diguanylate in the non-catalytic EAL domain of FimX induces a long-range conformational change. J Biol Chem. 2011 Jan 28;286(4):2910–2917.

300. Lee VT, Matewish JM, Kessler JL, Hyodo M, Hayakawa Y, Lory S. A cyclic-di-GMP receptor required for bacterial exopolysaccharide production. Mol Microbiol. 2007 Sep;65(6):1474–1484.

301. Starkey M, Hickman JH, Ma L, Zhang N, De Long S, Hinz A, et al. *Pseudomonas aeruginosa* rugose small-colony variants have adaptations that likely promote persistence in the cystic fibrosis lung. J Bacteriol. 2009 Jun;191(11):3492–3503.

302. Kuchma SL, Griffin EF, O'Toole GA. Minor pilins of the type IV pilus system participate in the negative regulation of swarming motility. J Bacteriol. 2012 Oct;194(19):5388–5403.

303. Jonas K, Edwards AN, Simm R, Romeo T, Römling U, Melefors O. The RNA binding protein CsrA controls cyclic di-GMP metabolism by directly regulating the expression of GGDEF proteins. Mol Microbiol. 2008 Oct;70(1):236–257.

304. Bai F, Morimoto YV, Yoshimura SDJ, Hara N, Kami-Ike N, Namba K, et al. Assembly dynamics and the roles of FliI ATPase of the bacterial flagellar export apparatus. Sci Rep. 2014 Oct 6; 4:6528.

305. Taylor TB, Mulley G, Dills AH, Alsohim AS, McGuffin LJ, Studholme DJ, et al. Evolution. Evolutionary resurrection of flagellar motility via rewiring of the nitrogen regulation system. Science. 2015 Feb 27;347(6225):1014–1017.

306. Lancero H, Caberoy NB, Castaneda S, Li Y, Lu A, Dutton D, et al. Characterization of a *Myxococcus xanthus* mutant that is defective for adventurous motility and social motility. Microbiology (Reading, Engl). 2004 Dec;150(Pt 12):4085–4093.

307. Römling U, Galperin MY, Gomelsky M. Cyclic di-GMP: the first 25 years of a universal bacterial second messenger. Microbiol Mol Biol Rev. 2013 Mar;77(1):1–52.

308. Skotnicka D, Petters T, Heering J, Hoppert M, Kaever V, Søgaard-Andersen L. Cyclic Di-GMP Regulates Type IV Pilus-Dependent Motility in *Myxococcus xanthus*. J Bacteriol. 2016 Jan;198(1):77–90.

309. Hedstrom RC, Funk CR, Kaper JB, Pavlovskis OR, Galloway DR. Cloning of a gene involved in regulation of exotoxin A expression in *Pseudomonas aeruginosa*. Infect Immun. 1986 Jan;51(1):37–42.

310. Wozniak DJ, Cram DC, Daniels CJ, Galloway DR. Nucleotide sequence and characterization of toxR: a gene involved in exotoxin A regulation in *Pseudomonas aeruginosa*. Nucleic Acids Res. 1987 Mar 11;15(5):2123–2135.

311. Duan K, Lafontaine ER, Majumdar S, Sokol PA. RegA, iron, and growth phase regulate expression of the *Pseudomonas aeruginosa* tol-oprL gene cluster. J Bacteriol. 2000 Apr;182(8):2077–2087.

312. Wolz C, Lehmann R, Vasil ML, Bischoff R, Döring G. A new extracellular protein of *Pseudomonas aeruginosa* PA103 regulated by *regA*. Microbiology (Reading, Engl). 1994 Jul;140 (Pt 7):1755–1761.

313. Guzzo CR, Dunger G, Salinas RK, Farah CS. Structure of the PilZ-FimXEAL-c-di-GMP Complex Responsible for the Regulation of Bacterial Type IV Pilus Biogenesis. J Mol Biol. 2013 Jun 26;425(12):2174–2197.

314. Caiazza NC, Shanks RMQ, O'Toole GA. Rhamnolipids modulate swarming motility patterns of *Pseudomonas aeruginosa*. J Bacteriol. 2005 Nov;187(21):7351–7361.

315. Martínez-Granero F, Navazo A, Barahona E, Redondo-Nieto M, Rivilla R, Martín M. The Gac-Rsm and SadB signal transduction pathways converge on AlgU to downregulate motility in *Pseudomonas fluorescens*. PLoS ONE. 2012 Feb 20;7(2):e31765.

316. Caiazza NC, Merritt JH, Brothers KM, O'Toole GA. Inverse regulation of biofilm formation and swarming motility by *Pseudomonas aeruginosa* PA14. J Bacteriol. 2007 May;189(9):3603–3612.

317. Bertrand JJ, West JT, Engel JN. Genetic analysis of the regulation of type IV pilus function by the Chp chemosensory system of *Pseudomonas aeruginosa*. J Bacteriol. 2010 Feb;192(4):994–1010.

318. Kang WK, Icho T, Isono S, Kitakawa M, Isono K. Characterization of the gene rimK responsible for the addition of glutamic acid residues to the C-terminus of ribosomal protein S6 in *Escherichia coli* K12. Mol Gen Genet. 1989 Jun;217(2-3):281–288.

319. Little RH, Grenga L, Saalbach G, Howat AM, Pfeilmeier S, Trampari E, et al. Adaptive Remodeling of the Bacterial Proteome by Specific Ribosomal Modification Regulates *Pseudomonas* Infection and Niche Colonisation. PLoS Genet. 2016 Feb 4;12(2): e1005837.

320. Ryan RP, McCarthy Y, Kiely PA, O'Connor R, Farah CS, Armitage JP, et al. Dynamic complex formation between HD-GYP, GGDEF and PilZ domain proteins regulates motility in *Xanthomonas campestris*. Mol Microbiol. 2012 Nov;86(3):557–567.

321. Weber H, Pesavento C, Possling A, Tischendorf G, Hengge R. Cyclic-di-GMP-mediated signalling within the sigma network of *Escherichia coli*. Mol Microbiol. 2006 Nov;62(4):1014–1034.

322. Mekalanos JJ. Environmental signals controlling expression of virulence determinants in bacteria. J Bacteriol. 1992 Jan;174(1):1–7.

323. Minamino T, Imada K, Tahara A, Kihara M, Macnab RM, Namba K. Crystallization and preliminary X-ray analysis of *Salmonella* FliI, the ATPase component of the type III flagellar protein-export apparatus. Acta Crystallographica Section F Structural Biology and Crystallization Communications. 2006 Oct 1;62(10):973–975.

324. Gómez-Gómez L, Boller T. Flagellin perception: a paradigm for innate immunity. Trends Plant Sci. 2002 Jun;7(6):251–256.

325. Sambongi Y, Iko Y, Tanabe M, Omote H, Iwamoto-Kihara A, Ueda I, et al. Mechanical rotation of the c subunit oligomer in ATP synthase (F0F1): direct observation. Science. 1999 Nov 26;286(5445):1722–1724.

326. Trampari E, Stevenson CEM, Little RH, Wilhelm T, Lawson DM, Malone JG. Bacterial Rotary Export ATPases Are Allosterically Regulated by the Nucleotide Second Messenger Cyclic-di-GMP. J Biol Chem. 2015 Oct 2;290(40):24470–24483.

Appendix 1:

False-positive capture compound screen proteins

Appendix 1: False-positive capture compound screen proteins

Chapter 3:

Negative binding results from proteins tested as part of the capture compound screen verification. Binding assays used are described more fully in Chapter 3.

Putative regulatory protein (PFLU_4895)

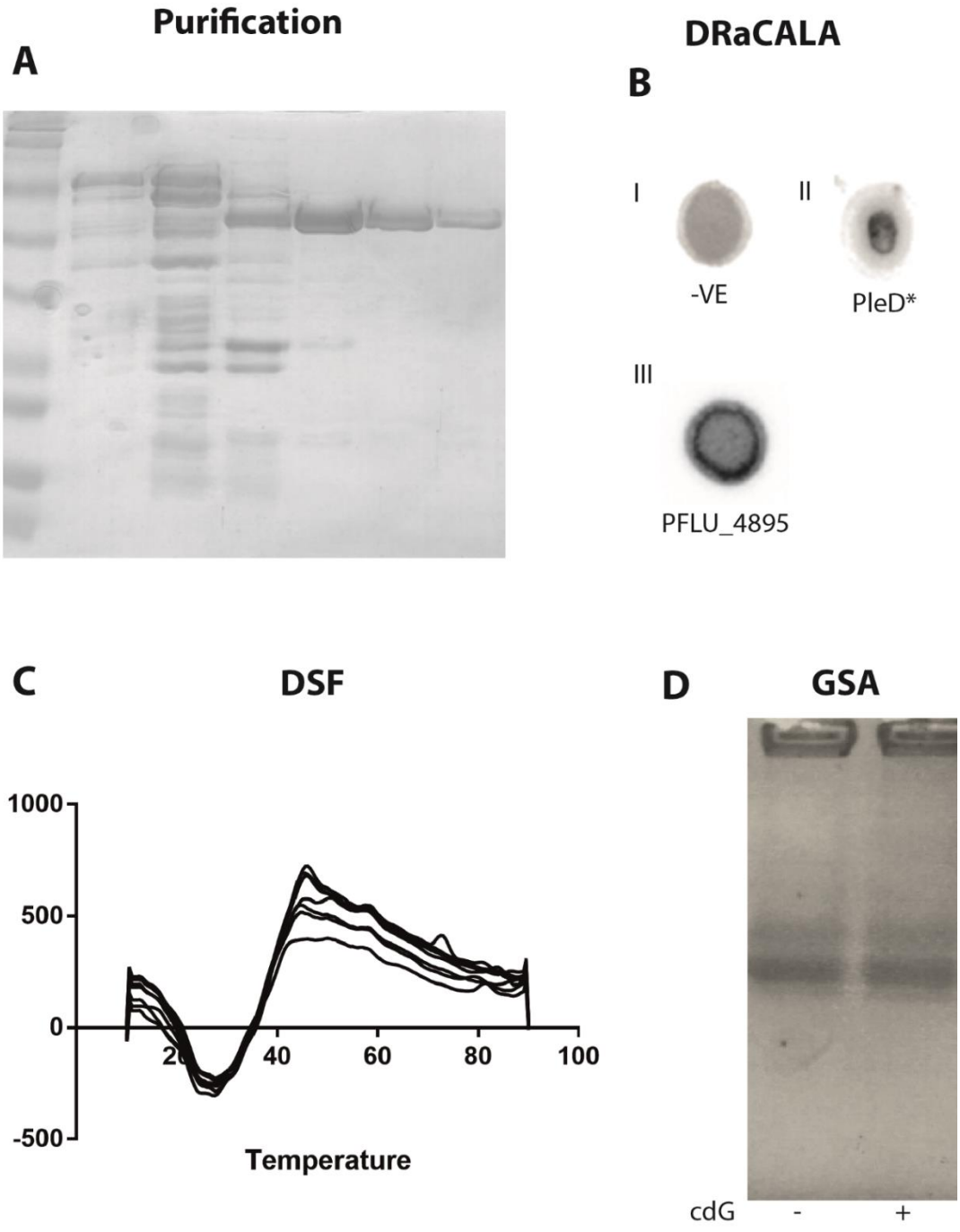

LysR family transcriptional regulator (PFLU_4531)

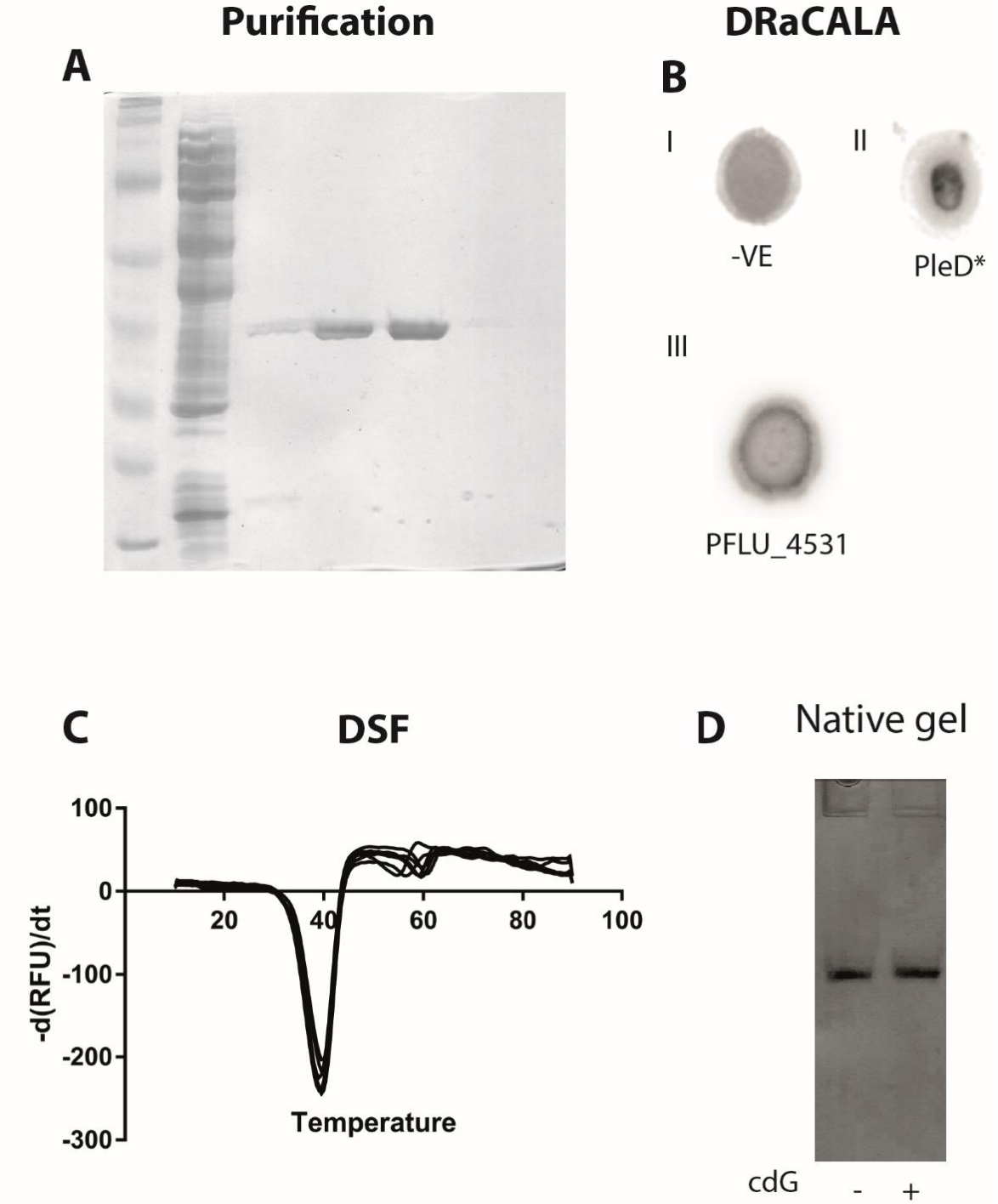

Appendix 2:

Publications

⌘ *Author's Choice*

THE JOURNAL OF BIOLOGICAL CHEMISTRY VOL. 290, NO. 40, pp. 24470–24483, October 2, 2015

Bacterial Rotary Export ATPases Are Allosterically Regulated by the Nucleotide Second Messenger Cyclic-di-GMP*[S]

Received for publication, April 30, 2015, and in revised form, August 10, 2015 Published, JBC Papers in Press, August 11, 2015, DOI 10.1074/jbc.M115.661439

Eleftheria Trampari[‡1], Clare E. M. Stevenson[§], Richard H. Little[‡], Thomas Wilhelm[¶], David M. Lawson[§], and Jacob G. Malone[‡‖2]

From the [‡]Molecular Microbiology Department and the [§]Biological Chemistry Department, John Innes Centre, Norwich NR4 7UH, United Kingdom, the [¶]Institute of Food Research, Norwich Research Park, Norwich NR4 7UA, United Kingdom, and the [‖]School of Biological Sciences, University of East Anglia, Norwich NR4 7TJ, United Kingdom

Background: AAA+ ATPase proteins play integral roles in the export apparatus of many bacterial organelles.
Results: The second messenger cyclic di-GMP binds specifically to multiple export ATPases at a highly conserved binding site.
Conclusion: Cyclic di-GMP binding is central to the function of many different bacterial export complexes.
Significance: This profoundly affects our understanding of numerous important bacterial organelles, including flagella, type III, and type VI secretion systems.

The widespread second messenger molecule cyclic di-GMP (cdG) regulates the transition from motile and virulent lifestyles to sessile, biofilm-forming ones in a wide range of bacteria. Many pathogenic and commensal bacterial-host interactions are known to be controlled by cdG signaling. Although the biochemistry of cyclic dinucleotide metabolism is well understood, much remains to be discovered about the downstream signaling pathways that induce bacterial responses upon cdG binding. As part of our ongoing research into the role of cdG signaling in plant-associated *Pseudomonas* species, we carried out an affinity capture screen for cdG binding proteins in the model organism *Pseudomonas fluorescens* SBW25. The flagella export AAA+ ATPase FliI was identified as a result of this screen and subsequently shown to bind specifically to the cdG molecule, with a K_D in the low micromolar range. The interaction between FliI and cdG appears to be very widespread. In addition to FliI homologs from diverse bacterial species, high affinity binding was also observed for the type III secretion system homolog HrcN and the type VI ATPase ClpB2. The addition of cdG was shown to inhibit FliI and HrcN ATPase activity *in vitro*. Finally, a combination of site-specific mutagenesis, mass spectrometry, and *in silico* analysis was used to predict that cdG binds to FliI in a pocket of highly conserved residues at the interface between two FliI subunits. Our results suggest a novel, fundamental role for cdG in controlling the function of multiple important bacterial export pathways, through direct allosteric control of export ATPase proteins.

Pseudomonas fluorescens is a widespread soil bacterium that forms commensal relationships with plant species. Members of the *P. fluorescens* species group nonspecifically colonize the rhizosphere and phyllosphere of many plants and promote plant growth, as well as providing potent antifungal and other biocontrol capabilities (1–3). The related bacterium *Pseudomonas syringae* is a Gram-negative phytopathogen and is responsible for numerous important plant diseases. *P. syringae* produces a large number of species-specific phytotoxins and type III-secreted effector molecules that subvert plant defenses (4, 5) and infects host plants by migration through open stomata and wounds on the plant surface. Two of the most important organelles for efficient host colonization by both commensal and pathogenic *Pseudomonas* sp. are the flagellum and the type III secretion system (T3SS).[3] Flagella-mediated motility is critical during the initial stages both of infection and benign plant colonization and is required to move through the soil toward plant roots, to colonize plant surfaces, and to migrate into the apoplastic space (6). Type III secretion systems, needle-like structures that inject effector proteins into plant cells, play a critical role in *P. syringae* virulence (4) and have also been shown to be important for rhizosphere colonization by *P. fluorescens* (6).

Assembly of the bacterial flagellum is tightly regulated and proceeds via the export of extracellular subunits through the central pore of the extending complex (7–9). The AAA+ ATPase FliI, together with FliH and FliJ, forms the soluble component of the flagellar export apparatus (8, 10, 11). FliI and FliH form a heterotrimer ($FliH_2$-FliI) *in vivo* and along with FliJ deliver export substrates from the cytoplasm to the flagellum export gate. There, FliI forms a hexameric ring and is anchored to the export gate by FliJ and FliH (12). Although the majority of the energy required for flagella formation is provided by the proton motive force, FliI ATPase activity is required for efficient flagella formation and plays a role in the initiation of protein export (13, 14). The secretion apparatus of flagella and T3SS share a conserved core architecture, with many proteins in common including the protein export apparatus (9, 13).

* This work was supported by Institute Strategic Program Grants awarded to the John Innes Centre (to J. G. M., R. L., C. E. M. S., and D. L.) and the Institute for Food Research (to T. W.) and by University of East Anglia start-up funding (to J. G. M.). The authors declare that they have no conflicts of interest with the contents of this article.
[S] This article contains supplemental Fig. S1.

[1] Supported by a Biotechnology and Biological Sciences Research Council Doctoral Training Partnership Ph.D. studentship.
[2] To whom correspondence should be addressed. Tel.: 44-1603-450-727; E-mail: jacob.malone@jic.ac.uk.

[3] The abbreviations used are: T3SS, type III secretion system; SPR, surface plasmon resonance; cdG, cyclic di-GMP; DRaCALA, differential radial capillary of ligand assay; MS-PSA, mass spectrometry peak-shift analysis.

TABLE 1
Strains and plasmids used in this study

	Description	Reference
Strains		
E. coli BL21-(DE3)	Sm^R, K12 *recF143 lacI*^{q} *lacZ*Δ*.M15*, *xylA*	Novagen
E. coli DH5α	*endA*1, *hsdR*17(r_K-m_K+), *supE*44, *recA*1, *gyrA* (Nal^R), *relA*1, Δ(*lacIZYA-argF*) U169, *deoR*, Φ80*dlac*Δ*(lacZ)M15*	Ref. 82
SBW25	Environmental *P. fluorescens* isolate	Ref. 47
Pto DC3000	Rif^R derivative of *P. syringae* pv. Tomato NCPPB 1106	Ref. 84
Salmonella enterica pv. typhimurium	Strain LT2	Ref. 51
Sinorhizobium meliloti	Strain 1020	Ref. 83
Plasmids		
pET*Nde*M-11	K_m^R, purification vector, N-terminal His_6 tag	Ref. 49
pET*Nde*M-11-overexpression vectors	Various overexpression vectors for *fliI* alleles, *hrcN*, and *clpB2* ligated between the NdeI and EcoRI sites of pET*Nde*M-11	This study

Investigations into the signaling pathways that control interactions between pathogenic and commensal *Pseudomonas* sp. and their host plants have highlighted a central role for the bacterial second messenger cyclic di-GMP (cdG) (15–21). cdG is a ubiquitous regulator of bacterial behavior, controlling the transition between motility and sessility, and chronic and virulent lifestyles in a wide range of bacteria. Recently, cdG has emerged as a crucial factor in the signaling pathways of most bacterial species, determining when, where, and how bacteria form biofilms, progress through the cell cycle, and regulate different aspects of motility and virulence (22). Broadly speaking, cdG production is associated with community behavior phenotypes such as biofilm formation and surface attachment. Conversely, low cdG levels are connected to unicellular, motile, and virulent lifestyles (22). cdG affects cell phenotypes by regulating the expression, production, and activity of different phenotypic output pathways. These outputs are controlled by cdG binding to effectors that function at transcriptional (23), translational (24), and post-translational, allosteric levels (25, 26). Individual phenotypic outputs may be controlled at multiple regulatory stages. For example, the expression of multiple flagella genes are controlled by the cdG-binding transcriptional regulator FleQ (23, 27). Flagella function is also allosterically controlled by cdG, with binding to the basal body-associated proteins YcgR and FlgZ leading to reduced flagella rotation speed in *Escherichia coli* and *Pseudomonas putida*, respectively (28, 29).

cdG-mediated signaling pathways are typically highly complex. Numerous species, including the pseudomonads, contain dozens of metabolic enzymes and display diverse cdG-triggered phenotypes (22). Although the synthesis and degradation of cdG by GGDEF, EAL, and HD-GYP proteins is fairly well understood (30–33), much remains to be discovered about the effector proteins that bind the dinucleotide molecule and elicit downstream responses in the cell. Although several predictable cdG binding folds are known, for example the PilZ (34) and degenerate GGDEF and EAL domains (35–37), cdG is a promiscuous molecule and binds to a diverse range of protein folds. In many cases, these cdG binding motifs are impossible to bioinformatically predict in advance (27, 38–41). This, combined with the complexity of cdG signaling and the diverse array of interconnected, cdG-associated phenotypes (22, 42, 43) suggests that a great many cdG binding proteins still await discovery.

Recent investigations by several research groups have made effective use of biochemical and spectrometric techniques for the isolation and identification of cdG binding proteins (44–46). These studies have both increased our understanding of the phenotypes and cellular functions controlled by this second messenger and substantially expanded the number of recognized binding motifs and protein domains (40, 42, 43). To better understand the role of cdG in the interactions between plant-associated *Pseudomonas* species and their hosts, we used a cdG capture compound assay (45) to screen for cdG binding proteins in the model *P. fluorescens* strain SBW25 (47). Among the proteins we identified in this screen was the flagella export ATPase FliI (PFLU4436). Subsequent biochemical analysis showed that SBW25 FliI specifically binds to cdG with a K_D in the low micromolar range. FliI-cdG binding was not confined to *P. fluorescens* but was also seen for FliI homologs from several other bacterial species, as well as the closely related T3SS export ATPase HrcN from *P. syringae* (PSPTO1400) and the significantly more divergent type VI secretion system secretion ATPase ClpB2 (PFLU6025).

In vitro addition of cdG induced a marked, concentration-dependent inhibition of ATPase activity for both FliI and HrcN. However, the association between ATPase activity and cdG binding is not absolute: mutation of critical active site residues in both FliI and HrcN abolishes ATP hydrolysis, whereas dinucleotide binding is unaffected. To further probe the relationship between FliI and cdG, a combination of mass spectrometry and *in silico* analysis was used to predict the FliI dinucleotide binding site. These results suggest that cdG may bind in a pocket of highly conserved residues at the interface between two domains of the FliI hexameric ring. Our results suggest a fundamental new role for the signaling molecule cdG, in the structure and function of multiple widespread and biologically important bacterial export pathways.

Experimental Procedures

Strains and Growth Conditions—Strains and plasmids are listed in Table 1. Primers are listed in Table 2. Unless otherwise stated, all *P. fluorescens* strains were grown at 28 °C and *E. coli* at 37 °C in lysogenic broth (48), solidified with 1.5% (w/v) agar where appropriate. For protein overexpression, terrific broth was used. Kanamycin was used at 50 μg/ml, carbenicillin was used at 100 μg/ml, and chloramphenicol was used at 30 μg/ml. For inducible plasmids, isopropyl β-D-thiogalactopyranoside was added to a final concentration 0.5 mM as appropriate.

Molecular Biology Procedures—Cloning was carried out in accordance with standard molecular biology techniques. The

TABLE 2
Primers

Name	Gene Target	Modification	Sequence (5′ → 3′)
A	*PFLU4436* (*fliI*)	None	TTACTTCATATGCGCCTTGATCGCACCAG
B	*PFLU4436* (*fliI*)	None	ATATTCAATTGTTAGCCGCCCGGCGCG
C	*PFLU4436* (*fliI*)	Δ1–18	TTACTTCATATGACATCGTTGCCCGGCCAG
D	*PSPTO1961* (*fliI*)	None	TTACTTCATATGCGCCTTGATCGCGTGAG
E	*PSPTO1961* (*fliI*)	None	AATATCAATTGTCAGCCGCCAGGGG
F	*STY2180* (*fliI*)	None	TTACTTCATATGACCACGCGCCTGACC
G	*STY2180* (*fliI*)	None	AATTGAGAATTCTCACACCGTCGGGAAAAT
H	*SMc03025* (*fliI*)	None	TTACTTCATATGGCACGCGAAGCCGCTG
I	*SMc03026* (*fliI*)	None	AATATCAATTGTCATCCCCTTCCGCGCA
J	*PSPTO1400* (*hrcN*)	None	TTACTTCATATGAACGCCGCACTGAACCAG
K	*PSPTO1400* (*hrcN*)	None	AATATGAATTCTTACTCCGGCAGTTGCGAG
L	*PFLU6025* (*clpB2*)	None	TTACTTCATATGGGTGAAATCAGTCGC
M	*PFLU6025* (*clpB2*)	None	AATATCAATTGTCAATCTGCGTCGC
N	*PFLU4436* (*fliI*)	G176A	CCTGTTCGCCGCTACCGGCGTGG
O	*PFLU4436* (*fliI*)	G176A	CCACGCCGGTAGCGGCGAACAGG
P	*PFLU4436* (*fliI*)	K181A	CGGCGTGGGTGCGTCGGTGTTGC
Q	*PFLU4436* (*fliI*)	K181A	GCAACACCGACGCACCCACGCCG
R	*PFLU4436* (*fliI*)	D265A	GTTGCTGATGGCCTCGCTCACGC
S	*PFLU4436* (*fliI*)	D265A	GCGTGAGCGAGGCCATCAGCAAC
T	*PSPTO1400* (*hrcN*)	K181A	GCGGCAAGGCCACGCTGATG
U	*PSPTO1400* (*hrcN*)	K181A	CATCAGCGTGGCCTTGCCGC

pET*Nde*M-11-*fliI*, *hrcN*, and *clpB2* purification vectors were produced by ligating PCR fragments (amplified with primers A–M from appropriate genomic DNA) between the NdeI and EcoRI sites of plasmid pET*Nde*M-11 (49) as appropriate. Strand overlap extension (50) was used to produce Walker A and Walker B mutants in FliI and HrcN using primers N–U, before cloning into expression vectors as appropriate.

cdG Capture Compound Experiments—Experiments were performed as described by Nesper *et al.* (45). *P. fluorescens* cells were grown in M9 0.4% (w/v) pyruvate medium ± 0.4% (w/v) casamino acids to stationary phase and to mid-logarithmic phase, lysogenic broth to stationary phase, and Kings B medium to logarithmic phase. Cells were collected by centrifugation for 5 min at 5,000 × *g*. The pellet was resuspended in lysis buffer (6.7 mM MES, 6.7 mM HEPES, pH 7.5, 200 mM NaCl, 6.7 mM sodium acetate and 10 mM β-mercaptoethanol) with protease inhibitors and DNase I (Roche). Cells were lysed using a French press (3 × 20,000 p.s.i.), and lysates were centrifuged at 100,000 × *g* for 1 h. The supernatant was then used to identify soluble cdG binding proteins. 600 μg of the soluble protein mixture was used and was mixed with 20 μl of capture buffer (100 mM HEPES, pH 7.5, 250 mM sodium acetate, 50 mM magnesium acetate, 50% (v/v) glycerol), plus 12.5 μl of 10 mM cdG for the control samples. Volumes were adjusted to 100 μl with water, and the reactions were then incubated for 2 h at 4 °C, before UV irradiation for 4 min using a caproBox (Caprotec Bioanalytics, Berlin, Germany). Magnetic streptavidin beads (50 μl) were added with 25 μl of 5× wash buffer (250 mM Tris, pH 7.5, 5 M NaCl, 0.1% (w/v) *n*-octyl-β-glucopyranoside), and the samples were incubated for 45 min at 4 °C on a rotary wheel. The beads were collected with a magnet, and the samples were washed six times with 200 μl of 1× wash buffer. The beads were resuspended in 20 μl of sample buffer, incubated for 10 min at 95 °C, and separated for 10 min on a precast 12% (w/v) SDS acrylamide gel at 100 V. Protein bands were then excised and sent for mass spectrometric analysis. The same protocol was followed for the competition experiment (see Fig. 1*C*). Similarly to the controls, 1 mM of each nucleotide was added to a protein mixture of 10 μM and preincubated for 1 h before the addition of the capture compound (10 μM).

Protein Purification—E. coli BL21-(DE3) pLysS overexpression cultures were inoculated from overnight cultures in a 1:100 ratio and grown at 37 °C to an OD_{600} of 0.4, before protein expression was induced overnight with 0.5 mM isopropyl β-D-thiogalactopyranoside at 18 °C. Cells were then lysed by French press (3 × 20,000 p.s.i.) and centrifuged, and the proteins purified were from the supernatant by nickel-nitrilotriacetic acid chromatography. 1-ml HiTrap chelating HP columns (Amersham Biosciences) were equilibrated with 10 volumes of washing buffer (20 mM HEPES, pH 7.5, 250 mM NaCl, 2 mM $MgCl_2$, and 2.5% (v/v) glycerol, pH 7.5) and loaded with cell lysate. Following protein immobilization, the column was washed with 10 volumes of buffer containing 50 mM imidazole, before proteins were eluted using 500 mM imidazole buffer in a single step elution.

Differential Radial Capillary of Ligand Assay (DRaCALA)—The method was performed as described by Roelofs *et al.* (44). Purified PleD* (52) was used to synthesize radiolabeled cdG from [γ-^{32}P]GTP. The assays were conducted using increasing concentrations of purified FliI proteins mixed with 4 nM radiolabeled cdG in each case. Samples were incubated for 2 min at room temperature with [γ-^{32}P]cdG in reaction buffer (25 mM Tris, 250 mM NaCl, 10 mM $MgCl_2$, 5 mM β-mercaptoethanol, pH 7.5). 5 μl of each sample were then spotted on nitrocellulose, samples were dried, and results were visualized using a PhosphorImager screen. In some cases 2′-Fluo-AHC-c-diGMP was used (BioLog 009) as an alternative to [γ-^{32}P]cdG, at a concentration of 0.6 μM. The results were visualized using a charge-coupled device camera. For the competition experiments, 1 mM of each nucleotide was mixed with 10 μM of $FliI_{\Delta 1-18}$ and incubated for 30 min before the addition of the fluorescent cdG.

Surface Plasmon Resonance (SPR)—SPR experiments were conducted at 25 °C with a Biacore T200 system (GE Healthcare) using a streptavidin SA sensor chip (GE Healthcare), which has four flow cells each containing SA preimmobilized to a carboxymethylated dextran matrix. Flow cells 1 and 3 were kept

blank to use for reference subtraction. The chip was first washed three times with 1 M NaCl, 50 mM NaOH to remove any unconjugated streptavidin. 100 nM biotinylated cdG (BioLog B098) was immobilized on flow cells 2 and 4 of the streptavidin chip at a 50-response unit immobilization level with a flow rate of 5 μl/min. Soluble proteins at the required concentrations were prepared in SPR buffer (10 mM HEPES, 150 mM NaCl, 0.1% (v/v) Tween 20, 2 mM $MgCl_2$) by adjusting the pH for the different proteins. For $FliI_{His}$, $FliI_{His}$ mutants, $HrcN_{His}$, $HrcN_{His}$ mutants, and ClpB2, the optimal pH was 6.5, whereas for $FliI_{SeT}$, the optimal pH was 7.5, and for $FliI_{\Delta 1-18}$ it was 5.5. Samples were injected with a flow rate of 5 μl/min over the reference and cdG cells for either 60, 90, or 120 s depending on their saturation level followed by buffer flow for either 60 or 90 s. The chip was washed at the end of each cycle with 1 M NaCl. Replicates for each protein concentration were included as appropriate. In certain cases (*e.g.* $FliI_{SeT}$), protein precipitation at higher concentrations prevented the acquisition of a saturated binding curve. In these cases, a representative data set is presented from at least three independent repetitions. All sensorgrams were analyzed using Biacore T200 BiaEvaluation software version 1.0 (GE Healthcare). The data were then plotted using Microsoft Excel and GraphPad Prism.

Linked Pyruvate Kinase/Lactate Dehydrogenase ATPase Activity Assay—ATPase activity was measured indirectly by monitoring NADH oxidation. The reaction buffer consisted of 50 mM Tris-Cl, pH 8.0, 2 mM $MgCl_2$, 1 mM DTT, and 10 mM KCl. Each reaction contained 5 mM NADH in 10 mM NaOH, 80 mM phosphoenolpyruvic acid, 1.5 μl of pyruvate kinase/lactate dehydrogenase (Sigma), and appropriate concentrations of FliI/HrcN and cdG and was initiated by the addition of ATP. Enzyme kinetics were determined by measuring A_{340} at 1-min intervals. Kinetic parameters were calculated by plotting the specific activity of the enzyme (nmol of ATP hydrolyzed/min/mg of protein) *versus* ATP concentration and by fitting the nonlinear enzyme kinetics model (Hill equation) in GraphPad Prism.

Mass Spectrometry of Cross-linked FliI—10 μM $FliI_{His}$ protein was incubated with 10 μM cdG capture compound (Caprotec) and cross-linked in a UV Stratalinker on ice for 4 min. Cross-linked sample was then separated from non-cross-linked using magnetic beads as described for the capture compound screen (above). Cross-linked FliI-cdG and a non-cross-linked control sample were then run into an SDS gel, and FliI bands were excised for protein identification. Samples were analyzed by Nano-LC-MS/MS on an Orbitrap Fusion™ Tribrid™ mass spectrometer coupled to an UltiMate® 3000 RSLCnano LC system (Thermo Scientific, Hemel Hempstead, UK). The sample was separated on a PepMap™ 100 C18 LC Column (C18, 2 μm, 500 × 0.75 mm; Thermo) using a gradient of 0.75% (v/v) min^{-1} acetonitrile from 6% to 40% (v/v) in water, 0.1% (v/v) formic acid at a flow rate of 0.3 μl min^{-1} and infused directly into the mass spectrometer. The mass spectrometer was run in positive ion mode, with no quad isolation, at 120K resolution over the mass range 350–1800 (m/z) for the precursor scans (Orbitrap). One microscan of 50 ms with an AGC target of $2e^5$ was used. MS2 threshold was set to $1.5e^4$, and precursors were fragmented by both CID and HCD with CE = 30 and an isolation window of 1.6 Da (quadrupole) using the automatic maximum speed option with ion injection for all available parallelizable time. Dynamic exclusion was set to 1 count and 30 s. Recalibrated peaklists were generated using MaxQuant 1.5.2.8, and the database search was performed with the merged HCD and CID peaklists using Mascot 2.4 (Matrixscience, London, UK). The search was performed with a precursor tolerance of 6 ppm and a fragment tolerance of 0.6 Da on a partial *E. coli* database, to which the expected $FliI_{His}$ protein sequence was added. The enzyme was set to trypsin/P with a maximum of two allowed missed cleavages. Carbamidomethyl (C) was set as fixed modification, and oxidation (M) and acetylation (Protein N-term) were used as variable modifications. The Mascot search results were imported into Scaffold 4.4.1.1 using identification probabilities of 99 and 95% for proteins and peptides.

Homology Model Production—A homology model of a *P. fluorescens* FliI monomer was created by the Phyre2 server (53) using the crystal structure of FliI from *Salmonella enterica* as a template (Protein Data Bank accession code 2DPY; 63% amino acid sequence identity) (54). FliI is predicted to be structurally homologous to the α and β subunits of F_1-ATPase, and the latter forms a hexameric ring of alternating α and β subunits around a single copy of a γ subunit. Using the secondary structure matching algorithm (55) within the program COOT (56), a model of a FliI hexamer was generated by superposing six copies of the monomer onto each of the α and β subunits of the bovine F_1-ATPase $\alpha_3\beta_3\gamma$ complex (Protein Data Bank accession code 2JIZ) (57). All structural figures were prepared using CCP4 mg (58).

Mass Spectrometry-Peak Shift Analysis (MS-PSA)—MS-PSA analysis of the sample containing the treated protein $FliI_{His}$ (*i.e.* cross-linked to cdG) was performed as described previously (44). We further improved the method to specifically search for spectra relations (*i.e.* modified *versus* unmodified peptide) between spectra from two different samples. Accordingly, we found many related peptides between the pure (untreated) $FliI_{His}$ sample and the treated sample ($FliI_{His}$ cross-linked to cdG), particularly for the peptide NVLLLMDSLTR. The following MS-PSA parameters were used for both analyses: num = 8 pmr = 0.001 t1 = 5 t2 = 100 fmr = 0.5 mnds = 2 clusterq = True signif = 1 tol = 1 outl = 0.1 nmfp = 20 mofp = 9 mnspg = 2 csf = 2 peakfreq = 2 nummods = 1 pwss = 4 cp = 3 qual1 = 0.2 qual2 = 0.2 qual1pl2 = 0.5 mrms = 150 maxdev = 1. MS-PSA parameters are defined in Fig. S1 of Ref. 44.

Results

The Flagellar ATPase FliI Binds Specifically to cdG—As part of our ongoing efforts to define the cdG regulon of *P. fluorescens* SBW25, we carried out a series of screening experiments for cdG binding proteins using a cdG capture compound assay (45) (Caprotec). These experiments identified homologs of confirmed binding proteins, including FleQ (23) and WspR (59), as well as several uncharacterized PilZ, GGDEF, and EAL domains and numerous proteins for which no previous experimental or predicted link to cdG signaling had been made. Among these previously unidentified cdG targets, the flagellar export protein FliI was identified in screens conducted under a number of different experimental conditions (Kings B medium

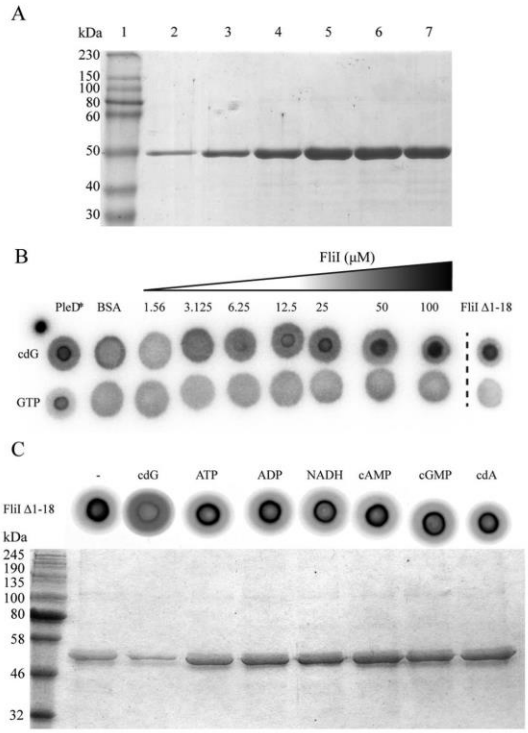

FIGURE 1. *A*, Coomassie-stained SDS-PAGE gel showing purified $FliI_{His}$ fractions eluted with 500 mM imidazole. *B*, DRaCALA for [^{32}P]cdG and [^{32}P]GTP binding to increasing concentrations of full-length FliI ($FliI_{His}$). Positive (10 μM PleD*) and negative (10 μM BSA) binding controls are included, as well as N-terminal truncated FliI (10 μM $FliI_{\Delta 1-18}$). *C*, DRaCALA competition experiment performed on $FliI_{\Delta 1-18}$. A variety of nucleotides were included in the reaction to test the specificity of cdG binding. SDS-PAGE gel showing protein bound to the capture compound after preincubation with different nucleotides.

log phase, lysogenic broth stationary phase, and M9 pyruvate + casamino acids). In addition to the suppression of flagellar gene expression (23) and flagellum rotation (29, 60), FliI-cdG binding suggests a central, previously unsuspected role for cdG in the regulation of flagellum protein export and assembly. Consequently, we selected FliI for further biochemical analysis. First, to confirm that SBW25 FliI binds to cdG *in vitro*, the full-length, His-tagged protein ($FliI_{His}$) was purified (Fig. 1*A*), and nucleotide binding was tested using the DRaCALA binding assay (44). $FliI_{His}$ bound strongly to ^{32}PcdG but did not bind to ^{32}PGTP even at far higher protein concentrations (Fig. 1*B*). To further test the specificity of FliI-cdG binding, competitive DRaCALA and capture compound experiments were performed (Fig. 1*C*). A variety of nucleotides (cyclic di-GMP, ADP, ATP, NADH, cAMP, cGMP, and cyclic di-AMP) were added in excess to compete the 2′-Fluo-AHC-c-diGMP and capture compound, respectively. In both experiments, binding was abolished only with the addition of cdG, strongly suggesting that cdG binding by FliI is specific. Our initial attempts to define the biochemical parameters of cdG binding to $FliI_{His}$ used isothermal titration calorimetry. This technique showed tight, concentration-dependent cdG binding with a K_D of ~10 μM (data not shown). However, we were unable to refine the isothermal titration calorimetry protocol sufficiently to produce publishable data. Consequently, we turned to SPR to examine $FliI_{His}$ binding to biotinylated cdG. In this experiment, $FliI_{His}$ bound to the cdG chip in a concentration-dependent manner with a K_D of 2.4 ± 0.2 μM (Fig. 2, *A* and *B*, and Table 3).

Much of the structural and functional analysis of FliI to date has been conducted in *S. enterica*, whose purified FliI homolog is unstable *in vitro* unless the N terminus of the protein is truncated (61). This modification affects FliI multimerization, with the truncated allele unable to form hexameric complexes *in vitro* (62). To examine the effects of removing the FliI N terminus on protein-ligand interactions, a truncated FliI allele missing the first 18 residues ($FliI_{\Delta 1-18}$) was purified and analyzed alongside full-length $FliI_{His}$. The $FliI_{\Delta 1-18}$ allele bound tightly and specifically to cdG in both DRaCALA and SPR experiments, with a dissociation constant of 0.75 ± 0.03 μM (Figs. 1*B* and 2, *C* and *D*). The binding constants for both full-length and truncated FliI fall comfortably within the affinity range of previously characterized cdG binding proteins (between the low nanomolar range and 10–15 μM (63)), indicating that FliI-cdG binding is likely to occur in *P. fluorescens* under physiologically relevant conditions.

FliI Homologs from Diverse Bacterial Species and the Export ATPases of Type III and Type VI Secretion Systems Bind cdG at Physiological Concentrations—Flagella-driven motility, and hence FliI-mediated export, is ubiquitous among Gram-negative bacteria. To investigate whether cdG-binding to FliI is similarly widespread, full-length FliI homologs from several bacterial species were cloned, expressed, purified, and then tested for cdG binding using SPR. FliI homologs were selected from human and plant pathogens, as well as commensal and symbiotic plant growth-promoting organisms. The tested FliI homologs included representatives from the α- and γ-proteobacterial classes and both monotrichous and polyflagellated bacteria. Concentration-dependent cdG binding was detected for full-length FliI alleles from the phytopathogen *P. syringae* pv. *tomato* (*Pto*) DC3000 ($FliI_{Pto}$), the human pathogen *S. enterica* serovar typhimurium ($FliI_{SeT}$), and the nitrogen-fixing symbiont *Sinorhizobium meliloti* ($FliI_{Sm}$) (Fig. 3 and Table 3). Despite a reasonably high degree of *fliI* amino acid sequence divergence (SBW25 and *S. meliloti fliI* share only 35.4% identity) and significant differences in flagella regulation and cdG signaling between the tested species, all four FliI homologs bound to the dinucleotide molecule with affinities well within the expected physiological range of intracellular cdG concentrations.

The export apparatus of the bacterial flagellum is closely related to that of the T3SS, with both complexes sharing a common ancestor (8). Furthermore, cdG has been associated with the control of T3SS function in the opportunistic pathogen *Pseudomonas aeruginosa* (64, 65), although the mechanism of this regulation is currently unclear. In light of this, our data for FliI-cdG binding implicate the T3SS export ATPase HrcN as a further potential cdG-binding target. To test this, we purified the full-length, His-tagged protein from *Pto* DC3000 ($HrcN_{His}$) and examined cdG binding using SPR. As predicted, $HrcN_{His}$

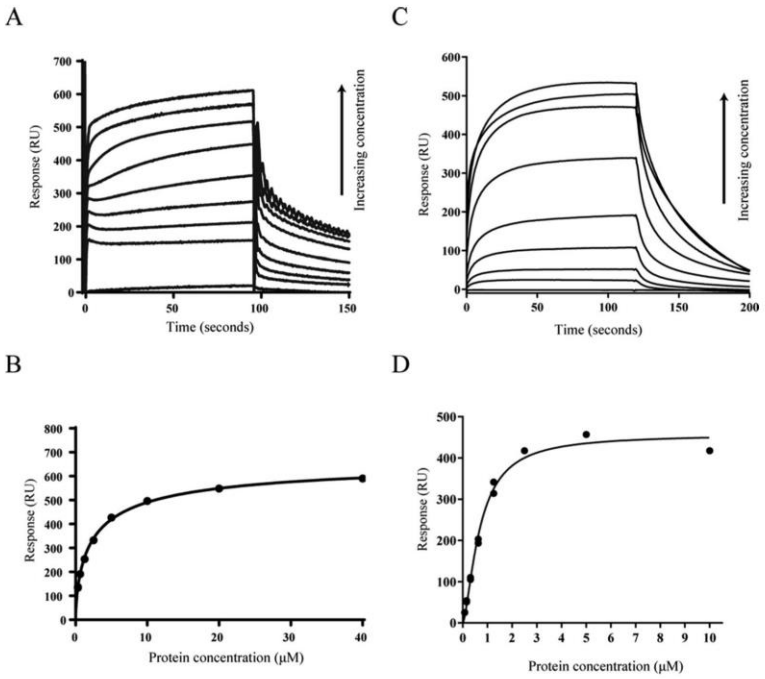

FIGURE 2. *A*, SPR sensorgrams showing affinity measurements for $FliI_{His}$ binding to biotinylated cdG. A range of $FliI_{His}$ concentrations was used (0.312, 0.625, 1.25, 2.5, 5, 10, 20, and 40 μM), and concentration replicates were included as appropriate together with buffer only and BSA controls. The protein binding and dissociation phases for all sensorgrams are shown. *B*, affinity fit for $FliI_{His}$-cdG binding. The binding response for each concentration was recorded 4 s before the end of the injection, and the K_D values for $FliI_{His}$ binding to cdG (2.4 $\pm$ 0.2 μM) were calculated using the BiaEvaluation software and confirmed by GraphPad Prism. *C*, SPR sensorgrams showing affinity measurements for $FliI_{\Delta 1-18}$ binding to biotinylated cdG. A range of protein concentrations was used (0.078, 0.156, 0.3125, 0.625, 1.25, 2.5, 5, and 10 μM), and concentration replicates were included as appropriate together with buffer only and BSA controls. The protein binding and dissociation phases for all sensorgrams are shown. *D*, affinity fit for $FliI_{\Delta 1-18}$-cdG binding. Binding responses were measured 4 s before the end of the injection, and the K_D values for $FliI_{\Delta 1-18}$ binding to cdG (0.8 $\pm$ 0.03 μM) were calculated using the BiaEvaluation software and confirmed by GraphPad Prism.

TABLE 3

Binding affinity data for tested FliI, HrcN, and ClpB2 variants

Dissociation constant (K_D) values for the ATPase proteins analyzed in this study are shown. Binding to $FliI_{SeT}$ was concentration-dependent but did not saturate in the kinetic experiment.

	K_D
	μM
$FliI_{His}$ (full-length)	2.4 $\pm$ 0.2
$FliI_{\Delta 1-18}$ (N-terminally truncated)	0.8 $\pm$ 0.03
$FliI_{\Delta 1-18}$ R170H	Not determined
$FliI_{\Delta 1-18}$ E208Q	Not determined
$FliI_{\Delta 1-18}$ R337H	Not determined
$FliI_{Pto}$ (*Pto* DC3000)	7.6 $\pm$ 0.8
$FliI_{SeT}$ (*S. enterica*)	Not determined
$FliI_{Sm}$ (*S. meliloti*)	3.2 $\pm$ 0.7
$HrcN_{His}$	3.2 $\pm$ 0.2
$ClpB2_{His}$	9.5 $\pm$ 0.5
FliI G176A (Walker A mutant)	11.0 $\pm$ 1.1
FliI K181A (Walker A mutant)	2.2 $\pm$ 0.2
HrcN K181A (Walker A mutant)	3.8 $\pm$ 0.4
FliI D265A (Walker B mutant)	4.5 $\pm$ 0.2

also bound strongly to cdG, with a dissociation constant of 3.2 $\pm$ 0.2 μM (Fig. 4, *A* and *B*). The type VI secretion system export ATPase (ClpB2) is far more distantly related to FliI, in terms of both primary sequence and organization of the ATPase subunits within the type VI secretion complex (66). Nonetheless, as ClpB2 is a rotary ATPase and type VI secretion is known to be under reciprocal, cdG-linked control with type III secretion (65), full-length ClpB2 ($ClpB2_{His}$) was purified and tested for cdG binding. To our surprise, ClpB2 also displayed strong, concentration-dependent binding to the cdG with a physiologically relevant binding affinity of 9.5 $\pm$ 0.5 μM (Fig. 4, *C* and *D*). These data strongly suggest that binding to the cdG second messenger is a widespread characteristic across diverse rotary ATPase export proteins.

Addition of cdG Inhibits FliI and HrcN ATPase Activity—The established model for cdG function associates increased dinucleotide levels with reduced motility and virulence (22). This has been shown to be the case for both *P. fluorescens* (67) and *P. syringae* (17, 18, 21). Consequently, we hypothesized that cdG binding may negatively affect the ATP-dependent export activity of FliI and/or HrcN. To examine the effect of cdG binding on FliI/HrcN ATPase activity, pyruvate kinase/lactate dehydrogenase-linked ATPase activity assays were conducted for the full-length protein alleles $FliI_{His}$ and $HrcN_{His}$. Purified $FliI_{His}$ metabolized ATP with a K_m of 0.48 $\pm$ 0.03 μM and a V_{max} of 1262 $\pm$ 54.46 nm ATP/min/mg. Addition of 50 μM cdG led to a noticeable drop in V_{max}, to 867.2 $\pm$ 51.65 nm ATP/min/mg (Fig. 5*A*). The IC_{50} of cdG for $FliI_{His}$ (36.7 $\pm$ 1.13 μM) was then determined by increasing cdG levels while maintaining a constant ATP concentration in the reaction (Fig. 5*B*). Similar cdG

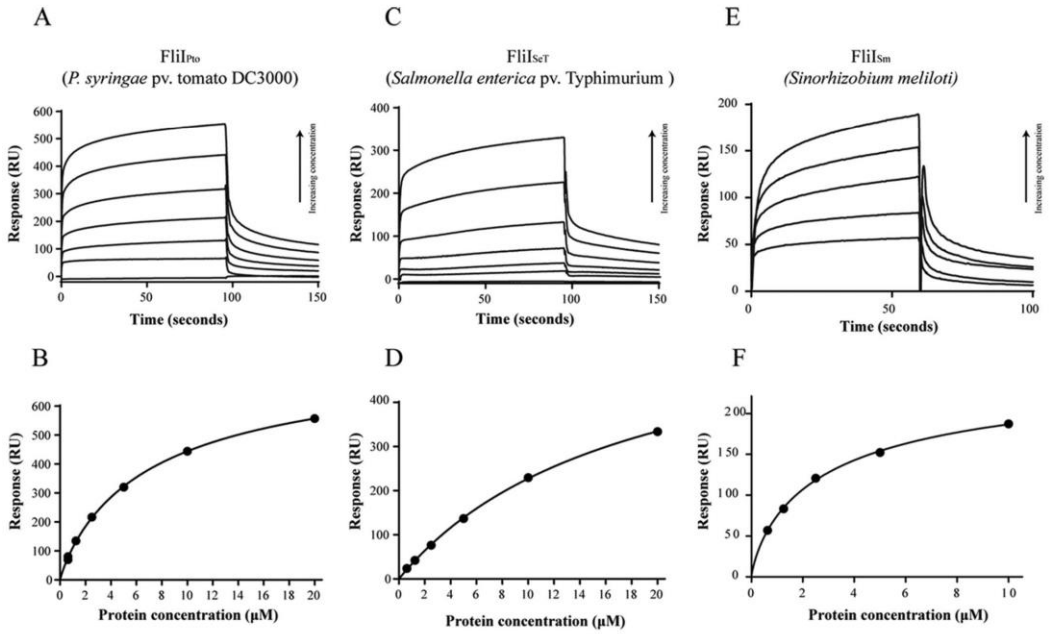

FIGURE 3. *A* and *B*, SPR sensorgrams and resulting affinity fit for FliI$_{Pto}$ binding to biotinylated cdG. *C* and *D*, SPR sensorgrams and affinity fit for FliI$_{SeT}$ binding to biotinylated cdG. *E* and *F*, SPR sensorgrams and affinity fit for FliI$_{Sm}$ binding to biotinylated cdG. In all three cases, a range of protein concentrations was used (0.625, 1.25, 2.5, 5, 10, and for FliI$_{Pto}$/FliI$_{SeT}$ 20 μM), and concentration replicates were included as appropriate together with buffer only and BSA controls. The protein binding and dissociation phases for all sensorgrams are shown. For the affinity fits, binding responses were measured 4 s before the end of the injection, and K_D values for each protein were calculated using the BiaEvaluation software and confirmed by GraphPad Prism (Table 3).

inhibitory activity was seen for FliI$_{\Delta 1-18}$, which metabolized ATP with K_m and V_{max} values of 0.45 ± 0.04 μM and 691.5 ± 41.90 nm ATP/min/mg without cdG. Upon addition of 50 μM of the dinucleotide molecule, V_{max} dropped to 375.4 ± 35.34 nm ATP/min/mg. FliI$_{\Delta 1-18}$ has an IC$_{50}$ value of 48.8 ± 0.159 μM. In agreement with DRaCALA results seen for FliI$_{His}$ (Fig. 1*B*), addition of GTP produced no change in ATPase activity, supporting a specific inhibitory role for cdG toward FliI ATPase activity (data not shown). Full-length HrcN showed a similar degree of ATPase inhibition to FliI, with V_{max} dropping from 1183 ± 68.2 to 832.4 ± 119.7 nm ATP/min/mg upon addition of 50 μM cdG, with an IC$_{50}$ of 25.11 ± 1.14 μM (Fig. 5, *C* and *D*). Addition of GTP had no effect on HrcN$_{His}$ ATPase activity (Fig. 5*D*), arguing once again for specific cdG inhibition of HrcN ATPase activity.

ATPase Activity and cdG Binding Are Uncoupled by Mutations in the FliI/HrcN Walker A and B Motifs—To further examine the relationship between ATP hydrolysis and cdG binding for FliI and HrcN, a series of full-length alleles were produced with residue substitutions in the conserved Walker A and Walker B motifs (68, 69) of the ATPase active site. The variant proteins were then purified and subjected to SPR analysis and ATPase activity assays as described above. Substitution of the critical FliI Walker A lysine residue for alanine (K181A) had very little effect on cdG binding affinity (Fig. 6*A* and Table 3) but entirely abolished ATPase activity (Fig. 6*B*). Conversely, substitution of the first conserved Walker A glycine to alanine (G176A) led to a mild reduction in FliI ATPase activity but almost entirely abolished the ability of the protein to bind cdG. Finally, a Walker B motif (D265A) substitution in FliI resulted in the complete abolition of ATPase activity but only a relatively small drop in the cdG binding affinity of the protein (Fig. 6, *A* and *B*, and Table 3). This is consistent with our previous results, which show that neither ATP nor ADP have any effect on cdG binding when included in DRaCALA assays (Fig. 1*C*). These results indicate that cdG binding and ATPase activity may be uncoupled.

Identifying the Site of cdG Capture Compound Binding in FliI—To further investigate the site of cdG binding on FliI, we constructed a homology model for SBW25 FliI based on the crystal structure of its *Salmonella* homolog (54) (Fig. 7). The location of ATP and the conserved residues across the six cdG-binding ATPases in this study were then mapped onto the model, and a predicted FliI hexameric complex was produced (Fig. 7*A*). Next, purified FliI$_{His}$ was incubated and UV cross-linked to the cdG capture compound. Following tryptic digestion and mass spectrometry, mass-shifted peptides were identified using MS-PSA, a recently developed analysis method for the identification of unexpected/unknown peptide modifications (70) (supplemental Fig. S1). Two MS-PSA analyses were performed, treated (*i.e.* cross-linked to cdG) *versus* untreated FliI$_{His}$ (S1A) and treated FliI$_{His}$ alone (S1B). In the treated sample, we expected to identify both pure FliI$_{His}$ and FliI$_{His}$ with bound cdG. Accordingly, many spectra relations correspond-

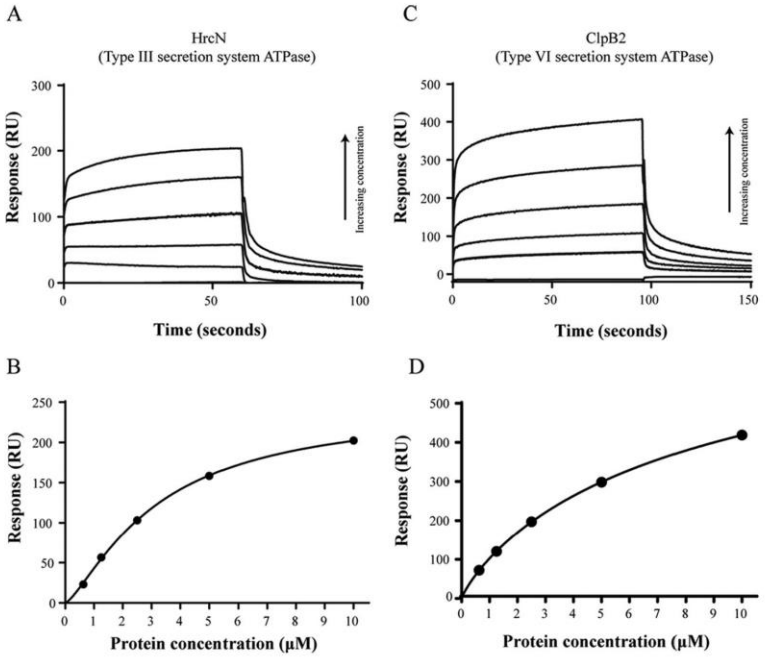

FIGURE 4. *A* and *B*, SPR sensorgram and resulting affinity fit for HrcN (type III export ATPase) binding to biotinylated cdG. *C* and *D*, SPR sensorgram and resulting affinity fit for ClpB2 (Type VI export ATPase) binding to biotinylated cdG. In both cases, a range of protein concentrations was used (0.625, 1.25, 2.5, 5, and 10 μM), and concentration replicates were included as appropriate together with buffer only and BSA controls. The protein binding and dissociation phases for all sensorgrams are shown. For the affinity fits, binding responses were measured 4 s before the end of the injection, and K_D values for each protein were calculated using the BiaEvaluation software and confirmed by GraphPad (Table 3).

ing to modified and unmodified peptides were identified (supplemental Fig. S1). Importantly, the most densely modified peptide following cdG capture compound cross-linking comprised residues 259–269 (NVLLLMDSLTR; supplemental Fig. S1). We identified 36 spectra relations where the lighter peptide was Mascot annotated NVLLLMDSLTR, and the heavier not-annotated partner carried a modification of >150 Da. By only comparing spectra between the treated and untreated sample, we identified 52 corresponding NVLLLMDSLTR spectra relations. The NVLLLMDSLTR peptide represents the central strand of a β-sheet at the core of the SBW25 FliI homology model, plus short loops at either end (Fig. 7*B*, *green*). The C terminus of the β-strand also contains the conserved aspartate (Asp-265) of the Walker B motif (Fig. 7*B*, *pink*). Interestingly, the end of the capture compound cross-linked peptide emerges close to a cluster of highly conserved residues that could form a pocket at the interface between two FliI subunits in our model (Fig. 7, *C* and *D*, *red*). As well as several glycine and proline residues, this conserved pocket contains two arginines (Arg-170 and Arg-337) from one subunit and a glutamate (Glu-208) from the second. Both arginine and glutamate are highly important for dinucleotide binding in all previously characterized cdG binding proteins (40, 42).

To confirm the importance of these residues to cdG binding, specific amino acid substitutions were produced (R170H, E208Q, and R337H) in $FliI_{\Delta 1-18}$. The solubility of the resulting $FliI_{\Delta 1-18}$ alleles was confirmed by gel filtration (data not shown), and then cdG binding and ATPase activity were tested. All three substitutions showed seriously compromised cdG binding, with K_D values that were too high to be accurately determined (Fig. 8*A* and Table 3) and a complete abolition of ATPase activity (Fig. 8*B*). Finally, we detected no cdG binding for the hexameric ATPase protein NtrC from *Azotobacter vinelandii*, which shares a tertiary structure fold with the export ATPases but does not have the residues of the proposed binding site (Fig. 8*C*). Together, these results strongly indicate that the binding indeed occurs at the proposed site shown in Fig. 7*D*.

Discussion

Here we show that the second messenger cdG binds to the bacterial flagellum export ATPase FliI. This cyclic dinucleotide binding is apparently widespread, with FliI homologs from multiple different bacterial species showing strong, concentration-dependent binding activity upon the addition of cdG. Excitingly, cdG binding at physiologically relevant (low micromolar) affinities was also determined for the closely related type III secretion exporter HrcN from *Pto* DC3000 and the much more distantly related *P. fluorescens* Type VI ATPase ClpB2. Our findings implicate cdG in the direct, allosteric regulation of both flagellar protein export and type III/type VI-mediated virulence for a range of pathogenic, commensal, and beneficial bacterial species.

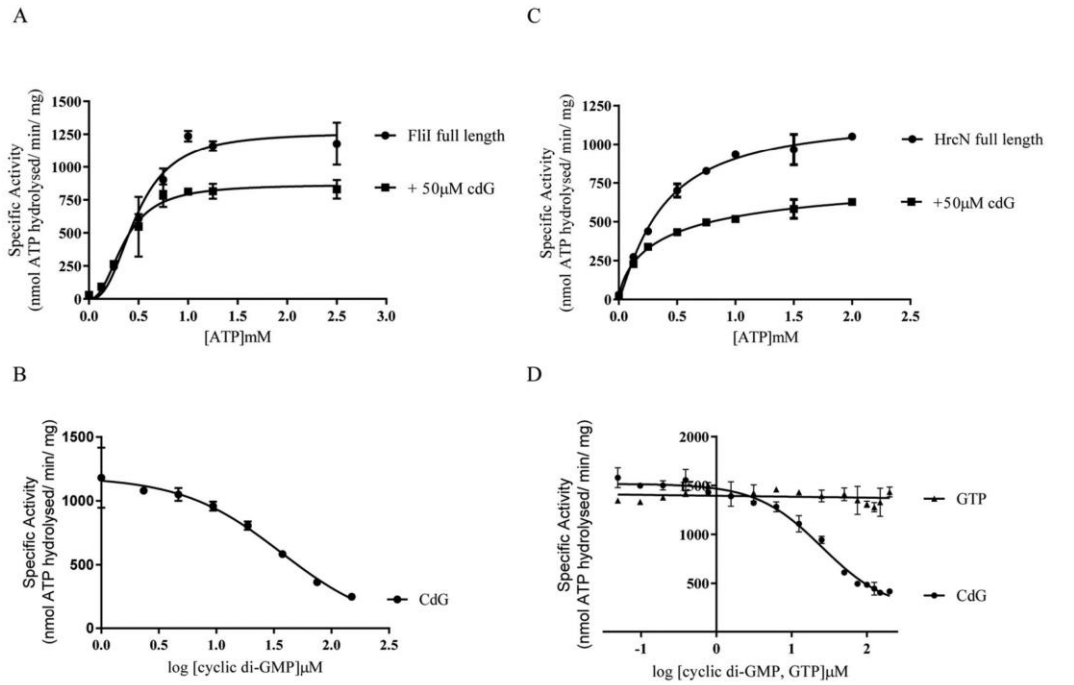

FIGURE 5. *A*, ATPase activity for $FliI_{His}$ ± 50 μM cdG. $FliI_{His}$ specific activity (nmol ATP hydrolyzed/min/mg protein) is shown for increasing ATP concentrations. Addition of cdG causes a decrease of the V_{max} of $FliI_{His}$ ATPase activity. *B*, IC_{50} curve for $FliI_{His}$ ATPase activity upon addition of increasing cdG concentrations. A constant concentration of ATP (1 mM) was included alongside 1 μg of $FliI_{His}$ protein. *C* and *D*, ATPase activity ± 50 μM cdG, and IC_{50} curve upon addition of increasing cdG concentrations, for HrcN. All parameters remain the same as in *A*. The IC_{50} curve also includes results for GTP titration showing no ATPase inhibition.

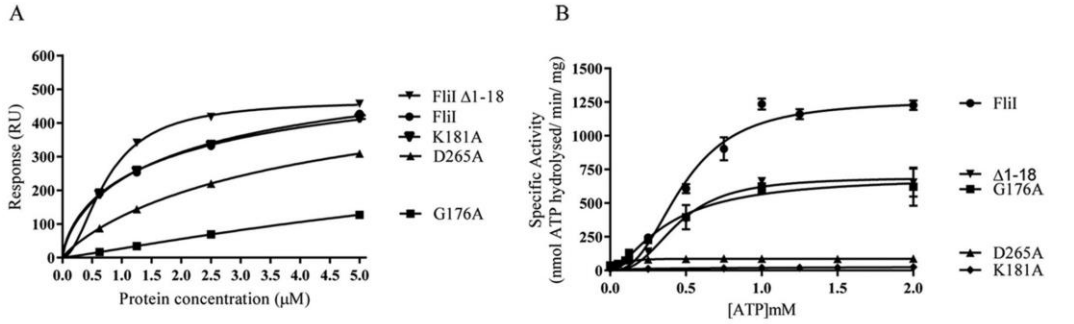

FIGURE 6. *A*, affinity fit for cdG binding to different FliI alleles ($FliI_{His}$, Δ1–18, K181A, D265A, and G176A). Sensorgrams obtained using biotinylated cdG (Figs. 1*D* and 2*B*) were used to calculate the K_D values for FliI binding to cdG (Table 3). At each protein concentration, the responses were recorded 4 s before the end of the injection. *B*, ATPase activity for different FliI alleles. Protein specific activity in each case (nmol ATP hydrolyzed/min/mg protein) is shown for increasing ATP concentrations.

The ATPase activity of both FliI and HrcN is suppressed by the addition of cdG. In this respect, the relationship between cdG and the export ATPase proteins is reminiscent of the transcriptional motility regulators FleQ (27) and FlrA (71). These proteins both contain AAA+ ATPase domains and bind cdG close to the Walker A motif of the protein. However, there appear to be important differences between the binding characteristics of FleQ/FlrA and the export ATPase proteins described here. In FleQ, cdG interacts with the Walker A site of the protein, leading to competitive inhibition of ATPase activity (27). Similarly, cdG binding to an arginine residue (Arg-176) downstream of the Walker A motif of FlrA inhibits binding to its target promoter sequence (71). In the case of the export ATPase proteins, we were able to uncouple ATPase activity from cdG binding. Our FliI/HrcN K181A mutants bound strongly to cdG but displayed no ATPase activity, whereas the G176A mutant retained substantial ATPase activity but showed severely compromised cdG binding. Furthermore, the FlrA R176 residue is conserved in FleQ but not in FliI/HrcN/ClpB2 (Fig. 9, *purple*), again suggesting a distinct cdG binding mechanism.

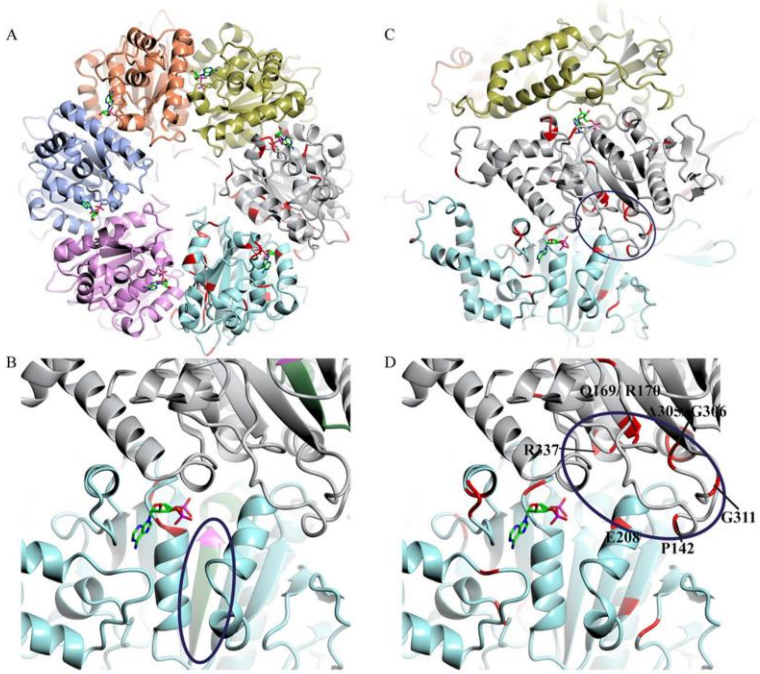

FIGURE 7. *A*, homology model of the predicted hexameric form of SBW25 FliI, based on the crystal structure of FliI from *S. typhimurium* (Protein Data Bank code 2DPY). Conserved residues between the six cdG-binding proteins tested in this study are marked in *red* (on the *gray* and *cyan*-colored subunits only), and ADP (stick model; taken from template structure) is shown bound at the interfaces between the individual FliI subunits. *B*, close-up of the interface between two FliI subunits, showing the NVLLLMDSLTR peptide implicated in cdG capture compound binding (*circled*, in *green*) and the conserved Walker B aspartate (Asp-265) in *pink*. *C*, locations of conserved residues between the six cdG-binding proteins tested in this study (*red*). *D*, close-up of the proposed cdG binding pocket (*circled*). Conserved residues suggested to form the cdG binding site are labeled.

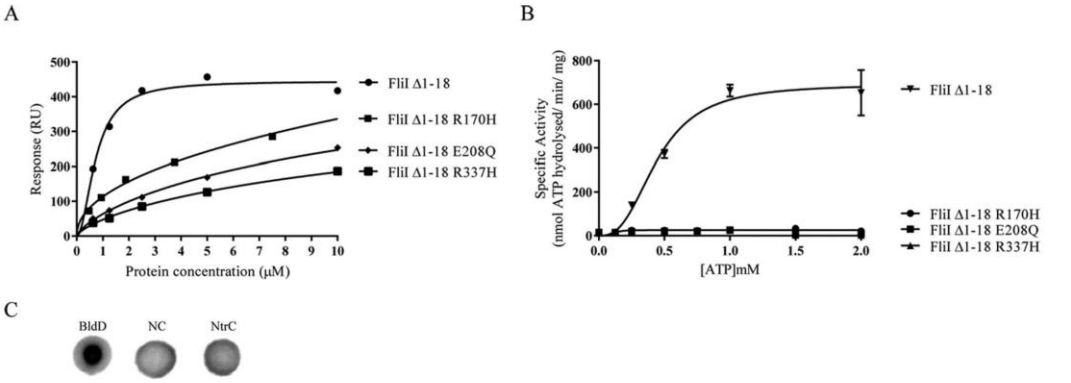

FIGURE 8. *A*, affinity fit for cdG binding to different FliI alleles ($FliI_{\Delta 1-18}$, $FliI_{\Delta 1-18}$ R170H, $FliI_{\Delta 1-18}$ E208Q, and $FliI_{\Delta 1-18}$ R337H). *B*, ATPase activity for different FliI alleles. Protein specific activity in each case (nmol ATP hydrolyzed/min/mg protein) is shown for increasing ATP concentrations. *C*, DRaCALA binding assay for [^{32}P]cdG to 10 μM NtrC (*A. vinelandii*). Positive (10 μM BldD*) and negative binding controls (*NC*) were included as appropriate.

Based on our biochemical and mutagenesis data for FliI/HrcN, mass spectrometric analysis of cdG cross-linked FliI, and *in silico* modeling of hexameric FliI, we identified an intriguing potential site for cdG binding to the rotary export ATPases. This site, at the interface between two protein monomers, contains highly conserved glutamate and arginine residues known to be required for cdG binding (42). The putative binding pocket also contains both a proline and two glycines, which may play a role in maintaining the structure of the binding pocket. Mutagenesis and subsequent *in vitro* binding tests confirmed that the conserved glutamate and arginine residues were indeed required for cdG binding. Although loss of binding was accom-

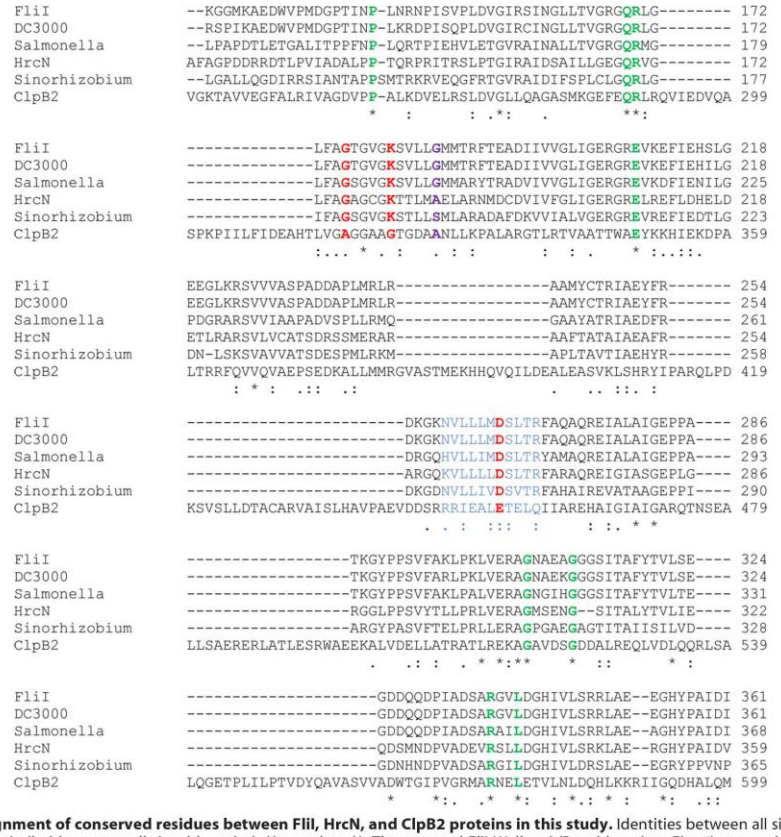

FIGURE 9. **Clustal alignment of conserved residues between FliI, HrcN, and ClpB2 proteins in this study.** Identities between all six residues are marked with *asterisks* (*), and similarities across all six with *periods* (.) or *colons* (:). The mutated FliI Walker A/B residues (see Fig. 6) are marked in *red*, the capture compound-binding NVLLLMDSLTR peptide is marked in *blue*, the position of the conserved cdG binding arginine in FlrA (Arg-176) is marked in *purple*, and the conserved residues of the proposed cdG binding site are marked in *green* (see Fig. 7).

panied by loss of ATPase activity in each case, this result is perhaps unsurprising given that the mutations made were at the FliI dimerization interface. Structural determination of FliI and HrcN in complex with cdG is underway and should allow us to determine exactly where and how cdG interacts with export ATPase complexes.

In general, cdG represses the production and function of flagella and type III secretion systems and promotes type VI secretion, although the relationship between cdG and these different pathways in *Pseudomonas* sp. is both highly complex and not fully understood. Flagella gene expression in *Pseudomonas* sp. is controlled by cdG through FleQ, which binds to numerous flagellar loci and whose inactivation by cdG binding (or deletion) abolishes flagella production (23). Flagella rotation is also likely to be under cdG control in *P. fluorescens* and *P. syringae*, because both contain close homologs to the *P. putida* rotation controller FlgZ (28). cdG has also been shown to control swarming motility in *P. aeruginosa* by switching between two different stator complexes; MotAB and MotCD (60). Other cdG-regulated pathways, such as pili synthesis (37) and exopolysaccharide production (23, 72) also have indirect impacts on both flagella deployment and motility (73, 74).

cdG is also known to control the level/activity of the *P. aeruginosa* type III and type VI secretion systems (64, 65), although here the regulatory pathways are less well understood. Moscoso *et al.* (65) show that cdG mediates the switch between production of type III and type VI secretion pathways and that this switch requires the sRNAs RsmY and RsmZ, linking cdG signaling to the small translational regulatory protein RsmA. Translation of both flagella and type III mRNAs are controlled by RsmA in *P. aeruginosa* (75), which is itself involved in a complex regulatory network involving downstream cdG signaling (76, 77). A role for cdG in the allosteric suppression of FliI/HrcN export *in vivo* is entirely consistent with the wider literature for both flagellar motility and type III secretion. Certainly, our biochemical data strongly suggest that increased intracellular cdG levels would suppress the ATPase activity and hence might be expected to suppress the export activity of these proteins. However, whether suppression of ATPase activity represents the actual *in vivo* function of export ATPase-cdG binding is currently uncertain.

Recently, Minamino *et al.* (14) showed that only residual FliI ATPase activity is actually required for flagellum production in *Salmonella*, with the majority of the energy for protein export provided by the proton motive force. FliI ATPase activity is still required for effective export to occur but is thought to play a gatekeeper role, where it provides the basal body with the energy required to initiate protein export (13, 14). If, as Minamino *et al.* suggest, reduced FliI ATPase activity upon cdG binding does not necessarily translate into reduced flagellar protein export, then what else might be the role of cdG? Our results show that cyclic dinucleotide binding is both widespread and highly conserved among export ATPases. Furthermore, the binding affinities we observed for cdG are sufficiently high that dinucleotide binding should occur frequently under "normal" environmental conditions.

We propose that FliI-cdG binding may play a more fundamental role in controlling flagella function and assembly. Specifically, a basal level of FliI-cdG binding may be required for the initiation of FliI export, via the promotion of multimerization, imposition of rotational asymmetry to the FliI hexamer (78) or another undefined mechanism. In support of this hypothesis, basal levels of cdG have been shown to be required for flagella synthesis in both *S. enterica* (79) and *Caulobacter crescentus* (80). In both cases, deletion of all GGDEF domain-containing proteins, and hence cdG, from the cell resulted in a loss of flagella-driven motility. In *Salmonella*, cdG removal led to increased expression of flagella basal body genes, but a severe defect in the export of FliC (79). Similarly for *C. crescentus*, the production of basal body proteins was unaffected by cdG removal, whereas class III and class IV gene expression was severely reduced (80). In this case, the reduced flagella gene expression could be explained by anti-σ factor-induced feedback upon the loss of flagellar export (81). Whether such a mechanism also applies to the ATPases of type III and type VI systems is unclear at this stage. Although the cdG-null strain of *S. enterica* showed a loss of virulence consistent with loss of T3SS function (79), more evidence is required to confidently propose a model for the relationship between cdG and HrcN/ClpB2 function. Research is ongoing to determine the exact nature of the relationship between cdG and the rotary ATPase proteins and the impact of cdG-ATPase binding on motility and virulence in bacterial species.

Author Contributions—E. T. conceived and designed the study, conducted most of the experimental work, produced Figs. 1–6 and 8, analyzed data, and contributed to writing the manuscript. C. E. M. S. contributed to the SPR work and relevant data analysis. D. M. L. produced Fig. 7, including modeling, figure preparation, and data analysis. T. W. conducted the in silico MS-PSA analysis and produced supplemental Fig. S1. R. H. L. purified proteins and provided technical assistance and support to this study. J. G. M. conceived and designed the study, produced Fig. 9, and wrote the manuscript.

Acknowledgments—We thank Mark Buttner for the kind gift of cdG capture compound, Gary Rowley and Philip Poole for samples of Salmonella and *Sinorhizobium DNA, respectively, Gerhard Saalbach for valuable assistance and advice with mass spectrometry, Natalia Tschowri for the kind gift of BldD protein, and Ray Dixon for the kind gift of the NtrC overexpression strain.*

References

1. Naseby, D. C., Way, J. A., Bainton, N. J., and Lynch, J. M. (2001) Biocontrol of *Pythium* in the pea rhizosphere by antifungal metabolite producing and non-producing *Pseudomonas* strains. *J. Appl. Microbiol.* **90,** 421–429
2. Haas, D., and Défago, G. (2005) Biological control of soil-borne pathogens by fluorescent pseudomonads. *Nat. Rev. Microbiol.* **3,** 307–319
3. Compant, S., Clement, C., and Sessitsch, A. (2010) Plant growth-promoting bacteria in the rhizo- and endosphere of plants: their role, colonization, mechnaisms onvolved and prospects for utilization. *Soil Biol. Biochem.* **42,** 669–678
4. Xin, X. F., and He, S. Y. (2013) *Pseudomonas syringae* pv. tomato DC3000: a model pathogen for probing disease susceptibility and hormone signaling in plants. *Annu. Rev. Phytopathol.* **51,** 473–498
5. Lindeberg, M., Cunnac, S., and Collmer, A. (2009) The evolution of *Pseudomonas syringae* host specificity and type III effector repertoires. *Mol. Plant Pathol.* **10,** 767–775
6. Lugtenberg, B. J., Dekkers, L., and Bloemberg, G. V. (2001) Molecular determinants of rhizosphere colonization by *Pseudomonas*. *Annu. Rev. Phytopathol.* **39,** 461–490
7. Macnab, R. M. (2003) How bacteria assemble flagella. *Annu. Rev. Microbiol.* **57,** 77–100
8. Macnab, R. M. (2004) Type III flagellar protein export and flagellar assembly. *Biochim. Biophys. Acta* **1694,** 207–217
9. Minamino, T., Imada, K., and Namba, K. (2008) Mechanisms of type III protein export for bacterial flagellar assembly. *Mol. Biosyst.* **4,** 1105–1115
10. Minamino, T., and MacNab, R. M. (2000) Interactions among components of the *Salmonella flagellar* export apparatus and its substrates. *Mol. Microbiol.* **35,** 1052–1064
11. Minamino, T., and Macnab, R. M. (1999) Components of the *Salmonella flagellar* export apparatus and classification of export substrates. *J. Bacteriol.* **181,** 1388–1394
12. Minamino, T., and Namba, K. (2008) Distinct roles of the FliI ATPase and proton motive force in bacterial flagellar protein export. *Nature* **451,** 485–488
13. Minamino, T. (2014) Protein export through the bacterial flagellar type III export pathway. *Biochim. Biophys. Acta* **1843,** 1642–1648
14. Minamino, T., Morimoto, Y. V., Kinoshita, M., Aldridge, P. D., and Namba, K. (2014) The bacterial flagellar protein export apparatus processively transports flagellar proteins even with extremely infrequent ATP hydrolysis. *Sci. Rep.* **4,** 7579
15. Gal, M., Preston, G. M., Massey, R. C., Spiers, A. J., and Rainey, P. B. (2003) Genes encoding a cellulosic polymer contribute toward the ecological success of *Pseudomonas fluorescens* SBW25 on plant surfaces. *Mol. Ecol.* **12,** 3109–3121
16. Barahona, E., Navazo, A., Yousef-Coronado, F., Aguirre de Cárcer, D., Martínez-Granero, F., Espinosa-Urgel, M., Martín, M., and Rivilla, R. (2010) Efficient rhizosphere colonization by *Pseudomonas fluorescens* f113 mutants unable to form biofilms on abiotic surfaces. *Environ. Microbiol.* **12,** 3185–3195
17. Pérez-Mendoza, D., Aragón, I. M., Prada-Ramírez, H. A., Romero-Jiménez, L., Ramos, C., Gallegos, M. T., and Sanjuán, J. (2014) Responses to elevated c-di-GMP levels in mutualistic and pathogenic plant-interacting bacteria. *PLoS One* **9,** e91645
18. Engl, C., Waite, C. J., McKenna, J. F., Bennett, M. H., Hamann, T., and Buck, M. (2014) Chp8, a diguanylate cyclase from *Pseudomonas syringae* pv. Tomato DC3000, suppresses the pathogen-associated molecular pattern flagellin, increases extracellular polysaccharides, and promotes plant immune evasion. *MBio* **5,** e01168–01114
19. Matilla, M. A., Travieso, M. L., Ramos, J. L., and Ramos-González, M. I. (2011) Cyclic diguanylate turnover mediated by the sole GGDEF/EAL response regulator in *Pseudomonas putida*: its role in the rhizosphere and an analysis of its target processes. *Environ. Microbiol.* **13,** 1745–1766
20. Aragón, I. M., Pérez-Mendoza, D., Gallegos, M. T., and Ramos, C. (2015) The c-di-GMP phosphodiesterase BifA is involved in the virulence of bacteria from the *Pseudomonas syringae* complex. *Mol. Plant Pathol.* **16,** 604–615
21. Pfeilmeier, S., Saur, I. M., Rathjen, J. P., Zipfel, C., and Malone, J. G.

(2015) High levels of cyclic-di-GMP in plant-associated *Pseudomonas* correlate with evasion of plant immunity. *Mol. Plant Pathol.* doi: 10.1111/mpp.12297
22. Hengge, R. (2009) Principles of c-di-GMP signalling in bacteria. *Nat. Rev. Microbiol.* **7,** 263–273
23. Hickman, J. W., and Harwood, C. S. (2008) Identification of FleQ from *Pseudomonas aeruginosa* as a c-di-GMP-responsive transcription factor. *Mol. Microbiol.* **69,** 376–389
24. Sudarsan, N., Lee, E. R., Weinberg, Z., Moy, R. H., Kim, J. N., Link, K. H., and Breaker, R. R. (2008) Riboswitches in eubacteria sense the second messenger cyclic di-GMP. *Science* **321,** 411–413
25. Newell, P. D., Boyd, C. D., Sondermann, H., and O'Toole, G. A. (2011) A c-di-GMP effector system controls cell adhesion by inside-out signaling and surface protein cleavage. *PLoS Biol.* **9,** e1000587
26. Benach, J., Swaminathan, S. S., Tamayo, R., Handelman, S. K., Folta-Stogniew, E., Ramos, J. E., Forouhar, F., Neely, H., Seetharaman, J., Camilli, A., and Hunt, J. F. (2007) The structural basis of cyclic diguanylate signal transduction by PilZ domains. *EMBO J.* **26,** 5153–5166
27. Baraquet, C., and Harwood, C. S. (2013) Cyclic diguanosine monophosphate represses bacterial flagella synthesis by interacting with the Walker A motif of the enhancer-binding protein FleQ. *Proc. Natl. Acad. Sci. U.S.A.* **110,** 18478–18483
28. Martínez-Granero, F., Navazo, A., Barahona, E., Redondo-Nieto, M., González de Heredia, E., Baena, I., Martín-Martín, I., Rivilla, R., and Martín, M. (2014) Identification of flgZ as a flagellar gene encoding a PilZ domain protein that regulates swimming motility and biofilm formation in *Pseudomonas*. *PLoS One* **9,** e87608
29. Boehm, A., Kaiser, M., Li, H., Spangler, C., Kasper, C. A., Ackermann, M., Kaever, V., Sourjik, V., Roth, V., and Jenal, U. (2010) Second messenger-mediated adjustment of bacterial swimming velocity. *Cell* **141,** 107–116
30. Schirmer, T., and Jenal, U. (2009) Structural and mechanistic determinants of c-di-GMP signalling. *Nat. Rev. Microbiol.* **7,** 724–735
31. Tchigvintsev, A., Xu, X., Singer, A., Chang, C., Brown, G., Proudfoot, M., Cui, H., Flick, R., Anderson, W. F., Joachimiak, A., Galperin, M. Y., Savchenko, A., and Yakunin, A. F. (2010) Structural insight into the mechanism of c-di-GMP hydrolysis by EAL domain phosphodiesterases. *J. Mol. Biol.* **402,** 524–538
32. Lovering, A. L., Capeness, M. J., Lambert, C., Hobley, L., and Sockett, R. E. (2011) The structure of an unconventional HD-GYP protein from Bdellovibrio reveals the roles of conserved residues in this class of cyclic-di-GMP phosphodiesterases. *MBio* **2** e00163–11
33. Wassmann, P., Chan, C., Paul, R., Beck, A., Heerklotz, H., Jenal, U., and Schirmer, T. (2007) Structure of BeF3-modified response regulator PleD: implications for diguanylate cyclase activation, catalysis, and feedback inhibition. *Structure* **15,** 915–927
34. Amikam, D., and Galperin, M. Y. (2006) PilZ domain is part of the bacterial c-di-GMP binding protein. *Bioinformatics* **22,** 3–6
35. Duerig, A., Abel, S., Folcher, M., Nicollier, M., Schwede, T., Amiot, N., Giese, B., and Jenal, U. (2009) Second messenger-mediated spatiotemporal control of protein degradation regulates bacterial cell cycle progression. *Genes Dev.* **23,** 93–104
36. Newell, P. D., Monds, R. D., and O'Toole, G. A. (2009) LapD is a bis-(3′,5′)-cyclic dimeric GMP-binding protein that regulates surface attachment by *Pseudomonas fluorescens* Pf0–1. *Proc. Natl. Acad. Sci. U.S.A.* **106,** 3461–3466
37. Qi, Y., Chuah, M. L., Dong, X., Xie, K., Luo, Z., Tang, K., and Liang, Z. X. (2011) Binding of cyclic diguanylate in the non-catalytic EAL domain of FimX induces a long-range conformational change. *J. Biol. Chem.* **286,** 2910–2917
38. Steiner, S., Lori, C., Boehm, A., and Jenal, U. (2013) Allosteric activation of exopolysaccharide synthesis through cyclic di-GMP-stimulated protein-protein interaction. *EMBO J.* **32,** 354–368
39. Fazli, M., O'Connell, A., Nilsson, M., Niehaus, K., Dow, J. M., Givskov, M., Ryan, R. P., and Tolker-Nielsen, T. (2011) The CRP/FNR family protein Bcam1349 is a c-di-GMP effector that regulates biofilm formation in the respiratory pathogen *Burkholderia cenocepacia*. *Mol. Microbiol.* **82,** 327–341
40. Tschowri, N., Schumacher, M. A., Schlimpert, S., Chinnam, N. B., Findlay, K. C., Brennan, R. G., and Buttner, M. J. (2014) Tetrameric c-di-GMP mediates effective transcription factor dimerization to control Streptomyces development. *Cell* **158,** 1136–1147
41. Krasteva, P. V., Fong, J. C., Shikuma, N. J., Beyhan, S., Navarro, M. V., Yildiz, F. H., and Sondermann, H. (2010) *Vibrio cholerae* VpsT regulates matrix production and motility by directly sensing cyclic di-GMP. *Science* **327,** 866–868
42. Ryan, R. P., Tolker-Nielsen, T., and Dow, J. M. (2012) When the PilZ don't work: effectors for cyclic di-GMP action in bacteria. *Trends Microbiol.* **20,** 235–242
43. Boyd, C. D., and O'Toole, G. A. (2012) Second messenger regulation of biofilm formation: breakthroughs in understanding c-di-GMP effector systems. *Annu. Rev. Cell Dev. Biol.* **28,** 439–462
44. Roelofs, K. G., Wang, J., Sintim, H. O., and Lee, V. T. (2011) Differential radial capillary action of ligand assay for high-throughput detection of protein-metabolite interactions. *Proc. Natl. Acad. Sci. U.S.A.* **108,** 15528–15533
45. Nesper, J., Reinders, A., Glatter, T., Schmidt, A., and Jenal, U. (2012) A novel capture compound for the identification and analysis of cyclic di-GMP binding proteins. *J. Proteomics* **75,** 4874–4878
46. Christen, M., Christen, B., Allan, M. G., Folcher, M., Jenö, P., Grzesiek, S., and Jenal, U. (2007) DgrA is a member of a new family of cyclic diguanosine monophosphate receptors and controls flagellar motor function in *Caulobacter crescentus*. *Proc. Natl. Acad. Sci. U.S.A.* **104,** 4112–4117
47. Rainey, P. B., and Bailey, M. J. (1996) Physical and genetic map of the *Pseudomonas fluorescens* SBW25 chromosome. *Mol. Microbiol.* **19,** 521–533
48. Miller, J. H. (1972) *Experiments in Molecular Genetics*, pp. 352–355, Cold Spring Harbor Laboratory, Cold Spring Harbor, New York
49. Little, R., Salinas, P., Slavny, P., Clarke, T. A., and Dixon, R. (2011) Substitutions in the redox-sensing PAS domain of the NifL regulatory protein define an inter-subunit pathway for redox signal transmission. *Mol. Microbiol.* **82,** 222–235
50. Ho, S. N., Hunt, H. D., Horton, R. M., Pullen, J. K., and Pease, L. R. (1989) Site-directed mutagenesis by overlap extension using the polymerase chain reaction. *Gene* **77,** 51–59
51. Lucchini, S., Rowley, G., Goldberg, M. D., Hurd, D., Harrison, M., and Hinton, J. C. (2006) H-NS Mediates the Silencing of Laterally Acquired Genes in Bacteria. *PLoS Pathog.* **2,** e81
52. Aldridge, P., Paul, R., Goymer, P., Rainey, P., and Jenal, U. (2003) Role of the GGDEF regulator PleD in polar development of *Caulobacter crescentus*. *Mol. Microbiol.* **47,** 1695–1708
53. Kelley, L. A., and Sternberg, M. J. (2009) Protein structure prediction on the Web: a case study using the Phyre server. *Nat. Protoc.* **4,** 363–371
54. Imada, K., Minamino, T., Tahara, A., and Namba, K. (2007) Structural similarity between the flagellar type III ATPase FliI and F1-ATPase subunits. *Proc. Natl. Acad. Sci. U.S.A.* **104,** 485–490
55. Krissinel, E., and Henrick, K. (2004) Secondary-structure matching (SSM), a new tool for fast protein structure alignment in three dimensions. *Acta Crystallogr. D Biol. Crystallogr.* **60,** 2256–2268
56. Emsley, P., and Cowtan, K. (2004) Coot: model-building tools for molecular graphics. *Acta Crystallogr. D Biol. Crystallogr.* **60,** 2126–2132
57. Gledhill, J. R., Montgomery, M. G., Leslie, A. G., and Walker, J. E. (2007) Mechanism of inhibition of bovine F1-ATPase by resveratrol and related polyphenols. *Proc. Natl. Acad. Sci. U.S.A.* **104,** 13632–13637
58. McNicholas, S., Potterton, E., Wilson, K. S., and Noble, M. E. (2011) Presenting your structures: the CCP4mg molecular-graphics software. *Acta Crystallogr. D Biol. Crystallogr.* **67,** 386–394
59. De, N., Pirruccello, M., Krasteva, P. V., Bae, N., Raghavan, R. V., and Sondermann, H. (2008) Phosphorylation-independent regulation of the diguanylate cyclase WspR. *PLoS Biol.* **6,** e67
60. Kuchma, S. L., Delalez, N. J., Filkins, L. M., Snavely, E. A., Armitage, J. P., and O'Toole, G. A. (2015) Cyclic di-GMP-mediated repression of swarming motility by *Pseudomonas aeruginosa* PA14 requires the MotAB stator. *J Bacteriol* **197,** 420–430
61. Minamino, T., Imada, K., Tahara, A., Kihara, M., Macnab, R. M., and Namba, K. (2006) Crystallization and preliminary x-ray analysis of *Salmonella* FliI, the ATPase component of the type III flagellar protein-export

apparatus. *Acta Crystallogr. Sect. F Struct. Biol. Cryst. Commun.* **62,** 973–975
62. Minamino, T., Kazetani, K., Tahara, A., Suzuki, H., Furukawa, Y., Kihara, M., and Namba, K. (2006) Oligomerization of the bacterial flagellar ATPase FliI is controlled by its extreme N-terminal region. *J. Mol. Biol.* **360,** 510–519
63. Pultz, I. S., Christen, M., Kulasekara, H. D., Kennard, A., Kulasekara, B., and Miller, S. I. (2012) The response threshold of *Salmonella* PilZ domain proteins is determined by their binding affinities for c-di-GMP. *Mol. Microbiol.* **86,** 1424–1440
64. Kulasakara, H., Lee, V., Brencic, A., Liberati, N., Urbach, J., Miyata, S., Lee, D. G., Neely, A. N., Hyodo, M., Hayakawa, Y., Ausubel, F. M., and Lory, S. (2006) Analysis of *Pseudomonas aeruginosa* diguanylate cyclases and phosphodiesterases reveals a role for bis-(3′-5′)-cyclic-GMP in virulence. *Proc. Natl. Acad. Sci. U.S.A.* **103,** 2839–2844
65. Moscoso, J. A., Mikkelsen, H., Heeb, S., Williams, P., and Filloux, A. (2011) The *Pseudomonas aeruginosa* sensor RetS switches type III and type VI secretion via c-di-GMP signalling. *Environ. Microbiol.* **13,** 3128–3138
66. Bingle, L. E., Bailey, C. M., and Pallen, M. J. (2008) Type VI secretion: a beginner's guide. *Curr. Opin. Microbiol.* **11,** 3–8
67. Navazo, A., Barahona, E., Redondo-Nieto, M., Martínez-Granero, F., Rivilla, R., and Martín, M. (2009) Three independent signalling pathways repress motility in *Pseudomonas fluorescens* F113. *Microb. Biotechnol.* **2,** 489–498
68. Bell, C. E. (2005) Structure and mechanism of *Escherichia coli* RecA ATPase. *Mol. Microbiol.* **58,** 358–366
69. Story, R. M., Weber, I. T., and Steitz, T. A. (1992) The structure of the *E. coli* recA protein monomer and polymer. *Nature* **355,** 318–325
70. Wilhelm, T., and Jones, A. M. (2014) Identification of related peptides through the analysis of fragment ion mass shifts. *J. Proteome Res.* **13,** 4002–4011
71. Srivastava, D., Hsieh, M. L., Khataokar, A., Neiditch, M. B., and Waters, C. M. (2013) Cyclic di-GMP inhibits *Vibrio cholerae* motility by repressing induction of transcription and inducing extracellular polysaccharide production. *Mol. Microbiol.* **90,** 1262–1276
72. Lee, V. T., Matewish, J. M., Kessler, J. L., Hyodo, M., Hayakawa, Y., and Lory, S. (2007) A cyclic-di-GMP receptor required for bacterial exopolysaccharide production. *Mol. Microbiol.* **65,** 1474–1484
73. Starkey, M., Hickman, J. H., Ma, L., Zhang, N., De Long, S., Hinz, A., Palacios, S., Manoil, C., Kirisits, M. J., Starner, T. D., Wozniak, D. J., Harwood, C. S., and Parsek, M. R. (2009) *Pseudomonas aeruginosa* rugose small-colony variants have adaptations that likely promote persistence in the cystic fibrosis lung. *J. Bacteriol.* **191,** 3492–3503
74. Kuchma, S. L., Griffin, E. F., and O'Toole, G. A. (2012) Minor pilins of the type IV pilus system participate in the negative regulation of swarming motility. *J. Bacteriol.* **194,** 5388–5403
75. Brencic, A., and Lory, S. (2009) Determination of the regulon and identification of novel mRNA targets of *Pseudomonas aeruginosa* RsmA. *Mol. Microbiol.* **72,** 612–632
76. Moscoso, J. A., Jaeger, T., Valentini, M., Hui, K., Jenal, U., and Filloux, A. (2014) The diguanylate cyclase SadC is a central player in Gac/Rsm-mediated biofilm formation in *Pseudomonas aeruginosa*. *J. Bacteriol.* **196,** 4081–4088
77. Jonas, K., Edwards, A. N., Simm, R., Romeo, T., Römling, U., and Melefors, O. (2008) The RNA binding protein CsrA controls cyclic di-GMP metabolism by directly regulating the expression of GGDEF proteins. *Mol. Microbiol.* **70,** 236–257
78. Iino, R., and Noji, H. (2013) Intersubunit coordination and cooperativity in ring-shaped NTPases. *Curr. Opin. Struct. Biol.* **23,** 229–234
79. Solano, C., García, B., Latasa, C., Toledo-Arana, A., Zorraquino, V., Valle, J., Casals, J., Pedroso, E., and Lasa, I. (2009) Genetic reductionist approach for dissecting individual roles of GGDEF proteins within the c-di-GMP signaling network in *Salmonella*. *Proc. Natl. Acad. Sci. U.S.A.* **106,** 7997–8002
80. Abel, S., Bucher, T., Nicollier, M., Hug, I., Kaever, V., Abel Zur Wiesch, P., and Jenal, U. (2013) Bi-modal distribution of the second messenger c-di-GMP controls cell fate and asymmetry during the *Caulobacter* cell cycle. *PLoS Genet.* **9,** e1003744
81. Hughes, K. T., Gillen, K. L., Semon, M. J., and Karlinsey, J. E. (1993) Sensing structural intermediates in bacterial flagellar assembly by export of a negative regulator. *Science* **262,** 1277–1280
82. Woodcock, D. M., Crowther, P. J., Doherty, J., Jefferson, S., DeCruz, E., Noyer-Weidner, M., Smith, S. S., Michael, M. Z., and Graham, M. W. (1989) Quantitative evaluation of *Escherichia coli* host strains for tolerance to cytosine methylation in plasmid and phage recombinants. *Nucleic Acids Res.* **17,** 3469–3478
83. Galibert, F., Finan, T. M., Long, S. R., Pühler, A., Abola, P., Ampe, F., Barloy-Hubler, F., Barnett, M. J., Becker, A., Boistard, P., Bothe, G., Boutry, M., Bowser, L., Buhrmester, J., Cadieu, E., Capela, D., Chain, P., Cowie, A., Davis, R. W., Dréano, S., Federspiel, N. A., Fisher, R. F., Gloux, S., Godrie, T., Goffeau, A., Golding, B., Gouzy, J., Gurjal, M., Hernandez-Lucas, I., Hong, A., Huizar, L., Hyman, R. W., Jones, T., Kahn, D., Kahn, M. L., Kalman, S., Keating, D. H., Kiss, E., Komp, C., Lelaure, V., Masuy, D., Palm, C., Peck, M. C., Pohl, T. M., Portetelle, D., Purnelle, B., Ramsperger, U., Surzycki, R., Thébault, P., Vandenbol, M., Vorhölter, F.-J., Weidner, S., Wells, D. H., Wong, K., Yeh, K.-C., and Batut, J. (2001) The composite genome of the legume symbiont *Sinorhizobium meliloti*. *Science* **293,** 668–672
84. Cuppels, D. A. (1986) Generation and characterization of Tn5 insertion mutations in *Pseudomonas syringae* pv. tomato. *Appl. Environ. Microbiol.* **51,** 323–327

PLOS | GENETICS

RESEARCH ARTICLE

Adaptive Remodeling of the Bacterial Proteome by Specific Ribosomal Modification Regulates *Pseudomonas* Infection and Niche Colonisation

Richard H. Little[1], Lucia Grenga[1,2], Gerhard Saalbach[1], Alexandra M. Howat[2], Sebastian Pfeilmeier[1,3], Eleftheria Trampari[1], Jacob G. Malone[1,2]*

1 Department of Molecular Microbiology, John Innes Centre, Norwich Research Park, Norwich, United Kingdom, **2** School of Biological Sciences, University of East Anglia, Norwich Research Park, Norwich, United Kingdom, **3** The Sainsbury Laboratory, Norwich Research Park, Norwich, United Kingdom

* jacob.malone@jic.ac.uk

OPEN ACCESS

Citation: Little RH, Grenga L, Saalbach G, Howat AM, Pfeilmeier S, Trampari E, et al. (2016) Adaptive Remodeling of the Bacterial Proteome by Specific Ribosomal Modification Regulates *Pseudomonas* Infection and Niche Colonisation. PLoS Genet 12(2): e1005837. doi:10.1371/journal.pgen.1005837

Editor: Christopher S Hayes, University of California, Santa Barbara, UNITED STATES

Received: August 27, 2015

Accepted: January 11, 2016

Published: February 4, 2016

Data Availability Statement: Mass spectrometry data have been deposited to the ProteomeXchange Consortium (http://proteomecentral.proteomexchange.org) via the PRIDE partner repository [73] [Dataset identifiers PXD001371 and PXD001376, Project DOI: 10.6019/PXD001376, PXD002573, Project DOI: 10.6019/PXD002573]. (PX reviewer accounts: PXD001371: reviewer16122@ebi.ac.uk, Password 5VGmVsYB, PXD001376: reviewer85562@ebi.ac.uk, Password K6l0HgKp, PXD002573: reviewer67993@ebi.ac.uk, Password:

Abstract

Post-transcriptional control of protein abundance is a highly important, underexplored regulatory process by which organisms respond to their environments. Here we describe an important and previously unidentified regulatory pathway involving the ribosomal modification protein RimK, its regulator proteins RimA and RimB, and the widespread bacterial second messenger cyclic-di-GMP (cdG). Disruption of *rimK* affects motility and surface attachment in pathogenic and commensal *Pseudomonas* species, with *rimK* deletion significantly compromising rhizosphere colonisation by the commensal soil bacterium *P. fluorescens*, and plant infection by the pathogens *P. syringae* and *P. aeruginosa*. RimK functions as an ATP-dependent glutamyl ligase, adding glutamate residues to the C-terminus of ribosomal protein RpsF and inducing specific effects on both ribosome protein complement and function. Deletion of *rimK* in *P. fluorescens* leads to markedly reduced levels of multiple ribosomal proteins, and also of the key translational regulator Hfq. In turn, reduced Hfq levels induce specific downstream proteomic changes, with significant increases in multiple ABC transporters, stress response proteins and non-ribosomal peptide synthetases seen for both Δ*rimK* and Δ*hfq* mutants. The activity of RimK is itself controlled by interactions with RimA, RimB and cdG. We propose that control of RimK activity represents a novel regulatory mechanism that dynamically influences interactions between bacteria and their hosts; translating environmental pressures into dynamic ribosomal changes, and consequently to an adaptive remodeling of the bacterial proteome.

Author Summary

Post-transcriptional control of protein abundance is a significant and underexplored regulatory process by which organisms respond to environmental change. We have discovered

6ze2VT7a). All other pertinent data is contained in the manuscript and its Supporting Information files.

Funding: This work was funded by the BBSRC (grant numbers BB/J004553/1, and BB/M002586/1, institute strategic program grant, and responsive mode grant to JGM respectively) and by start-up funding from the University of East Anglia. The funders had no role in study design, data collection and analysis, decision to publish, or preparation of the manuscript.

Competing Interests: The authors have declared that no competing interests exist.

an important new mechanism for this control in bacteria, based on the covalent modification of a small ribosomal protein by the widespread enzyme RimK. Here we show that the activity of RimK has specific effects on the levels of ribosomal proteins in the cell, which in turn affects the abundance of the important translational regulator Hfq. RimK is itself controlled by binding to the small regulatory proteins RimA and RimB and the widespread signalling molecule cyclic-di-GMP. Deletion of *rimK* compromises motility, virulence and plant colonisation/infection in several different *Pseudomonas* species. We propose that changes in intracellular RimK activity enable *Pseudomonas* to respond to environmental pressures by changing the nature of their ribosomes, leading in turn to an adaptive phenotypic response to their surroundings. This promotes motility and virulence during the initial stages of plant contact, and phenotypes including attachment, metabolite transport and stress control during long-term environmental adaptation.

Introduction

Post-transcriptional mechanisms for the regulation of protein abundance are critical for the control of diverse cellular processes including metabolism and nutritional stress responses [1,2], virulence and antibiotic production [3] and quorum sensing [4]. In addition to well-studied pathways for mRNA translational control by proteins such as RsmA and Hfq [4–6], riboswitches [1], and direct ribosomal interference [2], a further potential regulatory mechanism is the specific alteration of ribosome function by posttranslational modification of its associated proteins. Numerous ribosomal proteins undergo posttranslational modifications including methylation, acetylation and methylthiolation, as well as the addition and removal of C-terminal amino-acid residues. However, while there is some evidence that certain modifications affect translational accuracy, or ribosome stability, in most cases their functional and physiological significance is unknown [7].

In *Escherichia coli*, the α-L-glutamate ligase RimK catalyzes the unique, C-terminal addition of glutamate residues to the ribosomal 30S subunit protein S6 (RpsF). The biochemistry of the transferase reaction [8] and the synthesis of poly-α-L-glutamate peptides [9] have been studied *in vitro* for *E. coli* RimK, and a crystal structure for this protein is available [10]. However, while the phenomenon of glutamate addition by RimK is clearly documented, the significance of this modification for ribosomal function and cell behavior remains unknown. The *rimK* gene is widespread, with homologs in hundreds of prokaryotic and eukaryotic genomes, so determining the biological role of RimK has broad implications for our understanding of ribosome structure and function. Recently, the *rim* locus (*PFLU0261-0263*) was identified as part of an *In Vivo Expression Technology* (IVET) screen for up-regulated loci during *Pseudomonas fluorescens* interaction with sugar beet [11], prompting us to investigate further.

P. fluorescens is a Gram negative, soil-dwelling bacterium that non-specifically colonizes plant rhizospheres. Here, it utilizes root exudates as a carbon source and protects the host plant by positively affecting health and nutrition, and exhibiting potent antifungal and other biocontrol capabilities [12–14]. Successful plant colonisation by *P. fluorescens* is a complex process that requires the coordinated regulation of phenotypes including motility, the production of attachment factors such as exo/lipopolysaccharides, and the deployment of secondary metabolites [14–16]. Plant-colonizing bacteria must adapt both membrane transport and primary metabolism to exploit the carbon and nitrogen resources exuded by plant roots. A recent study of *Rhizobium leguminosarum* rhizosphere transcriptomes showed both a metabolic shift

towards the utilization of organic acids as the principle carbon source, and the up-regulation of ABC transporters for molecules including oligosaccharides and various amino acids [17].

The related species *P. syringae and P. aeruginosa* also encode the *rimABK* genes (*rimBK* only in *P. aeruginosa*). The phytopathogen *P. syringae* is responsible for a range of economically important plant diseases. It produces an array of species-specific type-III-secreted effectors and phytotoxins to subvert plant defences [18,19] and infects host plants by migration through open stomata and wounds on plant surfaces. It then colonizes the apoplastic space, multiplying rapidly and leading to chlorosis and tissue necrosis [18]. *P. aeruginosa* is an opportunistic pathogen of plants and humans, and the predominant infective bacterium in late stage cystic fibrosis lung infections [20]. It is a highly flexible pathogen, utilizing diverse phenotypic outputs to colonise and infect hosts including both plants and humans [21]. While responses to the environment by *P. aeruginosa* are complex, they may be broadly categorized as promoting either acute (virulent, cytotoxic and motile) or chronic (persistent, biofilm forming) lifestyles. Transitions between the two are frequently prompted by genetic adaptation during long-term infections [22].

In addition to *rimK* the *P. fluorescens rim* locus contains *rimB*, encoding a small uncharacterized protein, and *rimA*, which encodes an EAL (phosphodiesterase) domain for the ubiquitous bacterial second messenger cyclic-di-GMP (cdG). CdG signalling pathways control a wide range of processes involved in the transition between sessile, biofilm forming and unicellular, motile and virulent lifestyles in the majority of bacterial species [23,24]. In general, high cdG levels are associated with community behavior while low levels promote virulence and motility [23]. CdG influences bacterial phenotypes by binding and affecting the function of specific effector proteins, the identity of which can be difficult to predict in advance [25,26]. CdG signal transduction in *Pseudomonas* is highly complex, with dozens of metabolic proteins [27] and phenotypic outputs including exopolysaccharide and adhesin synthesis [28,29], virulence and cytotoxicity [27,30] and the production and control of flagella [28,31,32].

In this study we define the function of the RimABK system and its role in controlling interactions between *Pseudomonas* spp. and plants. Deletion of the *rimABK* genes down-regulates motility and virulence, and promotes phenotypes associated with sessile, surface-associated lifestyles in the commensal *P. fluorescens*, and the pathogens *P. syringae and P. aeruginosa*. RimK post-translationally modifies the ribosomal protein RpsF by the addition of glutamate residues to its C-terminus. This modification has profound effects on the *Pseudomonas* ribosome, with *rimK* deletion leading to significantly lower abundance of multiple ribosomal proteins, although the level of rRNA remains unaffected. Loss of modification by RimK manifests in specific changes in the proteome of *P. fluorescens*. These include a marked reduction in the important translational regulator Hfq and corresponding increases in non-ribosomal peptide synthetases (NRPS), stress response proteins and ABC transporters for peptides, polyamines and amino acids. RimK activity appears to be tightly controlled, both transcriptionally and via direct interaction with RimA, RimB and cdG, with addition of all three stimulating RimK enzymatic activity *in vitro*. We propose that control of RimK ribosomal modification represents a novel, high-level regulatory mechanism that enables bacteria to 'fine-tune' their proteomes to appropriately respond to the surrounding environment.

Results

RimABK influences *P. fluorescens* rhizosphere colonisation, root attachment and swarming motility

The *P. fluorescens* SBW25 *rimABK* locus is a predicted three gene polycistronic operon (Fig 1A). Following the observation that the *rim* locus is up-regulated in the plant environment

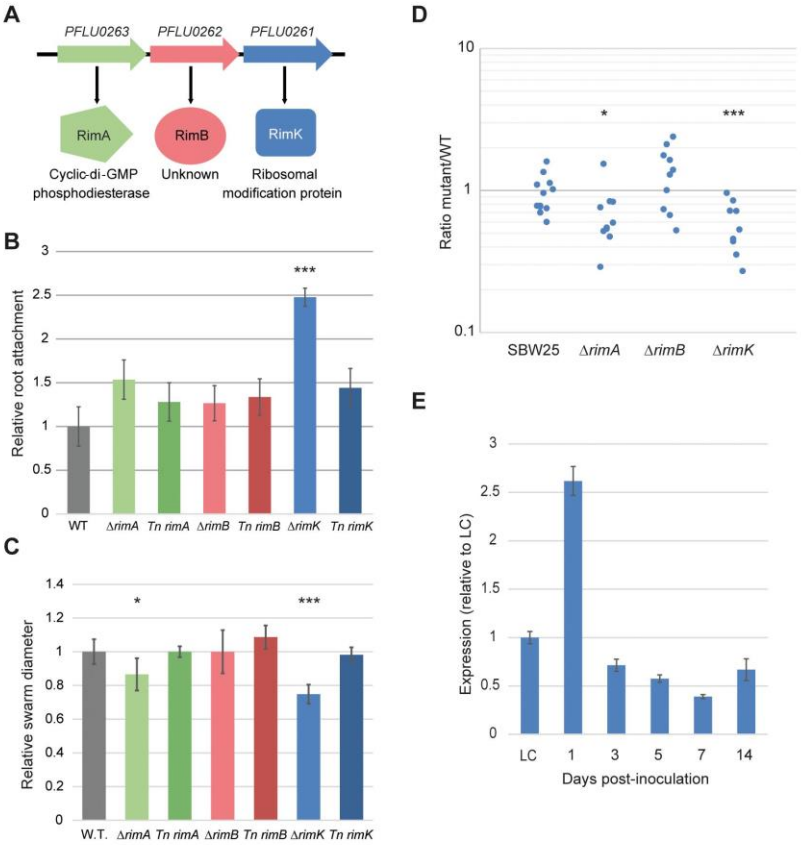

Fig 1. RimABK is important for *P. fluorescens* rhizosphere colonisation. 1A. The SBW25 *rimABK* operon consists of three co-transcribed genes. Gene numbers and predicted translated proteins are shown in each case. **1B.** Wheat root attachment by the Δ*rimABK* and complementation strains relative to SBW25 WT. **1C.** Swarming motility of the Δ*rimABK* and complementation strains relative to SBW25 WT. **1D.** Rhizosphere colonisation competition assays. The graph shows the ratio of SBW25 WT or Δ*rimABK* to WT-*lacZ* colony forming units (CFU) recovered from the rhizospheres of wheat plants seven days post-inoculation. Each dot represents CFU recovered from an individual plant. Statistically significant differences between SBW25 and Δ*rimABK* strains are indicated (*** = $p < 0.01$, * = $p < 0.05$) in each case. **1E.** SBW25 *rimK* mRNA abundance determined by qRT-PCR, for wheat rhizospheres sampled at various intervals post-inoculation. Expression of *rimK* is shown relative to M9 0.4% pyruvate liquid-culture (LC).

doi:10.1371/journal.pgen.1005837.g001

[11] we first examined how the three *rim* genes affect different phenotypes associated with plant interaction. To do this, we deleted the *rim* genes, and confirmed that neither of the two upstream deletions (*rimA/B*) had significant effects on transcription of the third gene, *rimK* (S1A Fig). Next, we complemented each deletion with a chromosomally-inserted copy under the predicted *rim* promoter at the *att*::Tn*7* locus [33]. Deletion of *rimK*, and to a lesser extent *rimA* led to enhanced wheat root attachment relative to WT SBW25 (Fig 1B), and also to a defect in swarming motility (Fig 1C). Both phenotypes were complemented in the relevant Tn*7* strain. To test the importance of *rimABK* for growth in the rhizosphere environment, we next

examined the ability of the *rim* mutants to competitively colonise the rhizospheres of wheat seedlings. After seven days, significantly fewer Δ*rimK* and Δ*rimA* colony forming units (CFUs) were recovered from model rhizospheres compared with the WT-*lacZ* competitor (Fig 1D). No differences in growth-rate were seen for the Δ*rimABK* mutants compared with WT in rich or poor defined media (S1B and S1C Fig), suggesting that the observed colonisation defects are specific to the rhizosphere environment. Finally, to test whether *rim* transcription varies as the surrounding environment changes, we examined *rimK* mRNA abundance at different points during wheat rhizosphere colonisation. SBW25 mRNA was extracted from inoculated wheat rhizospheres after incubation periods of between 1 and 14 days, and *rimK* mRNA levels assayed by qRT-PCR. 1-day colonisation samples showed significantly increased (261.7 ± 14.8%) transcript abundance compared with overnight growth in M9 pyruvate. However, *rimK* expression then decreased sharply as colonisation proceeded, with mRNA abundance after 7 days at 39.1 ± 2.1% of that seen in liquid-culture (Fig 1E), representing an almost seven-fold drop from the levels seen in day 1. This suggests that *rimABK* expression may be triggered by signals present in the early wheat rhizosphere, then down-regulated in the established root environment.

RimK also controls motility, attachment and virulence in plant and human pathogens

To examine whether RimK affects the plant-association behavior of related, pathogenic *Pseudomonas* species, we investigated the impact of *rimK* deletion in the phytopathogen *P. syringae* pv. *tomato* (*Pto*) DC3000 [34] and the opportunistic human pathogen *P. aeruginosa* PA01. Consistent with the findings for SBW25, deletion of *rimK* in *Pto* DC3000 led to increased Congo Red (CR) binding (an assay for lipo/exopolysaccharides and proteinaceous attachment factors [35]) and reduced swarming motility compared to WT (Fig 2A and 2B). Next, we examined the effect of *rimK* deletion on *Pto* DC3000 infection of *Arabidopsis thaliana* Col-0. Upon spray infection, Δ*rimK* presented both noticeably milder disease symptoms (Fig 2C) and significantly reduced bacterial proliferation in the apoplast. In contrast, no differences were observed between WT and Δ*rimK* in a leaf infiltration assay (Fig 2D), suggesting that *rimK* is important during the early stages of *P. syringae* plant infection only. Compared to WT PA01, Δ*rimK* also showed reduced swarming motility (Fig 2A) and significantly increased CR binding (Fig 2B). Furthermore, PA01 Δ*rimK* was markedly compromised both in its ability to infect lettuce leaves [36] and to induce β-hemolysis on blood agar plates (Fig 2E and 2F), while growth in liquid media was unaffected (S1D Fig).

RimK interacts with the ribosome and affects its function

E. coli RimK is an α-l-glutamate ligase and catalyzes both the ATP-dependent synthesis of poly-α-l-glutamate peptides [9], and the sequential addition of glutamate residues to the C-terminus of ribosomal protein RpsF [8]. To examine the relationship between these two proteins in *P. fluorescens*, SBW25 RimK and RpsF ($RimK_{Pf}$/$RpsF_{Pf}$) were purified and used to test the parameters of RimK enzyme activity. First, a linked pyruvate kinase-lactate dehydrogenase (PK/LDH) assay was used to test $RimK_{Pf}$ ATPase activity (Fig 3A). Alone, SBW25 RimK displayed low-level ATPase activity (K_m 0.37 ± 0.13 mM, V_{max} 14.84 ± 1.6 nmol/min/mg protein). The V_{max} of $RimK_{Pf}$ barely increased with $RpsF_{Pf}$ (to 17.8 ± 1.3 nmol/min/mg), but changed more noticeably upon glutamate addition (to 64.3 ± 2.8 nmol/min/mg). While K_m did not change markedly with the addition of either co-factor, V_{max}/K_m increased steadily (RimK = 39.7, +RpsF = 71, +Glu = 100.3, +both = 132.7), an indication of increasing enzymatic efficiency.

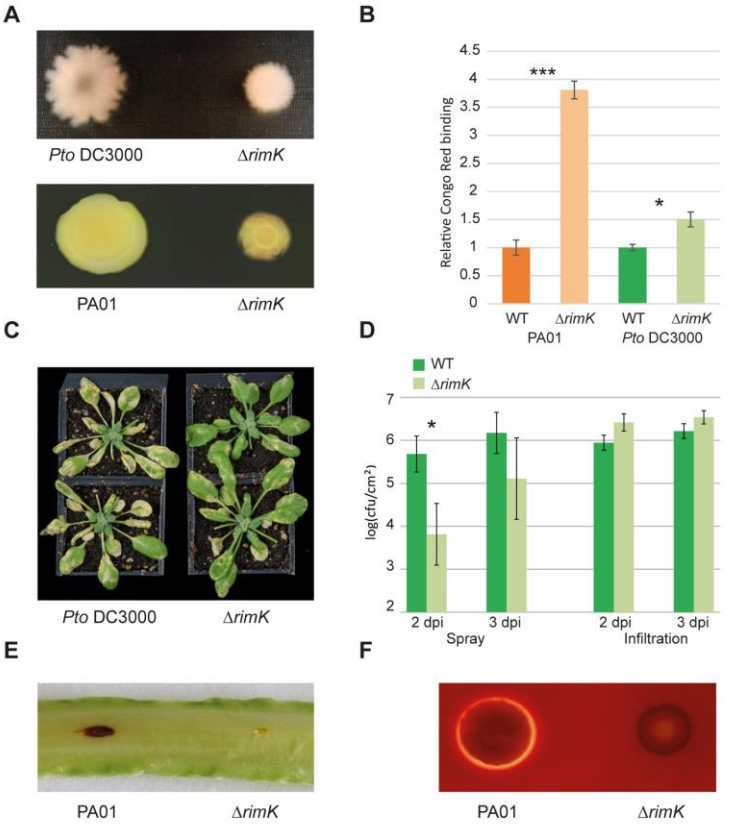

Fig 2. RimK is important for *P. syringae* and *P. aeruginosa* plant infection. 2A. Swarming motility of *Pto* DC3000 and PA01 Δ*rimK* relative to their respective WT strains. **2B.** Congo Red binding of *Pto* DC3000 and PA01 Δ*rimK* compared with their respective WT strains. **2C.** Representative spray-infected *Arabidopsis* Col-0 plants 4 days post-infection with *Pto* DC3000 WT/Δ*rimK*. Disease symptoms are less marked with Δ*rimK* infection. **2D.** log (*P. syringae* CFU per cm^2 leaf tissue) recovered from *Arabidopsis* Col-0 plants infected with *Pto* DC3000 WT or Δ*rimK*, 2 and 3 days post-infection (dpi). The infection method in each case is stated beneath the graph. **2E.** Lettuce leaf infections with *P. aeruginosa* WT/Δ*rimK* strains. Lesions photographed after 5 days. **2F.** β-hemolysis by *P. aeruginosa* WT/Δ*rimK* strains after 24 h growth on horse blood agar.

doi:10.1371/journal.pgen.1005837.g002

Next, we examined $RpsF_{Pf}$ glutamation using SDS-PAGE gel-shift assays adapted from Kino *et al.* [9]. Purified $RimK_{Pf}$ increased the mass of $RpsF_{Pf}$ (Fig 3B), consistent with previous observations for the addition of C-terminal glutamate residues [9]. MALDI-TOF analysis confirmed that the shifted band was overwhelmingly composed of RpsF peptides, although we were unable to detect the glutamated C-terminal RpsF peptide in this sample. This may be due to its large size (>3000 Da) and strong negative charge resulting in a failure to be retained on the reverse phase column. To examine the relationship between RimK and RpsF in more detail, we purified the *E. coli* homologs of both proteins ($RimK_{Ec}$/$RpsF_{Ec}$) and used these to carry out

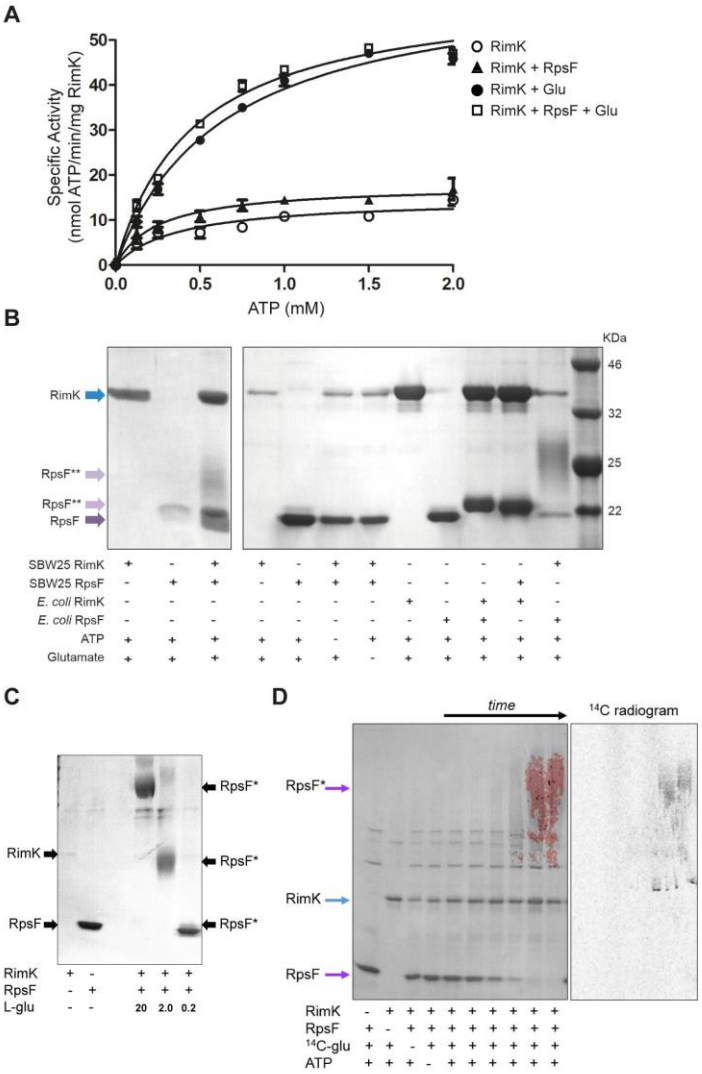

Fig 3. Biochemical analysis of RimK. 3A. ATPase activity of $RimK_{Pf}$ incubated with $RpsF_{Pf}$ and glutamate. $RimK_{Pf}$ specific activity (nmol ATP hydrolyzed/min/mg $RimK_{Pf}$) is shown for increasing concentrations of ATP (open circles). Addition of $RpsF_{Pf}$ (triangles), glutamate (filled circles) or both (square) increases the V_{max} of $RimK_{Pf}$ ATPase activity. **3B.** Glutamation assays with *E. coli* and SBW25 RimK and RpsF. The contents of each assay are indicated underneath the relevant lanes. Independent preparations of $RimK_{Pf}$ and $RpsF_{Pf}$ were used in the two panels, which were run separately and are shown side by side for comparative purposes only. Running positions of RimK, RpsF and glutamated-RpsF (RpsF**) are marked with arrows. **3C.** Glutamation assays with $RimK_{Pf}$ and $RpsF_{Pf}$. The contents of each assay are indicated, with 0.2, 2.0 and 20

mM glutamate added to the test samples as shown. Running positions of RimK, RpsF and glutamated-RpsF (RpsF*) are marked. **3D.** Glutamation assays with $RimK_{Pf}$, $RpsF_{Pf}$ and U-^{14}C- glutamate. The contents of each reaction is indicated underneath the relevant lane. Control samples were incubated overnight, while time-course samples show 5, 10, 30, 60, 180 minutes, and overnight incubation. The left hand panel shows an overlay of Coomassie stained and radiolabel visualizations of a single gel. The right hand panel shows radiolabel incorporation into RpsF alone.

doi:10.1371/journal.pgen.1005837.g003

additional gel-shift experiments (Fig 3B). Unlike $RimK_{Pf}$, ATPase activity for *E. coli* RimK was strictly glutamate dependent, with no activity seen for $RimK_{Ec}$ alone (S2 Fig). As expected, purified $RimK_{Ec}$ increased the mass of $RpsF_{Ec}$ by adding glutamate residues to its C-terminus [9]. Interestingly, the RimK proteins from *E. coli* and SBW25 were functionally interchangeable: $RimK_{Ec}$ was also able to shift $RpsF_{Pf}$, and $RimK_{Pf}$ successfully increased the mass of $RpsF_{Ec}$ (Fig 3B). The activity of both RimK homologs to modify RpsF was strictly dependent on the presence of glutamate and ATP in the reaction mix.

While we did occasionally see a conventional RpsF band-shift (Fig 3B), in many cases $RimK_{Pf}$ activity led to the formation of very large, diffuse RpsF bands (confirmed by MALDI-TOF) that ran poorly in SDS-PAGE. Formation of these large, diffuse bands was strictly dependent on the glutamate concentration in the assay, with lower levels producing more conventional band shifts (Fig 3C), and suggesting that the hyper-shifting band pattern seen with $RimK_{Pf}$ is due to uncontrolled RpsF glutamation in our assay conditions. To confirm that the RpsF in the large, diffuse complexes was indeed glutamated, gel-shift assays were repeated with radiolabeled ^{14}C-glutamate. Progressive incorporation of radiolabel into the RpsF band was seen over 24 hours (Fig 3D), confirming that $RimK_{Pf}$ functions as an α-l-glutamate ligase of RpsF.

To further investigate the effects of RpsF glutamation by RimK on the ribosome, we first examined the effect of *rimK* deletion on ribosomal RNA abundance by qRT-PCR of the 16S rRNA. No significant differences were observed between WT SBW25 and the *rimK* deletion mutant (Δ*rimK*/WT 16S rRNA = 1.27 ± 0.1). Next, we purified ribosomes from SBW25 WT and Δ*rimK* using sucrose cushion ultracentrifugation and examined the relative abundance of ribosomal proteins by semi-quantitative, comparative LFQ analysis using MaxQuant software. Strikingly, almost every detected ribosomal protein was present at a considerably lower level in Δ*rimK* compared with WT (S1 Table), despite their similar 16S rRNA levels. Consistent with a role for RimK in the regulation of ribosome function, *rimK* overexpression significantly increased SBW25 sensitivity to the 30S-targeting aminoglycosides gentamycin and kanamycin, but had no effect on sensitivity to the MurA inhibitor phosphomycin (S3 Fig). This suggests that excess RimK activity affects the ribosome in particular, rather than conferring a non-specific sensitivity to antibiotics in general.

RimK activity is controlled by RimA, RimB and the dinucleotide second messenger cdG

Next, we probed the protein-protein interactions of RimABK by co-immunoprecipitation with flag-tagged proteins. As expected, the RimK assay highlighted potential interactions with multiple ribosomally-associated proteins (Table 1), consistent with a role for RimK in ribosomal modification. Interestingly, both RimB and RimA also pulled down similar numbers of ribosomal protein peptides, alongside multiple peptides from the other two Rim proteins. These data suggest that the RimABK proteins associate both with each other and with the ribosome, and posit a role for RimA and RimB in the regulation of RimK activity.

To test this, $RimK_{Pf}$ ATPase assays were repeated with the addition of purified RimA/RimB proteins. Addition of RimB led to a substantial increase in $RimK_{Pf}$ activity (e.g. V_{max} = 691.2

Table 1. RimK interacting proteins. Numbers denote unique peptides detected in each sample.

	RimK	RimB	RimA	Negative Ctrl	Positive Ctrl
Ribosomal protein S6 modification protein RimK	**95**	17	10	0	0
Putative uncharacterized protein RimB	0	**46**	9	0	0
Conserved EAL domain protein RimA	0	0	**55**	0	0
50S ribosomal protein L18	7	7	6	1	2
Putative glycosyl transferase PFLU0478	7	4	0	0	0
50S ribosomal protein L2	6	12	2	0	3
Lon protease PFLU3927	5	4	2	0	0
30S ribosomal protein S13	5	4	1	0	2
Translation initiation factor IF-2	3	12	1	0	0
50S ribosomal protein L20	3	3	0	0	0
UPF0229 protein PFLU5583	3	1	2	0	0
Chorismate synthase AroC	1	11	0	0	0
Putative sulfite reductase PFLU2657	0	7	0	0	0
Putative peptidase PFLU2126	1	6	0	0	0
Putative uncharacterized protein PFLU4307	0	6	0	0	0
DNA-directed RNA polymerase subunit beta RpoB	0	4	1	0	0
30S ribosomal protein S21	0	4	0	1	0
30S ribosomal protein S11	1	3	1	0	0
30S ribosomal protein S12	1	3	0	0	0
Chaperone ClpB2	1	1	14	0	4
Cell division protein FtsA	0	1	12	0	2
Alanine—tRNA ligase AlaS	1	1	11	0	3
ATP-dependent Clp protease ATP-binding subunit ClpX	1	0	11	0	1
Putative carbamoyltransferase PFLU0475	0	0	7	0	0
Glycine—tRNA ligase alpha subunit GlyQ	0	0	7	0	0
Ribonucleoside-diphosphate reductase β-chain PFLU4768	0	0	6	0	0
Short chain dehydrogenase PFLU3332	0	0	6	0	0
2-dehydropantoate 2-reductase PFLU1707	0	0	6	0	0
Glutamate-ammonia-ligase adenylyl transferase GlnE	0	0	6	0	0
Putative uncharacterized protein PFLU1879	0	0	5	0	0
Putative uncharacterized protein PFLU5584	0	0	5	0	0
Putative histidine lyase PFLU0366	0	0	5	0	0

doi:10.1371/journal.pgen.1005837.t001

nmol/min/mg, 113.6 without RimB, Fig 4A), while RimA addition produced a consistent, but much smaller activity increase (e.g. V_{max} = 363.6 nmol/min/mg, 234.9 without RimA, Fig 4B). Again, increases in V_{max} were accompanied by corresponding enzyme efficiency increases. The modest effect of RimA was puzzling given the relative phenotypic effects of *rimA/rimB* disruption, and suggested another function for RimA besides direct stimulatory interaction with RimK. RimA contains an EAL domain, and is predicted to function as a phosphodiesterase (PDE) for the second messenger cdG. RimA PDE activity was subsequently confirmed (Fig 4C) using a chromatography-based assay alongside an established PDE; YhjH from *E. coli* [37]. This activity presented the intriguing possibility that cdG may play a role in the regulation of RimK activity, prompting us to test the relationship between cdG and RimK. Excitingly, both $RimK_{Pf}$ and $RimK_{Ec}$ were shown to bind strongly to cdG in biotinylated cdG pull-down assays and with surface plasmon resonance (SPR) after [38], with K_d values of 1.0 and 3.8 μM respectively (Fig 4D and 4E, and S4A Fig). Furthermore, cdG addition was shown to substantially

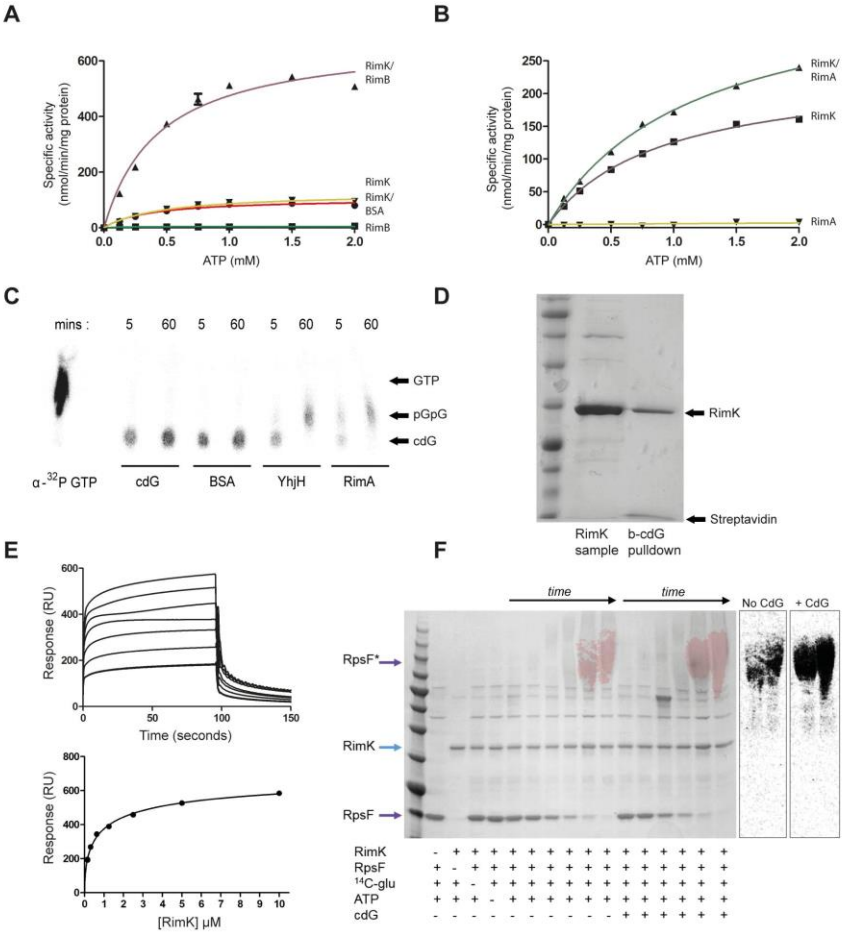

Fig 4. RimA, RimB and cdG impacts on RimK activity. 4A. ATPase activity of $RimK_{Pf}$ incubated with RimB, BSA and glutamate. $RimK_{Pf}$ specific activity (nmol ATP hydrolyzed/min/mg $RimK_{Pf}$) is shown for increasing concentrations of ATP (red, circles). Addition of RimB (purple, up-triangles) increases the $RimK_{Pf}$ V_{max}, while BSA (brown, down-triangles) does not. RimB alone displays no ATPase activity (green, squares). **4B.** ATPase activity of $RimK_{Pf}$ incubated with RimA and glutamate. $RimK_{Pf}$ specific activity (nmol ATP hydrolyzed/min/mg $RimK_{Pf}$) is shown for increasing concentrations of ATP (purple, squares). Addition of RimA (green, up-triangles) increases the $RimK_{Pf}$ V_{max}, while RimA alone displays no ATPase activity (yellow, down-triangles). **4C.** Thin layer chromatography of α-^{32}P-labeled cdG incubated with BSA, YhjH or RimA for the time periods shown. The product of cdG hydrolysis; pGpG, migrates further than cdG but less than α-^{32}P-GTP. **4D.** Biotinylated-cdG pulldown for $RimK_{Pf}$. *E. coli* overexpression cell lysate (RimK sample) is loaded alongside the washed cdG-bead sample (b-cdG pulldown). RimK and streptavidin are indicated with arrows. **4E.** SPR sensorgram and affinity data for $RimK_{Pf}$ binding to biotinylated cdG. A range of $RimK_{Pf}$ concentrations was used (0.156, 0.312, 0.625, 1.25, 2.5, 5, and 10 μM) and concentration replicates included as appropriate together with buffer only controls. Protein binding and dissociation phases are shown. For the affinity fit, binding responses were measured 4s before the end of the injection and K_d values for each protein calculated using BiaEvaluation software and confirmed by GraphPad. **4F.** The effect of cdG addition on glutamation of $RpsF_{Pf}$ by $RimK_{Pf}$. The contents of each reaction is indicated underneath the relevant lanes. Control samples were incubated overnight, while time-course samples show 5, 10, 30, 60, 180 minutes, and overnight incubation. The panel shows an overlay of Coomassie staining and radiolabel visualization (red) of the same gel, as with Fig 3C.

doi:10.1371/journal.pgen.1005837.g004

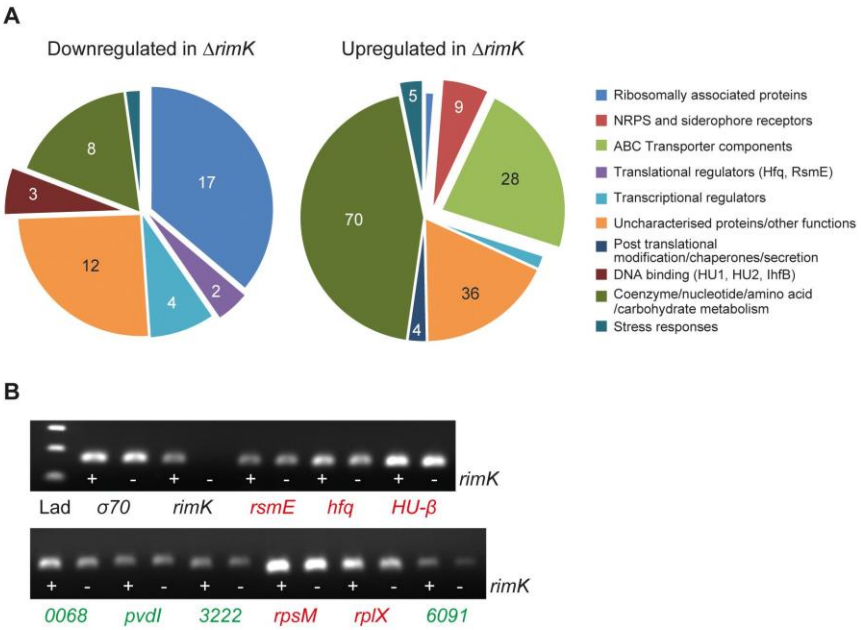

Fig 5. The RimK regulon in *Pseudomonas fluorescens*. 5A. Up and down-regulated proteins in the Δ*rimK* mutant compared with SBW25 WT. Pie chart sections indicate the proportion of significantly up- or down-regulated proteins in each functional category as shown. The numbers in each section of the chart refer to the total number of proteins in that category. Interesting or important functional groups are expanded from the chart in each case. **5B.** RT-PCR showing relative mRNA abundance in SBW25 WT (+) or Δ*rimK* (-) for selected RimK-regulated proteins. The housekeeping gene *rpoD* (σ^{70}) and *rimK* are included as controls. Down-regulated proteins in Δ*rimK* are shown in red, up-regulated proteins in green. (*PFLU*)-*0068* and *6091* encode ABC transporter components, *3222* an NRPS subunit.

doi:10.1371/journal.pgen.1005837.g005

increase both $RimK_{Pf}$ ATPase activity (S4B Fig) and the amount of radiolabeled glutamate incorporated into RpsF *in vitro* (to 225 ± 59% of the cdG- sample, Fig 4E). These data establish a role for cdG signalling in the direct control of RimK activity, and hence ribosome modification.

Deletion of *rimK* induces specific changes in the *P. fluorescens* proteome

To more closely examine how RimK affects ribosomal behaviour *in vivo*, and to probe the wider effects of this on the bacterial proteome, global quantitative mass-spectrometry analysis was conducted on soluble proteomes from liquid-culture grown SBW25 WT and Δ*rimK*. Approximately 1,000 proteins were identified in all tested proteomes (S6 Table, 2 biological replicates of WT and Δ*rimK*), of which 47 were significantly down-regulated and 157 up-regulated in Δ*rimK* across two independent experiments (Fig 5A, S2 Table). Once again, reduced levels of 17 ribosomal proteins were detected in the Δ*rimK* mutant relative to WT, alongside (possibly compensatory) increases in levels of elongation factor P (EF-P) and ribosome-recycling factor (Frr).

One of the most strongly down-regulated proteins in the Δ*rimK* proteome was the global translational regulator Hfq (Fig 5A, Table 2). Hfq is a small, hexameric RNA-binding protein

Table 2. Up- and Down-regulated proteins in the Δ*rimK* mutant background.

Down-regulated in mutant	***ΔrimK fold-change***		
	Assay 1	**Assay 2**	**Average**
Putative aldolase PFLU_4292	-12.84	-14.24	-13.54
Protein Hfq	-7.54	-2.92	-5.23
Putative D-hydantoinase PFLU_3942	-3.91	-5.39	-4.65
50S ribosomal protein L34 rpmH	-6.36	-2.06	-4.21
50S ribosomal protein L24 rplX	-5.28	-2.70	-3.99
Putative uncharacterized protein PFLU_1522	-5.00	-2.57	-3.78
Predicted RNA-binding protein, possibly ribosomal protein PFLU_5262	-5.36	-1.88	-3.62
Putative uncharacterized protein PFLU_2951	-3.46	-3.44	-3.45
Putative outer membrane protein PFLU_1327	-3.82	-2.63	-3.22
Putative uncharacterized protein PFLU_3617	-3.75	-2.26	-3.00
50S ribosomal protein L16 rplP	-3.57	-1.97	-2.77
Putative regulatory protein PFLU_2993	-3.40	-1.93	-2.66
30S ribosomal protein S15 rpsO	-3.65	-1.64	-2.64
Phosphate starvation-inducible protein psiF	-2.09	-3.16	-2.62
Transcriptional regulatory protein AlgP2	-2.91	-2.13	-2.52
Regulator of secondary metabolism RsmE PFLU_4165	-3.84	-1.18	-2.51
Transcriptional regulatory protein AlgP1 PFLU_5927	-2.81	-2.22	-2.51
DNA-binding protein HU1 hupA	-3.26	-1.64	-2.45
Ubiquinol-cytochrome c reductase iron-sulphur subunit petA	-2.95	-1.95	-2.45
30S ribosomal protein S13 rpsM	-2.92	-1.98	-2.45
Putative uncharacterized protein PFLU_5073	-3.02	-1.83	-2.42
30S ribosomal protein S21 rpsU	-3.22	-1.54	-2.38
Catalase katE	-1.63	-3.11	-2.37
2-nonaprenyl-3-methyl-6-methoxy-1,4-benzoquinol hydroxylase coq7	-2.40	-2.31	-2.36
Putative uncharacterized protein PFLU_0413	-3.43	-1.27	-2.35
Up-regulated in mutant	**Assay 1**	**Assay 2**	**Average**
Putative non-ribosomal peptide synthetase PFLU_3225	7.46	2.24	4.85
Putative amino-acid ABC transport system, substrate-binding protein PFLU_1000	5.49	4.29	4.89
Putative membrane protein PFLU_4501	5.85	4.63	5.24
Putative pyoverdin synthetase F PFLU_2547	5.65	4.83	5.24
Putative hydrolase PFLU_1856	6.71	3.82	5.26
Glutamate/aspartate ABC transport system, periplasmic binding protein gltI	6.45	4.17	5.31
Pyoverdin synthetase J pvdJ	7.75	2.93	5.34
Putative histidine-binding periplasmic protein PFLU_4765	5.65	5.35	5.50
Putative ABC transport system, exported protein PFLU_0246	5.75	5.26	5.51
Putative aminotransferase PFLU_5135	9.52	1.64	5.58
Putative uncharacterized protein PFLU_3504	9.52	1.66	5.59
Putative amino-acid transport system, substrate-binding protein PFLU_1311	6.10	5.29	5.69
Putative rhizopine-binding ABC transporter protein PFLU_2583	5.85	5.59	5.72
Aromatic-amino-acid aminotransferase PFLU_4209	8.00	3.73	5.87
Putative ubiquinol—cytochrome C reductase, cytochrome C1 PFLU_0843	9.26	3.00	6.13
Biopolymer transport membrane protein exbB	9.43	3.12	6.27
Putative branched amino-acid ABC transport system, substrate-binding protein livJ2	6.67	6.02	6.35
Dipeptide ABC transport system, substrate-binding protein dppA2	8.26	4.44	6.35
Putative amino-acid ABC transport system, membrane protein PFLU_0313	6.80	6.21	6.51
Putrescine ABC transport system, substrate-binding periplasmic protein potF1	6.67	6.45	6.56

(*Continued*)

Table 2. (*Continued*)

Putative exported protein PFLU_0215	5.41	7.87	6.64
Glucose-6-phosphate isomerase pgi	12.20	1.78	6.99
Diaminobutyrate—2-oxoglutarate aminotransferase PFLU_4378	7.52	6.62	7.07
Putative D-methionine ABC transport system, substrate-binding protein PFLU_0068	7.58	6.62	7.10
Dipeptide ABC transport system, substrate-binding protein dppA3	9.35	5.52	7.44
Branched amino-acid ABC transport system, substrate-binding protein livJ1	8.85	7.09	7.97
Preprotein translocase subunit PFLU_5076	13.89	2.29	8.09
Molybdate-binding periplasmic protein PFLU_2971	9.26	7.04	8.15
Pyoverdin synthetase I pvdI	12.82	3.53	8.18
Aspartate-semialdehyde dehydrogenase asd	11.76	4.90	8.33
UPF0312 protein PFLU_5725	8.06	8.62	8.34
Putative membrane protein PFLU_0832	14.71	4.35	9.53
Putative ABC transport system, periplasmic protein PFLU_6091	8.70	19.23	13.96

doi:10.1371/journal.pgen.1005837.t002

that exerts pleiotropic effects on mRNA translation by mechanisms that include facilitating the binding of regulatory sRNAs with their mRNA targets [5,39] and targeting the degradation of selected mRNAs [40–42]. Hfq may also act as a direct repressor of mRNA translation [43]. Δ*rimK* also contained markedly increased levels of numerous ABC transporter subunits, primarily those for amino acids, dipeptides and the polyamine putrescine. Several ABC-exported peptides were also strongly up-regulated (Table 2). Altered ABC transporter abundance has been linked to *hfq* deletion in several studies [44–46].

Seven NRPS genes, including three synthases for the iron scavenging siderophore pyoverdin (Pvd) were also significantly up-regulated in the Δ*rimK* strain. Hfq has been implicated in the control of iron homeostasis [44], again suggesting a link between these proteome changes and Hfq down-regulation. A further important class of Δ*rimK* up-regulated proteins are those involved in oxidative stress responses, including superoxide dismutase (SodA), thioredoxin and glutathione S-transferase and reductase [47]. Once again, regulation of these proteins has been linked to Hfq [48]. Also up-regulated were several enzymes involved in the secretion and post-translational modification of proteins such as the isomerase SurA, disulfide oxidoreductase DsbA and the pre-protein translocase YajC. The up-regulation of these proteins is consistent with a role in processing and folding the excess periplasmic ABC transporter peptides found in the Δ*rimK* background.

In addition to the drop in Hfq levels, a smaller decrease was observed for a second translational regulator, RsmE [6]. Rsm family proteins control phenotypes including virulence, motility, exopolysaccharide production, carbon metabolism and stress responses in numerous Gram-negative bacteria [49–51]. Reduced protein abundance was also seen for the chromatin organization and DNA bending proteins HU1, HU-beta, and IhfB [52,53] (S2 Table). Several transcriptional regulators, including AlgP1 and AlgP2 [54,55] were down-regulated, while the osmosis regulator OmpR was significantly more abundant in the Δ*rimK* background (S2 Table). Clearly, the proteomic changes that arise as a consequence of *rimK* deletion are both complex and pleiotropic, and determining their relevance and interconnection is the subject of active enquiry. Following the proteomic analysis, RT-PCR was used to examine the relative mRNA abundance of nine significantly up/down-regulated proteins in WT and Δ*rimK*. No discernable change was observed in the mRNA levels of *hfq*, *rsmE*, or any of the other RimK up- or down-regulated proteins tested (Fig 5B), supporting the hypothesis that the observed differences between the Δ*rimK* and WT proteomes predominantly occur post-mRNA transcription.

Downstream genetic analysis of the RimK regulon

To further test whether the *P. fluorescens* Δ*rimK* phenotypes may be attributed to reduced Hfq abundance, an SBW25 *hfq* deletion mutant was produced and tested for phenotypes including swarming and wheat rhizosphere colonisation. Deletion of *hfq* produced small, smooth colonies that took significantly longer to arise than WT SBW25. Similarly to Δ*rimK*, the Δ*hfq* mutant showed compromised swarming motility (Fig 6A), as well as enhanced Congo Red binding (Fig 6B). Rhizosphere colonisation was also significantly compromised (Fig 6C), with too few Δ*hfq* CFUs recovered (<0.1% of WT) to quantify in some cases. The phenotypes seen upon *hfq* deletion were markedly more severe than were seen for Δ*rimK*, although this is perhaps unsurprising as Hfq is still present in the Δ*rimK* background, albeit at a reduced abundance.

Next, SBW25 WT and Δ*hfq* soluble proteomes were isolated and separated by SDS-PAGE. The region between 25 and 58 kDa (corresponding to the size range of the most strongly upregulated proteins in Δ*rimK*) was then examined by comparative MaxQuant analysis. Consistent with the results for Δ*rimK*, *hfq* deletion led to up-regulation of multiple ABC transporter subunits, stress response proteins, secretion systems and proteins involved in the production/utilization of pyoverdin and other siderophores (S3 Table). A substantial degree of overlap was seen between the Δ*rimK* and Δ*hfq* proteomes. 25 significantly upregulated proteins were common to both datasets (Table 3, S3 Table), including ten ABC transporters, two stress response proteins including SodA, and three iron homeostasis proteins. These data support the hypothesis that many of the phenotypic and proteomic changes in Δ*rimK* are ultimately the result of reduced Hfq levels in this strain.

To confirm that the phenotypes associated with the *rimK* mutant arise specifically as a consequence of the loss of RpsF glutamation, we decided to abolish RpsF glutamation *in vivo* while disrupting RimK and RpsF as little as possible. To this end, we cloned and purified an allele of SBW25 RpsF with the penultimate C-terminal residue replaced with lysine (RpsF-D139K). This modification should prevent the C-terminal glutamation of RpsF [8]. We then tested the RpsF-D139K variant for glutamation by both SBW25 and *E. coli* RimK, and confirmed that neither protein could modify this allele *in vitro* (Fig 6C). Incidentally, RpsF-D139K consistently ran at a slightly different position to WT RpsF, which may be a consequence of neutralizing the strong negative charge of the RpsF C-terminus.

Next, we produced a chromosomal *rpsF-D139K* substitution mutant by allelic exchange, and tested it for plant association phenotypes alongside Δ*rimK*. As predicted, we observed both increased wheat root attachment and compromised rhizosphere colonisation to near-identical levels to those seen with the Δ*rimK* mutant (Fig 6D and 6E), strongly supporting the loss of *rpsF* glutamation as the major cause of the phenotypes seen in Δ*rimK*. Like Δ*rimK*, no differences in growth rate were observed between the *rpsF-D139K* strain and WT SBW25 in either rich or poor nutrient media (S5 Fig). Finally, we used a newly-raised polyclonal RpsF antiserum to examine levels of the RpsF protein in our various *rim/rpsF* mutant strains by Western blotting. Levels of the RpsF-D139K allele were comparable to WT RpsF, indicating that the non-glutamated allele is produced and stably maintained in the cell (Fig 6F), and supporting the idea that the phenotypes seen reflect the loss of modification rather than the complete loss of the RpsF protein.

Discussion

Here we identify a new mechanism for control of protein abundance based on differential, post-translational modification of the ribosomal protein RpsF, in the plant-associated bacteria *P. fluorescens* and *P. syringae* and the human pathogen *P. aeruginosa*. Glutamation of RpsF by

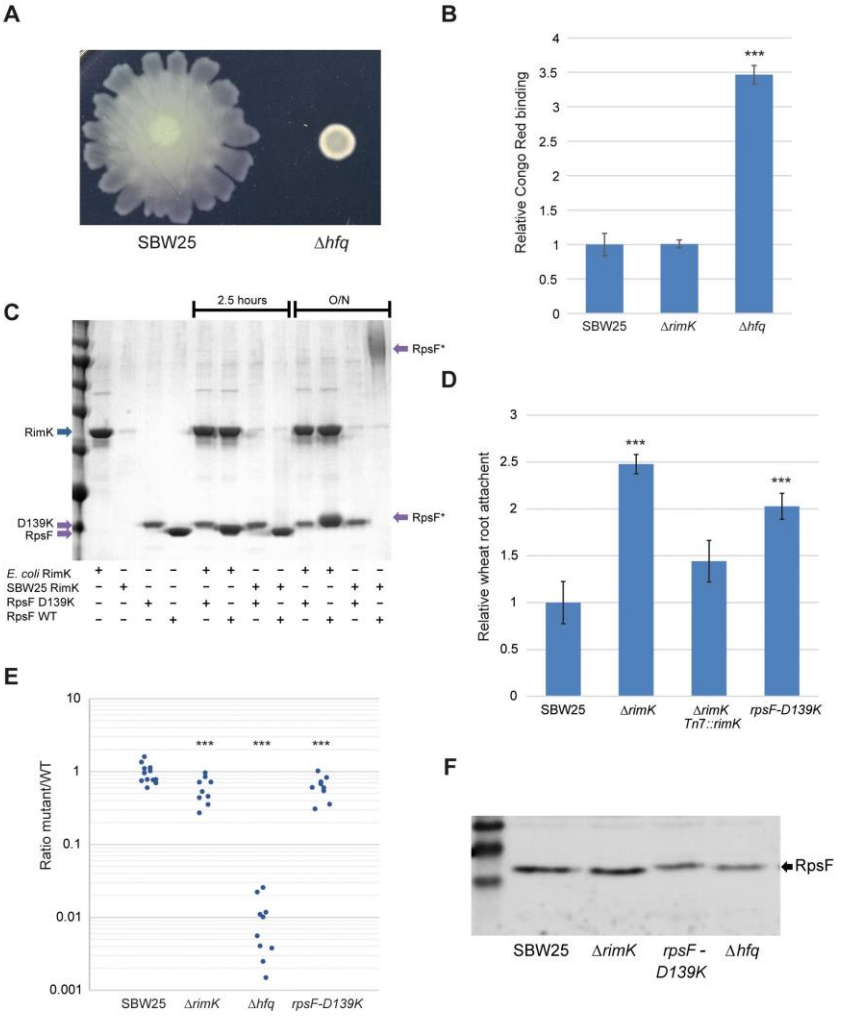

Fig 6. Comparison of the *P. fluorescens* Δ*rimK*, Δ*hfq* and *rpsF-D139K* mutant strains. 6A. Swarming motility of Δ*hfq* relative to SBW25 WT. **6B.** Congo Red binding of Δ*hfq*, compared to SBW25 WT and Δ*rimK*. **6C.** Glutamation assays with *E. coli* and SBW25 RimK, and RpsF/RpsF-D139K. The contents of each assay are indicated underneath the relevant lanes. Running positions of RimK, RpsF and glutamated-RpsF (RpsF*) are marked with arrows. Incubation time is shown above the gel image; all controls were incubated overnight. **6D.** Wheat root attachment assay for Δ*rimK*, Tn*7*::*rimK* and *rpsF-D139K*, relative to WT SBW25. **6E.** Rhizosphere colonisation competition assays for Δ*hfq*, Δ*rimK*, *rpsF-D139K* and WT SBW25. The graph shows the ratio of mutant to WT-*lacZ* CFU recovered from the rhizospheres of wheat plants seven days post-inoculation. Each dot represents CFU recovered from an individual plant. **6F.** Western blot showing RpsF levels in mutant cell lysates. Statistically significant differences between WT SBW25 and mutant strains are indicated throughout (*** = $p < 0.01$).

doi:10.1371/journal.pgen.1005837.g006

Table 3. Up-regulated proteins common to both Δ*hfq* and Δ*rimK* mutants.

Up-regulated protein	Fold change in Δ*hfq*	Fold change in Δ*rimK*
Ferripyoverdine receptor fpvA	77.43	2.65
Putative aminotransferase PFLU5135	49.45	5.58
Superoxide dismutase sodA	11.96	3.22
Putative exported protein PFLU3741	7.59	4.30
Putative ABC transport system ATP-binding protein PFLU1212	6.51	4.25*
Putative ABC transport system, substrate-binding protein PFLU2041	6.26	2.25
Phosphoenolpyruvate carboxykinase pckA	6.17	2.75
Putative uncharacterized protein PFLU6020	5.39	2.66
Putative sulfurylase PFLU4624	4.85	2.53
Putative uncharacterized protein PFLU5224	4.83	3.42
Dipeptide ABC transport system, substrate-binding protein dppA2	4.53	6.35
Putative iron utilization protein PFLU1089	4.40	3.88
Putative sugar ABC transport system, lipoprotein PFLU3117	4.38	3.39
Biopolymer transport membrane protein exbB	3.64	6.27
Glutamate/aspartate ABC transport system, periplasmic binding protein gltI	3.31	5.30
Putative sugar-binding exported protein PFLU3996	3.30	3.58
Putative uncharacterized protein PFLU5582	3.30	4.05
Lactoylglutathione lyase PFLU2991	3.27	2.64
Dipeptide ABC transport system, substrate-binding protein dppA3	3.13	7.43
Protein disulfide isomerase II PFLU5007	3.10	3.09
Putative oxidoreductase PFLU0041	3.05	4.35
Putative ABC transport system, exported protein PFLU0376	2.80	3.05
Putative hemin transport system, substrate-binding protein PFLU5229	2.70	2.60
Putative D-methionine ABC transport system, substrate-binding protein PFLU0068	2.67	7.09
Putative uncharacterized protein PFLU3219	2.56	3.00

*denotes fold-upregulation of PFLU1213 in Δ*rimK*.

doi:10.1371/journal.pgen.1005837.t003

the α-l-glutamate ligase RimK induces specific, adaptive changes in the bacterial proteome through modification of ribosomal behaviour. These RimK-induced proteomic shifts play an important role in the adaptation of both commensal and pathogenic *Pseudomonas* species to environmental changes, and contribute to efficient root colonisation and plant infection. RimK catalyzes the ATP-dependent addition of glutamate residues to the C-terminus of the ribosomal protein RpsF. This modification has important impacts on the bacterial ribosome, with *rimK* deletion leading to reduced ribosomal protein levels. Surprisingly however, the loss of RimK modification does not visibly affect bacterial vitality, as growth rates and colony morphology remain unaffected in the Δ*rimK* mutant. Similarly, ribosomal RNA levels are unaffected by *rimK* deletion. Deletion of *rimK* also leads to marked downstream changes in the *P. fluorescens* proteome. As these proteomic shifts are not linked to corresponding changes in mRNA abundance for any of the proteins tested, we propose that RimK modification of the ribosome changes its function in such a way as to promote or suppress the translation of

specific mRNAs and/or translational regulator abundance. The precise mechanism by which RimK activity affects ribosomal function, and the consequent remodeling of the proteome, is the subject of ongoing research.

While the proteomic changes that arise as a consequence of RimK activity are highly complex, many of the phenotypes and proteomic changes seen in Δ*rimK* may be confidently linked to the translational regulator Hfq, which is strongly down-regulated upon *rimK* deletion. Like Δ*rimK*, *hfq* deletion induces phenotypes including increased attachment factor production, and compromised motility and rhizosphere colonisation. Δ*hfq* also displayed significantly increased abundance of proteins associated with ABC transport, iron scavenging and utilization and oxidative stress responses, in common with the Δ*rimK* mutant. In support of this, biochemical and whole-cell analyses in various species have connected Hfq to proteomic changes associated with iron homeostasis [44], stress responses [48] and the production of multiple amino-acid ABC transporters in the context of rhizosphere adaptation. Microarray analysis of a *R. leguminosarum hfq* suppressor mutant shows that Hfq negatively regulates the mRNA stability of various amino-acid ABC transporters [45]. Furthermore, proteomic and transcriptomic studies in *S. meliloti* show Hfq repression of both solute-binding proteins and amino-acid ABC transporters [44,46]. Multiple proteins involved in amino-acid, nucleotide and carbohydrate metabolism are also up/down-regulated in the Δ*rimK* strain. Again, some of these changes may be linked to Hfq disruption. Alternatively, they may represent an adaptive response to altered amino-acid abundance, triggered by enhanced ABC transporter levels.

While reduced Hfq levels undoubtedly explain many of the Δ*rimK* phenotypes, numerous RimK-linked proteins were not identified in the published regulons for Hfq [44,46]. Altered abundance of several important regulatory proteins including RsmE, histone-like proteins and the transcriptional regulators AlgP1 and AlgP2 were seen in the Δ*rimK* mutant and may explain some aspects of Δ*rimK* behavior. While these changes may also be Hfq-mediated, it is also possible that translational regulation of some mRNAs may occur as a direct result of RimK ribosomal modification.

Critically, our data suggest that RimK modification of RpsF is not passive, but varies both with differential *rimK* transcription as the environment changes, and possibly also directly, through RimK interaction with RimA, RimB and the signalling molecule cdG. Both Rim proteins and cdG stimulate $RimK_{Pf}$ enzyme activity *in vitro*, and thus at first glance appear to function as positive regulators of RimK. However, it is likely that the *in vivo* situation is more complex. In the case of RimB, strong activation of RimK by protein-protein interaction *in vitro* does not correspond to noticeable plant-associated phenotypes. This suggests that the relationship between these two proteins is both context-specific, and dependent on additional, as-yet undetermined factors.

RimK is further controlled by direct binding to the important signalling molecule cdG, which increases the glutamate ligase activity of the *P. fluorescens* protein *in vitro*. This binding seems to be widespread, with low-μM binding affinities measured for both the *P. fluorescens* and *E. coli* RimK homologs. Uniform stimulation of RimK activity by cdG binding runs counter to the generally accepted model for cdG signalling, where increased cdG levels promote sessile, persistent lifestyles over motile, virulent ones. Again, this suggests that the true relationship between cdG and RimK activation is likely to be more complex than that seen in our biochemical assays.

Deletion of *rimA* produces effects consistent with a loss of *rimK in vivo*, suggesting that RimA functions as a positive regulator of RimK. While *rimB* is associated with *rimK* in around half of the genomes encoding a Rim system, *rimA* is restricted to plant-associated *Pseudomonas* species such as *P. fluorescens* and *P. syringae* [56]. For example, the *P. aeruginosa rim* operon lacks a *rimA* homolog. RimA thus appears to represent a particular refinement of the

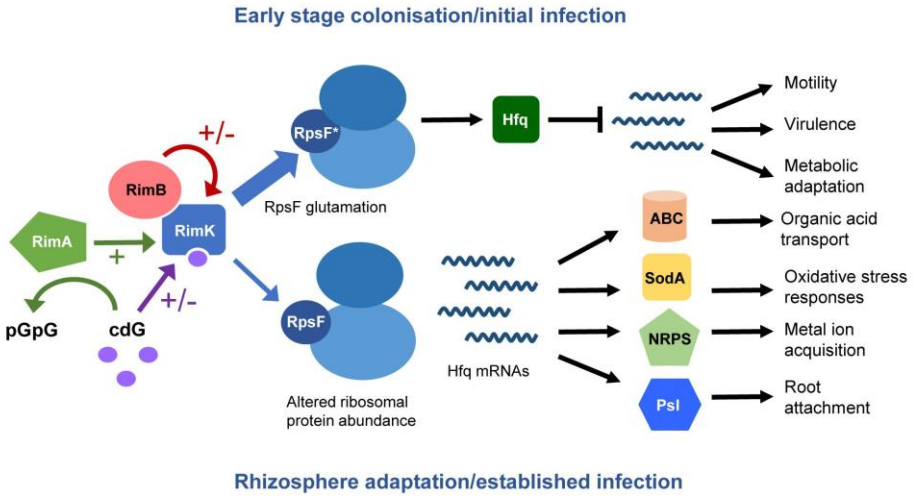

Fig 7. A model for RimABK function in *Pseudomonas* plant interactions. During early stage colonisation/initial infection (top row), increased RimK activity leads to increased RpsF glutamation. This leads to increased Hfq levels, with the resulting translational repression promoting phenotypes important for niche colonisation and the establishment of infection, including motility and virulence [4,44,51]. In the established rhizosphere/plant infection environment (bottom row), *rimK* transcription decreases. Less RpsF is glutamated, leading to altered ribosomal protein abundance and ribosome function, and lower Hfq levels. Release of Hfq translational repression leads to increased production of amino-acid transporters (ABC), oxidative stress response pathways (SodA), NRPSs and attachment factors. These changes promote resource acquisition, stress resistance and root attachment, and prioritize long-term adaptation to the plant environment. RimK activity is further regulated by direct interaction with the RimA/B proteins and the signalling molecule cdG. '+/-' denotes cases where the nature of protein/dinucleotide control is currently undefined.

doi:10.1371/journal.pgen.1005837.g007

regulatory system required for colonisation of the complex plant-associated niche. The relationship between RimK and RimA is probably based on more than just the modest, direct stimulation of RimK activity seen *in vitro*. It seems likely that RimA moderates the relationship between cdG and RimK in some way, although the nature of this control is currently unclear. RimA may play an active role; hydrolyzing RimK-associated cdG under certain circumstances, or a passive one; constitutively degrading cdG to buffer the impact of changing dinucleotide levels on RimK activity. Alternatively, it may act as a trigger enzyme, with cdG hydrolysis altering the RimA-RimK relationship in common with a recently characterized pathway in *E. coli* [57]. While the details of the RimABK-cdG regulatory circuit remain to be fully established, it is clear that control of RimK activity represents a high-level regulatory mechanism that integrates cdG-signalling with post-translational ribosome modification, and hence control of bacterial protein production. In turn, this enables bacteria to rapidly fine tune their proteomes to optimally respond to the surrounding environment (Fig 7).

In our experiments, *P. fluorescens rimK* mRNA abundance peaked during initial wheat rhizosphere colonisation, but then progressively declined as the rhizosphere community matured over the next six days. We propose that enhanced RimK levels during the initial stages of root colonisation equates to enhanced RpsF glutamation. This in turn leads to increased abundance of Hfq (and possibly other regulators such as RsmE), and reduced translation of target mRNAs including those for ABC transporters and NRPS pathways. Our model suggests that an early peak in *rimK* expression promotes a state where organic acid transport, siderophore utilization and a sessile, surface-adherent lifestyle are downplayed in favor of increased motility and rapid

colonisation of the spatial environment of the rhizosphere (Fig 7). Reduced *rimK* transcription in the established wheat rhizosphere would lead to decreased Hfq abundance, and consequently to increased root attachment, production of siderophores and deployment of ABC transporters for polyamines, peptides and organic acids (Fig 7). Organic acid catabolism is the predominant form of carbon metabolism in the rhizosphere [17], necessitating a shift towards ABC transporter expression and metabolic enzyme reorganization. Similarly, siderophore production plays an important survival role in the competitive rhizosphere environment [14], scavenging iron and other metals and providing a measure of oxidative stress-protection [58]. Reduced RimK/Hfq abundance in the established rhizosphere also corresponds to up-regulation of oxidative stress response proteins such as SodA. Again, this is logical in the context of a global strategy for adaptation to the rhizosphere environment, where oxidative stress is a constant threat [59]. Induction of the *soxR* regulon has been shown upon RpsF glutamation in *E. coli*, and a similar mechanism may function in *P. fluorescens* [60]. Down-regulating RimK production may therefore represent an effective strategy for optimizing the bacterial proteome to the established rhizosphere environment (Fig 7).

RimABK regulatory effects appear to be both subtle and global; 'tuning' the ribosome for optimal performance in a particular environment rather than acting as a checkpoint for a specific phenotype in response to an input signal. This is reflected in the relatively modest phenotypes seen for *P. fluorescens* Δ*rimK* compared to Δ*hfq*. For example, compromised rhizosphere colonisation by Δ*rimK* is likely to stem from multiple interconnected factors, including an inability to fully adapt the surface transporter complement to optimally exploit the organic-acid rich environment of the rhizosphere [17], putrescine transporter overproduction leading to H_2O_2 toxicity [61,62], and disruption of the complex relationship between motility and attachment during rhizoplane colonisation [6,14,63].

In addition to controlling phenotypes associated with colonisation and metabolic adaptation, RimK plays an important role in the virulence of both human and plant pathogenic pseudomonads. In *P. syringae*, RimK is important for the initial stages of plant infection but is not required for apoplastic proliferation. This is in agreement with the results seen for *rimK* expression during *P. fluorescens* rhizosphere colonisation, and suggests that RimK fulfils a similar, global adaptation role in both species. Thus, RimK activity in the early stages of infection would promote bacterial migration from plant surfaces into the apoplast through stomata and wounds on the plant surface. Once infection is underway, *P. syringae* changes the expression of metabolic genes to exploit the nutrient availability of the apoplast [64,65], and up-regulates multiple additional loci including genes for polysaccharide synthesis, stress tolerance and nutrient uptake [65]. RimK would therefore become redundant under these conditions. For the opportunistic human pathogen *P. aeruginosa*, the loss of virulence associated with *rimK* deletion was more general; occurring even in stabbed lettuce leaves and accompanied by the loss of β-hemolytic activity. This suggests that virulence loci are directly under *rimK*/*hfq* control in *P. aeruginosa*. While significant parallels exist between the RimK regulons of *P. fluorescens*, *P. syringae* and *P. aeruginosa*, there are nonetheless also important differences between them. We are actively investigating the differences between the Δ*rimK* proteomes of various *Pseudomonas* species, and how they impact on the relationship between pathogenic and commensal microbes and their respective hosts.

Methods

Strains and growth conditions

Strains and plasmids are listed in S4 Table. Primers are listed in S5 Table. Unless otherwise stated all *P. fluorescens* and *P. syringae* strains were grown at 28°C, and *P. aeruginosa* and *E.*

coli at 37°C in lysogenic broth (LB) [66], solidified with 1.3% agar where appropriate. Gentamycin was used at 25 μg/ml, carbenicillin at 100 μg/ml, piperacillin and fosfomycin at 2 mg/ml and tetracycline (Tet) at 12.5 μg/ml (50 μg/ml for *P. aeruginosa*). For inducible plasmids, IPTG was added to a final concentration 0.2 (SBW25) or 1 mM (*E. coli*) as appropriate.

Molecular biology procedures

Cloning was carried out in accordance with standard molecular biology techniques. The pME-*rimA/B/K* plasmids were constructed by ligation of the appropriate PCR fragments (amplified with primers 5/6, 3/4 and 1/2 respectively, from SBW25 genomic DNA), between the *Eco*RI and *Kpn*I sites of plasmid pME6032 [67]. The C-terminal flag-tagged *rim* plasmids were produced from these by the method described by Yu et al. following flag cassette amplification from pSUB11 with primers 9/10, 8/10 and 7/10 [68]. The kanamycin gene inserted downstream of the *rim* gene was then excised by transformation of the *E. coli* host with pFLP2 [69] followed by sucrose counter-selection. The pETM11-*rpsF*, pETM11-*rimB*, pETM11-*rimA* and pET42b(+)-*rimK* purification vectors were produced by ligating PCR fragments (amplified with primers 21/22, 29/30, 13/14, 15/16, 11/12 and 27/28) between the *Nde*I and *Xho*I sites of plasmids pET*Nde*M-11 [70] and pET42b(+) (Novagen) as appropriate. Reverse-transcriptase PCR (RT-PCR) was conducted using primers (31–52). The SBW25 *rimABK* complementation vectors were constructed by ligation of the relevant *rimABK* PCR fragments (amplified from appropriate *rim* deletion strains with primers 74–77) between the *Hin*dIII and *Bam*HI sites of pUC18T-mini-Tn*7*T-Gm.

Gene deletions

P. fluorescens, *P. syringae* and *P. aeruginosa* deletion mutants were constructed via an adaptation of the protocol described elsewhere [71]. Up- and downstream flanking regions to the target genes were amplified using primers 17–20, 53–56, 57–60, 23–26 and 61–64. PCR products in each case were ligated into pME3087 between *Eco*RI-*Bam*HI. The resulting vectors were transformed into the target strain, and single crossovers were selected on Tet and re-streaked. Cultures from single crossovers were grown overnight in LB medium, then diluted 1:100 into fresh medium. After 2 hours, 5 μg/ml Tet (20 μg/ml for *P. aeruginosa*) was added to inhibit the growth of cells that had lost the Tet cassette. After a further hour of growth, samples were pelleted and re-suspended in fresh LB containing Tet and 2 mg/ml piperacillin and phosphomycin to kill growing bacteria. Cultures were grown for a further 4–6 hours, washed once in LB and a dilution series plated onto LB agar. Individual colonies were patched onto LB plates ± Tet, and Tet-sensitive colonies tested for gene deletion/modification by colony PCR.

rpsF-D139K point mutation

The mutant allele with flanking regions for the SBW25 *D139K* point mutation in *rpsF* (*PFLU0533*) was prepared by primer extension PCR. Primer pairs 66/68 and 67/69 were used to produce PCR products that were subsequently combined in a second PCR with primer pair 66/69 to produce the mutant allele with flanking regions. This product was ligated into pME3087 between *Xho*I-*Bam*HI and introduced into the *P. fluorescens* chromosome as detailed above.

Phenotypic assays

The Congo Red (CR) binding assay was adapted from [72]. Five 10 μl drops of LB overnight cultures per strain were grown on 20 ml King's B agar plates for 24 hours at 28°C. Each colony was then re-suspended in 1 ml 0.005% (w/v) CR (Sigma) and incubated for 2 h at 37°C with

shaking. Colony material was pelleted by centrifugation and CR remaining in the supernatant determined by measurement of A_{490} compared to appropriate CR standards. To measure swarming motility, 0.3–0.5% Kings B agar plates (as indicated) were poured and allowed to set and dry for 1 hour in a sterile flow chamber. Plates were then inoculated with 2 μl spots of overnight cultures, and incubated overnight at room temperature. Each sample was tested in triplicate. Disc inhibition assays were carried out using paper discs impregnated with 20 μg/ml gentamycin, on LB + 0.004% CR plates spread with 100 μl of OD 1.0 overnight cultures. Plates were then incubated overnight at 28°C. Assays were repeated at least once independently, and statistical significance assessed using Students t-tests where appropriate.

Growth assays

Bacterial growth was monitored in a microplate spectrophotometer (BioTek Instruments) using a minimum of 3 experimental replicates/sample. Wells (of a 96-well plate) contained 150μL of the indicated growth medium, supplemented with 0.1 mM IPTG and 12.5 μg/ml tetracycline where appropriate. For the antibiotic inhibition assays (S3 Fig), gentamycin, kanamycin and carbenicillin were added to the concentrations noted. Growth was initiated by the addition of 5μL of cell culture with an OD_{600} = 0.01. Plates were covered with adhesive sealing sheets and incubated statically at 28°C.

Wheat root attachment

SBW25 strains containing the bioluminescent plasmid pIJ-11-282 [73] were grown overnight in M9 0.4% pyruvate media. Cultures were normalized by luminescence using a GloMax Multi JR luminometer (Promega) and diluted 1:100 in 10 ml 25 mM pH7.5 phosphate buffer in sterile 50 ml tubes, each containing 12–15 1.5 cm long sterile 3 day-old wheat root tips. Tubes were incubated for 2 hours at room temperature with gentle shaking, before supernatant was discarded and the roots washed twice with phosphate buffer. 10 roots per sample were transferred to individual tubes and luminescence measured and compared with that obtained for wild-type SBW25. The assay was repeated twice independently, and statistical significance assessed using Students t-tests.

Rhizosphere colonization

Paragon wheat seeds were sterilized with 70% ethanol and 5% hypochlorite, washed, and germinated on sterile 0.8% MS agar for 72 h in the dark. Seedlings were then transferred into sterile 50 ml tubes containing medium grain vermiculite and rooting solution (1 mM $CaCl_2.2H_2O$, 100 μM KCl, 800 μM $MgSO_4$, 10 μM FeEDTA, 35 μM H_3BO_3, 9 μM $MnCl_2.4H_2O$, 0.8 μM $ZnCl_2$, 0.5 μM $Na_2MoO_4.2H_2O$, 0.3 μM $CuSO_4.5H_2O$, 6 mM KNO_3, 18.4 mM KH_2PO_4, and 20 mM Na_2HPO_4), and transferred to a controlled environment room (25°C, 16 h light cycle). WT-*lacZ* and mutant SBW25 strains were grown overnight in M9 0.4% pyruvate media, then diluted in phosphate buffer and 1 x 10^3 CFU of mutant and WT-*lacZ* bacteria used to inoculate seven day-old seedlings. Plants were grown for a further seven days, after which shoots were removed, 20 ml PBS was added to each tube and vortexed thoroughly to resuspend bacteria. A dilution series was plated onto XGal + IPTG plates and WT-*lacZ*/mutant colonies distinguished by blue/white selection. Assays were conducted for 8–12 plants/mutant, repeated at least twice independently, and statistical significance assessed using Mann-Whitney tests.

Bacterial plant infection

P. aeruginosa lettuce leaf infections were carried out after [36]. For *P. syringae* infections, *Arabidopsis thaliana* ecotype *Columbia* (Col-0) plants were grown at 20–22°C under 10 h light

period for 4 weeks. *Pto* DC3000 cultures were grown overnight, re-suspended in 10 mM $MgCl_2$ and adjusted to OD_{600} = 0.0002 (10^5 CFU/ml) for syringe infiltration and OD_{600} = 0.05 (10^7 CFU/ml) for spray infection. Shortly before spraying 0.02% Silwet L77 was added to the suspension, plants were sprayed until run-off. All plants were covered with vented lids for five days. Six leaf discs (7 mm diameter) from six different plants per strain were collected in 10 mM $MgCl_2$ and homogenized using a drill-adapted pestle. Serial dilutions were plated and CFUs determined in each case. The assay was repeated three times independently and statistical significance assessed using Students t-tests.

Co-immunoprecipitation

SBW25 pME-*rimA/B/K-flag* overnight cultures were pelleted by centrifugation, re-suspended in ice-cold IP buffer (20 mM HEPES pH 7.4, 100 mM NaCl, 1 mM EDTA, 1.0% $^{v}/_{v}$ Triton X-100, protease inhibitor), and incubated at 4°C with end-over-end agitation for 6 hours. Samples were then centrifuged (15,000 g, 20 min, 4°C), and the supernatant removed and incubated with 20 μg/ml protein-A agarose beads (4°C, end-over-end agitation, 30 min) to remove non-specifically binding proteins. Samples were then centrifuged (3,000 g, 1 min 4°C) to pellet the beads, an aliquot of the supernatant was taken for analysis, and the remaining supernatant was incubated overnight with 20 μg/ml ANTI-FLAG M2 affinity gel (Sigma) (4°C, end-over-end agitation). Samples were pelleted by centrifugation (3,000 g, 1 min 4°C), the supernatant was discarded and the beads re-suspended in 1.0 ml ice-cold IP buffer. This wash step was repeated 5 times. The beads were then re-suspended in SDS sample buffer, boiled, and pelleted by centrifugation. The presence of Flag-tagged Rim proteins in the supernatant was confirmed by immunoblotting, and interacting proteins were detected by Orbitrap mass spectrometry. Results were compared with two control datasets (M2 bead-only, and a non-specific protein control based on immunoprecipitation of unrelated flag-tagged proteins (PFLU3129 and PFLU3130)).

Ribosomal enrichment

Ribosomal enrichment was adapted from the method described in [74]. 500 ml SBW25 WT and Δ*rimK* overnight cultures were grown in M9 0.4% pyruvate. 1 mM chloramphenicol was added, and samples were incubated on ice for 20 minutes. Cells were pelleted by centrifugation, re-suspended in 2ml lysis buffer (20 mM Hepes pH 7.8, 6 mM $MgCl_2$, 100 mM NaCl, 16% ($^{w}/_{v}$) sucrose), and incubated on ice with 2 mg/ml lysozyme for 1 hour. Samples were then sonicated for 30 seconds, and centrifuged twice (10,000 g, 15 min, 4°C) to remove cell debris. The resulting lysates were diluted threefold with running buffer (20 mM Hepes pH 7.8, 6 mM $MgCl_2$, 100 mM NaCl, 2 mM EDTA, protease inhibitor), loaded onto 2 ml 35% sucrose cushions and ultracentrifuged for 2 hours (300,000 g, 4°C). Pellets from the ultracentrifugation step were washed twice and re-suspended in running buffer before analysis by SDS-PAGE and Orbitrap mass spectrometry.

Purification of Rim and RpsF proteins

1.0 litre *E. coli* BL21-(DE3) pLysS overexpression cultures were inoculated from overnights and grown at 30°C to an OD_{600} of 0.6, before protein expression was induced for 2 hours with 1mM IPTG. Cells were then lysed by French press and His_6-tagged proteins purified by NTA-Ni chromatography. 1 ml HiTrap chelating HP columns (Amersham) were equilibrated with 25 mM KH_2PO_4, 200 mM NaCl, pH 8.0 (SBW25 RimA/B/K), 50 mM Tris-Cl, 2.5% glycerol, pH 8.0 (SBW25 RpsF) or 50 mM Tris, 300 mM NaCl, 10 mM imidazole, pH 9.0 (*E. coli* RimK and RpsF), and loaded with cell lysate. Following protein immobilization, elution was accomplished using a linear gradient to 500 mM imidazole over a 15 ml elution volume.

RpsF glutamation assays

The glutamation assay was adapted from Kino et al. [9]. Briefly, purified RpsF and Rim proteins in a 1:1 ratio were incubated for the indicated times at room temperature in reaction buffer (20 mM glutamate, 20 mM ATP, 20 mM $MgSO_4 \cdot 7H_2O$, 100 mM Tris-HCl pH 9). The reaction products were then analyzed using Tricine-SDS-PAGE gels and MALDI-TOF spectroscopy. Reactions were supplemented as indicated with a 1:1 ratio of purified RimA/RimB, 150 μM cdG (Sigma), and/or 13 μM L-[^{14}C(U)]-Glutamic Acid (Perkin Elmer). For the experiments in Fig 4F, assays were repeated in triplicate and radiolabel incorporation was quantified using MultiGauge software (Fuji Film).

Linked Pyruvate Kinase / Lactate Dehydrogenase (PK/LDH) ATPase activity assay

ATPase activity was measured indirectly by monitoring NADH oxidation. The reaction buffer consisted of 50 mM Tris-Cl (pH 8.0), 2 mM MgCl2, 1 mM DTT and 10mM KCl. Each 100 μL reaction contained 0.4 mM NADH, 0.8 mM phosphoenolpyruvic acid, 1 μM RimK/RpsF protein, 0.7 μl PK/LDH (Sigma) and was initiated by the addition of 10 μL ATP. Enzyme kinetics were determined by measuring A_{340} at 1 minute intervals. Kinetic parameters were calculated by plotting the specific activity of the enzyme (nmol ATP hydrolysed/ min/ mg of protein) versus ATP concentration and by fitting the non-linear enzyme kinetics model (Hill equation) in GraphPad Prism. 25 μM cdG or 1 μM RimB/RimA proteins were included as appropriate.

Phosphodiesterase activity assay

The assay was carried out after Christen et al. [75]. Briefly, ^{32}P-cdG was produced enzymatically with PleD*, then 100 μM cdG supplemented with 0.07 μM ^{32}P-cdG was incubated with 1.5 μM YhjH, RimA or BSA at 30°C. The reaction buffer contained 25 mM Tris pH 8.0, 100 mM NaCl, 10 mM $MgCl_2$, 5 mM β-mercaptoethanol and 5% glycerol. Aliquots were removed after 5 and 60 min, and the reaction stopped with 0.25 M EDTA before TLC separation and visualization.

Biotinylated cdG pull-down experiment

Cell lysates overexpressing RimK were prepared by sonicating 5 ml of culture, previously induced with 0.5mM IPTG for 5 hours at 28°C. The lysed cells were pelleted (20,000 g, 1 hr.) and 45 μL of the soluble fraction was collected and mixed with biotinylated cdG (BioLog B098) at a final concentration of 30 μM. Samples were then incubated overnight with end-over-end rotation at 8°C. Samples were then cross linked for 4 minutes in a UV Stratalinker (Stratagene) before addition of 25μl of streptavidin magnetic beads (Invitrogen) and a further hour of incubation with end-over-end rotation at 8°C. Streptavidin magnetic beads were recovered with a magnet and washed five times with 200 μL of protein wash buffer (20 mM HEPES pH 7.5, 250 mM NaCl, 2 mM $MgCl_2$, 2.5% (v/v) glycerol), to remove unbound proteins. Samples were then run on an SDS-PAGE gel and visualized with colloidal Coomassie stain.

Surface plasmon resonance

SPR experiments were conducted at 25°C with a Biacore T200 system using a Streptavidin SA sensor chip (GE healthcare) with four flow cells each containing SA pre-immobilized to a carboxymethylated dextran matrix. Flow cell one (FC1) and flow cell three (FC3) were kept blank for reference subtraction. The chip was first washed three times with 1 M NaCl, 50 mM NaOH to remove unconjugated streptavidin. 100 nM biotinylated cdG (BioLog B098) was then

immobilised on FC2 and FC4 at a 50 RU immobilisation level with a flow rate of 5 μL/min. Soluble RimK alleles at the required concentration were prepared in SPR buffer (10 mM HEPES, 150 mM NaCl, 0.1% Tween 20, 2 mM $MgCl_2$, pH 6.5). Samples were injected with a flow rate of 5 μL/min over the reference and cdG cells for 90 seconds, followed by buffer flow for 60 seconds. The chip was washed at the end of each cycle with 1 M NaCl. Replicates for each protein concentration were included as appropriate. Sensorgrams were analysed using Biacore T200 BiaEvaluation software 1.0 (GE Healthcare).

Quantitative analysis using isobaric labelling (iTRAQ)

50 ml SBW25 WT and Δ*rimK* overnight cultures were grown in M9 0.4% pyruvate. Cellular activity was then frozen by addition of 30 ml of 'RNAlater' (saturated $(NH_4)_2SO_4$, 16.7 mM Na-Citrate, 13.3 mM EDTA, pH 5.2) and protease inhibitors. Cells were pelleted by centrifugation and washed three times with 10 mM HEPES pH 8.0 + protease inhibitors, before re-suspension in 200 μL. 700 μL pre-cooled RLT + β-mercaptoethanol buffer (RNeasy Mini Kit, QIAGEN) was added and samples lysed with two 30 second Ribolyser 'pulses' at speed 6.5. The supernatant was removed, and the soluble fraction separated by ultracentrifugation (279,000 g, 30 minutes, 4°C). Soluble proteomes were acetone precipitated and protein concentrations determined. The proteomic samples were then subjected to iTRAQ quantitative mass spectrometry.

Specifically, samples were reduced, alkylated and digested with trypsin [76], then labelled with iTRAQ tags according to the manufacturer's instructions (AB Sciex). Samples were then mixed, desalted on a SepPak column (Waters) and fractionated by high-pH reversed phase chromatography on an Xterra HPLC column (Waters). The fractionated samples were analyzed by LC-MS/MS on a Synapt G2 mass spectrometer coupled to a nanoAcquity UPLC system (Waters). Peaklist (.pkl) files were generated in ProteinLynx Global Server 2.5.2 (Waters).

Label-free analysis of protein extracts by LC-MS/MS

Ribosome protein samples were acetone precipitated and re-dissolved in 8 M urea, 100 mM Tris-HCl pH 8.0. Eluates from Co-IPs were run into an SDS gel and bands cut out for protein identification. All samples were reduced, alkylated, and digested with trypsin [76], then analyzed by LC-MS/MS on an LTQ-Orbitrap™ mass spectrometer (Thermo Fisher) coupled to a nanoAcquity UPLC system (Waters). Data dependent analysis was carried out in Orbitrap-IT parallel mode using CID fragmentation of the 5 most abundant ions in each cycle. The Orbitrap was run with a resolution of 30,000 over the MS range from m/z 350 to m/z 1800, an MS target of 10^6 and 1 s maximum scan time. The MS2 was triggered by a minimal signal of 1000 with an AGC target of $3x10^4$ ions and 150 ms scan time using the chromatography function for peak apex detection. Dynamic exclusion was set to 1 count and 60 s exclusion with an exclusion mass window of ±20 ppm. Raw files were processed with MaxQuant version 1.5.0.30 (http://maxquant.org). For relative label-free quantitation (LFQ) the following parameters were used: min. unique peptides = 2, peptides for quantitation = unique, include oxidised (M) peptides, maximum missed cleavages = 1, min. LFQ ratio count = 1, match between runs = yes, intensity determination = sum FWHM (smooth).

Protein identification from gel bands by MALDI-TOF

Gel slices were treated and digested with trypsin [76] and peptides spotted onto a PAC II plate (Bruker Daltonics). The spots were washed briefly with 10 mM NH_4PO_4, 0.1% TFA according to the manufacturer, dried and analyzed by MALDI-TOF on an Ultraflex TOF/TOF (Bruker). The instrument was calibrated using the pre-spotted standards (ca. 200 laser shots). Samples

were analyzed using a laser power of approx. 25%, and spectra were summed from ca. 10 x 30 laser shots. Data processing was conducted using FlexAnalysis (Bruker).

Database searches in each case were performed using an in-house Mascot 2.4 Server (Matrixscience) on a *P. fluorescens* protein database (www.uniprot.org). Mascot search results were imported into Scaffold (Proteome Software) for evaluation and comparison. Mass spectrometry data have been deposited to the ProteomeXchange Consortium (http://proteomecentral.proteomexchange.org) via the PRIDE partner repository [77] [Dataset identifiers PXD001371 and PXD001376, Project DOI: 10.6019/PXD001376, PXD002573, Project DOI: 10.6019/PXD002573].

RNA extraction

To obtain SBW25 rhizosphere RNA, shoots were removed from 8 wheat seedlings, each previously inoculated with 10^8 CFU bacteria. 20 ml of 60% RNAlater (in PBS) was added to each tube, and sealed tubes were vortexed for 10 min at 4°C. The 8 samples were combined and filtered through 4 layers of muslin into sterile tubes, and the filtrate was centrifuged (200 g, 4°C, 1 min) to remove heavy particulate contamination. Cells were then pelleted (10,000 rpm, 4°C, 10 min) and lysed by mechanical disruption before RNA was purified from the lysate by column capture (QIAGEN RNeasy Mini Kit). Purified RNA was subjected to an additional DNase treatment (Turbo™ DNase, Ambion). RNA quantification was performed by specific fluorometric quantitation (Qubit®, Life Technologies).

Quantitative real-time PCR (qRT-PCR) analysis

cDNA synthesis was performed using SuperScript II reverse transcriptase and random primers (Invitrogen) in the presence of RNasin ribonuclease inhibitor (Promega). The quantity of total RNA used was dictated by the lowest concentration sample in each assay in the case of rhizosphere samples. cDNA was then used as template in qRT-PCR performed with a SensiFAST SYBR No-ROX kit (Bioline). Three technical replicates were used for each gene. Specific qPCR primers (31–34 and 70–73) were used to amplify reference and target genes. To normalize for differing primer efficiency, a standard curve was constructed (in duplicate) using chromosomal DNA. Melting curve analysis was used to confirm the production of a specific single product from each primer pair. qRT-PCR was performed using a CFX96 Touch instrument using hard-shell white PCR plates (Bio Rad). PCR products were detected with SYBR green fluorescent dye and amplified according to the following protocol: 95°C, 3 min, then 50 cycles at 95°C 5 sec, 62°C 10 sec and 72°C 7 sec. Melting curves were generated at 65 to 95°C with 0.5°C increments. Primers were used at a final concentration of 1 μM. The entire experiment (including RNA extraction) was repeated once independently.

Supporting Information

S1 Fig. mRNA abundance and growth curves for Δ*rimA*, *B* and *K* mutants. A. *rimK* mRNA abundance in Δ*rimA*, *B* and *K* mutant backgrounds, relative to WT SBW25. **B.** Growth curves for SBW25 WT and Δ*rimA*, *B* and *K* in rooting solution + 0.4% pyruvate, 0.4% glucose (see Methods, Rhizosphere colonisation). **C.** Growth curves for SBW25 WT and Δ*rimA*, *B* and *K* in rooting solution + 0.4% pyruvate. **D.** Growth curve for PA01 and Δ*rimK* in rooting solution + 0.4% pyruvate, 0.4% glucose. No significant differences in growth rate were seen between WT and any of the *rim* mutants under the tested conditions. Experiments were repeated at least twice independently.
(TIF)

S2 Fig. ATPase activity of *E. coli* His_6-RimK ($RimK_{Ec}$) incubated with glutamate. $RimK_{Ec}$ specific activity (nmol ATP hydrolyzed/min/mg RimK) is shown for increasing concentrations of ATP.
(TIF)

S3 Fig. *rimK* overexpression effects on antibiotic susceptibility. A. Growth curves in rooting solution + 0.4% pyruvate (RSP) plus gentamycin (Gent) for SBW25 either containing an empty vector (WT) or overexpressing *rimK* (p-*rimK*). **B.** Growth curves in RSP plus kanamycin (Kan) for SBW25 either containing an empty vector (WT) or overexpressing *rimK* (p-*rimK*). **C.** Growth curves in RSP plus phosphomycin (Phos) for SBW25 either containing an empty vector (WT) or overexpressing *rimK* (p-*rimK*). **D.** Gentamycin disc inhibition assays for SBW25 containing empty vector (WT) or overexpressing *rimK* (p-*rimK*). Congo Red dye was added to the plates to improve contrast.
(TIF)

S4 Fig. CdG effects on RimK. A. SPR sensorgram and affinity data for $RimK_{Ec}$ binding to biotinylated cdG. A range of $RimK_{Ec}$ concentrations was used (1.25, 2.5, 5, 10, 20, and 40 μM) and concentration replicates included as appropriate together with buffer only controls. Protein binding and dissociation phases are shown. For the affinity fit, binding responses were measured 4s before the end of the injection and K_d values for each protein calculated using BiaEvaluation software, and confirmed using GraphPad. **B.** ATPase activity of $RimK_{Pf}$ incubated with glutamate and cdG. $RimK_{Pf}$ specific activity (V_{max} = 234.9 nmol ATP/min/mg protein) is shown for increasing concentrations of ATP (squares). Addition of 25 μM cdG (circles) increases V_{max} to 471.0 nmol ATP/min/mg.
(TIF)

S5 Fig. The *rpsF-D139K* mutation does not affect growth. Growth curves for SBW25 WT, Δ*rimK* and *rpsF-D139K* in rooting solution + 0.4% pyruvate, ± 0.4% glucose. No significant differences in growth rate were seen between WT and *rpsF-D139K* in either condition.
(TIF)

S1 Table. Ribosomal proteins detected in SBW25 WT and Δ*rimK*.
(DOCX)

S2 Table. Up and down-regulated proteins in SBW25 Δ*rimK*.
(DOCX)

S3 Table. Up-regulated proteins in SBW25 Δ*hfq*.
(DOCX)

S4 Table. Strains and plasmids.
(DOCX)

S5 Table. Primers.
(DOCX)

S6 Table. Relative protein abundances in SBW25 WT and Δ*rimK*.
(XLSX)

Acknowledgments

The authors would like to thank Ramakrishnan Karunakaran and Corinne Appia-Ayme for advice concerning RNA extraction and quantification, Cyril Zipfel for advice and support for the plant infection experiments, and Barrie Wilkinson, Ray Dixon and Mark Buttner for

helpful comments on the manuscript. The PRIDE proteome database team provided assistance with uploading proteomic datasets.

Author Contributions

Conceived and designed the experiments: RHL GS LG JGM. Performed the experiments: RHL GS LG AMH ET SP JGM. Analyzed the data: RHL GS LG SP JGM. Contributed reagents/materials/analysis tools: GS. Wrote the paper: RHL GS LG JGM.

References

1. Winkler WC, Breaker RR. Regulation Of Bacterial Gene Expression By Riboswitches. Annual review of microbiology. 2005; 59:487–517. PMID: 16153177.
2. Potrykus K, Cashel M. (p)ppGpp: still magical? Annual review of microbiology. 2008; 62:35–51. Epub 2008/05/06. doi: 10.1146/annurev.micro.62.081307.162903 PMID: 18454629.
3. Wilf NM, Williamson NR, Ramsay JP, Poulter S, Bandyra KJ, Salmond GP. The RNA chaperone, Hfq, controls two luxR-type regulators and plays a key role in pathogenesis and production of antibiotics in Serratia sp. ATCC 39006. Environ Microbiol. 2011; 13(10):2649–66. Epub 2011/08/10. doi: 10.1111/j.1462-2920.2011.02532.x PMID: 21824244.
4. Brencic A, Lory S. Determination of the regulon and identification of novel mRNA targets of Pseudomonas aeruginosa RsmA. Mol Microbiol. 2009; 72(3):612–32. Epub 2009/05/12. MMI6670 [pii] doi: 10.1111/j.1365-2958.2009.06670.x PMID: 19426209.
5. Moller T, Franch T, Hojrup P, Keene DR, Bachinger HP, Brennan RG, et al. Hfq: a bacterial Sm-like protein that mediates RNA-RNA interaction. Mol Cell. 2002; 9(1):23–30. Epub 2002/01/24. PMID: 11804583.
6. Reimmann C, Valverde C, Kay E, Haas D. Posttranscriptional repression of GacS/GacA-controlled genes by the RNA-binding protein RsmE acting together with RsmA in the biocontrol strain Pseudomonas fluorescens CHA0. J Bacteriol. 2005; 187(1):276–85. Epub 2004/12/17. doi: 10.1128/JB.187.1.276–285.2005 PMID: 15601712; PubMed Central PMCID: PMC538806.
7. Nesterchuk MV, Sergiev PV, Dontsova OA. Posttranslational Modifications of Ribosomal Proteins in Escherichia coli. Acta naturae. 2011; 3(2):22–33. Epub 2011/04/01. PMID: 22649682; PubMed Central PMCID: PMC3347575.
8. Kang WK, Icho T, Isono S, Kitakawa M, Isono K. Characterization of the gene rimK responsible for the addition of glutamic acid residues to the C-terminus of ribosomal protein S6 in Escherichia coli K12. Molecular & general genetics: MGG. 1989; 217(2–3):281–8. Epub 1989/06/01. PMID: 2570347.
9. Kino K, Arai T, Arimura Y. Poly-alpha-glutamic acid synthesis using a novel catalytic activity of RimK from Escherichia coli K-12. Appl Environ Microbiol. 2011; 77(6):2019–25. Epub 2011/02/01. doi: 10.1128/AEM.02043-10 PMID: 21278279; PubMed Central PMCID: PMC3067337.
10. Zhao G, Jin Z, Wang Y, Allewell NM, Tuchman M, Shi D. Structure and function of Escherichia coli RimK, an ATP-grasp fold, l-glutamyl ligase enzyme. Proteins. 2013. Epub 2013/04/24. doi: 10.1002/prot.24311 PMID: 23609986.
11. Silby MW, Cerdeno-Tarraga AM, Vernikos GS, Giddens SR, Jackson RW, Preston GM, et al. Genomic and genetic analyses of diversity and plant interactions of Pseudomonas fluorescens. Genome Biol. 2009; 10(5):R51. PMID: 19432983. doi: 10.1186/gb-2009-10-5-r51
12. Naseby DC, Way JA, Bainton NJ, Lynch JM. Biocontrol of Pythium in the pea rhizosphere by antifungal metabolite producing and non-producing Pseudomonas strains. J Appl Microbiol. 2001; 90(3):421–9. Epub 2001/04/12. jam1260 [pii]. PMID: 11298238.
13. Barahona E, Navazo A, Yousef-Coronado F, Aguirre de Carcer D, Martinez-Granero F, Espinosa-Urgel M, et al. Efficient rhizosphere colonization by Pseudomonas fluorescens f113 mutants unable to form biofilms on abiotic surfaces. Environ Microbiol. 2010; 12(12):3185–95. Epub 2010/07/16. doi: 10.1111/j.1462-2920.2010.02291.x EMI2291 [pii]. PMID: 20626456.
14. Haas D, Defago G. Biological control of soil-borne pathogens by fluorescent pseudomonads. Nat Rev Microbiol. 2005; 3(4):307–19. Epub 2005/03/11. nrmicro1129 [pii] doi: 10.1038/nrmicro1129 PMID: 15759041.
15. Barahona E, Navazo A, Martinez-Granero F, Zea-Bonilla T, Perez-Jimenez RM, Martin M, et al. Pseudomonas fluorescens F113 Mutant with Enhanced Competitive Colonization Ability and Improved Biocontrol Activity against Fungal Root Pathogens. Appl Environ Microbiol. 2011; 77(15):5412–9. Epub 2011/06/21. AEM.00320-11 [pii] doi: 10.1128/AEM.00320-11 PMID: 21685161; PubMed Central PMCID: PMC3147442.

16. Rodriguez-Navarro DN, Dardanelli MS, Ruiz-Sainz JE. Attachment of bacteria to the roots of higher plants. FEMS Microbiol Lett. 2007; 272(2):127–36. Epub 2007/05/25. doi: 10.1111/j.1574-6968.2007.00761.x PMID: 17521360.

17. Ramachandran VK, East AK, Karunakaran R, Downie A, Poole PS. Adaptation of Rhizobium leguminosarum to pea, alfalfa and sugar beet rhizospheres investigated by comparative transcriptomics. Genome Biol. 2011; 12(10):R106. Epub 2011/10/25. gb-2011-12-10-r106 [pii] doi: 10.1186/gb-2011-12-10-r106 PMID: 22018401.

18. Xin XF, He SY. Pseudomonas syringae pv. tomato DC3000: a model pathogen for probing disease susceptibility and hormone signaling in plants. Annual review of phytopathology. 2013; 51:473–98. Epub 2013/06/04. doi: 10.1146/annurev-phyto-082712-102321 PMID: 23725467.

19. Lindeberg M, Cunnac S, Collmer A. The evolution of Pseudomonas syringae host specificity and type III effector repertoires. Molecular plant pathology. 2009; 10(6):767–75. Epub 2009/10/24. doi: 10.1111/j.1364-3703.2009.00587.x PMID: 19849783.

20. Harrison F. Microbial ecology of the cystic fibrosis lung. Microbiology. 2007; 153:917–23. PMID: 17379702

21. Walker TS, Bais HP, Deziel E, Schweizer HP, Rahme LG, Fall R, et al. Pseudomonas aeruginosa-plant root interactions. Pathogenicity, biofilm formation, and root exudation. Plant physiology. 2004; 134 (1):320–31. doi: 10.1104/pp.103.027888 PMID: 14701912; PubMed Central PMCID: PMC316311.

22. Rau MH, Hansen SK, Johansen HK, Thomsen LE, Workman CT, Nielsen KF, et al. Early adaptive developments of Pseudomonas aeruginosa after the transition from life in the environment to persistent colonization in the airways of human cystic fibrosis hosts. Environ Microbiol. 2010; 12(6):1643–58. Epub 2010/04/22. EMI2211 [pii] doi: 10.1111/j.1462-2920.2010.02211.x PMID: 20406284.

23. Hengge R. Principles of c-di-GMP signalling in bacteria. Nat Rev Microbiol. 2009; 7(4):263–73. PMID: 19287449. doi: 10.1038/nrmicro2109

24. Jenal U, Malone J. Mechanisms of cyclic-di-GMP signaling in bacteria. Annual review of genetics. 2006; 40:385–407. PMID: 16895465.

25. Ryan RP, Tolker-Nielsen T, Dow JM. When the PilZ don't work: effectors for cyclic di-GMP action in bacteria. Trends in microbiology. 2012; 20(5):235–42. Epub 2012/03/27. doi: 10.1016/j.tim.2012.02.008 PMID: 22444828.

26. Boyd CD, O'Toole GA. Second messenger regulation of biofilm formation: breakthroughs in understanding c-di-GMP effector systems. Annual review of cell and developmental biology. 2012; 28:439–62. Epub 2012/10/13. doi: 10.1146/annurev-cellbio-101011-155705 PMID: 23057745.

27. Kulasakara H, Lee V, Brencic A, Liberati N, Urbach J, Miyata S, et al. Analysis of Pseudomonas aeruginosa diguanylate cyclases and phosphodiesterases reveals a role for bis-(3'-5')-cyclic-GMP in virulence. Proc Natl Acad Sci U S A. 2006; 103(8):2839–44. PMID: 16477007.

28. Hickman JW, Harwood CS. Identification of FleQ from Pseudomonas aeruginosa as a c-di-GMP-responsive transcription factor. Mol Microbiol. 2008; 69(2):376–89. PMID: 18485075. doi: 10.1111/j.1365-2958.2008.06281.x

29. Borlee BR, Goldman AD, Murakami K, Samudrala R, Wozniak DJ, Parsek MR. Pseudomonas aeruginosa uses a cyclic-di-GMP-regulated adhesin to reinforce the biofilm extracellular matrix. Mol Microbiol. 2010; 75(4):827–42. PMID: 20088866. doi: 10.1111/j.1365-2958.2009.06991.x

30. Moscoso JA, Jaeger T, Valentini M, Hui K, Jenal U, Filloux A. The diguanylate cyclase SadC is a central player in Gac/Rsm-mediated biofilm formation in Pseudomonas aeruginosa. J Bacteriol. 2014; 196 (23):4081–8. doi: 10.1128/JB.01850-14 PMID: 25225264; PubMed Central PMCID: PMC4248864.

31. Kulasekara BR, Kamischke C, Kulasekara HD, Christen M, Wiggins PA, Miller SI. c-di-GMP heterogeneity is generated by the chemotaxis machinery to regulate flagellar motility. eLife. 2013; 2:e01402. doi: 10.7554/eLife.01402 PMID: 24347546; PubMed Central PMCID: PMC3861689.

32. Kuchma SL, Delalez NJ, Filkins LM, Snavely EA, Armitage JP, O'Toole GA. Cyclic Di-GMP-Mediated Repression of Swarming Motility by Pseudomonas aeruginosa PA14 Requires the MotAB Stator. J Bacteriol. 2015; 197(3):420–30. doi: 10.1128/JB.02130-14 PMID: 25349157; PubMed Central PMCID: PMC4285984.

33. Choi KH, Gaynor JB, White KG, Lopez C, Bosio CM, Karkhoff-Schweizer RR, et al. A Tn7-based broad-range bacterial cloning and expression system. Nature methods. 2005; 2(6):443–8. PMID: 15908923.

34. Whalen MC, Innes RW, Bent AF, Staskawicz BJ. Identification of Pseudomonas syringae pathogens of Arabidopsis and a bacterial locus determining avirulence on both Arabidopsis and soybean. The Plant cell. 1991; 3(1):49–59. Epub 1991/01/01. doi: 10.1105/tpc.3.1.49 PMID: 1824334; PubMed Central PMCID: PMC159978.

35. Malone JG, Williams R, Christen M, Jenal U, Spiers AJ, Rainey PB. The structure–function relationship of WspR, a Pseudomonas fluorescens response regulator with a GGDEF output domain. Microbiology. 2007; 153(4):980–94. doi: 10.1099/mic.0.2006/002824-0

36. Starkey M, Rahme LG. Modeling Pseudomonas aeruginosa pathogenesis in plant hosts. Nature protocols. 2009; 4(2):117–24. doi: 10.1038/nprot.2008.224 PMID: 19180083.

37. Pesavento C, Becker G, Sommerfeldt N, Possling A, Tschowri N, Mehlis A, et al. Inverse regulatory coordination of motility and curli-mediated adhesion in Escherichia coli. Genes Dev. 2008; 22 (17):2434–46. Epub 2008/09/04. doi: 10.1101/gad.475808 PMID: 18765794; PubMed Central PMCID: PMC2532929.

38. Trampari E, Stevenson CE, Little RH, Wilhelm T, Lawson DM, Malone JG. Bacterial Rotary Export ATPases Are Allosterically Regulated by the Nucleotide Second Messenger Cyclic-di-GMP. J Biol Chem. 2015; 290(40):24470–83. doi: 10.1074/jbc.M115.661439 PMID: 26265469; PubMed Central PMCID: PMC4591828.

39. Maki K, Uno K, Morita T, Aiba H. RNA, but not protein partners, is directly responsible for translational silencing by a bacterial Hfq-binding small RNA. Proc Natl Acad Sci U S A. 2008; 105(30):10332–7. Epub 2008/07/25. doi: 10.1073/pnas.0803106105 PMID: 18650387; PubMed Central PMCID: PMC2492515.

40. Moll I, Afonyushkin T, Vytvytska O, Kaberdin VR, Blasi U. Coincident Hfq binding and RNase E cleavage sites on mRNA and small regulatory RNAs. Rna. 2003; 9(11):1308–14. Epub 2003/10/17. PMID: 14561880; PubMed Central PMCID: PMC1287052.

41. Afonyushkin T, Vecerek B, Moll I, Blasi U, Kaberdin VR. Both RNase E and RNase III control the stability of sodB mRNA upon translational inhibition by the small regulatory RNA RyhB. Nucleic Acids Res. 2005; 33(5):1678–89. Epub 2005/03/23. doi: 10.1093/nar/gki313 PMID: 15781494; PubMed Central PMCID: PMC1069011.

42. Morita T, Maki K, Aiba H. RNase E-based ribonucleoprotein complexes: mechanical basis of mRNA destabilization mediated by bacterial noncoding RNAs. Genes Dev. 2005; 19(18):2176–86. Epub 2005/09/17. doi: 10.1101/gad.1330405 PMID: 16166379; PubMed Central PMCID: PMC1221888.

43. Desnoyers G, Masse E. Noncanonical repression of translation initiation through small RNA recruitment of the RNA chaperone Hfq. Genes Dev. 2012; 26(7):726–39. Epub 2012/04/05. doi: 10.1101/gad.182493.111 PMID: 22474262; PubMed Central PMCID: PMC3323883.

44. Sobrero P, Schluter JP, Lanner U, Schlosser A, Becker A, Valverde C. Quantitative proteomic analysis of the Hfq-regulon in Sinorhizobium meliloti 2011. PLoS One. 2012; 7(10):e48494. Epub 2012/11/03. doi: 10.1371/journal.pone.0048494 PMID: 23119037; PubMed Central PMCID: PMC3484140.

45. Mulley G, White JP, Karunakaran R, Prell J, Bourdes A, Bunnewell S, et al. Mutation of GOGAT prevents pea bacteroid formation and N2 fixation by globally downregulating transport of organic nitrogen sources. Mol Microbiol. 2011; 80(1):149–67. Epub 2011/02/01. doi: 10.1111/j.1365-2958.2011.07565.x PMID: 21276099.

46. Gao M, Barnett MJ, Long SR, Teplitski M. Role of the Sinorhizobium meliloti global regulator Hfq in gene regulation and symbiosis. Molecular plant-microbe interactions: MPMI. 2010; 23(4):355–65. Epub 2010/03/03. doi: 10.1094/MPMI-23-4-0355 PMID: 20192823.

47. Jozefczak M, Remans T, Vangronsveld J, Cuypers A. Glutathione is a key player in metal-induced oxidative stress defenses. International journal of molecular sciences. 2012; 13(3):3145–75. Epub 2012/04/11. doi: 10.3390/ijms13033145 PMID: 22489146; PubMed Central PMCID: PMC3317707.

48. Zhang A, Altuvia S, Tiwari A, Argaman L, Hengge-Aronis R, Storz G. The OxyS regulatory RNA represses rpoS translation and binds the Hfq (HF-I) protein. The EMBO journal. 1998; 17(20):6061–8. Epub 1998/10/17. doi: 10.1093/emboj/17.20.6061 PMID: 9774349; PubMed Central PMCID: PMC1170932.

49. Burrowes E, Baysse C, Adams C, O'Gara F. Influence of the regulatory protein RsmA on cellular functions in Pseudomonas aeruginosa PAO1, as revealed by transcriptome analysis. Microbiology. 2006; 152(Pt 2):405–18. PMID: 16436429.

50. Irie Y, Starkey M, Edwards AN, Wozniak DJ, Romeo T, Parsek MR. Pseudomonas aeruginosa biofilm matrix polysaccharide Psl is regulated transcriptionally by RpoS and post-transcriptionally by RsmA. Mol Microbiol. 2010; 78(1):158–72. Epub 2010/08/26. doi: 10.1111/j.1365-2958.2010.07320.x PMID: 20735777; PubMed Central PMCID: PMC2984543.

51. Timmermans J, Van Melderen L. Post-transcriptional global regulation by CsrA in bacteria. Cellular and molecular life sciences: CMLS. 2010; 67(17):2897–908. Epub 2010/05/07. doi: 10.1007/s00018-010-0381-z PMID: 20446015.

52. Lynch TW, Read EK, Mattis AN, Gardner JF, Rice PA. Integration host factor: putting a twist on protein-DNA recognition. J Mol Biol. 2003; 330(3):493–502. Epub 2003/07/05. PMID: 12842466.

53. Swinger KK, Rice PA. IHF and HU: flexible architects of bent DNA. Current opinion in structural biology. 2004; 14(1):28–35. Epub 2004/04/23. doi: 10.1016/j.sbi.2003.12.003 PMID: 15102446.

54. Konyecsni WM, Deretic V. DNA sequence and expression analysis of algP and algQ, components of the multigene system transcriptionally regulating mucoidy in Pseudomonas aeruginosa: algP contains multiple direct repeats. J Bacteriol. 1990; 172(5):2511–20. Epub 1990/05/01. PMID: 2110144; PubMed Central PMCID: PMC208891.

55. Matsumoto K, Matsusaki H, Taguchi K, Seki M, Doi Y. Isolation and characterization of polyhydroxyalkanoates inclusions and their associated proteins in Pseudomonas sp. 61–3. Biomacromolecules. 2002; 3(4):787–92. Epub 2002/07/09. PMID: 12099824.

56. Winsor GL, Lam DK, Fleming L, Lo R, Whiteside MD, Yu NY, et al. Pseudomonas Genome Database: improved comparative analysis and population genomics capability for Pseudomonas genomes. Nucleic Acids Res. 2011; 39(Database issue):D596–600. Epub 2010/10/12. doi: 10.1093/nar/gkq869 PMID: 20929876; PubMed Central PMCID: PMC3013766.

57. Lindenberg S, Klauck G, Pesavento C, Klauck E, Hengge R. The EAL domain protein YciR acts as a trigger enzyme in a c-di-GMP signalling cascade in E. coli biofilm control. The EMBO journal. 2013; 32 (14):2001–14. Epub 2013/05/28. doi: 10.1038/emboj.2013.120 PMID: 23708798; PubMed Central PMCID: PMC3715855.

58. Dimkpa CO, Merten D, Svatos A, Buchel G, Kothe E. Metal-induced oxidative stress impacting plant growth in contaminated soil is alleviated by microbial siderophores. Soil Biol Biochem. 2009; 41 (1):154–62. doi: 10.1016/j.soilbio.2008.10.010 PMID: WOS:000262250900020.

59. Lamb C, Dixon RA. The Oxidative Burst in Plant Disease Resistance. Annual review of plant physiology and plant molecular biology. 1997; 48:251–75. Epub 1997/06/01. doi: 10.1146/annurev.arplant.48.1.251 PMID: 15012264.

60. Greenberg JT, Monach P, Chou JH, Josephy PD, Demple B. Positive control of a global antioxidant defense regulon activated by superoxide-generating agents in Escherichia coli. Proc Natl Acad Sci U S A. 1990; 87(16):6181–5. Epub 1990/08/01. PMID: 1696718; PubMed Central PMCID: PMC54496.

61. Schneider BL, Reitzer L. Pathway and enzyme redundancy in putrescine catabolism in Escherichia coli. J Bacteriol. 2012; 194(15):4080–8. Epub 2012/05/29. doi: 10.1128/JB.05063-11 PMID: 22636776; PubMed Central PMCID: PMC3416515.

62. Kuiper I, Bloemberg GV, Noreen S, Thomas-Oates JE, Lugtenberg BJ. Increased uptake of putrescine in the rhizosphere inhibits competitive root colonization by Pseudomonas fluorescens strain WCS365. Molecular plant-microbe interactions: MPMI. 2001; 14(9):1096–104. Epub 2001/09/12. doi: 10.1094/MPMI.2001.14.9.1096 PMID: 11551074.

63. Lapouge K, Schubert M, Allain FH, Haas D. Gac/Rsm signal transduction pathway of gamma-proteobacteria: from RNA recognition to regulation of social behaviour. Mol Microbiol. 2008; 67(2):241–53. Epub 2007/12/01. doi: 10.1111/j.1365-2958.2007.06042.x PMID: 18047567.

64. Rico A, Preston GM. Pseudomonas syringae pv. tomato DC3000 uses constitutive and apoplast-induced nutrient assimilation pathways to catabolize nutrients that are abundant in the tomato apoplast. Molecular plant-microbe interactions: MPMI. 2008; 21(2):269–82. Epub 2008/01/11. doi: 10.1094/MPMI-21-2-0269 PMID: 18184070.

65. Boch J, Joardar V, Gao L, Robertson TL, Lim M, Kunkel BN. Identification of Pseudomonas syringae pv. tomato genes induced during infection of Arabidopsis thaliana. Mol Microbiol. 2002; 44(1):73–88. Epub 2002/04/23. PMID: 11967070.

66. Miller JH. Experiments in molecular genetics. Cold Spring Harbor Laboratory, Cold Spring Harbor, New York. 1972:352–5.

67. Heeb S, Itoh Y, Nishijyo T, Schnider U, Keel C, Wade J, et al. Small, stable shuttle vectors based on the minimal pVS1 replicon for use in gram-negative, plant-associated bacteria. Molecular plant-microbe interactions: MPMI. 2000; 13(2):232–7. PMID: 10659714.

68. Yu D, Ellis HM, Lee EC, Jenkins NA, Copeland NG, Court DL. An efficient recombination system for chromosome engineering in Escherichia coli. Proc Natl Acad Sci U S A. 2000; 97(11):5978–83. PMID: 10811905.

69. Hoang TT, Karkhoff-Schweizer RR, Kutchma AJ, Schweizer HP. A broad-host-range Flp-FRT recombination system for site-specific excision of chromosomally-located DNA sequences: application for isolation of unmarked Pseudomonas aeruginosa mutants. Gene. 1998; 212(1):77–86. PMID: 9661666.

70. Little R, Salinas P, Slavny P, Clarke TA, Dixon R. Substitutions in the redox-sensing PAS domain of the NifL regulatory protein define an inter-subunit pathway for redox signal transmission. Mol Microbiol. 2011; 82(1):222–35. Epub 2011/08/23. doi: 10.1111/j.1365-2958.2011.07812.x PMID: 21854469.

71. Voisard C, Bull CT, Keel C, Laville J, Maurhofer M, U S. Biocontrol of root diseases by Pseudomonas fluorescens CHA0: current concepts and experimental approaches. O'Gara F, Dowling DN, Boesten B (eds) Molecular Ecology of Rhizosphere Microorganisms 1994:67–89.

72. Spiers AJ, Bohannon J, Gehrig SM, Rainey PB. Biofilm formation at the air-liquid interface by the Pseudomonas fluorescens SBW25 wrinkly spreader requires an acetylated form of cellulose. Mol Microbiol. 2003; 50(1):15–27. PMID: 14507360.

73. Frederix M, Edwards A, Swiderska A, Stanger A, Karunakaran R, Williams A, et al. Mutation of praR in Rhizobium leguminosarum enhances root biofilms, improving nodulation competitiveness by increased expression of attachment proteins. Mol Microbiol. 2014; 93(3):464–78. doi: 10.1111/mmi.12670 PMID: 24942546; PubMed Central PMCID: PMCPMC4149787.

74. Bommer UA, Burkhardt N, Jonemann R, Spahn CMT, Triana-Alonso FJ, Nierhaus KH. Subcellular fractionation. A practical approach Graham J., Rickwoods D, editors. Oxford, UK: Oxford University Press; 1996.

75. Christen M, Christen B, Folcher M, Schauerte A, Jenal U. Identification and Characterization of a Cyclic di-GMP-specific Phosphodiesterase and Its Allosteric Control by GTP. J Biol Chem. 2005; 280 (35):30829–37. PMID: 15994307.

76. Shevchenko A, Tomas H, Havlis J, Olsen JV, Mann M. In-gel digestion for mass spectrometric characterization of proteins and proteomes. Nature protocols. 2006; 1(6):2856–60. Epub 2007/04/05. doi: 10.1038/nprot.2006.468 PMID: 17406544.

77. Vizcaino JA, Cote RG, Csordas A, Dianes JA, Fabregat A, Foster JM, et al. The PRoteomics IDEntifications (PRIDE) database and associated tools: status in 2013. Nucleic Acids Res. 2013; 41(Database issue):D1063–9. Epub 2012/12/04. doi: 10.1093/nar/gks1262 PMID: 23203882; PubMed Central PMCID: PMC3531176.

PLOS | GENETICS

RESEARCH ARTICLE

A Minimal Threshold of c-di-GMP Is Essential for Fruiting Body Formation and Sporulation in *Myxococcus xanthus*

Dorota Skotnicka[1], Gregory T. Smaldone[2☯], Tobias Petters[1☯], Eleftheria Trampari[3], Jennifer Liang[2], Volkhard Kaever[4], Jacob G. Malone[3,5], Mitchell Singer[2]*, Lotte Søgaard-Andersen[1]*

1 Department of Ecophysiology, Max Planck Institute for Terrestrial Microbiology, Marburg, Germany, **2** Department of Microbiology and Molecular Genetics, University of California - Davis, Davis, California, United States of America, **3** Molecular Microbiology Department, John Innes Centre, Norwich, United Kingdom, **4** Research Core Unit Metabolomics, Hannover Medical School, Hannover, Germany, **5** School of Biological Sciences, University of East Anglia, Norwich, United Kingdom

☯ These authors contributed equally to this work.
* mhsinger@ucdavis.edu (MS); sogaard@mpi-marburg.mpg.de (LSA)

OPEN ACCESS

Citation: Skotnicka D, Smaldone GT, Petters T, Trampari E, Liang J, Kaever V, et al. (2016) A Minimal Threshold of c-di-GMP Is Essential for Fruiting Body Formation and Sporulation in *Myxococcus xanthus*. PLoS Genet 12(5): e1006080. doi:10.1371/journal.pgen.1006080

Editor: Josep Casadesús, Universidad de Sevilla, SPAIN

Received: February 1, 2016

Accepted: May 4, 2016

Published: May 23, 2016

Data Availability Statement: All relevant data are within the paper and its Supporting Information files.

Funding: This work was funded by: German Research Council within the framework of the Collaborative Research Center SFB987 "Microbial Diversity in Environmental Signal Response" (www.dfg.de/en/): to LSA; Max Planck Society (http://www.mpg.de/en): to LSA; and National Science Foundation grant MCB-1024989 (http://www.nsf.gov/): to MS. The funders had no role in study design, data collection and analysis, decision to publish, or preparation of the manuscript.

Abstract

Generally, the second messenger bis-(3'-5')-cyclic dimeric GMP (c-di-GMP) regulates the switch between motile and sessile lifestyles in bacteria. Here, we show that c-di-GMP is an essential regulator of multicellular development in the social bacterium *Myxococcus xanthus*. In response to starvation, *M. xanthus* initiates a developmental program that culminates in formation of spore-filled fruiting bodies. We show that c-di-GMP accumulates at elevated levels during development and that this increase is essential for completion of development whereas excess c-di-GMP does not interfere with development. MXAN3735 (renamed DmxB) is identified as a diguanylate cyclase that only functions during development and is responsible for this increased c-di-GMP accumulation. DmxB synthesis is induced in response to starvation, thereby restricting DmxB activity to development. DmxB is essential for development and functions downstream of the Dif chemosensory system to stimulate exopolysaccharide accumulation by inducing transcription of a subset of the genes encoding proteins involved in exopolysaccharide synthesis. The developmental defects in the *dmxB* mutant are non-cell autonomous and rescued by co-development with a strain proficient in exopolysaccharide synthesis, suggesting reduced exopolysaccharide accumulation as the causative defect in this mutant. The NtrC-like transcriptional regulator EpsI/Nla24, which is required for exopolysaccharide accumulation, is identified as a c-di-GMP receptor, and thus a putative target for DmxB generated c-di-GMP. Because DmxB can be—at least partially—functionally replaced by a heterologous diguanylate cyclase, these results altogether suggest a model in which a minimum threshold level of c-di-GMP is essential for the successful completion of multicellular development in *M. xanthus*.

Competing Interests: The authors have declared that no competing interests exist.

Author Summary

The nucleotide-based second messenger c-di-GMP is ubiquitous in bacteria and generally regulates the switch between motile and sessile lifestyles. We show that c-di-GMP regulates multicellular morphogenesis and cellular differentiation during the starvation-induced developmental program that culminates in fruiting body formation in *Myxococcus xanthus*. DmxB is identified as a diguanylate synthase that is regulated at multiple levels and responsible for the increased c-di-GMP synthesis during development. A Δ*dmxB* mutant has reduced exopolysaccharide accumulation and is rescued by co-development with strains proficient in exopolysaccharide accumulation, suggesting reduced exopolysaccharide accumulation as the causative defect in this mutant. We propose that a minimum threshold level of c-di-GMP is required for successful completion of starvation-induced development in *M. xanthus*.

Introduction

Bacteria synthesize a variety of nucleotide-based second messengers that have important functions in adaptation and differentiation processes in response to environmental changes. Among these bis-(3'-5')-cyclic dimeric GMP (c-di-GMP) has emerged as ubiquitous and highly versatile. Regulation by c-di-GMP often relates to lifestyle changes involving transitions between motility and sessility with the specific processes regulated including motility, adhesion, exopolysaccharide (EPS) synthesis, biofilm formation, cell cycle progression and virulence [for reviews, see [1–3]]. However, c-di-GMP also regulates multicellular development and cellular differentiation processes that do not appear to relate to this transition such as aerial mycelium formation in *Streptomyces venezuelae* and heterocyst formation in filaments of *Anabaena* sp. strain PCC 7120 [4, 5]. c-di-GMP is synthesized from two molecules of GTP by diguanylate cyclases (DGCs) [6, 7] that share the so-called GGDEF domain named after a conserved sequence motif in the active- (A) site [8]. GGDEF domains often contain an inhibitory- (I) site with the consensus sequence RxxD that binds c-di-GMP resulting in allosteric feedback inhibition of DGC activity [8]. c-di-GMP is degraded by phosphodiesterases (PDEs) that contain either a catalytic EAL or HD-GYP domain both of which are also named after conserved sequence motifs in their active site [9–12]. c-di-GMP interacts with a range of effectors to regulate downstream responses at the transcriptional, (post-)translational or allosteric level, as well as by mediating protein-protein interactions [1, 5, 13]. Effectors include degenerate GGDEF and EAL domain proteins that do not have catalytic activity [14–18], different transcription factor families [5, 19–24], PilZ domain-containing proteins [25–31], and riboswitches [32].

In response to nutrient starvation, the social bacterium *Myxococcus xanthus* initiates a multicellular developmental program that results in the formation of fruiting bodies that each contains ~100,000 spores [for review, see [33]]. Fruiting body formation proceeds in distinct morphological stages. After 4–6 hrs of starvation, the rod-shaped cells change motility behavior and start to aggregate to form translucent mounds [34]. By 24 hrs, the aggregation process is complete and those cells that have accumulated inside fruiting bodies differentiate to spherical spores with spore maturation completed by 72 hrs. While gliding motility is dispensable [35], type IV pili (T4P)-dependent motility is important for fruiting body formation and lack of T4P causes a delay or even blocks fruiting body formation while sporulation still proceeds [35, 36]. In *M. xanthus* T4P-dependent motility depends on EPS because it stimulates T4P retraction [37] and lack of EPS completely blocks fruiting body formation and sporulation [38–40]. EPS

synthesis depends on the *eps* locus, which encodes structural proteins for EPS biosynthesis and transport [41]. Multiple regulators of EPS accumulation have been identified; however, only the NtrC-like transcriptional regulator EpsI/Nla24, which is encoded in the *eps* locus, and the Dif chemosensory system are essential for EPS synthesis [40–43]. Interestingly, lack of EPS causes a non-cell autonomous defect in development and development of mutants that lack EPS can be rescued by co-development with a strain proficient in EPS synthesis or by addition of purified EPS [38–40].

We recently demonstrated that *M. xanthus* accumulates c-di-GMP during growth and that c-di-GMP regulates T4P-dependent motility in growing cells by regulating transcription of the *pilA* gene, which encodes the major pilin of T4P, and EPS accumulation [44]. *M. xanthus* encodes 24 proteins containing a GGDEF, EAL or HD-GYP domain [15, 44]. A systematic genetic analysis using single gene mutations identified three of these genes (*dmxA*, *sgmT* and *tmoK*) as important for T4P-dependent motility whereas single mutations in the remaining 21 genes neither interfered with growth nor with motility [44]. Here, we identify c-di-GMP as an essential regulator of development in *M. xanthus* and show that reduced c-di-GMP levels cause a non-cell autonomous defect in EPS accumulation during development whereas increased c-di-GMP levels do not interfere with development. Moreover, we identify a novel DGC, DmxB, that only functions during development and is responsible for the increase in c-di-GMP levels that is essential for fruiting body formation and sporulation to go to completion. Moreover, we demonstrate that DmxB is essential for transcription of subset of genes involved in EPS synthesis and that the NtrC-like transcriptional regulator EpsI/Nla24 is a c-di-GMP receptor. Our results suggest a scenario in which a minimal threshold level of c-di-GMP is essential for progression of the developmental program in *M. xanthus* and binds to EpsI/Nla24 to stimulate EPS synthesis.

Results

c-di-GMP level increases significantly during development

We previously demonstrated that *M. xanthus* cells grown in suspension in rich medium accumulate c-di-GMP [44]. *M. xanthus* only forms fruiting bodies when starved on a surface. Therefore, to determine if *M. xanthus* accumulates c-di-GMP during development, exponentially growing wild-type (WT) DK1622 cells were removed from rich medium and starved on a solid surface in submerged culture for 48 hrs. c-di-GMP levels were quantified at different time points during development using liquid chromatography coupled tandem mass spectrometry [45]. c-di-GMP was detected at all time points of development. The c-di-GMP level increased ~20-fold from 0 hrs (4.4 ± 0.7 pmol/mg protein) to 48 hrs (84.8 ± 15.9 pmol/mg protein) of development (Fig 1). To determine if this increase in c-di-GMP was a specific response to starvation and not to a solid surface, cells were exposed to starvation in suspension. Under these conditions, the c-di-GMP level also increased ~20-fold from 0 hrs (6.2 ± 0.7 pmol/mg protein) to 48 hrs (118.5 ± 35.0 pmol/mg protein) of starvation (Fig 1). While the c-di-GMP level increased ~20-fold under both starvation conditions, the c-di-GMP level was generally lower in cells starved on a solid surface. Moreover, the c-di-GMP accumulation profile was slightly different, i.e. cells starved on a surface showed a significant increase in c-di-GMP after 24 hrs and cells starved in suspension a significant increase after 6 hrs of starvation. Importantly, because the level of c-di-GMP does not increase significantly in stationary phase cells [44], these data demonstrate that the increase in the c-di-GMP level is a specific response to starvation and that the c-di-GMP level increases during development. Because the c-di-GMP levels

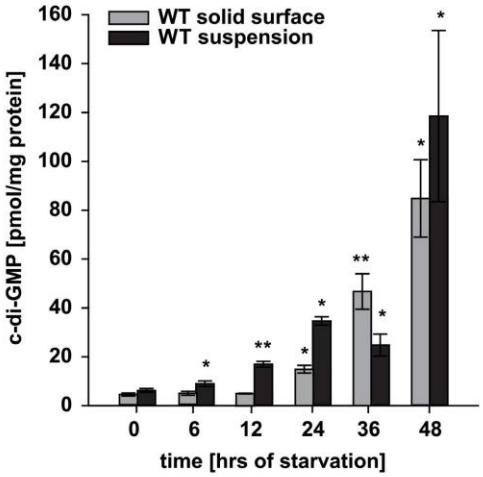

Fig 1. c-di-GMP accumulates at increased levels in developing and starving *M. xanthus* cells. DK1622 WT cells were starved in MC7 buffer on a solid surface in submerged culture or in suspension. At the indicated time points the c-di-GMP levels were determined and correlated to protein concentration. The c-di-GMP level is shown as mean ± standard deviation (SD) calculated from three biological replicates. * $p < 0.05$, ** $p < 0.001$ in Student's t-test in which samples from individual time points were compared to the relevant 0 hrs sample.

doi:10.1371/journal.pgen.1006080.g001

in suspension-starved WT cells overall correlated with that in developing WT, we from now measured c-di-GMP levels in cells starved in suspension.

c-di-GMP level is important for fruiting body formation and sporulation

To determine if the c-di-GMP level is important for development, we used previously generated strains [44] that constitutively produce a heterologous DGC ($DgcA^{WT}$ of *Caulobacter crescentus*), a heterologous PDE ($PA5295^{WT}$ of *Pseudomonas aeruginosa*) or their active site variants $DgcA^{D164A}$ or $PA5295^{E328A}$ in WT cells. Production of $DgcA^{WT}$ and $PA5295^{WT}$ causes a significant increase and decrease, respectively in the c-di-GMP level during vegetative growth whereas the two active site variants do not [44]. Consistently, after 24 hrs of starvation in suspension, the c-di-GMP level was significantly increased in cells producing $DgcA^{WT}$ compared to WT and significantly decreased in cells expressing $PA5295^{WT}$ (Fig 2A).

On TPM agar as well as in submerged culture, WT and the strains producing $DgcA^{D164A}$ or $PA5295^{E328A}$ aggregated to form nascent fruiting bodies after 24 hrs and had formed darkened spore-filled fruiting bodies after 120 hrs (Fig 2B). The strain producing $DgcA^{WT}$ still formed fruiting bodies and sporulated but the fruiting bodies were smaller than in WT, possibly due to the defect that this strain has in T4P-dependent motility during vegetative growth [44]. By contrast, the $PA5295^{WT}$ producing strain displayed delayed fruiting body formation on TPM agar, did not form fruiting bodies in submerged culture even after 120 hrs and its sporulation was strongly reduced. We conclude that a decreased c-di-GMP level impedes fruiting body formation and sporulation whereas an increased level of c-di-GMP does not.

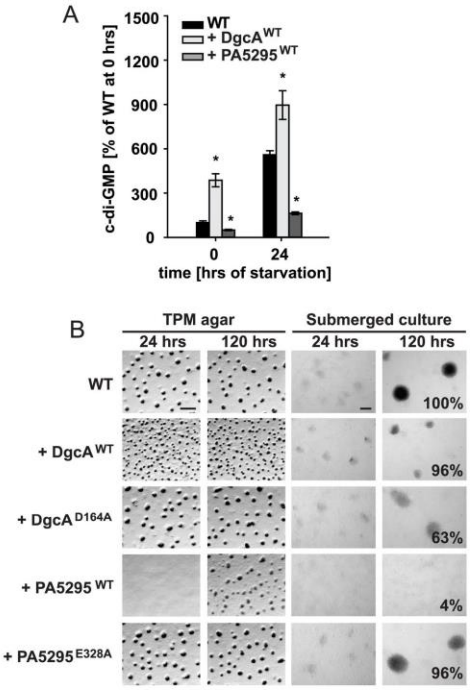

Fig 2. c-di-GMP level is important for development. (A) c-di-GMP levels in cells expressing the indicated proteins during starvation in suspension. The c-di-GMP levels are shown as mean ± SD from three biological replicates relative to WT at 0 hrs. * $p < 0.05$ in Student's t-test comparing different mutants to the WT at the respective time points. Note that the data for WT are the same as in Fig 1. (B) Fruiting body formation and sporulation under two different starvation conditions. Numbers after 120 hrs of starvation in submerged culture indicate heat- and sonication resistant spores formed after 120 hrs of starvation in submerged culture in percentage of WT (100%) from one representative experiment. Scale bars, TPM agar 500 μm, submerged culture 100 μm.

doi:10.1371/journal.pgen.1006080.g002

Identification of GGDEF, EAL and HD-GYP domain proteins important for development

We previously identified 24 genes in *M. xanthus* encoding proteins containing either a GGDEF (17 proteins), EAL (two proteins) or HD-GYP domain (five proteins) [15, 44]. Based on single gene mutations, three of these proteins are important for T4P-dependent motility: DmxA is a DGC, SgmT is a hybrid histidine protein kinase that binds c-di-GMP using its C-terminal degenerate GGDEF domain but does not have DGC activity, and TmoK is a hybrid histidine protein kinase with a C-terminal GGDEF domain that neither synthesizes nor binds c-di-GMP [15, 44].

To further investigate the function of these 24 proteins, we screened strains with single in-frame deletions in these genes or an insertion mutation in the case of *dmxA* for development-related phenotypes. Single gene mutations in 20 of the 24 genes did not affect development

(S1 Fig). These 20 genes included *dmxA* and *actA*. ActA has previously been suggested to be important for development [46]. For generation of the in-frame deletion of *actA*, we reannotated *actA* taking into account the GC content in the third position of codons and by comparisons to orthologous genes (S2 Fig). Based on this re-annotation, the original Δ*actA* mutation extends into the promoter region of the *act* operon. *actA* is located upstream of *actB*, which is important for development (S2 Fig) [46]. Because the original Δ*actA* mutant phenocopies the Δ*actB* mutant, we speculate that the developmental defects observed for the original Δ*actA* mutant are caused by a polar effect on *actB*. We conclude that ActA is not required for development. Lack of the DGC DmxA did also not affect development and, thus, specifically causes a defect in T4P-dependent motility in vegetative cells.

As previously reported, lack of SgmT caused defects in fruiting body formation and sporulation [15]. Moreover, lack of TmoK caused delayed aggregation and reduced sporulation in submerged culture while aggregation was normal on TPM agar (S1 Fig).

Mutations in two genes caused developmental defects without affecting growth or motility in vegetative cells [44]. MXAN3735, henceforth DmxB (DGC from *M. xanthus* B), is a predicted cytoplasmic protein with an N-terminal receiver domain of two component system and a C-terminal GGDEF domain that contains the conserved residues for catalytic activity (G^{219}GDEF) and an intact I-site (R^{210}ESD), which allows c-di-GMP binding and allosteric feedback inhibition of DGC activity (Fig 3A; [44]). A mutant lacking DmxB neither aggregated on TPM agar nor in submerged culture and was strongly reduced in sporulation (S1 Fig and Fig 3B). MXAN2061, henceforth PmxA (PDE from *M. xanthus* A), is a predicted integral membrane protein and contains an N-terminal periplasmic Cache domain followed by a transmembrane segment, a HAMP domain and a HD-GYP domain with all the residues required for catalytic activity (H^{424}D-G^{485}YP) (Fig 3A; [44]). The Δ*pmxA* mutant formed highly irregular translucent fruiting bodies on TPM agar, did not aggregate in submerged culture (S1 Fig and Fig 3B) and only sporulated at 15% of WT levels (S1 Fig and Fig 3B). Moreover, the Δ*dmxB* Δ*pmxA* double mutant had the same developmental phenotype as the Δ*dmxB* strain (Fig 3B).

The developmental defects in all four mutants were complemented by ectopic expression of the relevant WT gene from its native promoter on plasmids integrated at the Mx8 *attB* site (Fig 3B and [15]). Because SgmT and TmoK are important for T4P-dependent motility, we speculate that the developmental defects caused by lack of either of these two proteins may be caused by a defect in T4P-dependent motility. From here on, we focused on DmxB and PmxA that are only important for development.

DmxB and PmxA have enzymatic activity and DmxB binds c-di-GMP *in vitro*

To test *in vitro* for enzymatic activity of DmxB and PmxA, we overexpressed His_6-tagged full-length variants of DmxB and truncated variants of PmxA (Fig 4A and 4B) in *Escherichia coli* and purified them as soluble proteins.

Similarly to the control protein $DgcA^{WT}$, DmxB produced c-di-GMP when incubated with [α-^{32}P]-GTP as detected after separation of nucleotides by thin layer chromatography (TLC), while an active site variant $DmxB^{D221A}$ did not (Fig 4A). To test whether DmxB binds c-di-GMP *in vitro* we used a differential radial capillary action of ligand assay (DRaCALA) with [α-^{32}P]-labeled c-di-GMP [48]. In agreement with the predictions from sequence analyses, DmxB specifically bound [α-^{32}P]-c-di-GMP whereas the I-site mutant $DmxB^{R210A}$ did not (Fig 4C). Moreover, the I-site mutant had slightly increased DGC activity *in vitro* in comparison to

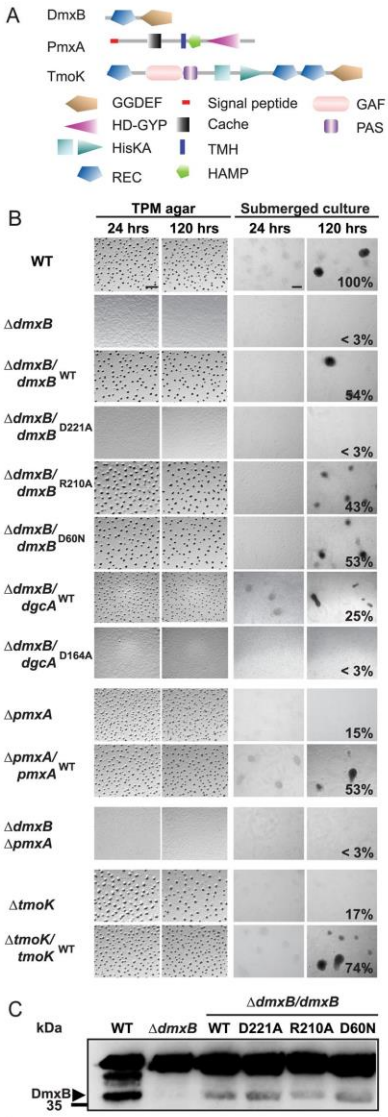

Fig 3. Complementation experiments with Δ*dmxB*, Δ*pmxA* and Δ*tmoK* mutants. (A) Domain structure of DmxB, PmxA and TmoK. The primary sequences of the indicated proteins were analyzed for domain structure using [47]. (B) Fruiting body formation and sporulation under two different starvation conditions. Cells were treated and spores enumerated as described in Fig 2B. Scale bars: TPM agar 500 μm, submerged culture 100 μm. (C) Immunoblot detection of DmxB in total cell extracts. Total cell lysates from cells of the

indicated genotypes were harvested from starvation agar at 24 hrs of development, separated by SDS-PAGE and probed with rabbit, polyclonal α-DmxB serum. Protein from the same calculated number of cells was loaded per lane. DmxB has a calculated molecular mass of 35.3 kDa. Molecular mass marker is indicated on the left. The non-specific band above the band corresponding to DmxB serves as an internal loading control.

doi:10.1371/journal.pgen.1006080.g003

the WT protein consistent with impaired feedback inhibition (Fig 4A). PmxA$^{384\text{-}568}$, which contains the predicted cytoplasmic part of PmxA, displayed PDE activity and degraded [α-^{32}P]-labeled c-di-GMP to linear pGpG, whereas the active site variant PmxA$^{H424A,\ D425A}$ did not (Fig 4B).

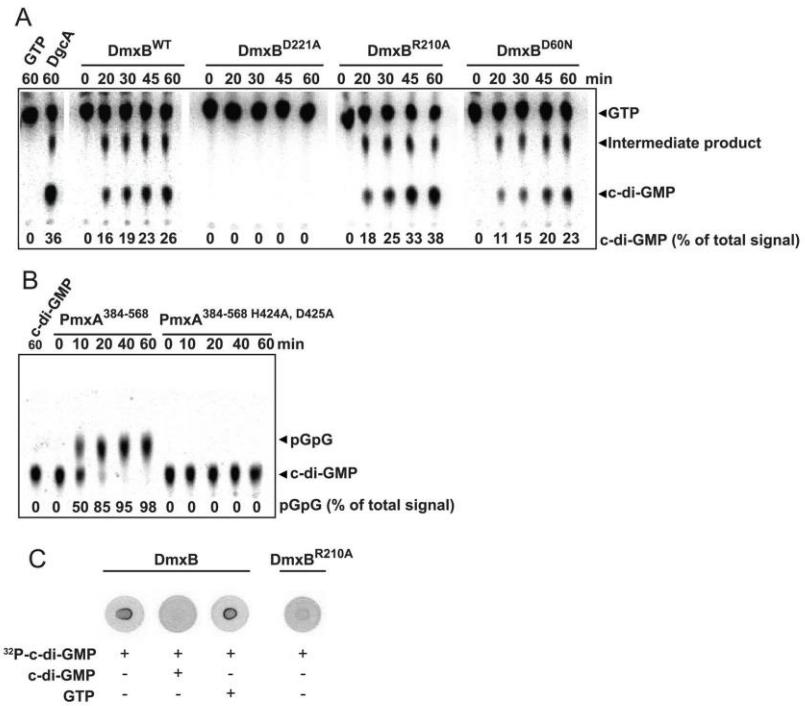

Fig 4. *In vitro* assay for enzyme activity and c-di-GMP binding. (A) DGC assay of DmxB variants. The indicated His6-tagged full-length DmxB variants were incubated with [α-^{32}P]-GTP for the indicated periods of time followed by separation of nucleotides by TLC. Full-length DgcA^{WT} was used as a positive control. GTP and c-di-GMP are indicated. The intermediate product indicated was described as a product formed during the DGC-dependent synthesis of c-di-GMP [49]. Numbers at the bottom indicate levels of c-di-GMP in % of the total signal in each lane. (B) PDE activity assay of PmxA. The indicated PmxA variants were incubated with [α-^{32}P]-labeled c-di-GMP for the indicated periods of time followed by separation of nucleotides by TLC. pGpG and c-di-GMP are indicated. Numbers at the bottom indicate levels of pGpG in % of the total signal in each lane. (C) DRaCALA to detect c-di-GMP binding. The indicated full-length DmxB variants were incubated with [α-^{32}P]-c-di-GMP with or without unlabeled c-di-GMP or GTP as competitors as indicated. 10 μl of the reaction mixtures were transferred to a nitrocellulose filter, dried and imaged.

doi:10.1371/journal.pgen.1006080.g004

Lack of DmxB but not PmxA causes changes in the c-di-GMP level during starvation

To determine if lack of DmxB or PmxA had an effect on c-di-GMP levels *in vivo*, we determined the c-di-GMP level in the Δ*dmxB and* Δ*pmxA* mutants starved in suspension for 48 hrs. In the Δ*pmxA* mutant, the c-di-GMP level in vegetative cells as well as during starvation was similar to that in WT (Fig 5A). In the Δ*dmxB* mutant, the c-di-GMP level in vegetative cells was also similar to that in WT and essentially remained constant throughout the entire time

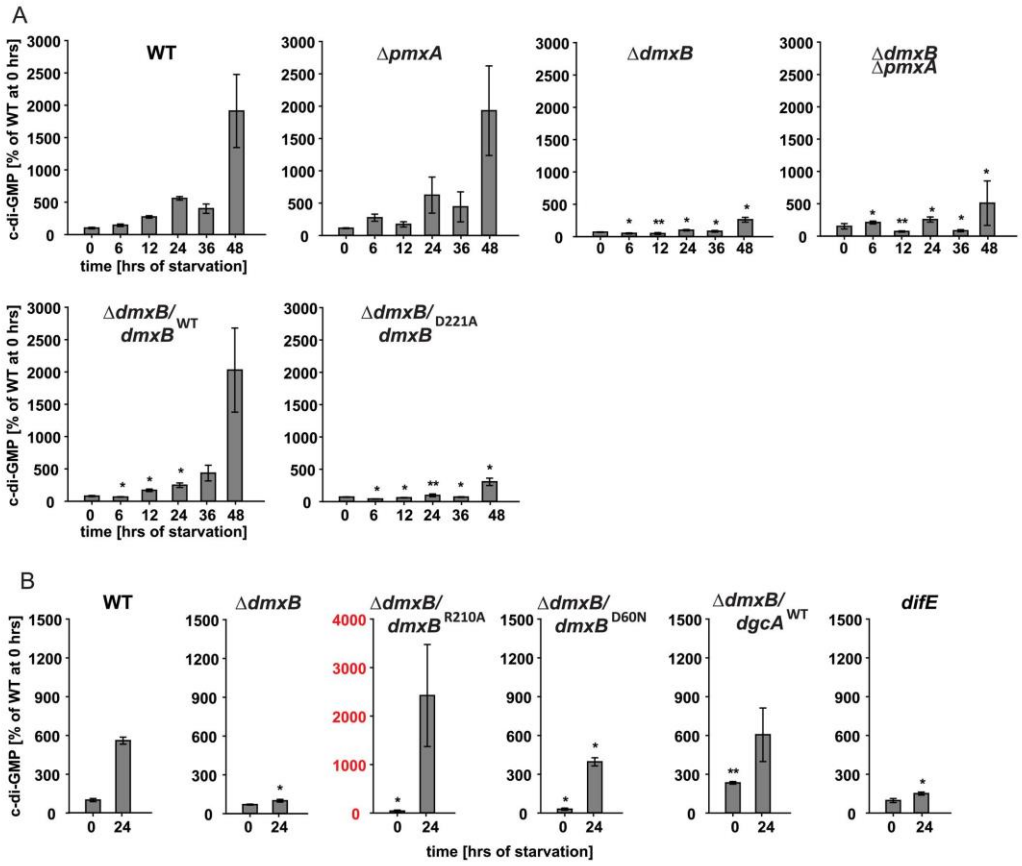

Fig 5. c-di-GMP levels in cells of the indicated mutants during starvation. (A, B) c-di-GMP levels in cells of the indicated genotypes were determined from three biological replicates as described in Fig 1. Note that the data for the WT are the same as in Fig 1 and in (B) the data for the WT and Δ*dmxB* strains are the same as in (A) and are shown again for the indicated time points for comparison. Note the different scale in (B) and for the Δ*dmxB/ dmxB*^{R210A} strain. * $p < 0.05$, ** $p < 0.001$ in Student's t-test comparing the different mutants to the WT at the same time points.

doi:10.1371/journal.pgen.1006080.g005

course without showing the ~20-fold increase observed in WT (Fig 5A). Moreover, the Δ*dmxB* Δ*pmxA* double mutant accumulated c-di-GMP at a similar low level as the Δ*dmxB* mutant (Fig 5A) consistent with the observation that the double mutant has the same developmental phenotype as the Δ*dmxB* mutant. Because the Δ*pmxA* mutant did not show significant changes in c-di-GMP levels during development and the Δ*dmxB* Δ*pmxA* double mutant accumulated c-di-GMP at a similar low level as the Δ*dmxB* mutant, we focused on elucidating the function of DmxB in development.

In the Δ*dmxB*/*dmxB*^{WT} complementation strain but not in the Δ*dmxB*/*dmxB*^{D221A} strain containing the active site variant of DmxB, the c-di-GMP level during starvation was restored to that in WT (Fig 5A). Importantly, the Δ*dmxB*/*dmxB*^{D221A} strain phenocopied the Δ*dmxB* mutant and did not aggregate and was strongly reduced in sporulation (Fig 3B). Moreover, development of the strain Δ*dmxB*/*dmxB*^{R210A}, which contains the DmxB variant with a substitution of the conserved Arg residue in the I-site, proceeded as in WT. This strain had a c-di-GMP level that was ~4-fold higher than in WT at 24 hrs of starvation (Fig 5B—third panel, note scale on y-axis) consistent with the increased DGC activity *in vitro* (Fig 4A) and the notion that DmxB^{R210A} is no longer subject to feedback inhibition by c-di-GMP. In all three complementation strains, the DmxB variants had accumulated at the same level at 24 hrs and this level was lower than in the DK1622 WT (Fig 3C; Cf. below). We conclude that complementation of the Δ*dmxB* mutant depends on DGC activity by DmxB and not only on its presence, that DmxB is responsible for the ~20-fold increase in the c-di-GMP level during development and that this increase is essential for development whereas an even higher increase in c-di-GMP levels does not interfere with development.

Because DmxB contains an N-terminal receiver domain with the conserved phosphorylatable Asp residue conserved (D60), we asked if DmxB phosphorylation is involved in regulating DmxB activity. To this end, we ectopically expressed *dmxB*^{D60N}, which encodes a DmxB variant in which this Asp residue has been substituted with non-phosphorylatable Asn. DmxB^{D60N} accumulated similarly to DmxB^{WT} in the Δ*dmxB*/*dmxB*^{WT} complementation strain (Fig 3C), complemented the developmental defects in the Δ*dmxB* mutant (Fig 3B) and largely restored c-di-GMP accumulation (Fig 5B). *In vitro* DmxB^{D60N} displayed DGC activity similar to DmxB^{WT} (Fig 4A). Altogether, these observations suggest that phosphorylation of the N-terminal receiver domain in DmxB is not essential for DmxB function. Of note, MXAN3734 located downstream of *dmxB* encodes a response regulator; however, under the conditions tested, this protein is not required for development (S3 Fig).

Δ*dmxB* mutant is partially complemented by expression of a heterologous DGC

Strains that accumulate significantly more c-di-GMP than WT (WT/DgcA^{WT} and Δ*dmxB*/*dmxB*^{R210A}) developed whereas the strains (WT/PA5295^{WT}, Δ*dmxB*, and Δ*dmxB*/*dmxB*^{D221A}) that accumulate significantly less c-di-GMP did not, suggesting that a minimal threshold level of c-di-GMP is essential for development and that significantly higher c-di-GMP levels do not interfere with development. Because DmxB is responsible for reaching this threshold, this raised the question if the only function of DmxB is to contribute to the cellular pool of c-di-GMP. To address this question, we expressed the heterologous DgcA^{WT} or its active site variant DgcA^{D164A} in the Δ*dmxB* mutant. Interestingly, fruiting body formation and sporulation were largely restored by expression of DgcA^{WT} but not by DgcA^{D164A} (Fig 3B) and in the DgcA^{WT} containing strain the level of c-di-GMP was similar to that in WT at 24 hrs of starvation (Fig 5B) suggesting that the major function of DmxB is to contribute to a cellular pool of c-di-GMP in developing *M. xanthus* cells without engaging in specific protein-protein interactions.

DmxB specifically accumulates during development

To deduce how lack of DmxB only causes developmental defects and not a defect in T4P-dependent motility in growing cells, we determined the expression pattern of *dmxB* using qRT-PCR. The *dmxB* transcript level increased >100-fold during the first 24 hrs of development in comparison to growing cells (Fig 6A). Also, immunoblot analysis revealed that DmxB was undetectable in growing cells and that accumulation increased during development (Fig 6B). Together, these data demonstrate that DmxB accumulation is regulated at the transcriptional level and induced in response to starvation.

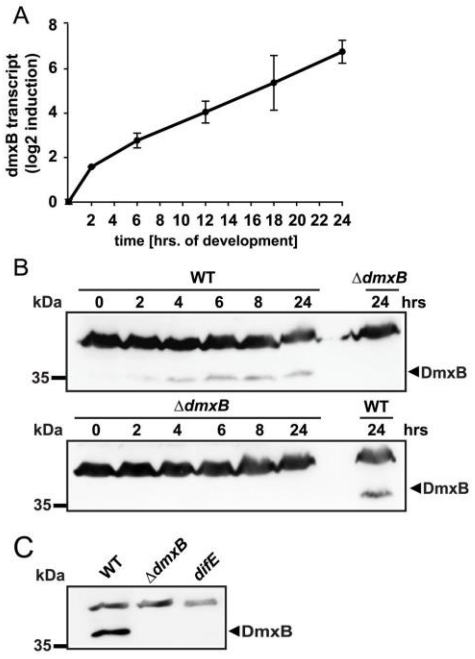

Fig 6. Determination of *dmxB* transcript and DmxB accumulation levels. (A) qRT-PCR analysis of *dmxB* expression. Total RNA was isolated from WT developed in submerged culture at the indicated time points. *dmxB* transcript level is shown as the mean ± standard deviation from two biological replicates with each three technical replicates relative to WT at 0 hrs. (B) Immunoblot detection of DmxB in total cell extracts. Total cell lysates were prepared from cells of the indicated genotypes harvested from starvation agar plates at the indicated time points of development. Immunoblots were prepared as described in Fig 3C. Protein from the same calculated number of cells was loaded per lane. Molecular mass marker is indicated on the left. The non-specific band above the band corresponding to DmxB serves as an internal loading control. (C) Immunoblot detection of DmxB in total cell extract of WT, Δ*dmxB* and *difE* strains. Total cell lysates from cells harvested from starvation agar after 24 hrs of development were prepared. Immunoblots were prepared as described in Fig 3C. Protein from the same calculated number of cells was loaded per lane. Molecular mass marker is indicated on the left. The non-specific band above the band corresponding to DmxB serves as an internal loading control.

doi:10.1371/journal.pgen.1006080.g006

Lack of DmxB causes reduced EPS accumulation

In growing cells c-di-GMP is important for T4P-dependent motility by regulating T4P formation and EPS accumulation. To elucidate the mechanism underlying the developmental defects of the Δ*dmxB* mutant, we therefore tested this mutant for PilA accumulation and T4P formation. In WT cells as well as in the Δ*dmxB* mutant the level of PilA in total cell extracts increased from 0 to 24 hrs of development as previously reported for WT [50] (Fig 7A). Also, the level of PilA incorporated into T4P increased significantly in both strains and even more in the Δ*dmxB* mutant than in the WT (Fig 7A). As expected, PilA was not detected in the Δ*pilA* mutant and also not in T4P fraction of the *pilC* mutant that served as negative controls (Fig 7A).

EPS accumulation was determined using an assay in which trypan blue binding to EPS is used to visualize EPS. For this purpose, cells were inoculated on solid medium containing trypan blue in the presence or absence of nutrients. As expected, in the presence of nutrients, no differences in trypan blue staining were observed between WT, a *fruA* mutant, which has a developmental defect [51], the Δ*dmxB* mutant and the Δ*dmxB* mutant complemented with $dmxB^{WT}$, $dmxB^{D221A}$, $dgcA^{WT}$ or $dgcA^{D164A}$ whereas the *difE* mutant, which lacks the histidine protein kinase DifE of the Dif chemosensory system that is essential for EPS accumulation, did not stain with trypan blue (Fig 7B). By contrast, in the absence of nutrients, only the WT, Δ*dmxB*/$dmxB^{WT}$ and Δ*dmxB*/$dgcA^{WT}$ strains accumulated high levels of EPS as indicated by the dark blue coloration, while the Δ*dmxB*, Δ*dmxB*/$dmxB^{D221A}$ and Δ*dmxB*/$dgcA^{D164A}$ strains, similarly to the *difE* strain, bound trypan blue at a much reduced level (Fig 7B). Importantly, the development-deficient *fruA* mutant bound trypan blue similarly to WT providing evidence that the reduced EPS accumulation in the Δ*dmxB*, Δ*dmxB*/$dmxB^{D221A}$ and Δ*dmxB*/$dgcA^{D164A}$ strains was not a simple consequence of lack of development. Together, these data strongly indicate that an increase in the c-di-GMP level is required for EPS accumulation during development and that DmxB is responsible for this increase in WT.

Lack of DmxB causes non-cell autonomous developmental defects

The developmental defects of the Δ*dmxB* mutant are similar to those of the *difE* mutant, i.e. no aggregation, strongly reduced sporulation and strongly reduced EPS accumulation. Therefore, we hypothesized that *difE* would also be important for DmxB accumulation. As shown in Fig 6C, the *difE* mutant is strongly reduced in DmxB accumulation. Consistently, the *difE* mutant was found to be strongly reduced in c-di-GMP accumulation after 24 hrs of starvation (Fig 5B).

Because the developmental defects of a *difE* mutant can be rescued by extracellular complementation by WT in co-development assays, we reasoned that the Δ*dmxB* mutant would also be rescued by co-development with WT if the primary defect in this mutant is reduced EPS accumulation during development. To this end, cells of the tetracycline resistant Δ*dmxB* mutant (Δ*dmxB*/$dmxB^{D221A}$) were mixed with tetracycline sensitive WT cells in a 1:1 ratio and co-developed in submerged culture. Subsequently, spores formed by the two strains were enumerated. In this experiment, 53% of germinating spores derived from the Δ*dmxB*/$dmxB^{D221A}$ strain (Fig 7C). Importantly, the Δ*dmxB* mutant was not rescued by co-development with the *difE* mutant and the Δ*dmxB* mutant did not rescue sporulation of the *difE* mutant whereas the WT efficiently rescued sporulation by the *difE* mutant, supporting the notion that the mechanism underlying the Δ*dmxB* developmental defects is indeed reduced EPS accumulation.

Dictyostelium discoideum is the only eukaryote where c-di-GMP has been identified and lack of the DGC DgcA blocks fruiting body formation [52]. Development of a *dgcA* mutant is restored by exogenous c-di-GMP at a final concentration of 1 mM. Therefore, we tested if exogenous c-di-GMP would restore development of the Δ*dmxB* mutant. Estimates of the

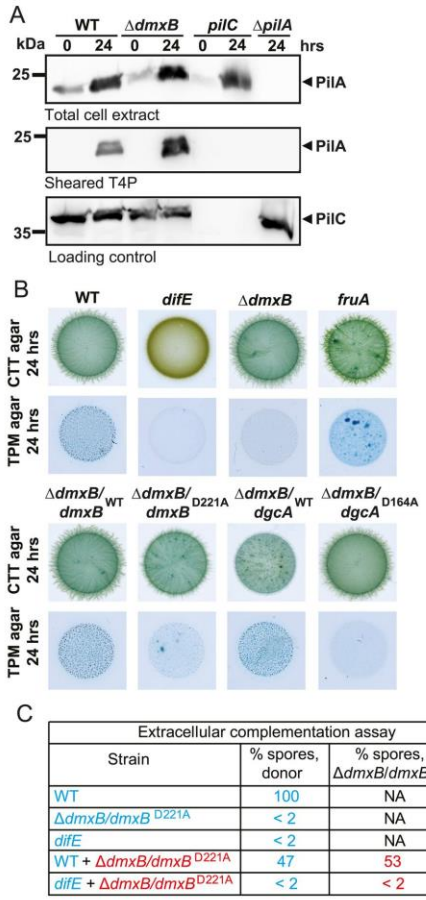

C

Extracellular complementation assay		
Strain	% spores, donor	% spores, ΔdmxB/dmxB^{D221A}
WT	100	NA
ΔdmxB/dmxB^{D221A}	< 2	NA
difE	< 2	NA
WT + ΔdmxB/dmxB^{D221A}	47	53
difE + ΔdmxB/dmxB^{D221A}	< 2	< 2

Fig 7. T4P formation and EPS accumulation in various mutants. (A) Immunoblot detection of PilA in total cell extracts and in the sheared T4P fraction. In the upper and lower blots, total cell extracts were isolated from the indicated strains developed in submerged culture at the indicated time points. In the middle blot, T4P were sheared off from the same number of cells and concentrated by MgCl2 precipitation. In all three blots, protein from the same calculated number of cells was loaded per lane. The upper and middle blots were probed with α-PilA antibodies. The lower blot was probed against PilC, which is important for T4P assembly and served as a loading control. PilA and PilC have a calculated molecular mass 23.4 kDa and 45.2 kDa, respectively. Molecular mass marker is indicated on the left. (B) Quantification of EPS accumulation in *dmxB* mutants. 20 μl aliquots of exponentially growing cells of the indicated genotypes were spotted at a density of 7×10^9 cells/ml on 1.5% agar supplemented with 0.5% CTT and 20 μg/ml trypan blue or on TPM starvation agar supplemented with 20 μg/ml trypan blue and incubated at 32°C for 24 hrs. (C) Extracellular complementation assay of Δ*dmxB* mutant. Cells of the indicated genotypes were either developed alone as described in Fig 2B in submerged culture or mixed at a 1:1 ratio and co-developed in submerged culture. Sporulation levels are enumerated after 120 hrs of starvation as the number of germinating heat- and sonication resistant spores relative to WT (100%).

doi:10.1371/journal.pgen.1006080.g007

intracellular concentration of c-di-GMP in different bacterial species range between 130 nM to a few μM [53, 54]. Therefore, we added exogenous c-di-GMP at 0 or 24 hrs to a final concentration of 1 mM to the Δ*dmxB* mutant in submerged culture. However, development of the mutant was not restored by exogenous c-di-GMP under these conditions.

Transcription of *eps* genes is reduced in the Δ*dmxB* mutant

The *eps* locus encodes proteins involved in EPS synthesis and transport and at least 10 of the genes in this locus are essential for development [41] (S4A Fig). We measured the expression profile in WT and the Δ*dmxB* mutant during development of ten of the *eps* genes, which encode proteins with different functions in EPS synthesis and transport using qRT-PCR (Fig 8 and S5AB Fig). For seven of the ten genes we did not observe significant differences in the expression profiles between the two strains (S4B Fig); however, three genes (*epsA*, *epsB* and *epsD*) were transcribed at a significantly lower level in the Δ*dmxB* mutant than in WT at the late time points (Fig 8). These three genes have been suggested to form a single transcriptional unit together with two additional genes [41] (S4A Fig). *epsA* and *epsD* encode predicted glycosyltransferases and have been shown to be essential for EPS accumulation and development while e*psB* encodes a predicted glycosyl hydrolase that is neither important for EPS accumulation nor for development [41].

These data suggest that the DmxB-dependent high level of c-di-GMP that accumulates during development functions to stimulate transcription of at least three genes in the *eps* locus. The only transcription regulator known to be required for EPS synthesis in *M. xanthus* is the NtrC-like transcriptional regulator EpsI/Nla24 [41–43], which is encoded in the *eps* locus (S4A Fig). Two NtrC-like transcriptional regulators have been shown to bind to c-di-GMP [22, 23], suggesting a possible route for c-di-GMP regulation of EPS synthesis via direct allosteric control of EpsI/Nla24. To test whether EpsI/Nla24 binds to c-di-GMP, we first used a biotinylated c-di-GMP pull-down experiment. As shown in Fig 9A, EpsI/Nla24-His_6 was successfully pulled-down from *E. coli* whole-cell extracts containing overexpressed EpsI/Nla24-His_6, strongly suggesting c-di-GMP binding. Direct c-di-GMP binding by EpsI/Nla24 was subsequently confirmed using Surface Plasmon Resonance (SPR) with a chip containing biotinylated c-di-GMP bound to streptavidin, and the purified protein (Fig 9B) [55]. The K_D of c-di-GMP binding to EpsI/Nla24 was calculated as 0.53 ±0.06 μM, well within the physiological range of published c-di-GMP binding proteins (Fig 9B) [56].

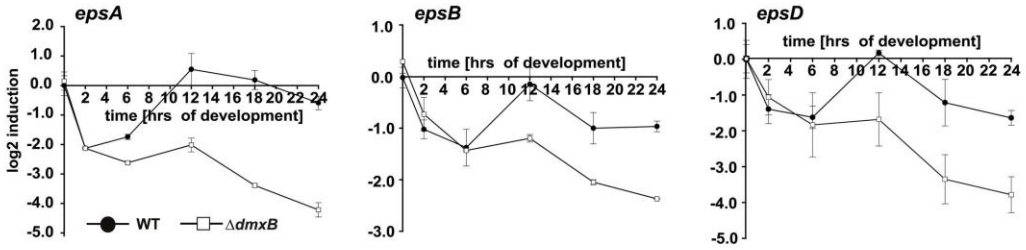

Fig 8. c-di-GMP regulates *epsABD* transcription. Total RNA was isolated at the indicated time points from cells of WT (closed circles) and the Δ*dmxB* mutant (open squares) developed in submerged culture. Transcript levels are shown as mean ± standard deviation from two biological replicates with each three technical replicates relative to WT at 0 hrs.

doi:10.1371/journal.pgen.1006080.g008

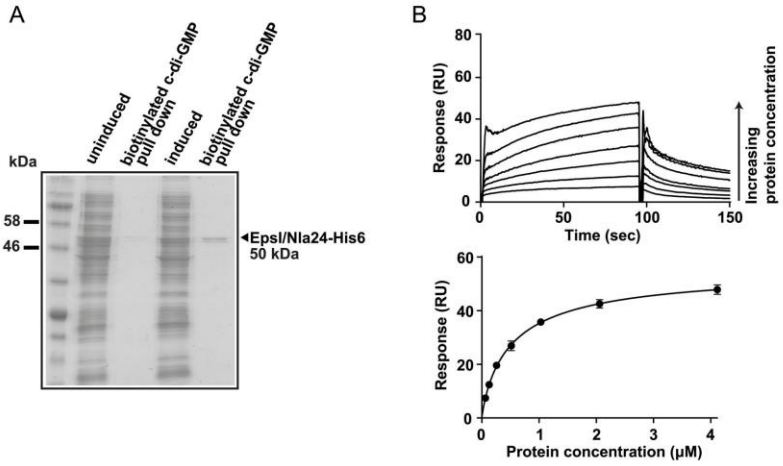

Fig 9. Transcriptional regulator EpsI/Nla24 binds c-di-GMP. (A) Pull-down experiment with the soluble fraction of *E. coli* cell lysates before and after induction of EpsI/Nla24 synthesis using biotinylated c-di-GMP immobilized on streptavidin magnetic beads. Cell extract from the uninduced sample was used as a negative control. Pulled-down protein is indicated with an arrow. EpsI/Nla24-His_6 has a calculated molecular mass of 50 kDa. (B) SPR sensorgrams and resulting affinity fit data for EpsI/Nla24 binding to biotinylated c-di-GMP. Upper panel, sensorgrams of EpsI/Nla24 binding to biotinylated c-di-GMP immobilized on sensor chip. The concentration of EpsI/Nla24 ranged from 62.5 nM (lowest curve) to 4 μM (highest curve) and concentration replicates were included as appropriate. The protein binding and dissociation phases for all sensorgrams are shown. Lower panel, affinity fit of EpsI/Nla24 binding to biotinylated c-di-GMP. For this fit, binding responses were measured 4 sec before the end of the injection.

doi:10.1371/journal.pgen.1006080.g009

Discussion

Here, we show that c-di-GMP is an essential regulator of starvation-induced development with fruiting body formation and sporulation in *M. xanthus*. To assess c-di-GMP accumulation during starvation, *M. xanthus* cells were starved on a solid surface or in suspension. While starvation in suspension is not conducive to development, starvation on a solid surface is. Under both conditions, the c-di-GMP level increased significantly (~20-fold over 48 hrs). Because the level of c-di-GMP does not increase significantly in stationary phase *M. xanthus* cells [44], we conclude that the increase in the c-di-GMP level is a specific response to starvation and that the c-di-GMP level increases during development. In otherwise WT cells, further increasing the c-di-GMP level by expression of a heterologous DGC did not prevent progression of development whereas reducing the c-di-GMP level by expression of a heterologous PDE caused defects in fruiting body formation as well as in sporulation suggesting that a threshold level of c-di-GMP is essential for development to proceed to completion.

By systematically analyzing a set of mutants with single mutations in the 24 gene encoding proteins with a GGDEF, EAL or HD-GYP domain, we identified a single catalytically active DGC, DmxB, which is not only specifically required for development but also responsible for the increase in the c-di-GMP level during starvation. DGC activity by DmxB is essential for development. Moreover, the DmxB-dependent increase in the c-di-GMP level during development is necessary for EPS accumulation and our data suggests that the stimulation of EPS accumulation proceeds via stimulation of the transcription of a subset of the genes in the *eps* locus. This subset of genes code for predicted glycosyltransferases that have previously been shown to

be important for EPS accumulation and development (EpsA, EpsD) and a glycosyl hydrolase (EpsB) that is neither important for EPS accumulation nor for development [41]. Also, the developmental defects caused by lack of DmxB are non-cell autonomous and development of the Δ*dmxB* mutant can be rescued by co-development with a strain proficient in EPS accumulation strongly suggesting that the defects in development in the Δ*dmxB* mutant are caused by lack of EPS. DmxB can be largely functionally replaced by a heterologous DGC both with respect to development and EPS accumulation. Because it is unlikely that this DGC would be able to engage in the same protein-protein interactions as DmxB, we infer that the increase in c-di-GMP level, rather than DmxB *per se*, is important for development and EPS accumulation. Finally, because all strains with significant increases in the level of c-di-GMP, irrespective of the DGC involved, develop whereas strains with reduced c-di-GMP levels have strong defects in development, we surmise that a minimal threshold level of c-di-GMP is essential for development to be successfully completed and that c-di-GMP levels in excess of this threshold do not interfere with development. In WT cells, this minimal threshold level of c-di-GMP is generated by DmxB. It should be noted that simply increasing the c-di-GMP level in vegetative cells to that observed during development by expression of a heterologous DGC is not sufficient to initiate fruiting body formation [44]. Thus, as opposed to the second messenger (p)ppGpp, which is required and sufficient for initiating the developmental program in *M. xanthus* [57, 58], the increased c-di-GMP level is necessary for development but not sufficient to initiate this program. In *S. venezuelae* c-di-GMP also regulates multicellular development with the formation of aerial hyphae. However, in this organism, a high level of c-di-GMP inhibits development by binding to the transcription factor BldD, which inhibits expression of sporulation genes, and a decrease in the c-di-GMP level stimulates development [5]. Thus, c-di-GMP has opposite effects on multicellular development in *S. venezuelae* and *M. xanthus*.

EPS synthesis is a target of c-di-GMP-dependent regulation in several bacterial species [for review, see [1]]. This regulation can occur at the transcriptional and post-translational level. Among transcription factors regulating the expression of genes for EPS synthesis, c-di-GMP has been shown to bind to and modulate the activity of the NtrC-like transcriptional regulators FleQ in *P. aeruginosa* [22] and VpsR in *Vibrio cholerae* [23] as well as the response regulator VpsT in *V. cholerae* [24]. FleQ alone inhibits transcription of the *pel* operon involved in EPS synthesis while binding of c-di-GMP to FleQ inhibits its binding to the *pel* promoter in that way causing derepression of *pel* transcription [22]. VpsR binds to its cognate promoters independently of c-di-GMP; however, it only functions as a transcriptional activator in the c-di-GMP bound state and it is currently not known how c-di-GMP modulates VpsR activity [23]. The NtrC-like transcriptional regulator EpsI/Nla24 is the only transcription regulator known to be required for EPS synthesis in *M. xanthus* and is composed of three domains, an N-terminal receiver domain of two component system, a AAA+ domain, and a helix-turn-helix DNA-binding domain (S5 Fig). As shown here, EpsI/Nla24 binds tightly to c-di-GMP, with a K_D in the low μM range. This strongly suggests that regulation of EPS synthesis during development by c-di-GMP in *M. xanthus* proceeds through control of transcription factor activity, and hence *eps* transcription, by direct c-di-GMP binding to EpsI/Nla24. Recently, structural insights into how the AAA+ domain in FleQ from *P. aeruginosa* binds c-di-GMP were reported and several important motifs for c-di-GMP binding were identified [59] (S5 Fig). Alignment of the AAA+ domains of EpsI/Nla24 and FleQ revealed that not all of these motifs are present in EpsI/Nla24 but confirmed the presence of two Arg residues in EpsI/Nla24 (S5 Fig) that are important for c-di-GMP binding by FleQ [59]. Similarly, VpsR from *V. cholera* does not have all the binding residues reported for FleQ [59] but still binds c-di-GMP [23].

EpsI/Nla24 has been suggested to regulate *eps* gene transcription not only in developing cells but also during vegetative growth [43]. To explain the effect of lack of DmxB and by

implication low c-di-GMP levels on *eps* gene expression during development, we suggest three scenarios. First, as the level of c-di-GMP in vegetative WT cells is similar to the c-di-GMP level in starving Δ*dmxB* cells, it is possible that EpsI/Nla24 binds c-di-GMP at this level in vegetative cells as well as in starving Δ*dmxB* cells. At this c-di-GMP level, EpsI/Nla24 in complex with c-di-GMP activates transcription of all the tested *eps* genes in vegetative cells and a subset of the tested *eps* genes in developing cells; however, a higher level of c-di-GMP is required for *epsABD* expression during development. Alternatively, EpsI/Nla24 functions independently of c-di-GMP in vegetative cells and only binds c-di-GMP during development and this binding requires the high concentration of c-di-GMP that is observed in starving WT cells. In this scenario, EpsI/Nla24 in complex with c-di-GMP specifically functions to activate *epsABD* expression. Of note, c-di-GMP modulates FleQ activity at different promoters differentially [60]. In a third scenario, an additional transcriptional regulator could be involved in the response to the high c-di-GMP level during development. In future experiments, the molecular mechanism of EpsI/Nla24 in the expression of *eps* genes will be analyzed.

Several lines of evidence suggest that synthesis and activity of DmxB is tightly regulated. First, DmxB only accumulates in starving cells but not in growing cells. Measurements of *dmxB* transcript levels strongly suggest that DmxB accumulation is regulated at the transcriptional level. DmxB consists of an N-terminal receiver domain and the C-terminal catalytically active GGDEF domain. An active DGC is an obligate dimer [8] and it was previously reported that DGCs can be induced to dimerize by phosphorylation of their receiver domain as in the case of PleD and WspR [61, 62]. However, the non-phosphorylatable variant $DmxB^{D60N}$ was fully functional *in vivo* as well as *in vitro* suggesting that DmxB forms a dimer independently of phosphorylation of the N-terminal receiver domain. Second, a DmxB variant with a mutated I-site showed higher activity *in vitro* and accumulated ~4-fold more c-di-GMP than WT during development suggesting that DmxB is subject to allosteric feedback inhibition of DGC activity by c-di-GMP. The DmxB variant with the mutated I-site developed normally, suggesting that allosteric feedback inhibition of DGC activity by DmxB is not essential. We speculate that this feedback serves to minimize futile c-di-GMP synthesis during starvation. In total, these observations suggest that DmxB is regulated at the transcriptional level as well as post-translationally by allosteric feedback inhibition.

The Dif chemosensory system is essential for EPS synthesis in growing as well as in starving cells [40], however, it is not known how the Dif system stimulates EPS synthesis. Here, we show that the DifE histidine protein kinase is essential for DmxB accumulation and c-di-GMP accumulation during development, strongly suggesting that during development the Dif system functions by stimulating DmxB accumulation and in that way c-di-GMP and EPS synthesis. Because DmxB specifically accumulates during development and does not accumulate in growing cells, these data also argue that Dif functions through a different downstream target in growing cells to stimulate EPS synthesis.

In addition to DmxB, we also identified the enzymatically active PDE PmxA as specifically important for development. Interestingly, the Δ*pmxA* mutant did not show significant changes in the c-di-GMP levels during development suggesting that the developmental defects in the Δ*pmxA* mutant are not a simple consequence of changes in the global cellular c-di-GMP level but may involve protein-protein interaction and possibly also a local c-di-GMP pool. Interestingly, the HD-GYP domain protein RpfG from *Xanthomonas campestris* was found to interact directly with several GGDEF domain proteins. This interaction was independent on PDE activity of RpfG and DGC activity of the GGDEF domain proteins [63, 64]. It remains to be shown if PDE activity is essential for PmxA function *in vivo* and if PmxA interacts with other proteins involved in c-di-GMP metabolism in *M. xanthus*.

Proteins involved in c-di-GMP metabolism and regulation are ubiquitous with some species encoding >100 proteins with GGDEF, EAL, HD-GYP and effector domains [1]. Yet, mutation of individual genes can give rise to specific defects raising the question how these enzymes and effectors are regulated to obtain specific output responses. It has been suggested that individual signaling modules can be temporally separated by differentially regulating their synthesis, spatially separated by complex formation or by localizing to distinct subcellular locations, or by effectors having different binding affinities for c-di-GMP [1, 53, 54, 65]. Among the 17 GGDEF domain proteins in *M. xanthus*, 11 are predicted to have DGC activity [44]. We previously showed that DmxA has DGC activity and is involved in regulating EPS accumulation in growing *M. xanthus* cells. Lack of DmxA causes a slight but significant increase in the c-di-GMP level and a ~4-fold increase in EPS accumulation and in that way also cause a defect in T4P-dependent motility [44]. However, lack of DmxA does not cause developmental defects. Vice versa, lack of DmxB only causes developmental defects and not motility defects in growing cells. The finding here that DmxB is exclusively synthesized in developing cells provides evidence that *M. xanthus* restricts the synthesis of at least one DGC to a distinct stage of its life cycle suggesting that temporal regulation of proteins involved in c-di-GMP metabolism could be of general importance in *M. xanthus*. Similarly, it was recently demonstrated that *Bdellovibrio bacteriovorus* uses different DGCs at different stages of its predatory life cycle [66].

Materials and Methods

M. xanthus strains, growth and development

All *M. xanthus* strains are derivatives of the WT strain DK1622 [67]. *M. xanthus* strains and plasmids used in this work are listed in Tables 1 and 2, respectively. *M. xanthus* cells were grown in liquid 1% CTT medium or on 1% CTT agar plates at 32°C [68]. For development, cells were grown as described, harvested and resuspended in MC7 buffer (10 mM MOPS pH 7.0, 1 mM $CaCl_2$) to a calculated density of 7×10^9 cells/ml. 20 μl aliquots of cells were placed on TPM agar (10 mM Tris-HCl pH 7.6, 1 mM K_2HPO_4/KH_2PO_4 pH 7.6, 8 mM $MgSO_4$); for development in submerged culture, 50 μl of the cell suspension were mixed with 350 μl MC7 buffer and placed in a 18 mm diameter microtiter dish. Cells were visualized at the indicated time points using a Leica MZ8 stereomicroscope or a Leica IMB/E inverted microscope and imaged using Leica DFC280 and DFC350FX CCD cameras, respectively. Sporulation levels were determined after development for 120 hrs in submerged culture as the number of sonication- and heat-resistant spores relative to WT [51]. In extracellular complementation experiments, spore titers were determined as the number of germinating spores relative to WT. Spores of mixed strains were enumerated by replica plating onto plates containing relevant antibiotics. Because the results of sporulation assay are highly variable, we considered it as significant only if the difference between strains were 3-fold or more. Kanamycin and oxytetracycline were added to *M. xanthus* cells at concentrations of 40 μg/ml or 10 μg/ml, respectively. Growth was measured as an increase in OD at 550 nm.

E. coli strains were grown in LB broth in the presence of relevant antibiotics [69]. All plasmids were propagated in *E. coli* Mach1 (Δ*recA*1398 *endA*1 *tonA* Φ80Δ*lacM*15 Δ*lacX*74 *hsdR* (r_K^- m_K^+)) unless otherwise stated.

Trypan blue binding assay

Cells were grown in CTT to a density of 7×10^8 cells/ml, harvested and resuspended in 1% CTT or MC7 buffer to a calculated density of 7×10^9 cells/ml. 20 μl aliquots of the cell suspensions were placed on 0.5% agar supplemented with 0.5% CTT and 20 μg/ml trypan blue or on

Table 1. *M. xanthus* strains used in this work.

M. xanthus strains	Genotype [a, b]	Reference
DK1622	Wild-type	[67]
DK1300	*pilC*	[35]
SA3502	Δ*sgmT*	[15]
SW501	*difE*::kan^{R}	[75]
DK10410	Δ*pilA*	[76]
DK11063	*fruA*::*Tn5 lacΩ7540*; kan^{R}	[51]
SA3535	*attB*::pTP110; (P_{pilA}-PA5295^{WT}-strepII)	[44]
SA3537	*attB*::pTP112; (P_{pilA}-PA5295^{E328A}-strepII)	[44]
SA3543	*attB*::pTP114; (P_{pilA}-*dgcA*^{WT}-strepII)	[44]
SA3559	*attB*::pTP131; (P_{pilA}-*dgcA*^{D164A}-strepII)	[44]
SA3524	Δ*MXAN2424* (5–256/275)	[44]
SA3525	Δ*MXAN2530* (11-406/416)	[44]
SA3544	Δ*MXAN4232* (6–407/412)	[44]
SA3546	Δ*pmxA* (16–559/569)	[44]
SA3554	Δ*tmoK* (11–1101/1110)	[44]
SA3533	Δ*MXAN5791* (11–338/348)	[44]
SA3545	Δ*MXAN5199* (6–297/304)	[44]
SA3548	Δ*MXAN4675* (11–352/372)	[44]
SA3555	Δ*MXAN1525* (6–289/294)	[44]
SA3556	Δ*MXAN2643* (11–355/265)	[44]
SA3557	Δ*MXAN4029* (6–286/292)	[44]
SA3558	Δ*MXAN2807* (6–655/661)	[44]
SA3569	Δ*MXAN4257* (6–589/595)	[44]
SA3599	Δ*actA* (11-292/302)	[44]
SA5524	Δ*MXAN2997* (9–641/646)	[44]
SA5600	Δ*MXAN4463* (46–433/458)	[44]
SA5605	Δ*dmxB* (10–310/319)	[44]
SA5606	Δ*MXAN7362* (10–665/674)	[44]
SA5607	Δ*MXAN5366* (10–312/321)	[44]
SA5525	Δ*MXAN5340* (50–542/547)	[44]
SA5526	Δ*MXAN5053* (6–612/617)	[44]
SA5527	Δ*MXAN6098* (6–495/501)	[44]
SA5619	Δ*dmxB*; *attB*::pDJS27 (P_{nat}-*dmxB*^{WT})	This study
SA5620	Δ*dmxB*; *attB*::pDJS37 (P_{nat}-*dmxB*^{D221A})	This study
SA5621	Δ*dmxB*; *attB*::pDJS33 (P_{nat}-*dmxB*^{D60N})	This study
SA5622	Δ*dmxB*; *attB*::pDJS38 (P_{nat}-*dmxB*^{R210A})	This study
SA5636	Δ*dmxB*; *attB*::pTP114 (P_{pilA}-*dgcA*^{WT}-strepII)	This study
SA5637	Δ*dmxB*; *attB*::pTP131 (P_{pilA}-*dgcA*^{D164A}-strepII)	This study
SA5629	Δ*pmxA*; *attB*::pDJS56 (P_{nat}-*pmxA*^{WT})	This study
SA5630	Δ*tmoK*; *attB*::pDJS57 (P_{nat}-*tmoK*^{WT})	This study

[a] For in-frame deletions, numbers in brackets indicate the codons deleted over the total number of codons in a given gene).

[b] For strains containing plasmids integrated at the Mx8 *attB* site, the gene expressed including the promoter driving the expression is indicated in brackets.

doi:10.1371/journal.pgen.1006080.t001

Table 2. Plasmids used in this work.

Plasmids	Description	Reference
pBJ114	kan^R, *galK*	[77]
pSWU30	tet^R	[50]
pSW105	P_{pilA}, kan^R	[78]
pET24b(+)	kan^R, expression vector	Novagen
pMALc2x	amp^R, expression vector	New England Biolabs
pDJS27	pSWU30; P_{nat}-$dmxB^{WT}$; tet^R	This study
pDJS37	pSWU30; P_{nat}-$dmxB^{D221A}$; tet^R	This study
pDJS33	pSWU30; P_{nat}-$dmxB^{D60N}$; tet^R	This study
pDJS38	pSWU30; P_{nat}-$dmxB^{R210A}$; tet^R	This study
pDJS56	pSWU30; P_{nat}-*pmxA*; tet^R	This study
pDJS57	pSWU30; P_{nat}-*tmoK*; tet^R	This study
pDJS31	pET24b(+); $dgcA^{WT}$; kan^R	[44]
pDJS30	pET24b(+); $dmxB^{WT}$; kan^R	This study
pDJS39	pET24b(+); $dmxB^{D221A}$; kan^R	This study
pDJS42	pET24b(+); $dmxB^{R210A}$; kan^R	This study
pDJS45	pET24b(+); $dmxB^{D60N}$; kan^R	This study
pDJS71	pET24b(+); $pmxA^{384\text{-}568}$; kan^R	This study
pDJS75	pET24b(+); $pmxA^{384\text{-}568\ H424A,\ D425A}$; kan^R	This study
pDJS79	pET24b(+); *epsI/nla24*; kan^R	This study
pTP114	pSW105, P_{pilA}-$dgcA^{WT}$-strepII, kan^R	[44]
pTP131	pSW105, P_{pilA}-$dgcA^{D164A}$-strepII, kan^R	[44]

doi:10.1371/journal.pgen.1006080.t002

TPM agar supplemented 20 μg/ml trypan blue. Plates were incubated at 32°C for 24 hrs and then visualized using a Leica MZ8 stereomicroscope and imaged using Leica DFC280 camera.

c-di-GMP quantification

Quantifications of c-di-GMP levels in starving *M. xanthus* cells were performed as described [45]. Briefly, exponentially growing cells were harvested from CTT growth medium and resuspended to a cell density of 10^9 cells/ml in MC7 (10 mM MOPS pH 7.0, 1 mM $CaCl_2$) starvation buffer, and incubated in submerged culture on a solid surface or in suspension with shaking. At the indicated time points, cells were harvested at 4°C, 2500× g, 20 min. Cells were lysed in extraction buffer (HPLC grade acetonitrile/methanol/water (2/2/1, v/v/v)), supernatants pooled and evaporated to dryness in a vacuum centrifuge. Pellets were dissolved in HPLC grade water for analysis by LC-MS/MS. All experiments were done in biological triplicates. For all samples, protein concentrations were determined in parallel using a Bradford assay (Bio-Rad).

qRT-PCR analysis

Total RNA was isolated from cells developed in submerged culture using a hot-phenol extraction method as described [70]. RNA was treated with DNase I (Ambion) and purified with the RNeasy kit (Qiagen). RNA was confirmed to be free of DNA by PCR analysis. 1 μg of RNA was used to synthesize cDNA with the High capacity cDNA Archive kit (Applied Biosystems) using random hexamers primers. qRT-PCR was performed in 25 μl reaction volume using SYBR green PCR master mix (Applied Biosystems) and 0.1 μM primers specific to the target gene in a 7300 Real Time PCR System (Applied Biosystems). Relative gene expression levels

were calculated using the comparative Ct method. All experiments were done with two biological replicates each with three technical replicates.

Immunoblot analysis

Immunoblots were carried out as described [69]. Rabbit polyclonal α-PilA [50], α-PilC [71] and α-DmxB antibodies were used together with horseradish-conjugated goat anti-rabbit immunoglobulin G (Sigma) as secondary antibody. Blots were developed using Luminata crescendo Western HRP Substrate (Millipore). T4P were sheared from cells developed in submerged culture, purified, followed by immunoblot analyses with α-PilA antibodies as described [50]. To generate rabbit, polyclonal α-DmxB antibodies, purified DmxB-His_6 was used to immunize rabbits using standard procedures [69].

Protein purification

For expression and purification of His_6-tagged proteins, proteins were expressed in *E. coli* Rosetta 2(DE3) (F^- *ompT hsdS*$_B$(r_B^- m_B^-) *gal dcm* (DE3) pRARE2) at 18°C or 37°C. His_6-tagged proteins were purified using Ni-NTA affinity purification. Briefly, cells were resuspended in buffer A (50 mM Tris-HCl, 150 mM NaCl, 10 mM imidazole, 1 mM DTT, 10% glycerol, pH 8) and lysed using a French pressure cell. To purify DmxB variants and PmxA, after centrifugation (1 hr, 48000× g, 4°C) lysates were loaded on a Ni-NTA agarose column (Qiagen) and washed with 20x column volume using buffer B (50 mM Tris-HCl, 300 mM NaCl, 20 mM imidazole, pH 8). Proteins were eluted with buffer C (50 mM Tris-HCl, 300 mM NaCl, 200 mM imidazole, pH 8). To purify EpsI/Nla24, 1 ml HiTrap chelating HP columns (GE Healthcare, Life Sciences) were equilibrated with 10 volumes of washing buffer (20 mM HEPES pH 7.5, 250 mM NaCl, 2 mM $MgCl_2$, and 2.5% (v/v) glycerol pH 6.8) and loaded with cell lysate. Following protein immobilization, the column was washed with 10 volumes of washing buffer containing 50mM imidazole, before proteins were eluted using washing buffer containing 500mM imidazole.

In vitro DGC and PDE assays

DGC and PDE activities were determined as described [72, 73]. Briefly, assays were performed with 10 μM of purified proteins (final concentration) in a final volume of 40 μl. Reaction mixtures were pre-incubated for 5 min at 30°C in reaction buffer (50 mM Tris-HCl pH 8.0, 300 mM NaCl, 10 mM $MgCl_2$). DGC reactions were initiated by adding 1 mM GTP/[α-^{32}P]-GTP (0.1 μCi/μl) and incubated at 30°C for the indicated periods of time. PDE reactions were initiated by adding ^{32}P-labeled c-di-GMP. Reactions were stopped by addition of one volume 0.5 M EDTA. Reaction products were analyzed by polyethyleneimine-cellulose TLC chromatography as described [12]. Plates were dried prior to exposing a phosphor-imaging screen (Molecular Dynamics). Data were collected and analyzed using a STORM 840 scanner (Amersham Biosciences) and ImageJ 1.46r, respectively.

Preparation of [α-^{32}P]-labeled c-di-GMP

[α-^{32}P]-labeled c-di-GMP was prepared by incubating 10 μM His_6-$DgcA^{WT}$ (final concentration) with 1 mM GTP/[α-^{32}P]-GTP (0.1 μCi/μl) in reaction buffer (50 mM Tris-HCl pH 8.0, 300 mM NaCl, 10 mM $MgCl_2$) in a total volume of 200 μl overnight at 30°C. The reaction mixture was then incubated with 5 units of calf intestine alkaline phosphatase (Fermentas) for 1 hr at 22°C to hydrolyze unreacted GTP. The reaction was stopped by incubation for 10 min at

95°C. The reaction was centrifuged (10 min, 15000× g, 20°C) and the supernatant used for the PDE assay.

In vitro c-di-GMP binding assay

In the DRaCALA [48, 74] [α-^{32}P]-c-di-GMP was mixed with 20 μM of the relevant protein and incubated for 10 min at 22°C in binding buffer (10 mM Tris, pH 8.0, 100 mM NaCl, 5 mM $MgCl_2$). 10 μl of this mixture was transferred to a nitrocellulose filter (GE Healthcare), allowed to dry and imaged using a STORM 840 scanner (Amersham Biosciences). For competition experiments, 0.4 mM unlabelled c-di-GMP (Biolog) or GTP (Sigma) was used. In the SPR-based method [55], experiments were done at 25°C with a Biacore T200 system (GE Healthcare) using a Streptavidin SA sensor chip (GE Healthcare), which has four flow cells each containing Streptavidin pre-immobilized to a carboxymethylated dextran matrix. Flow cell (FC) one (FC1) and FC3 were kept blank to use for reference subtraction. To remove unconjugated Streptavidin, the chip was washed three times with 1 M NaCl, 50 mM NaOH. 100 nM biotinylated c-di-GMP (BioLog) was immobilised on FC2 and FC4 of the Streptavidin SA chip at a 50 RU immobilisation level with a flow rate of 5 μl/min. Purified, soluble EpsI/Nla24-His_6 was prepared in SPR buffer (10 mM HEPES, 150 mM NaCl, 0.1% (v/v) Tween 20, 2 mM $MgCl_2$, pH 6.8). Samples were injected with a flow rate of 5 μl/min over the four flow cells for 90 sec followed by buffer flow for 60 sec. The chip was washed at the end of each cycle with 1 M NaCl. An increasing range of protein concentrations (62.5 nM, 125 nM, 250 nM, 500 nM, 1.0 μM, 2.0 μM, 4.0 μM) was used, with replicates for certain protein concentrations as appropriate. Sensorgrams were analysed using Biacore T200 BiaEvaluation version 1.0 (GE Healthcare). Data were plotted using Microsoft Excel and GraphPad Prism. The experiment was repeated three times independently.

Biotinylated c-di-GMP pull-down

E. coli whole cell lysates before and after induction (0.5mM IPTG for 5 hrs at 28°C) of EpsI/Nla24 were prepared by sonication. The lysed cells were centrifuged (1 hr, 13000× g, 4°C) and 45 μl of the soluble fraction was collected and mixed with biotinylated c-di-GMP (BioLog B098) at a final concentration of 30 μM. The mixture was incubated O/N on a rotary wheel at 8°C. The next day, UV cross-linking was carried out using a UV Stratalinker (Stratagene) for 4 min on ice, to stabilise c-di-GMP/protein complexes. 25μl of Streptavidin magnetic beads (Invitrogen) were added to the mixture, and incubated for 1 hr on a rotary wheel at 8°C. A magnet was used to isolate the Streptavidin magnetic beads and five washing steps were carried out using 200 μl of the protein wash buffer each time (20 mM HEPES pH 7.5, 250 mM NaCl, 2 mM $MgCl_2$, and 2.5% (v/v) glycerol pH 6.8), to remove non-bound proteins. The washed Streptavidin beads were resuspended in 15 μl wash buffer, 4× SDS loading buffer was added, incubated at 95°C for 10 min and then loaded on a 12% SDS-PAGE protein gel. The gel was then developed using InstantBlue (Expedeon).

Supporting Information

S1 Fig. Systematic analysis of *M. xanthus* genes encoding proteins containing a GGDEF, EAL or HD-GYP domain. Cells were treated and spores enumerated as described in Fig 2B. Scale bars: TPM agar 500 μm, submerged culture 100 μm. Strains indicated in red have defects in development only.
(EPS)

S2 Fig. Bioinformatics analysis of actA gene and ActA protein. (A) Flanking genome region of *actA*. Old and new annotation of *actA* gene is indicated in black. Red line marks the region deleted from *actA* in strain DK10605 [46]. Green line marks the region deleted from *actA* in strain SA3599 used in this work. Numbers indicate position in bp relatively to the first nucleotide in the newly annotated *actA* (+1). Direction of gene transcription is indicated by the arrows. (B) Sequence comparison of ActA homologs. The first two lines indicate the old and new annotation of ActA, respectively. From top to bottom: ActA from *M. xanthus*, *M. fulvus*, *M. stipitatus*, *Corallococcus coralloides* and *Stigmatella aurantiaca*.
(EPS)

S3 Fig. Genetic neighborhood of *MXAN3735* (*dmxB*) and phenotype of Δ*MXAN3734* mutant during development. (A) *dmxB* locus. Direction of transcription of *dmxB* (*MXAN3735*) and genes flanking *dmxB* are indicated by the arrows. Numbers indicate position in bp relatively to start of *dmxB* (+1). Domain structure of proteins encoded by *dmxB* and flanking genes is indicated on the right. Domain structure was analyzed using [47]. (B) Cells of the indicated genotypes were treated and spores enumerated as described in Fig 2B. Scale bars, TPM agar 500 μm, submerged culture 100 μm.
(EPS)

S4 Fig. qRT-PCR analysis of *eps* gene transcription in WT and the Δ*dmxB* mutant during development. (A) The *eps* locus in *M. xanthus*. Analyzed genes are indicated (red arrows) in the schematic of the *eps* locus together with the predicted function of the corresponding proteins indicated. The five genes in the dashed box have been suggested to form an operon [41]. (B) Total RNA was isolated at the indicated time points from cells of WT (closed circles) and the Δ*dmxB* mutant (open squares) developed in submerged culture. Transcript levels are shown as mean ± standard deviation from two biological replicates with each three technical replicates relative to WT at 0 hrs.
(EPS)

S5 Fig. Domain structure of EpsI/Nla24 and sequence comparison of AAA+ domains of EpsI/Nla24, FleQ and VpsR. Domain structure was analyzed using [47]. Conserved features important for AAA+ activity (Walker A, Walker B, R finger) and interaction with σ^{54} (Loop L1, Loop L2) are indicated in different colors. c-di-GMP binding motifs identified in FleQ [59] are marked by red boxes, conserved residues in these motifs as identified in [59] are in bold. Red arrows below the alignment indicate conserved Arg residues in FleQ important for c-di-GMP binding, black arrows indicate other c-di-GMP-interacting residues identified in the FleQ structure [59].
(EPS)

Acknowledgments

We gratefully acknowledge Annette Garbe for technical assistance in performing the c-di-GMP quantifications.

Author Contributions

Conceived and designed the experiments: DS GTS TP ET VK JGM MS LSA. Performed the experiments: DS GTS TP ET JL VK. Analyzed the data: DS GTS TP ET VK JGM MS LSA. Contributed reagents/materials/analysis tools: DS GTS TP ET VK JGM MS LSA. Wrote the paper: DS GTS ET VK JGM MS LSA.

References

1. Römling U, Galperin MY, Gomelsky M. Cyclic di-GMP: the first 25 years of a universal bacterial second messenger. Microbiol Mol Biol Rev. 2013; 77: 1–52. doi: 10.1128/MMBR.00043-12 PMID: 23471616
2. Krasteva PV, Giglio KM, Sondermann H. Sensing the messenger: The diverse ways that bacteria signal through c-di-GMP. Protein Sci. 2012; 21: 929–948. doi: 10.1002/pro.2093 PMID: 22593024
3. Boyd CD, O'Toole GA. Second messenger regulation of biofilm formation: Breakthroughs in understanding c-di-GMP effector systems. Annu Rev Cell Dev Biol 2012; 28: 439–462. doi: 10.1146/annurev-cellbio-101011-155705 PMID: 23057745
4. Neunuebel MR, Golden JW. The *Anabaena* sp. strain PCC 7120 gene *all2874* encodes a diguanylate cyclase and is required for normal heterocyst development under high-light growth conditions. J Bacteriol. 2008; 190: 6829–6836. doi: 10.1128/JB.00701-08 PMID: 18723619
5. Tschowri N, Schumacher MA, Schlimpert S, Chinnam NB, Findlay KC, Brennan RG, et al. Tetrameric c-di-GMP mediates effective transcription factor dimerization to control *Streptomyces* development. Cell. 2014; 158: 1136–1147. doi: 10.1016/j.cell.2014.07.022 PMID: 25171413
6. Paul R, Weiser S, Amiot NC, Chan C, Schirmer T, Giese B, et al. Cell cycle-dependent dynamic localization of a bacterial response regulator with a novel di-guanylate cyclase output domain. Genes Dev. 2004; 18: 715–727. PMID: 15075296
7. Ryjenkov DA, Tarutina M, Moskvin OV, Gomelsky M. Cyclic diguanylate is a ubiquitous signaling molecule in bacteria: Insights into biochemistry of the GGDEF protein domain. J Bacteriol. 2005; 187: 1792–1798. PMID: 15716451
8. Schirmer T, Jenal U. Structural and mechanistic determinants of c-di-GMP signalling. Nat Rev Micro. 2009; 7: 724–735.
9. Schmidt AJ, Ryjenkov DA, Gomelsky M. The ubiquitous protein domain EAL is a cyclic diguanylate-specific phosphodiesterase: Enzymatically active and inactive EAL domains. J Bacteriol. 2005; 187: 4774–4781. PMID: 15995192
10. Tamayo R, Tischler AD, Camilli A. The EAL domain protein VieA is a cyclic diguanylate phosphodiesterase. J Biol Chem. 2005; 280: 33324–33330. PMID: 16081414
11. Ryan RP, Fouhy Y, Lucey JF, Crossman LC, Spiro S, He Y-W, et al. Cell–cell signaling in *Xanthomonas campestris* involves an HD-GYP domain protein that functions in cyclic di-GMP turnover. Proc Natl Acad Sci USA. 2006; 103: 6712–6717. PMID: 16611728
12. Christen M, Christen B, Folcher M, Schauerte A, Jenal U. Identification and characterization of a cyclic di-GMP-specific phosphodiesterase and its allosteric control by GTP. J Biol Chem. 2005; 280: 30829–30837. PMID: 15994307
13. Steiner S, Lori C, Böhm A, Jenal U. Allosteric activation of exopolysaccharide synthesis through cyclic di-GMP-stimulated protein-protein interaction. EMBO J. 2013; 32: 354–368. doi: 10.1038/emboj.2012.315 PMID: 23202856
14. Duerig A, Abel S, Folcher M, Nicollier M, Schwede T, Amiot N, et al. Second messenger-mediated spatiotemporal control of protein degradation regulates bacterial cell cycle progression. Genes Dev. 2009; 23: 93–104. doi: 10.1101/gad.502409 PMID: 19136627
15. Petters T, Zhang X, Nesper J, Treuner-Lange A, Gomez-Santos N, Hoppert M, et al. The orphan histidine protein kinase SgmT is a c-di-GMP receptor and regulates composition of the extracellular matrix together with the orphan DNA binding response regulator DigR in *Myxococcus xanthus*. Mol Microbiol. 2012; 84: 147–165. doi: 10.1111/j.1365-2958.2012.08015.x PMID: 22394314
16. Qi Y, Chuah MLC, Dong X, Xie K, Luo Z, Tang K, et al. Binding of cyclic diguanylate in the non-catalytic EAL domain of FimX induces a long-range conformational change. J Biol Chem. 2011; 286: 2910–2917. doi: 10.1074/jbc.M110.196220 PMID: 21098028
17. Newell PD, Monds RD, O'Toole GA. LapD is a bis-(3',5')-cyclic dimeric GMP-binding protein that regulates surface attachment by *Pseudomonas fluorescens* Pf0-1. Proc Natl Acad Sci USA. 2009; 106: 3461–3466. doi: 10.1073/pnas.0808933106 PMID: 19218451
18. Navarro MV, De N, Bae N, Wang Q, Sondermann H. Structural analysis of the GGDEF-EAL domain-containing c-di-GMP receptor FimX. Structure. 2009; 17: 1104–1116. doi: 10.1016/j.str.2009.06.010 PMID: 19679088
19. Li W, He ZG. LtmA, a novel cyclic di-GMP-responsive activator, broadly regulates the expression of lipid transport and metabolism genes in *Mycobacterium smegmatis*. Nucl Acids Res. 2012; 40: 11292–11307. doi: 10.1093/nar/gks923 PMID: 23047950
20. Chin KH, Lee YC, Tu ZL, Chen CH, Tseng YH, Yang JM, et al. The cAMP receptor-like protein CLP is a novel c-di-GMP receptor linking cell-cell signaling to virulence gene expression in *Xanthomonas campestris*. J Mol Biol 2010; 396: 646–662. doi: 10.1016/j.jmb.2009.11.076 PMID: 20004667

21. Fazli M, O'Connell A, Nilsson M, Niehaus K, Dow JM, Givskov M, et al. The CRP/FNR family protein Bcam1349 is a c-di-GMP effector that regulates biofilm formation in the respiratory pathogen *Burkholderia cenocepacia*. Mol Microbiol. 2011; 82: 327–341. doi: 10.1111/j.1365-2958.2011.07814.x PMID: 21883527

22. Hickman JW, Harwood CS. Identification of FleQ from *Pseudomonas aeruginosa* as a c-di-GMP-responsive transcription factor. Mol Microbiol. 2008; 69: 376–389. doi: 10.1111/j.1365-2958.2008.06281.x PMID: 18485075

23. Srivastava D, Harris RC, Waters CM. Integration of cyclic di-GMP and quorum sensing in the control of *vpsT* and *aphA* in *Vibrio cholerae*. J Bacteriol. 2011; 193: 6331–6341. doi: 10.1128/JB.05167-11 PMID: 21926235

24. Krasteva PV, Fong JC, Shikuma NJ, Beyhan S, Navarro MV, Yildiz FH, et al. Vibrio cholerae VpsT regulates matrix production and motility by directly sensing cyclic di-GMP. Science. 2010; 327: 866–868. doi: 10.1126/science.1181185 PMID: 20150502

25. Amikam D, Galperin MY. PilZ domain is part of the bacterial c-di-GMP binding protein. Bioinformatics. 2006; 22: 3–6. PMID: 16249258

26. Ryjenkov DA, Simm R, Römling U, Gomelsky M. The PilZ domain is a receptor for the second messenger c-di-GMP: The PilZ domain protein YcgR controls motility in enterobacteria. J Biol Chem. 2006; 281: 30310–30314. PMID: 16920715

27. Christen M, Christen B, Allan MG, Folcher M, Jeno P, Grzesiek S, et al. DgrA is a member of a new family of cyclic diguanosine monophosphate receptors and controls flagellar motor function in *Caulobacter crescentus*. Proc Natl Acad Sci U S A. 2007; 104: 4112–4117. PMID: 17360486

28. Pratt JT, Tamayo R, Tischler AD, Camilli A. PilZ domain proteins bind cyclic diguanylate and regulate diverse processes in *Vibrio cholerae*. J Biol Chem. 2007; 282: 12860–12870. PMID: 17307739

29. Ramelot TA, Yee A, Cort JR, Semesi A, Arrowsmith CH, Kennedy MA. NMR structure and binding studies confirm that PA4608 from *Pseudomonas aeruginosa* is a PilZ domain and a c-di-GMP binding protein. Proteins: Structure, Function, and Bioinformatics. 2007; 66: 266–271.

30. Merighi M, Lee VT, Hyodo M, Hayakawa Y, Lory S. The second messenger bis-(3'-5')-cyclic-GMP and its PilZ domain-containing receptor Alg44 are required for alginate biosynthesis in *Pseudomonas aeruginosa*. Mol Microbiol. 2007; 65: 876–895. PMID: 17645452

31. Wilksch JJ, Yang J, Clements A, Gabbe JL, Short KR, Cao H, et al. MrkH, a novel c-di-GMP-dependent transcriptional activator, controls *Klebsiella pneumoniae* biofilm formation by regulating type 3 fimbriae expression. PLoS Pathog. 2011; 7: e1002204. doi: 10.1371/journal.ppat.1002204 PMID: 21901098

32. Sudarsan N, Lee ER, Weinberg Z, Moy RH, Kim JN, Link KH, et al. Riboswitches in eubacteria sense the second messenger cyclic di-GMP. Science. 2008; 321: 411–413. doi: 10.1126/science.1159519 PMID: 18635805

33. Konovalova A, Petters T, Søgaard-Andersen L. Extracellular biology of *Myxococcus xanthus*. FEMS Microbiol Rev. 2010; 34: 89–106. doi: 10.1111/j.1574-6976.2009.00194.x PMID: 19895646

34. Jelsbak L, Søgaard-Andersen L. Pattern formation by a cell surface-associated morphogen in *Myxococcus xanthus*. Proc Natl Acad Sci USA. 2002; 99: 2032–2037. PMID: 11842199

35. Hodgkin J, Kaiser D. Genetics of gliding motility in *Myxococcus xanthus* (Myxobacterales): Two gene systems control movement. Mol Gen Genet. 1979; 171: 177–191.

36. Wu SS, Wu J, Cheng YL, Kaiser D. The *pilH* gene encodes an ABC transporter homologue required for type IV pilus biogenesis and social gliding motility in *Myxococcus xanthus*. Mol Microbiol. 1998; 29: 1249–1261. PMID: 9767592

37. Li Y, Sun H, Ma X, Lu A, Lux R, Zusman D, et al. Extracellular polysaccharides mediate pilus retraction during social motility of *Myxococcus xanthus*. Proc Natl Acad Sci USA. 2003; 100: 5443–5448. PMID: 12704238

38. Chang BY, Dworkin M. Isolated fibrils rescue cohesion and development in the Dsp mutant of *Myxococcus xanthus*. J Bacteriol. 1994; 176: 7190–7196. PMID: 7961490

39. Shimkets LJ. Role of cell cohesion in *Myxococcus xanthus* fruiting body formation. J Bacteriol. 1986; 166: 842–848. PMID: 3011748

40. Yang Z, Ma X, Tong L, Kaplan HB, Shimkets LJ, Shi W. *Myxococcus xanthus dif* genes are required for biogenesis of cell surface fibrils essential for social gliding motility. J Bacteriol. 2000; 182: 5793–5798. PMID: 11004179

41. Lu A, Cho K, Black WP, Duan XY, Lux R, Yang Z, et al. Exopolysaccharide biosynthesis genes required for social motility in *Myxococcus xanthus*. Mol Microbiol. 2005; 55: 206–220. PMID: 15612929

42. Caberoy NB, Welch RD, Jakobsen JS, Slater SC, Garza AG. Global mutational analysis of NtrC-like activators in *Myxococcus xanthus*: identifying activator mutants defective for motility and fruiting body development. J Bacteriol. 2003; 185: 6083–6094. PMID: 14526020

43. Lancero H, Caberoy NB, Castaneda S, Li YN, Lu A, Dutton D, et al. Characterization of a *Myxococcus xanthus* mutant that is defective for adventurous motility and social motility. Microbiology-Sgm. 2004; 150: 4085–4093.

44. Skotnicka D, Petters T, Heering J, Hoppert M, Kaever V, Søgaard-Andersen L. c-di-GMP regulates type IV pili-dependent-motility in *Myxococcus xanthus*. J Bacteriol. 2016; 198: 77–90.

45. Spangler C, Bohm A, Jenal U, Seifert R, Kaever V. A liquid chromatography-coupled tandem mass spectrometry method for quantitation of cyclic di-guanosine monophosphate. J Microbiol Methods. 2010; 81: 226–231. doi: 10.1016/j.mimet.2010.03.020 PMID: 20385176

46. Gronewold TM, Kaiser D. The *act* operon controls the level and time of C-signal production for *Myxococcus xanthus* development. Mol Microbiol. 2001; 40: 744–756. PMID: 11359579

47. Letunic I, Doerks T, Bork P. SMART: recent updates, new developments and status in 2015. Nucleic Acids Res. 2015; 43: D257–D260. doi: 10.1093/nar/gku949 PMID: 25300481

48. Roelofs KG, Wang JX, Sintim HO, Lee VT. Differential radial capillary action of ligand assay for high-throughput detection of protein-metabolite interactions. Proc Natl Acad Sci USA. 2011; 108: 15528–15533. doi: 10.1073/pnas.1018949108 PMID: 21876132

49. Bharati BK, Sharma IM, Kasetty S, Kumar M, Mukherjee R, Chatterji D. A full-length bifunctional protein involved in c-di-GMP turnover is required for long-term survival under nutrient starvation in *Mycobacterium smegmatis*. Microbiology. 2012; 158: 1415–1427. doi: 10.1099/mic.0.053892-0 PMID: 22343354

50. Wu SS, Kaiser D. Regulation of expression of the *pilA* gene in *Myxococcus xanthus*. J Bacteriol. 1997; 179: 7748–7758. PMID: 9401034

51. Søgaard-Andersen L, Slack FJ, Kimsey H, Kaiser D. Intercellular C-signaling in *Myxococcus xanthus* involves a branched signal transduction pathway. Genes Dev. 1996; 10: 740–754. PMID: 8598300

52. Chen ZH, Schaap P. The prokaryote messenger c-di-GMP triggers stalk cell differentiation in *Dictyostelium*. Nature. 2012; 488: 680–683. doi: 10.1038/nature11313 PMID: 22864416

53. Massie JP, Reynolds EL, Koestler BJ, Cong J-P, Agostoni M, Waters CM. Quantification of high-specificity cyclic diguanylate signaling. Proc Natl Acad Sci USA. 2012; 109: 12746–12751. doi: 10.1073/pnas.1115663109 PMID: 22802636

54. Abel S, Bucher T, Nicollier M, Hug I, Kaever V, Abel zur Wiesch P, et al. Bi-modal distribution of the second messenger c-di-GMP controls cell fate and asymmetry during the *Caulobacter* cell cycle. PLOS Genet. 2013; 9: e1003744. doi: 10.1371/journal.pgen.1003744 PMID: 24039597

55. Trampari E, Stevenson CEM, Little RH, Wilhelm T, Lawson DM, Malone JG. Bacterial rotary export ATPases are allosterically regulated by the nucleotide second messenger cyclic-di-GMP. J Biol Chem. 2015; 290: 24470–24483. doi: 10.1074/jbc.M115.661439 PMID: 26265469

56. Pultz IS, Christen M, Kulasekara HD, Kennard A, Kulasekara B, Miller SI. The response threshold of *Salmonella* PilZ domain proteins is determined by their binding affinities for c-di-GMP. Mol Microbiol. 2012; 86: 1424–1440. doi: 10.1111/mmi.12066 PMID: 23163901

57. Harris BZ, Kaiser D, Singer M. The guanosine nucleotide (p)ppGpp initiates development and A-factor production in *Myxococcus xanthus*. Genes Dev. 1998; 12: 1022–1035. PMID: 9531539

58. Singer M, Kaiser D. Ectopic production of guanosine penta- and teraphosphate can initiate early developmental gene expression in *Myxococcus xanthus*. Genes Dev. 1995; 9: 1633–1644. PMID: 7628697

59. Matsuyama BY, Krasteva PV, Baraquet C, Harwood CS, Sondermann H, Navarro MVAS. Mechanistic insights into c-di-GMP-dependent control of the biofilm regulator FleQ from *Pseudomonas aeruginosa*. Proc Natl Acad sci USA. 2016; 113: E209–E218. doi: 10.1073/pnas.1523148113 PMID: 26712005

60. Baraquet C, Harwood CS. Cyclic diguanosine monophosphate represses bacterial flagella synthesis by interacting with the Walker A motif of the enhancer-binding protein FleQ. Proc Natl Acad Sci USA. 2013; 110: 18478–18483. doi: 10.1073/pnas.1318972110 PMID: 24167275

61. Paul R, Abel S, Wassmann P, Beck A, Heerklotz H, Jenal U. Activation of the diguanylate cyclase PleD by phosphorylation-mediated dimerization. J Biol Chem. 2007; 282: 29170–29177. PMID: 17640875

62. Hickman JW, Tifrea DF, Harwood CS. A chemosensory system that regulates biofilm formation through modulation of cyclic diguanylate levels. Proc Natl Acad Sci USA. 2005; 102: 14422–14427. PMID: 16186483

63. Ryan RP, McCarthy Y, Andrade M, Farah CS, Armitage JP, Dow JM. Cell–cell signal-dependent dynamic interactions between HD-GYP and GGDEF domain proteins mediate virulence in *Xanthomonas campestris*. Proc Natl Acad Sci USA. 2010; 107: 5989–5994. doi: 10.1073/pnas.0912839107 PMID: 20231439

64. Ryan RP, McCarthy Y, Kiely PA, O'Connor R, Farah CS, Armitage JP, et al. Dynamic complex formation between HD-GYP, GGDEF and PilZ domain proteins regulates motility in *Xanthomonas campestris*. Mol Microbiol. 2012; 86: 557–567. doi: 10.1111/mmi.12000 PMID: 22924852

65. Hengge R. Principles of c-di-GMP signalling in bacteria. Nat Rev Microbiol. 2009; 7: 263–273. doi: 10.1038/nrmicro2109 PMID: 19287449

66. Hobley L, Fung RK, Lambert C, Harris MA, Dabhi JM, King SS, et al. Discrete cyclic di-GMP-dependent control of bacterial predation versus axenic growth in *Bdellovibrio bacteriovorus*. PLOS Pathog. 2012; 8: e1002493. doi: 10.1371/journal.ppat.1002493 PMID: 22319440

67. Kaiser D. Social gliding is correlated with the presence of pili in *Myxococcus xanthus*. Proc Natl Acad Sci USA. 1979; 76: 5952–5956. PMID: 42906

68. Hodgkin J, Kaiser D. Cell-to-cell stimulation of movement in nonmotile mutants of *Myxococcus*. Proc Natl Acad Sci U S A. 1977; 74: 2938–2942. PMID: 16592422

69. Sambrook J, Russell DW. Molecular Cloning—A Laboratory Manual. 3rd Edition ed. Cold Spring Harbor, New York: Cold Spring Harbor Laboratory Press; 2001.

70. Overgaard M, Wegener-Feldbrügge S, Søgaard-Andersen L. The orphan response regulator DigR is required for synthesis of extracellular matrix fibrils in *Myxococcus xanthus*. J Bacteriol. 2006; 188: 4384–4394. PMID: 16740945

71. Bulyha I, Schmidt C, Lenz P, Jakovljevic V, Höne A, Maier B, et al. Regulation of the type IV pili molecular machine by dynamic localization of two motor proteins. Mol Microbiol. 2009; 74: 691–706. doi: 10.1111/j.1365-2958.2009.06891.x PMID: 19775250

72. Bordeleau E, Brouillette E, Robichaud N, Burrus V. Beyond antibiotic resistance: integrating conjugative elements of the SXT/R391 family that encode novel diguanylate cyclases participate to c-di-GMP signalling in *Vibrio cholerae*. Environ Microbiol. 2010; 12: 510–523. doi: 10.1111/j.1462-2920.2009.02094.x PMID: 19888998

73. Sultan SZ, Pitzer JE, Boquoi T, Hobbs G, Miller MR, Motaleb MA. Analysis of the HD-GYP domain cyclic dimeric GMP phosphodiesterase reveals a role in motility and the enzootic life cycle of *Borrelia burgdorferi*. Infect Immun. 2011; 79: 3273–3283. doi: 10.1128/IAI.05153-11 PMID: 21670168

74. Fang X, Ahmad I, Blanka A, Schottkowski M, Cimdins A, Galperin MY, et al. GIL, a new c-di-GMP-binding protein domain involved in regulation of cellulose synthesis in enterobacteria. Mol Microbiol. 2014; 93: 439–452. doi: 10.1111/mmi.12672 PMID: 24942809

75. Yang ZM, Geng YZ, Xu D, Kaplan HB, Shi WY. A new set of chemotaxis homologues is essential for *Myxococcus xanthus* social motility. Mol Microbiol. 1998; 30: 1123–1130. PMID: 9988486

76. Wu SS, Kaiser D. Markerless deletions of pil genes in *Myxococcus xanthus* generated by counterselection with the *Bacillus subtilis sacB* gene. J Bacteriol. 1996; 178: 5817–5821. PMID: 8824635

77. Julien B, Kaiser AD, Garza A. Spatial control of cell differentiation in *Myxococcus xanthus*. Proc Natl Acad Sci U S A. 2000; 97: 9098–9103. PMID: 10922065

78. Jakovljevic V, Leonardy S, Hoppert M, Søgaard-Andersen L. PilB and PilT are ATPases acting antagonistically in type IV pilus function in *Myxococcus xanthus*. J Bacteriol. 2008; 190: 2411–2421. doi: 10.1128/JB.01793-07 PMID: 18223089